

Copyright  
by  
David Reed Price  
2009

The Dissertation Committee for David Reed Price  
certifies that this is the approved version of the following dissertation:

**Parallel Computation of Analytic Second Derivatives  
with Applications to Benzene and [10]Annulene**

Committee:

---

John F. Stanton, Supervisor

---

Peter Rossky

---

Dimtrii Makarov

---

Eric Anslyn

---

Kent Milfeld

**Parallel Computation of Analytic Second Derivatives  
with Applications to Benzene and [10]Annulene**

by

**David Reed Price, B.A., M.A.**

**DISSERTATION**

Presented to the Faculty of the Graduate School of

The University of Texas at Austin

in Partial Fulfillment

of the Requirements

for the Degree of

**DOCTOR OF PHILOSOPHY**

THE UNIVERSITY OF TEXAS AT AUSTIN

May 2009

Dr. Juana Vázquez por su incansable trabajo sobre el benceno, su paciente  
revisión de este documento en numerosas ocasiones y su necesitada asistencia  
para comprender “vibrational perturbation theory. ”

# Acknowledgments

“If I have seen a little further, it is by standing on the shoulders of Giants.” The author acknowledges the assistance of the following individuals and organizations:

Dr. Juana Vázquez for her tireless work on benzene, her patient review of this document on numerous occasions and her needed assistance in understanding vibrational perturbation theory.

Dr. John F. Stanton for his patient support and resources used in this study.

Dr. Peter Szalay for his assistance in the implementation of the coarse grained parallelization scheme.

Dr. Michael E. Harding for his assistance in debugging and testing the coarse grained parallelization scheme in conjunction with the current parallelization in ACESII MAB and his insights on the NMR spectrum of [10]annulene.

Dr. Kent Milfeld for his assistance in testing ACESII MAB on **lone-star**.

Alexander A. Price and Karen Norman for their assistance in proof reading this document.

Texas Advanced Computing Center (TACC) at The University of Texas at Austin for providing HPC resources used in this study.

# Parallel Computation of Analytic Second Derivatives with Applications to Benzene and [10]Annulene

Publication No. \_\_\_\_\_

David Reed Price, Ph.D.  
The University of Texas at Austin, 2009

Supervisor: John F. Stanton

CCSD(T) has been used in the past to accurately predict compute the spectra and structures of small molecules. However, the large execution times required for these calculations has limited their use in larger molecules such as benzene and [10]annulene. The parallelization of analytic second derivatives of post Hartree-Fock methods, including CCSD(T), has enabled the VPT2+D treatment of the vibrational states of benzene. The fundamental frequencies and infrared active two quantum transitions that result are within  $20\text{ cm}^{-1}$  of the experimental values when treated for Fermi and Darling-Dennison resonances and empirical estimates for the harmonic frequencies and equilibrium bond lengths are determined to be within  $12\text{ cm}^{-1}$  and  $0.004\text{ \AA}$  of the values at the CCSD(T)/ANO2(fc) level of theory. The parallelization also facilitated the identification of two candidates for the structures of two isomers of [10]annulene. The harmonic frequencies of several conformations proposed in the literature were computed at the CCSD/DZP level of theory with five of the conformations being ground states. The NMR shifts of four of these structures

were computed using CCSD(T)/tzp and conformation **6**( $C_2$  “twist”) was identified as the likeliest structure for one of the isomers isolated. The remaining compound was identified as conformation **2b**( $C_2$  “boat”) due to a low conformation barrier and the proximity of its average NMR shifts to experiment. The identification of both compounds rely on properties computed using analytic derivatives not entirely on the relative energies of optimized geometries.

# Table of Contents

<b>Acknowledgments</b>	<b>v</b>
<b>Abstract</b>	<b>vi</b>
<b>List of Tables</b>	<b>xii</b>
<b>List of Figures</b>	<b>xv</b>
<b>Chapter 1. An Overview of Certain Aspects of Quantum Chemistry</b>	<b>1</b>
1.1 Introduction . . . . .	1
1.2 Hartree-Fock Approximation and Self Consistent Field Method	2
1.3 Electron-Correlation Methods . . . . .	8
1.3.1 Second-Order Many-Body Perturbation Theory . . . . .	9
1.3.2 Coupled-Cluster Theory . . . . .	12
1.3.2.1 Coupled-Cluster Singles and Doubles (CCSD) .	14
1.3.2.2 Non-iterative Triples Correction (CCSD(T)) . .	17
1.4 Basis Sets . . . . .	18
1.5 Analytic Gradients and Second Derivatives . . . . .	22
1.5.1 Coupled-Perturbed Hartree-Fock Equations . . . . .	23
1.5.2 Second-Order Many-Body Perturbation Theory . . . . .	27
1.5.3 Coupled-Cluster Theory . . . . .	32
1.5.4 Analytic Derivatives of Perturbative Triples . . . . .	37
1.6 Serial Implementation of Analytic Second Derivatives for MBPT and CC methods . . . . .	39



<b>Chapter 2. Coarse-Grained Scheme for Parallel Calculation of Post Hartree-Fock Analytic Second Derivatives</b>	<b>43</b>
2.1 Rationale: Infrared Spectra and Other Observable Properties .	43
2.2 Current Parallelization of Quantum Chemistry Programs . . .	44
2.3 Coarse Grained Parallelization of the Computation Analytic Second Derivatives . . . . .	45
2.4 Testing . . . . .	47
2.5 Performance . . . . .	48
2.5.1 Performance Metrics: Speed up and Sequential Fraction	48
2.5.2 Comparison to Current Parallelization . . . . .	50
2.5.3 Other Comparisons . . . . .	55
2.5.4 Scalability . . . . .	59
2.6 Summary . . . . .	61
 <b>Chapter 3. Vibrational Spectroscopy and Second-Order Vibrational Perturbation Theory</b>	 <b>63</b>
3.1 Systems of Harmonic Oscillators . . . . .	63
3.2 Limitations of the Harmonic Approximation . . . . .	67
3.3 Second-Order Vibrational Perturbation Theory . . . . .	68
3.3.1 Resonances . . . . .	72
3.4 Other Methods for Treating the Vibrational Problem . . . . .	76
3.4.1 Comparison of Other Methods to VPT2 . . . . .	78
 <b>Chapter 4. Benzene</b>	 <b>82</b>
4.1 History . . . . .	82
4.2 Background . . . . .	84
4.2.1 Infrared Spectra . . . . .	86
4.2.2 Raman Spectra . . . . .	88
4.2.3 Two Photon Spectroscopy . . . . .	89
4.2.4 Combination Bands . . . . .	90
4.2.5 Other Experiment: $\nu_{13}(b_{1u})$ CH Stretch . . . . .	91
4.2.6 <i>Ab Initio</i> and Density Functional Studies . . . . .	92
4.2.7 Empirical and Experimental Estimates of Harmonic Frequencies . . . . .	93

4.3	Computational Details . . . . .	95
4.4	<i>Ab Initio</i> and Empirical Geometries . . . . .	97
4.4.1	Equilibrium Bond Lengths . . . . .	97
4.4.2	Empirical Equilibrium Bond Lengths . . . . .	100
4.4.3	Distance and Position Averages . . . . .	105
4.4.4	Effective Bond Lengths . . . . .	107
4.5	Harmonic Frequencies . . . . .	109
4.5.1	<i>Ab Initio</i> Frequencies . . . . .	109
4.5.2	Empirical Estimates . . . . .	114
4.6	Spectral Predictions . . . . .	117
4.6.1	Fundamental Frequencies . . . . .	119
4.6.2	Combination Bands and Overtones . . . . .	125
4.7	Summary . . . . .	136
<b>Chapter 5.</b>	<b>[10]Annulene</b>	<b>138</b>
5.1	Introduction . . . . .	138
5.2	Computational Details . . . . .	140
5.3	Structures of Conformations . . . . .	141
5.4	<i>Ab Initio</i> Energies of the Studied Conformations . . . . .	150
5.5	Harmonic Frequencies . . . . .	153
5.6	NMR Shifts . . . . .	160
5.7	Summary . . . . .	165
<b>Chapter 6.</b>	<b>Conclusion</b>	<b>166</b>
	<b>Appendices</b>	<b>167</b>
<b>Appendix A.</b>	<b>Parallel Timings</b>	<b>168</b>
<b>Appendix B.</b>	<b>Benzene Supporting Information</b>	<b>182</b>
B.1	Literature Values . . . . .	182
B.2	Geometry . . . . .	184
B.3	Harmonic Frequencies . . . . .	185
B.4	Fundamental Frequencies . . . . .	189
B.5	Two Quantum Transitions . . . . .	192

<b>Appendix C. [10]Annulene Supporting Information</b>	<b>197</b>
C.1 Literature Values . . . . .	197
C.2 Structures of Conformations . . . . .	198
C.3 Relative Energies . . . . .	206
C.4 Harmonic Frequencies . . . . .	207
C.5 NMR Shifts . . . . .	219
<b>Bibliography</b>	<b>222</b>
<b>Index</b>	<b>252</b>
<b>Vita</b>	<b>254</b>

# List of Tables

1.1	Description of basis sets used in this work. The primitive Gaussian type orbitals (PGTO) are contracted into $N$ basis functions of contracted Gaussian type orbitals (CGTO). . . . .	21
1.2	Properties calculated from derivatives of the energy from Table 10.1 of Reference [103]. . . . .	24
2.1	Comparison of execution times (s) of current parallelization versus coarse grained scheme for harmonic frequency calculations using analytic second derivatives. <b>Part 1:</b> Initial unperturbed calculation. <b>Part 2:</b> $N$ perturbations. <b>Part 3:</b> Final summation. Numbers in parenthesis are the number of perturbations treated and the number of basis functions. . . . .	50
2.2	Comparison of speed up and sequential fraction ( $\bar{Z}$ ) for the current parallelization versus the coarse grained scheme for harmonic frequency calculations using analytic second derivatives. Part 2: $N$ perturbations, given in parenthesis. . . . .	53
3.1	Elements of Hamiltonian grouped by order of magnitude . . .	71
3.2	Comparison of methods for treating the vibrational problem: the fundamental vibrational frequencies of formaldehyde . . .	79
4.1	Observed gas-phase fundamental frequencies ( $\text{cm}^{-1}$ ) . . . . .	87
4.2	Calculated equilibrium bond lengths, $r_e$ , mean internuclear distances, $r_g$ and distances between mean internuclear positions, $r_z$ (Units: Å). All of these calculations were carried out at CCSD(T) level of theory. . . . .	98
4.3	CCSD(T) ground-state rotational constants, calculated vibrational corrections and empirical equilibrium rotational constants of benzene isotopomers in MHz . . . . .	103
4.4	Empirical equilibrium bond lengths $r_e$ and effective bond lengths $r_0$ (Å). All calculations were performed using CCSD(T). . . .	104
4.5	CCSD(T) harmonic frequencies ( $\text{cm}^{-1}$ ) <sup>a</sup> . . . . .	108

4.6	Comparison of empirical harmonic frequencies ( $\text{cm}^{-1}$ ) estimated with CCSD(T) to the estimates of other levels of theory and experiment <sup>a</sup> . . . . .	115
4.7	CCSD(T) fundamental frequencies: VPT2 ( $\text{cm}^{-1}$ ) . . . . .	120
4.8	Comparison of CCSD(T)/ANO2/1(fc) straight forward VPT2 fundamental frequencies with deperturbed and diagonalized or dressed frequencies ( $\text{cm}^{-1}$ ). . . . .	124
4.9	CCSD(T) two quantum transitions: VPT2 ( $\text{cm}^{-1}$ ) . . . . .	126
5.1	Relative energies of conformations and transition states for [10]-annulene (in $\text{kcal mol}^{-1}$ ) . . . . .	151
A.1	Timing (s) and Speed Up . . . . .	168
B.1	Previous experimental effective bond lengths ( $r_0$ ) and electron diffraction ( $r_a$ ) ( $\text{\AA}$ ) . . . . .	182
B.2	Bond distances from previous studies . . . . .	182
B.3	Fundamental frequencies: Literature ( $\text{cm}^{-1}$ ) . . . . .	184
B.4	Bond distances $r_e$ for other levels of theory ( $\text{\AA}$ ) . . . . .	185
B.5	Bond distances $r_g$ and $r_z$ for other levels of theory ( $\text{\AA}$ ) . . . . .	185
B.6	Harmonic frequencies for SCF level of theory ( $\text{cm}^{-1}$ ) . . . . .	185
B.7	Harmonic frequencies for MP2 level of theory ( $\text{cm}^{-1}$ ) . . . . .	186
B.8	Harmonic Frequencies for CCSD level of theory ( $\text{cm}^{-1}$ ) . . . . .	187
B.9	CCSD(T) Harmonic Frequencies for Other Basis Sets ( $\text{cm}^{-1}$ ) . . . . .	188
B.10	VPT2 Fundamental Frequencies for SCF level of theory ( $\text{cm}^{-1}$ ) . . . . .	189
B.11	Dressed VPT2 Fundamental Frequencies for SCF level of theory ( $\text{cm}^{-1}$ ) . . . . .	190
B.12	VPT2 Fundamental Frequencies for MP2 level of theory ( $\text{cm}^{-1}$ ) . . . . .	190
B.13	Dressed VPT2 Fundamental Frequencies for MP2 level of theory ( $\text{cm}^{-1}$ ) . . . . .	191
B.14	VPT2 Fundamental Frequencies for CCSD(T) level of theory ( $\text{cm}^{-1}$ ) . . . . .	191
B.15	Dressed VPT2 Fundamental Frequencies for CCSD(T) level of theory ( $\text{cm}^{-1}$ ) . . . . .	192
B.16	CCSD(T) two quantum transitions: VPT2 ( $\text{cm}^{-1}$ ) . . . . .	192

C.1	Previously reported relative energy for conformations of [10]annulene relative to conformation <b>6</b> (kcal mol <sup>-1</sup> ) . . . . .	197
C.2	Geometry of conformation <b>1a</b> ( <i>D</i> <sub>5h</sub> ) and <b>1b</b> ( <i>D</i> <sub>10h</sub> ) (Å) . . . . .	198
C.3	Geometry of conformation <b>2a</b> ( <i>C</i> <sub>s</sub> ) (Å) . . . . .	198
C.4	Geometry of conformation <b>2b</b> ( <i>C</i> <sub>2</sub> ) (Å) . . . . .	199
C.5	Geometry of conformation <b>3a</b> ( <i>C</i> <sub>2</sub> ) (Å) . . . . .	200
C.6	Geometry of conformation <b>3b</b> ( <i>C</i> <sub>1</sub> ) (Å) . . . . .	201
C.7	Geometry of conformation <b>4</b> ( <i>C</i> <sub>s</sub> ) (Å) . . . . .	203
C.8	Geometry of conformation <b>5</b> ( <i>C</i> <sub>2</sub> ) (Å) . . . . .	204
C.9	Geometry of conformation <b>6</b> ( <i>C</i> <sub>2</sub> ) (Å) . . . . .	205
C.10	Relative energies of conformations and transition states for [10]annulene (kcal mol <sup>-1</sup> ) . . . . .	207
C.11	Harmonic frequencies for conformation <b>2a</b> in cm <sup>-1</sup> . Infrared intensities in parenthesis (km mol <sup>-1</sup> ). . . . .	207
C.12	Harmonic frequencies for conformation <b>2b</b> in cm <sup>-1</sup> . Infrared intensities in parenthesis in km mol <sup>-1</sup> . . . . .	209
C.13	Harmonic frequencies for conformation <b>3a</b> in cm <sup>-1</sup> . Infrared intensities in parenthesis in km mol <sup>-1</sup> . . . . .	211
C.14	Harmonic frequencies for conformation <b>3b</b> in cm <sup>-1</sup> . Infrared intensities in parenthesis in km mol <sup>-1</sup> . . . . .	212
C.15	Harmonic frequencies for conformation <b>4</b> in cm <sup>-1</sup> . Infrared intensities in parenthesis in km mol <sup>-1</sup> . . . . .	214
C.16	Harmonic frequencies for conformation <b>5</b> in cm <sup>-1</sup> . Infrared intensities in parenthesis in km mol <sup>-1</sup> . . . . .	216
C.17	Harmonic frequencies for conformation <b>6</b> in cm <sup>-1</sup> . Infrared intensities in parenthesis in km mol <sup>-1</sup> . . . . .	217
C.18	NMR shifts for conformation <b>2b</b> in ppm. . . . .	219
C.19	NMR shifts for conformation <b>4</b> in ppm. . . . .	220
C.20	NMR shifts for conformation <b>5</b> in ppm. . . . .	220
C.21	NMR shifts for conformation <b>6</b> in ppm. . . . .	221
C.22	<sup>13</sup> C NMR shifts using CCSD(T)/qz2p for conformation <b>6</b> with vibrational correction (v.c.) and temperature correction (t.c.) determined using SCF/tzp in ppm. . . . .	221

# List of Figures

1.1	Sequential computational algorithm for MP and CC methods as outlined by Ref. [77]. Part 1: Initial unperturbed calculation. Part 2: $N$ perturbations. Part 3: Final summation. . . . .	42
2.1	General parallel scheme for calculating analytic second derivatives for MP and CC methods. Based on the sequential algorithm outlined in the previous chapter. Part 1: Initial unperturbed calculation. Part 2: $N$ perturbations, number in parenthesis. Part 3: Final summation. . . . .	46
2.2	Timing of current parallelization versus coarsed grain scheme for $C_3H_6$ CCSD(T)/cc-pVTZ. Part 1: Initial unperturbed calculation. Part 2: 24 perturbations. Part 3: Final summation. .	52
2.3	Comparison of the overall speed up of ACESII MAB Current parallelization versus the coarse grained scheme for $C_3H_6$ using CCSD(T)/ cc-pVTZ. . . . .	54
2.4	Comparison of the speed up of Part 2 using different methods: MP2, CCSD, and CCSD(T) with cc-pVTZ basis set for $C_3H_6$ . . . . .	55
2.5	Comparison of the speed up of Part 2 using different basis sets in the correlation consistent Dunning series cc-pVXZ ( $X = D, T$ and $Q$ ) which contain 52, 118 and 225 basis functions for $C_3H_2$ using CCSD(T). . . . .	56
2.6	Comparison of the speed up of Part 2 using different molecular sizes: $C_3H_2$ , $C_3H_6$ and $C_6H_5OH$ using CCSD(T)/cc-pVDZ. . .	57
2.7	Comparison of the speed up of Part 2 of the coarse grained scheme combined with the current parallelization: $SCl_2$ and $C_3H_2$ using CCSD(T)/ cc-pVQZ. . . . .	58
2.8	Comparison of the speed up of Part 2 using different point groups: $D_{2h}$ , $C_{2h}$ and $C_1$ for $CO_2$ CCSD(T)/cc-pVTZ. . . . .	60
4.1	Several historic structures of benzene: (a) Landengburg's prism, (b) Kekulé's ring and (c) Pauling's regular hexagon . . . . .	83
4.2	Infrared active two quantum transitions in the $5920\text{ cm}^{-1}$ to $6040\text{ cm}^{-1}$ region. . . . .	133
4.3	Additional infrared active mode in the $b_{2u}$ symmetry subgroup. . . . .	134

4.4	Additional infrared active mode in the $b_{3u}$ symmetry subgroup.	135
5.1	Conformation <b>1a</b> ( $D_{5h}$ ) of [10]annulene . . . . .	142
5.2	Conformation <b>1b</b> ( $D_{10h}$ ) of [10]annulene . . . . .	143
5.3	Conformation <b>2a</b> ( $C_s$ ) of [10]annulene . . . . .	144
5.4	Conformation <b>2b</b> ( $C_2$ ) of [10]annulene . . . . .	145
5.5	Conformation <b>3a</b> ( $C_2$ ) of [10]annulene . . . . .	146
5.6	Conformation <b>3b</b> ( $C_1$ ) of [10]annulene . . . . .	147
5.7	Conformation <b>4</b> of [10]annulene . . . . .	148
5.8	Conformation <b>5</b> of [10]annulene . . . . .	149
5.9	Conformation <b>6</b> of [10]annulene . . . . .	150
5.10	Infrared spectra of Conformation <b>2b</b> based on harmonic frequencies and IR intensities calculated using CCSD/DZP. . . .	155
5.11	Infrared spectra of Conformation <b>3b</b> based on harmonic frequencies and IR intensities calculated using CCSD/DZP. . . .	156
5.12	Infrared spectra of Conformation <b>4</b> based on harmonic frequencies and IR intensities calculated using CCSD/DZP. . . . .	157
5.13	Infrared spectra of Conformation <b>5</b> based on harmonic frequencies and IR intensities calculated using CCSD/DZP. . . . .	158
5.14	Infrared spectra of Conformation <b>6</b> based on harmonic frequencies and IR intensities calculated using CCSD/DZP. . . . .	159
5.15	$^{13}\text{C}$ NMR shifts relative to TMS computed using CCSD(T)/DZP at geometries optimized at the CCSD(T)/DZd level from Ref. [113]. The NMR shifts have been corrected to account for the basis set effect as described in the text. . . . .	161
5.16	$^{13}\text{C}$ NMR shifts relative to TMS computed using CCSD(T)/tzp at geometries optimized at the CCSD(T)/DZP level. . . . .	162
5.17	$^{13}\text{C}$ NMR shifts relative to TMS computed using CCSD(T)/DZP, CCSD(T)/tzp and CCSD(T)/qz2p at geometries optimized using CCSD(T)/DZP. The vibrational corrections (vc) for conformation <b>6</b> and TMS were computed using SCF/tzp and then added to the $^{13}\text{C}$ NMR shifts. . . . .	163



# Chapter 1

## An Overview of Certain Aspects of Quantum Chemistry

### 1.1 Introduction

In spite of its success in describing small systems such as a hydrogen atom and a harmonic oscillator, the equation Erwin Schrödinger [202–205] proposed cannot be solved analytically in most cases of interest to chemists. As the Hamiltonian of the system becomes more complex, approximations are made, but the results become more uncertain. For instance, the Hamiltonian of water may be written as:

$$\begin{aligned} \hat{H} = & - \sum_{i=1}^{10} \frac{\hbar}{2m_e} \nabla_i^2 - \sum_{\alpha=1}^3 \frac{\hbar}{2M_\alpha} \nabla_\alpha^2 - \sum_{i=1}^{10} \sum_{\alpha=1}^3 \frac{Z_\alpha e^2}{4\pi\epsilon_0 |\mathbf{r}_i - \mathbf{R}_\alpha|} \\ & + \sum_{i=1}^{10} \sum_{j>i}^{10} \frac{e^2}{4\pi\epsilon_0 |\mathbf{r}_i - \mathbf{r}_j|} + \sum_{\alpha=1}^3 \sum_{\beta>\alpha}^3 \frac{Z_\alpha Z_\beta e^2}{4\pi\epsilon_0 |\mathbf{R}_\alpha - \mathbf{R}_\beta|}, \end{aligned} \quad (1.1)$$

contains terms that describe the kinetic energy of the nuclei  $((\hbar/2M_\alpha)\nabla_\alpha^2)$  and electrons  $((\hbar/2m_e)\nabla_i^2)$  and the potential energy between electrons and nuclei  $(Z_\alpha e^2/4\pi\epsilon_0 |\mathbf{r}_i - \mathbf{R}_\alpha|)$ , between two electrons  $(e^2/4\pi\epsilon_0 |\mathbf{r}_i - \mathbf{r}_j|)$  and two nuclei  $(Z_\alpha Z_\beta e^2/4\pi\epsilon_0 |\mathbf{R}_\alpha - \mathbf{R}_\beta|)$ . To determine the ground state energy of water, the first approximation, the Born-Oppenheimer approximation [29], separates the motion of the nuclei from the electrons and allows the molecular wavefunction to be defined as a product of a wavefunction,  $|\Phi_n(\mathbf{q}; \mathbf{Q})\rangle$ , where the electrons

depend parametrically on the positions of the nuclei  $\mathbf{Q}$ , and a wavefunction,  $|\chi_i(\mathbf{Q})\rangle$ , describing the nuclei:

$$|\psi(\mathbf{q}, \mathbf{Q})\rangle = \sum_{i=1}^{\infty} |\chi_i(\mathbf{Q})\rangle |\Phi_i(\mathbf{q}; \mathbf{Q})\rangle, \quad (1.2)$$

where the electronic wavefunction  $|\Phi_n(\mathbf{q}; \mathbf{Q})\rangle$  satisfies:

$$\hat{H}_e |\Phi_i(\mathbf{q}; \mathbf{Q})\rangle = E_i(\mathbf{Q}) |\Phi_i(\mathbf{q}; \mathbf{Q})\rangle. \quad (1.3)$$

For water, the electronic part of the Hamiltonian,  $\hat{H}_e$ , is:

$$\begin{aligned} \hat{H}_e = & - \sum_{i=1}^{10} \frac{\hbar}{2m_e} \nabla_i^2 - \sum_{i=1}^{10} \sum_{\alpha=1}^3 \frac{Z_{\alpha} e^2}{4\pi\epsilon_0 |\mathbf{r}_i - \mathbf{R}_{\alpha}|} \\ & + \sum_{i=1}^{10} \sum_{j>i}^{10} \frac{e^2}{4\pi\epsilon_0 |\mathbf{r}_i - \mathbf{r}_j|} + \sum_{\alpha=1}^3 \sum_{\beta>\alpha}^3 \frac{Z_{\alpha} Z_{\beta} e^2}{4\pi\epsilon_0 |\mathbf{R}_{\alpha} - \mathbf{R}_{\beta}|} \end{aligned} \quad (1.4)$$

This Hamiltonian generalizes (in atomic units) to:

$$\hat{H}_e = - \sum_{i=1}^N \nabla_i^2 - \sum_{i=1}^N \sum_{\alpha=1}^M \frac{Z_{\alpha} e^2}{|\mathbf{r}_i - \mathbf{R}_{\alpha}|} + \sum_{i=1}^N \sum_{j>i}^N \frac{1}{|\mathbf{r}_i - \mathbf{r}_j|} + \sum_{\alpha=1}^M \sum_{\beta>\alpha}^M \frac{Z_{\alpha} Z_{\beta}}{|\mathbf{R}_{\alpha} - \mathbf{R}_{\beta}|} \quad (1.5)$$

for an arbitrary molecule with  $N$  electrons and  $M$  nuclei<sup>1</sup>.

## 1.2 Hartree-Fock Approximation and Self Consistent Field Method

The electron-electron interaction terms in the electronic Hamiltonian, Equation 1.5, prevent analytic solutions to Equation 1.3 for systems with more

---

<sup>1</sup> $i$  and  $j$  are indices used to identify particular electrons and  $\alpha$  and  $\beta$  are used here as indices used to identify particular nuclei.

than one electron. The first *ab initio*<sup>2</sup> method proposed independently by D. Hartree and V. Fock solved Equation 1.3 by treating these electron-electron interaction as the average field of the other electrons [59, 73, 95]. In the 1930s, J. C. Slater incorporated the Pauli Exclusion principle<sup>3</sup> and represented the electronic wavefunction as a sum of the product of spin orbitals  $|\phi_i\rangle = \phi_i(r_j; \sigma_j)$  - a function of the spin orbit,  $\sigma_j$ , and the spacial coordinate  $r_j$  of  $j$ th electron, and proposed the molecular wavefunction maybe written as a determinant [209, 210]:

$$|\Phi_0\rangle = \frac{1}{\sqrt{n!}} \begin{vmatrix} |\phi_1(1)\rangle & |\phi_2(1)\rangle & \cdots & |\phi_n(1)\rangle \\ |\phi_1(2)\rangle & |\phi_2(2)\rangle & \cdots & |\phi_n(2)\rangle \\ \vdots & \vdots & \ddots & \vdots \\ |\phi_1(n)\rangle & |\phi_2(n)\rangle & \cdots & |\phi_n(n)\rangle \end{vmatrix}. \quad (1.6)$$

The Hartree-Fock energy,  $E_{HF}$ , of the electronic Hamiltonian, Equation 1.3, for the Slater determinant is:

$$E_{HF} = \sum_i^N \langle \Phi_0 | \hat{h}_i | \Phi_0 \rangle + \sum_i^N \sum_{j>i}^N \langle \Phi_0 | \hat{J}_i - \hat{K}_i | \Phi_0 \rangle + \langle \Phi_0 | \hat{V}_{nn} | \Phi_0 \rangle, \quad (1.7)$$

where the one electron operator,  $\hat{h}_i$ , is defined by:

$$\hat{h}_i = -\frac{1}{2} \nabla_i^2 - \sum_{\alpha}^M \frac{Z_{\alpha}}{|\mathbf{R}_{\alpha} - \mathbf{r}_i|}, \quad (1.8)$$

the Coulomb operator,  $\hat{J}_i$ , is:

$$\hat{J}_i = \frac{1}{|\mathbf{r}_1 - \mathbf{r}_2|} |\phi_i(1)\rangle |\phi_j(2)\rangle, \quad (1.9)$$

---

<sup>2</sup>A Latin phrase meaning from the beginning. Here, it refers to methods which begin with first principles and rely exclusively on quantum mechanics.

<sup>3</sup>If any two electrons are exchanged in a given wavefunction, the new wavefunction must be antisymmetric to the first wavefunction.

the exchange operator,  $\hat{K}_i$  is defined by:

$$\hat{K}_i = \frac{1}{|\mathbf{r}_1 - \mathbf{r}_2|} |\phi_j(1)\rangle |\phi_i(2)\rangle, \quad (1.10)$$

where the orbitals containing the electrons have been exchanged and finally, the nuclear repulsion operator,  $\hat{V}_{nn}$ , is:

$$\hat{V}_{nn} = \sum_{\alpha}^M \sum_{\beta > \alpha}^M \frac{Z_{\alpha} Z_{\beta}}{|\mathbf{R}_{\alpha} - \mathbf{R}_{\beta}|}. \quad (1.11)$$

More simply:

$$E_{HF} = \sum_i^N \langle \Phi_0 | \hat{F}_i | \Phi_0 \rangle + \langle \Phi_0 | \hat{V}_{nn} | \Phi_0 \rangle, \quad (1.12)$$

if the one electron, Coulomb and exchange operators are combined to form the Fock operator,  $\hat{F}_i$ :

$$\hat{F}_i = \hat{h}_i + \sum_{j > i}^N (\hat{J}_j - \hat{K}_j). \quad (1.13)$$

Then, Equation 1.7 reduces to:

$$E_{HF} = \sum_i^N h_i + \sum_i^N \sum_{j > i}^N \langle ij || ij \rangle + V_{nn}, \quad (1.14)$$

where the one electron integrals determined from the expectation value of the one electron operator (Equation 1.8):

$$h_i = \langle \phi_i | \hat{h}_i | \phi_i \rangle, \quad (1.15)$$

the two electron integrals determined from the expectation value of the difference of the Coulomb and exchange operators (Equations 1.9 and 1.10):

$$\begin{aligned} \langle ij || ij \rangle &= \langle \phi_i(1) | \langle \phi_j(2) | \frac{1}{|\mathbf{r}_1 - \mathbf{r}_2|} | \phi_i(1) \rangle | \phi_j(2) \rangle \\ &\quad - \langle \phi_i(1) | \langle \phi_j(2) | \frac{1}{|\mathbf{r}_1 - \mathbf{r}_2|} | \phi_j(1) \rangle | \phi_i(2) \rangle, \end{aligned} \quad (1.16)$$

and the nuclear repulsion energy:

$$V_{nn} = \sum_{\alpha}^M \sum_{\beta > \alpha}^M \frac{Z_{\alpha} Z_{\beta}}{|\mathbf{R}_{\alpha} - \mathbf{R}_{\beta}|}. \quad (1.17)$$

To determine the electronic energy,  $E_{HF}$ , Lagrange undetermined multipliers were used by C. C. J. Roothan [193] and G. G. Hall [86] to minimize the energy subject to the constraint  $\langle \Phi_0 | \Phi_0 \rangle - 1 = 0$  (i.e. the normalization of the wavefunction  $|\Phi_0\rangle$ )<sup>4</sup>:

$$L = E_{HF} - \sum_{i,j} \lambda_{ij} (\langle \phi_i | \phi_j \rangle - \delta_{ij}). \quad (1.18)$$

Optimizing  $L$  leads to<sup>5</sup>:

$$\delta L = \delta E_{HF} - \sum_{i,j} \lambda_{ij} (\langle \delta \phi_i | \phi_j \rangle + \langle \phi_i | \delta \phi_j \rangle) = 0, \quad (1.19)$$

where,

$$\delta E_{HF} = \sum_i (\langle \delta \phi_i | \hat{F}_i | \phi_i \rangle + \langle \phi_i | \hat{F}_i | \delta \phi_i \rangle). \quad (1.20)$$

Equation 1.19 may be rearranged to form:

$$\begin{aligned} \delta L &= \sum_i (\langle \delta \phi_i | \hat{F}_i | \phi_i \rangle + \langle \phi_i | \hat{F}_i | \delta \phi_i \rangle) - \sum_{i,j} \lambda_{ij} (\langle \delta \phi_i | \phi_j \rangle + \langle \phi_i | \delta \phi_j \rangle) \\ &= \sum_i \langle \delta \phi_i | \hat{F}_i | \phi_i \rangle - \sum_{i,j} \lambda_{ij} \langle \delta \phi_i | \phi_j \rangle + \text{complex conjugate} \\ &= 0. \end{aligned} \quad (1.21)$$

---

<sup>4</sup>This derivation mirrors what C. C. J. Roothaan and G. G. Hall published independently in 1951 [86, 193], and follows the derivation presented by in reference [103].

<sup>5</sup>Lagrange multipliers are a mathematical method of optimizing a function  $f$  subject to the constraints of an additional function  $g$ . The Lagrange functions  $L$  is typically the difference between the function to be optimized  $f$  and the product of the constraint  $g$  and a constant  $\lambda$ .

For an arbitrary  $\delta\phi_i$ , Equation 1.21 reduces to:

$$\hat{F}_i|\phi_i\rangle = \sum_j \lambda_{ij}|\phi_j\rangle. \quad (1.22)$$

A unitary transformation of  $|\phi_i\rangle$  such that  $\lambda_{ij} = 0$  for  $i \neq j$  and  $\lambda_{ii} = \epsilon_i$  simplifies Equation 1.22 to:

$$\hat{F}_i|\phi_i\rangle = \epsilon_i|\phi_i\rangle. \quad (1.23)$$

If each molecular orbital  $|\phi_i\rangle$  is approximated by a linear combination of atomic orbitals (AO)  $|\chi_\nu\rangle$  scaled by a set of coefficients,  $c_{\nu i}$ , to be determined, i.e.:

$$|\phi_i\rangle = \sum_{\nu}^{N_{AO}} c_{\nu i}|\chi_\nu\rangle, \quad (1.24)$$

then Equation 1.23 becomes:

$$\hat{F}_i \sum_{\nu}^{N_{AO}} c_{\nu i}|\chi_\nu\rangle = \epsilon_i \sum_{\nu}^{N_{AO}} c_{\nu i}|\chi_\nu\rangle. \quad (1.25)$$

The expectation value with respect to  $\langle\chi_\mu|$  simplifies Equation 1.25 to the Roothaan-Hall equations [86, 193]:

$$\sum_{\nu}^{N_{AO}} (F_{\mu\nu} - \epsilon_i S_{\mu\nu}) c_{\nu i} = 0, \quad (1.26)$$

These equations may also be expressed in matrix form as:

$$\mathbf{FC} = \mathbf{SC}\epsilon, \quad (1.27)$$

where  $\mathbf{S}$ , the overlap matrix, has elements:

$$S_{\mu\nu} = \langle\chi_\mu|\chi_\nu\rangle \quad (1.28)$$

$\mathbf{F}$  is the Fock matrix whose elements are:

$$\begin{aligned}
F_{\mu\nu} &= \langle \chi_\mu | \hat{F} | \chi_\nu \rangle \\
&= \langle \chi_\mu | \hat{h} | \chi_\nu \rangle + \sum_i^N \langle \chi_\mu | \hat{J}_i - \hat{K}_i | \chi_\nu \rangle \\
&= h_{\mu\nu} + \sum_\rho^{N_{AO}} \sum_\sigma^{N_{AO}} D_{\rho\sigma} \langle \chi_\mu \chi_\rho | | \chi_\nu \chi_\sigma \rangle,
\end{aligned} \tag{1.29}$$

The vector  $\boldsymbol{\epsilon}$  contains the set of Lagrange multipliers or eigenvalues to be determined by solving Equation 1.26 and  $\mathbf{C}$ , is the matrix of coefficients that solves the same equation<sup>6</sup>.  $D_{\rho\sigma}$  is the  $\rho\sigma$  element of the density matrix and is defined by the set of coefficients of the orbitals occupied by an electron, i.e.:

$$D_{\rho\sigma} = \sum_i^N c_{\rho i}^* c_{\sigma i}. \tag{1.30}$$

The Hartree-Fock energy, Equation 1.14, may now be expressed as:

$$E_{HF} = \sum_{\mu\nu} D_{\mu\nu} h_{\mu\nu} + \frac{1}{2} \sum_{\mu\nu\rho\sigma} D_{\mu\nu} D_{\rho\sigma} \langle \chi_\mu \chi_\rho | | \chi_\nu \chi_\sigma \rangle + V_{nn} \tag{1.31}$$

where the one electron AO integrals,  $h_{\mu\nu}$ , are:

$$h_{\mu\nu} = \langle \chi_\mu | \hat{h}_\nu | \chi_\nu \rangle \tag{1.32}$$

and the two electron AO intergals,  $\langle \chi_\mu \chi_\rho | | \chi_\nu \chi_\sigma \rangle$ , are:

$$\begin{aligned}
\langle \chi_\mu \chi_\rho | | \chi_\nu \chi_\sigma \rangle &= \langle \chi_\mu(1) \chi_\rho(2) | \frac{1}{|\mathbf{r}_1 - \mathbf{r}_2|} | \chi_\nu(1) \chi_\sigma(2) \rangle \\
&\quad - \langle \chi_\mu(1) \chi_\rho(2) | \frac{1}{|\mathbf{r}_1 - \mathbf{r}_2|} | \chi_\sigma(1) \chi_\nu(2) \rangle.
\end{aligned} \tag{1.33}$$

---

<sup>6</sup>The operators  $\hat{J}_i$  and  $\hat{K}_i$  each contain the molecular orbitals  $|\phi_i\rangle$  which yields a sum of the products of the coefficients,  $c_{\rho i} c_{\sigma i}$ , and is expressed more compactly as the density matrix element  $D_{\rho\sigma}$ .

To obtain a set of coefficients needed for the calculation of  $E_{HF}$ , Equation 1.27 is typically solved iteratively as described in the literature [5, 86, 103, 193] until  $\mathbf{C}^{(n)} - \mathbf{C}^{(n-1)}$  is below the specified tolerance. The set of coefficients that results represents a self consistent field in Equation 1.27 and the energy computed is also referred in the literature as SCF energy ( $E_{SCF}$ ).

Before concluding this section note that the spin orbitals  $|\phi_i\rangle$  contain both a spacial function and an orthonormal spin function -  $\alpha$  and  $\beta$ . Under the Hartree-Fock approximation spin orbitals may be restricted (RHF), such that each spacial function corresponds to two electrons - one with spin  $\alpha$  and the other spin  $\beta$ :

$$\Phi_{RHF} = \frac{1}{\sqrt{(n)!}} \begin{vmatrix} |\phi_1(1)\alpha\rangle & |\phi_1(1)\beta\rangle & \cdots \\ |\phi_1(2)\alpha\rangle & |\phi_1(2)\beta\rangle & \cdots \\ \vdots & \vdots & \ddots \end{vmatrix} \quad (1.34)$$

or unrestricted (UHF), such that there are no restrictions to the spacial functions:

$$\Phi_{UHF} = \frac{1}{\sqrt{(2n)!}} \begin{vmatrix} |\phi_1(1)\alpha\rangle & |\phi_1(1)\beta\rangle & \cdots \\ |\phi_2(2)\alpha\rangle & |\phi_2(2)\beta\rangle & \cdots \\ \vdots & \vdots & \ddots \end{vmatrix} \quad (1.35)$$

The molecules examined in subsequent chapters have even numbers of electrons (close shell) and their molecular electronic wavefunction will be defined using restricted Hartree-Fock (RHF) spin orbits as the reference wavefunction. Thus, no additional reference to UHF will be needed.

### 1.3 Electron-Correlation Methods

The Hartree-Fock energy is above the expected electronic ground state energy. The electrons in atoms and molecules move with respect to each other



to lower their repulsion energy and do not experience an average field. This energy difference (or electron correlation) has two components: “static” and “dynamic”. The static correlation corresponds to the interactions between a pair of electrons in the same orbital while dynamical correlation results from the Coulomb repulsion between pairs of electrons in different spin orbitals.

Two approaches are used for computing correlation energy. The first (or dynamic) approach begins with a single reference wavefunction (often the HF determinate) and introduces excited states from this reference to account for the dynamic correlation. Alternatively, in the second approach, the initial wavefunction is augmented by additional wavefunctions to account for static correlation before accounting for dynamical correlation if desired [16].

The *ab initio* methods used in this study, MP2, CCSD and CCSD(T), account for the correlation energy using the dynamical approach and the theory behind them will be outlined in this section<sup>7</sup>.

### 1.3.1 Second-Order Many-Body Perturbation Theory

Using Lord Rayleigh’s method, Erwin Schrödinger suggested that any Hamiltonian,  $\hat{H}$ , may be divided into two parts - a zero order reference Hamiltonian and a perturbation,  $\hat{H}_1$ :

$$\hat{H} = \hat{H}_0 + \lambda\hat{H}_1. \tag{1.36}$$

---

<sup>7</sup>Other methods such as configuration interaction (CI) and density functional theory (DFT) are also used to account for the dynamic correlation, but have not been included here. For a detailed explanation of DFT and CI methods, the reader is referred to Frank Jensen’s *Introduction to Computational Chemistry* Chapter 6 and Sections 4.2 to 4.7, respectively [103]. I will forgo discussing DFT and CI methods in favor of MBPT and CC methods used in this study. Some of the multireference methods used to account for static correlation are also included. Reference [16] has additional references and discussion of the multireference approaches.

In practice,  $\lambda$  is the perturbation parameter which takes on values between 0 and 1. The reference Hamiltonian,  $\hat{H}_0$ , is chosen such that a fully defined set of wavefunctions  $\{\varphi_n^{(0)}\}$  and eigenvalues  $E_n^{(0)}$  exist. The Schrödinger equation:

$$\hat{H}|\psi_n\rangle = E_n|\psi_n\rangle, \quad (1.37)$$

now writes as:

$$(\hat{H}_0 + \lambda\hat{H}_1)|\psi_n\rangle = E_n|\psi_n\rangle, \quad (1.38)$$

and the energy,  $E_n$ , and the wavefunction,  $|\psi_n\rangle$  may then be written in terms of a perturbation parameter,  $\lambda$ :

$$E_n = E_n^{(0)} + \lambda E_n^{(1)} + \lambda^2 E_n^{(2)} + \lambda^3 E_n^{(3)} + \dots \quad (1.39)$$

and

$$|\psi_n\rangle = |\varphi_n^{(0)}\rangle + \lambda|\varphi_n^{(1)}\rangle + \lambda^2|\varphi_n^{(2)}\rangle + \lambda^3|\varphi_n^{(3)}\rangle + \dots \quad (1.40)$$

Inserting Equations 1.39 and 1.40 into Equation 1.38 and after following a series of manipulations leads to expressions for each correction to the energy<sup>8</sup>,  $E_n^{(i)}$ , and wavefunction,  $|\varphi_n^{(i)}\rangle$ . The reference energy,  $E_n^{(0)}$ , and first two corrections to the energy are listed below in terms of the zero order or reference wavefunction:

$$E_n^{(0)} = \langle\varphi_n^{(0)}|\hat{H}_0|\varphi_n^{(0)}\rangle, \quad (1.41)$$

$$E_n^{(1)} = \langle\varphi_n^{(0)}|\hat{H}_1|\varphi_n^{(0)}\rangle, \quad (1.42)$$

and

$$E_n^{(2)} = \sum_{n \neq k} \frac{\langle\varphi_n^{(0)}|\hat{H}_1|\varphi_k^{(0)}\rangle\langle\varphi_k^{(0)}|\hat{H}_1|\varphi_n^{(0)}\rangle}{E_n^{(0)} - E_k^{(0)}}. \quad (1.43)$$

---

<sup>8</sup>The superscripts in Equations 1.39 and 1.40 represent the order of the correction to the reference energy and wavefunction.

To apply perturbation theory to atoms and molecules, C. Møller and M. S. Plesset [145] suggested in 1934 that the Hamiltonian could be divided as follows:

$$\hat{H}_0 = \sum_{i=1}^N (\hat{h}_i + \sum_{j=1}^N (\hat{J}_{ij} - \hat{K}_{ij})) + \hat{V}_{nn} \quad (1.44)$$

and

$$\hat{H}_1 = \sum_{i=1}^N \sum_{j>i}^N \frac{1}{|\mathbf{r}_i - \mathbf{r}_j|} - \sum_{i=1}^N \sum_{j=1}^N (\hat{J}_{ij} - \hat{K}_{ij}) \quad (1.45)$$

Here, the reference Hamiltonian,  $\hat{H}_0$ , corresponds to the Fock operator, note the sum includes the electron-electron repulsion energy. Subsequently, the perturbation corresponds to the difference between the original Hamiltonian and the reference. When they used a Slater determinant,  $|\Phi_0\rangle$ , as the reference wavefunction for the zero order Hamiltonian, the first two energy terms become:

$$E^{(0)} = \sum_{i=1}^N h_i + \sum_{i=1}^N \sum_{j=1}^N \langle ij || ij \rangle + V_{nn} \quad (1.46)$$

and

$$E^{(1)} = \sum_{i=1}^N \sum_{j>i}^N \langle ij || ij \rangle. \quad (1.47)$$

However, combining Equations 1.46 and 1.47 only yield the HF energy obtained given in Equation 1.14.

For higher order corrections to the energy, i.e.  $E^{(2)}$ ,  $E^{(3)}$ , ..., wavefunctions, are now defined by Slater determinants where one or more electrons are promoted from occupied orbitals ( $N_{occ}$ )  $\phi_i$ ,  $\phi_j$ ,  $\phi_k$ , ..., to unoccupied orbitals ( $N_{vir}$ ),  $\phi_a$ ,  $\phi_b$ ,  $\phi_c$ , ... . These wavefunctions are in general denoted as  $|\Phi_{ijk...}^{abc...}\rangle$ <sup>9</sup>. For example, the second-order correction,  $E^{(2)}$  or  $E_{MP2}$ , utilizes doubly

---

<sup>9</sup>From this point forward,  $i, j, \dots, n$  will denote occupied molecular orbitals (MO) ( $\phi$ ),

excited Slater determinants  $|\Phi_{ij}^{ab}\rangle^{10}$  as a basis:

$$E_{MP2} = \sum_{j>i}^{N_{occ}} \sum_{b>a}^{N_{vir}} \frac{\langle \Phi_0 | \hat{H}_1 | \Phi_{ij}^{ab} \rangle \langle \Phi_{ij}^{ab} | \hat{H}_1 | \Phi_0 \rangle}{E^{(0)} - E_{ij}^{ab}}. \quad (1.48)$$

Equation 1.48 simplifies to:

$$E_{MP2} = \sum_{j>i}^{N_{occ}} \sum_{b>a}^{N_{vir}} \langle ij || ab \rangle t_{ij}^{ab} \quad (1.49)$$

where:

$$t_{ij}^{ab} = \frac{\langle ij || ab \rangle}{f_{ii} + f_{jj} - f_{aa} - f_{bb}}, \quad (1.50)$$

and  $f_{pp}$  are the diagonal elements of Fock matrix in the MO basis:

$$f_{ii} = h_i + \langle im || im \rangle \quad (1.51)$$

and

$$f_{aa} = h_a + \langle ae || ae \rangle \quad (1.52)$$

for occupied and virtual orbitals, respectively.

### 1.3.2 Coupled-Cluster Theory

As illustrated above, MP2 computes the correlation energy from double excitations of electrons of a given reference wavefunction (generally, the occupied orbitals of the Slater Determinant obtained by the HF approximation) to virtual orbitals. Higher orders of many-body perturbation theory include more

---

$a, b, \dots, f$  will denote unoccupied or virtual MO orbitals, and  $p, q, r$  and  $s$  will denote arbitrary MO orbitals. Greek letters  $\mu, \nu, \rho$  and  $\sigma$  will be used to denote AO orbitals ( $\chi$ ). Also, Einstein summation notation will be used where  $e$  and  $f$  imply summation over  $N_{vir}$  virtual orbitals and  $m$  and  $n$  imply summation over  $N_{occ}$  occupied orbitals.

<sup>10</sup>The doubly excited Slater determinant is chosen as a basis since the Hamiltonian is a two electron operator and the singly excited determinant  $\langle \Phi_0 | \hat{H}_1 | \Phi_i^a \rangle = 0$ .

such excitations: single, triple, quadruple, etc. To include all these excitations to infinite order, Čížek and Paldus [50–52] proposed an ansatz:

$$|\Psi\rangle = e^{\hat{T}}|\Phi_0\rangle, \quad (1.53)$$

where  $\hat{T}$  is the cluster operator defined as  $\hat{T} = \hat{T}_1 + \hat{T}_2 + \hat{T}_3 + \dots$  whose components ( $\hat{T}_1, \hat{T}_2, \dots$ ) promote electrons from occupied orbitals to virtual orbitals as follows

$$\begin{aligned} \hat{T}_1|\Phi_0\rangle &= \sum_i \sum_a t_i^a |\Phi_i^a\rangle \\ \hat{T}_2|\Phi_0\rangle &= \sum_{j>i} \sum_{b>a} t_{ij}^{ab} |\Phi_{ij}^{ab}\rangle \\ &\vdots \end{aligned} \quad (1.54)$$

where  $t_i^a$  and  $t_{ij}^{ab}$  are the coupled cluster or  $T$  amplitudes and correspond to the weight of each excited state. By expanding  $e^{\hat{T}}$ , the new wavefunction becomes:

$$\begin{aligned} |\Psi\rangle &= (1 + \hat{T}_1 + \frac{1}{2}\hat{T}_1^2 + \hat{T}_2 + \frac{1}{6}\hat{T}_1^3 + \hat{T}_2\hat{T}_1 + \hat{T}_3 + \frac{1}{24}\hat{T}_1^4 \\ &\quad + \frac{1}{2}\hat{T}_2\hat{T}_1^2 + \hat{T}_3\hat{T}_1 + \hat{T}_4 + \dots)|\Phi_0\rangle. \end{aligned} \quad (1.55)$$

The energy,  $E$ , found from the expectation value of the Schrödinger equation:

$$\hat{H}e^{\hat{T}}|\Phi_0\rangle = Ee^{\hat{T}}|\Phi_0\rangle \quad (1.56)$$

with respect to  $\langle\Phi_0|$ , is:

$$\begin{aligned} \langle\Phi_0|\hat{H}e^{\hat{T}}|\Phi_0\rangle &= E\langle\Phi_0|e^{\hat{T}}|\Phi_0\rangle \\ &= E\langle\Phi_0|(1 + \hat{T} + \frac{1}{2}\hat{T}^2 + \dots)|\Phi_0\rangle \\ &= E. \end{aligned} \quad (1.57)$$

The right hand side of Equation 1.57 reduces to  $E$  since the excited wavefunctions are orthogonal to the reference wavefunction (i.e.  $\langle\Phi_0|\Phi_{ij\dots}^{ab\dots}\rangle = 0$ ).

The left hand side of Equation 1.57 also may be reduced. Since the electronic Hamiltonian is a two electron operator, only the second-order terms,  $\hat{T}_1^2$  and  $\hat{T}_2$  do not vanish. Thus, the energy:

$$\begin{aligned}
E &= \langle \Phi_0 | \hat{H} (1 + \hat{T}_1 + \hat{T}_2 + \frac{1}{2} \hat{T}_2^2) | \Phi_0 \rangle \\
&= E_{HF} + \sum_{j>i} \sum_{b>a} (t_{ij}^{ab} + t_i^a t_j^b - t_i^b t_j^a) \langle \Phi_0 | \hat{H} | \Phi_{ij}^{ab} \rangle \\
&= E_{HF} + \sum_{j>i} \sum_{b>a} (t_{ij}^{ab} + t_i^a t_j^b - t_i^b t_j^a) (\langle ij || ab \rangle).
\end{aligned} \tag{1.58}$$

correction corresponds to the single and double excitations ( $t_i^a$  and  $t_{ij}^{ab}$ )<sup>11</sup>.

### 1.3.2.1 Coupled-Cluster Singles and Doubles (CCSD)

To compute  $t_i^a$  and  $t_{ij}^{ab}$  needed in Equation 1.58, the cluster operator may be truncated to include only singles and doubles:  $\hat{T} \equiv \hat{T}_1 + \hat{T}_2$ . The  $T$  amplitudes needed to compute this energy are then determined by<sup>12</sup>:

$$\langle \Phi_i^a | e^{-\hat{T}} \hat{H} e^{\hat{T}} | \Phi_0 \rangle = 0 \tag{1.59}$$

and

$$\langle \Phi_{ij}^{ab} | e^{-\hat{T}} \hat{H} e^{\hat{T}} | \Phi_0 \rangle = 0. \tag{1.60}$$

---

<sup>11</sup>The effect of higher order excitations ( $t_{ijk}^{abc}, \dots$ ) are included in the determination of  $t_i^a$  and  $t_{ij}^{ab}$ .

<sup>12</sup>The operators  $e^{-\hat{T}} \hat{H} e^{\hat{T}}$  in Equations 1.59 and 1.60 can be represented by the effective Hamiltonian  $\bar{H}$ . The effect of higher order excitations ( $t_{ijk\dots}^{abc\dots}$ ) are included by solving the additional equations:  $\langle \Phi_{ijk\dots}^{abc\dots} | \bar{H} | \Phi_0 \rangle = 0$ . Although  $t_{ijk\dots}^{abc\dots}$  are not included explicitly in Equation 1.58, they have an effect on  $t_i^a$  and  $t_{ij}^{ab}$  which can be sizable and will be discussed in the next section.

Using Equations 1.59 and 1.60, equations for  $t_i^a$  and  $t_{ij}^{ab}$  result in [56, 78, 81, 211]<sup>13</sup>:

$$0 = f_{ai} + \tilde{\mathcal{F}}_{ae} t_i^a - t_m^a \tilde{\mathcal{F}}_{mi} + \tilde{\mathcal{F}}_{me} t_{im}^{ae} + t_m^e \langle am || ie \rangle - \frac{1}{2} t_{mn}^{ae} \langle mn || ie \rangle + \frac{1}{2} \langle am || ef \rangle t_{im}^{ef} \quad (1.61)$$

and

$$\begin{aligned} 0 = & \langle ab || ij \rangle + P_-(ab) t_{ij}^{ae} \left\{ \tilde{\mathcal{F}}_{be} - \frac{1}{2} t_m^b \tilde{\mathcal{F}}_{me} \right\} - P_-(ij) t_{im}^{ab} \left\{ \tilde{\mathcal{F}}_{mj} + \frac{1}{2} t_j^e \tilde{\mathcal{F}}_{me} \right\} \\ & + \frac{1}{2} \tau_{mn}^{ab} \tilde{\mathcal{W}}_{mni} + \frac{1}{2} \tilde{\mathcal{W}}_{abef} \tau_{ij}^{ef} + P_-(ij) P_-(ab) \left\{ t_{im}^{ae} \tilde{\mathcal{W}}_{mbej} - t_i^e t_m^a \langle mb || ej \rangle \right\} \\ & + P_-(ij) \langle ab || ej \rangle t_i^e - P_-(ab) t_m^a \langle mb || ij \rangle. \end{aligned} \quad (1.62)$$

Expressions for one-particle intermediates,  $\tilde{\mathcal{F}}_{pq}$ , two-particle intermediates and  $\tilde{\mathcal{W}}_{pqrs}$  are included in Reference [78].  $f_{pq}$  are elements of the Fock matrix in MO basis (See Equation 1.51 for an example) and  $P_-(pq)$  is a permutation operator:  $P_-(pq)g(p, q) = g(p, q) - g(q, p)$ .

An alternative description of coupled-cluster in terms of creation ( $\hat{a}_p^\dagger$ ) and annihilation operators ( $\hat{a}_q$ ) and the one electron  $f_{pq}$  and two electron  $\langle pq || rs \rangle$  operators is given by the second quantization [56]:

$$\begin{aligned} \hat{H}_{cc} = & \sum_{p,q} (\hat{h}_{pq} + \sum_i \langle pi || qi \rangle) \{ \hat{a}_p^\dagger \hat{a}_q \} + \frac{1}{4} \sum_{p,q,r,s} \langle pq || rs \rangle \{ \hat{a}_p^\dagger \hat{a}_q^\dagger \hat{a}_r \hat{a}_s \} \\ = & \sum_{p,q} f_{pq} \{ \hat{a}_p^\dagger \hat{a}_q \} + \frac{1}{4} \sum_{p,q,r,s} \langle pq || rs \rangle \{ \hat{a}_p^\dagger \hat{a}_q^\dagger \hat{a}_r \hat{a}_s \} \end{aligned} \quad (1.63)$$

Here, the excited state  $|\Phi_i^a\rangle$  from an arbitrary Slater determinant ground state  $|\Phi_0\rangle$  or  $|\chi_1 \dots \chi_i \dots \chi_N\rangle$  is created by removing the  $i$ th state:

$$\hat{a}_i |\chi_1 \dots \chi_i \dots \chi_N\rangle = |\chi_1 \chi_N\rangle, \quad (1.64)$$

---

<sup>13</sup>For a thorough derivation of these amplitude equations, the reader is referred to T. Daniel Crawford and Henry F. Schaefer, III's *An Introduction to Coupled Cluster Theory for Computational Chemists* [56].

then inserting the  $a$ th state in its place:

$$\hat{a}_a^\dagger |\chi_1 \dots \chi_N\rangle = |\chi_1 \dots \chi_a \dots \chi_N\rangle. \quad (1.65)$$

In this description, the one particle intermediates correspond to  $\hat{f}\{\hat{a}_p^\dagger \hat{a}_q\}$  and the two particle intermediates correspond to  $\langle ab || ij \rangle \{\hat{a}_p^\dagger \hat{a}_q^\dagger \hat{a}_r \hat{a}_s\}$ . The Schrödinger equation becomes:

$$\hat{H}_{cc}|\Phi\rangle = E_{cc}|\Phi\rangle \quad (1.66)$$

and considering  $|\Phi\rangle = e^{\hat{T}}|\Phi_0\rangle$

$$\underbrace{e^{-\hat{T}} \hat{H}_{cc} e^{\hat{T}}}_{\bar{H}} |\Phi_0\rangle = E_{cc} |\Phi_0\rangle \quad (1.67)$$

where  $\bar{H}$  is the effective coupled cluster Hamiltonian.

To numerically solve for  $t_i^a$  and  $t_{ij}^{ab}$ , Equations 1.61 and 1.62 may be written as:

$$D_i^a t_i^a = f_{ai} + \sum_c (1 - \delta_{ca}) f_{ac} t_i^c - \sum_k (1 - \delta_{ik}) f_{ik} t_k^a + \dots \quad (1.68)$$

and

$$D_{ij}^{ab} t_{ij}^{ab} = \langle ab || ij \rangle + P(ab) \sum_c (1 - \delta_{bc}) f_{bc} t_{ij}^{ac} - P(ij) \sum_k (1 - \delta_{kj}) f_{kj} t_{ik}^{ab} + \dots \quad (1.69)$$

where  $D_i^a \equiv f_{ii} - f_{aa}$  and  $D_{ij}^{ab} \equiv f_{ii} + f_{jj} - f_{aa} - f_{bb}$ . Then,  $t_i^a = f_{ai}/D_i^a$  and  $t_{ij}^{ab} = \langle ab || ij \rangle / D_{ij}^{ab}$  can be used as initial guesses, and Equations 1.68 and 1.69 are used to determine new values for  $t_i^a$  and  $t_{ij}^{ab}$ . This iterative process is repeated until  $t_i^a$  and  $t_{ij}^{ab}$  converge. Non-iterative approaches can also be used and will be described in the next section.



### 1.3.2.2 Non-iterative Triples Correction (CCSD(T))

It has been shown that the CCSD approximation, described in the previous section, does not satisfactorily predict molecular properties<sup>14</sup>. These cases suggest that more terms of the cluster operator,  $\hat{T}$ , are needed to improve the agreement of coupled-cluster predictions with experimental observations. A perturbative approach to the contribution of triples<sup>15</sup>,  $\hat{T}_3$ , has improved the agreement between theory and experiment<sup>16</sup>. To determine this correction from triples to the CCSD energy, the following correction can be computed:

$$E_{CCSD(T)} = \frac{1}{36} \sum_{ijk} \sum_{abc} t_{ijk}^{abc} D_{ijk}^{abc} \left\{ t_{ijk}^{abc} + \tilde{t}_{ijk}^{abc} \right\}, \quad (1.70)$$

where the connected triples<sup>17</sup>,  $t_{ijk}^{abc}$ , are defined by:

$$t_{ijk}^{abc} = P(ijk)P(abc) \frac{t_{ij}^{ae} \langle bc || ek \rangle - t_{im}^{ab} \langle mc || jk \rangle}{f_{ii} + f_{jj} + f_{kk} - f_{aa} - f_{bb} - f_{cc}}, \quad (1.71)$$

the disconnected triples<sup>18</sup>,  $\tilde{t}_{ijk}^{abc}$ , write as:

$$\tilde{t}_{ijk}^{abc} = P(ijk)P(abc) \frac{t_i^a \langle bc || jk \rangle}{f_{ii} + f_{jj} + f_{kk} - f_{aa} - f_{bb} - f_{cc}} \quad (1.72)$$

and

$$D_{ijk}^{abc} = f_{ii} + f_{jj} + f_{kk} - f_{aa} - f_{bb} - f_{cc}. \quad (1.73)$$

The permutator  $P(q/qr)$  in Equations 1.71 and 1.72 corresponds to:

$$P(pqr)g(p, q, r) = g(p, q, r) + g(q, p, r) + g(r, q, p). \quad (1.74)$$

---

<sup>14</sup>Several of these cases have been discussed in References [119] and [103].

<sup>15</sup> $\hat{T}_3$  is connected to fourth-order perturbation theory as discussed in Reference [56]. This connection was used originally by K. Raghavachari *et al.* [182] to derive Equation 1.70.

<sup>16</sup>CCSD(T) has been compared extensively to other methods. These comparisons can be found in References [119], [103] and [217] and the references therein.

<sup>17</sup>Due to the fourth-order energy correction of the perturbative triples correction.

<sup>18</sup>Due to the fifth-order energy correction of the perturbative triples correction.

## 1.4 Basis Sets

The methods described in the previous sections require a set of basis functions,  $|\chi\rangle$  of Equation 1.24. A hydrogen atom may be represented by a Slater-type wavefunction consisting of an angular component,  $Y_{l,m}(\theta, \phi)$  and a radial component:

$$R_{nl}(r) = N_{nl} r^l e^{-r/n} L_{2l+1, n+l} \left( \frac{2r}{n} \right) \quad (1.75)$$

where  $L_{2l+1, n+l}$  is an associated Laguerre polynomial. However, it has been difficult and expensive to extend these types of orbitals beyond diatomics. For polyatomic molecules,  $e^{-r/n}$  is replaced by a Gaussian function  $e^{-\zeta r^2}$ :

$$\chi_{n,l,m} = N Y_{l,m}(\theta, \phi) \underbrace{r^{(2n-2-l)} e^{-\zeta r^2}}_{R_{n,l}(r)} \quad (1.76)$$

or in Cartesian terms:

$$\chi_{l_x, l_y, l_z} = N x^{l_x} y^{l_y} z^{l_z} e^{-(x^2+y^2+z^2)} \quad (1.77)$$

where  $l_x + l_y + l_z = l$  to form Gaussian types of orbitals (GTO). The parameter,  $\zeta$ , of these orbitals may then be optimized so that the energy corresponds to the total energy of a particular atom for a type of calculation.

An optimization of  $\zeta$  by S. Huzinaga using Hartree-Fock to compute atomic energies led to a set of GTO consisting of nine  $s$  ( $l = 0$ ) and five  $p$  functions  $9s5p$  for C, N, O, etc and four  $s$  functions for H [101]. Subsequently, T. H. Dunning contracted these functions (primitive Gaussian type orbitals or  $\chi^{PGTO}$ ) by:

$$\chi^{CGTO} = \sum_i c_i \chi^{PGTO}, \quad (1.78)$$

into sets of  $4s2p$  contracted Gaussian type orbitals or  $\chi^{CGTO}$  for C, N, O, etc and  $2s$  for H to form the double-zeta (DZ) basis sets [61] as seen in Table 1.1. Larger basis sets such as triple-zeta (TZ) and quadruple-zeta (QZ) add additional PGTO that are then contracted [62, 101]. To achieve the same level of convergence for correlated calculation, these basis sets are augmented with one or two polarization functions. DZP for example, add  $1d$  function to row one elements and  $1p$  function to hydrogen atoms while TZ2P contracts  $3d$  to  $2d$  for row one elements and  $3p$  to  $2d$  for hydrogen.

The development and implementation of correlation methods such as MP2 prompted a search for new basis sets which include  $f$  and  $g$  functions and provided better agreement with experiment [208]. One such basis set (Atomic Natural Orbitals or ANO) proposed by J. Almlöf and P. R. Taylor [6, 7] combine a set of primitive GTO consisting of thirteen  $s$  and eight  $p$  functions for first row elements from a number of sources with a set of six  $d$ , four  $f$  and two  $g$  polarization functions optimized for correlated methods and  $8s6p4d3f$  for hydrogen. These primitive orbitals are contracted to  $3s2p1d/2s1p$  (ANO0),  $4s3p2d1f/4s2p1d$  (ANO1) and  $5s4p3d2f1g/4s3p2d1f$  (ANO2) depending on the size of the basis set desired (see Table 1.1). The contraction coefficients are obtained by diagonalization of the unrelaxed density matrix of the atoms at the CISD level of theory with core electrons frozen. For calculations including electron-correlation, the core electrons are generally excluded from the correlation treatment (i.e. frozen core which will be denoted as ANOn(fc)).

The success of ANO basis sets prompted Dunning to optimise a smaller set of orbitals [63]. Reducing the number of primitives compared to ANO and including polarization functions ( $d$ ,  $f$ ,  $g$ , etc) as seen in Table 1.1, the set of correlation consistent basis sets accounts for 99% of the correlation energy

ANO basis sets. These basis sets designated as correlation consistent polarized valence double/triple/quadruple zeta or cc-pVXZ where  $X = D, T, Q$ , etc and correspond to the double-zeta, triple-zeta, and quadruple-zeta basis sets developed earlier. However, studies of the harmonic and fundamental frequencies of acetylene [133] and benzene [133] found them unsuited for bending frequencies when compared to ANO basis sets<sup>19</sup>.

Alternative basis sets dz, tz and qz proposed by A. Schäfer, H. Horn and R. Ahlrichs [197] analytically optimized both the exponents ( $\zeta$ ) and contraction coefficients at the HF level of theory. These basis sets contain fewer GTO in comparison to DZ as seen in Table 1.1; however, previous experience found them well suited for calculations of NMR chemical shifts when polarization functions are included [11, 75, 171]. Although there exists other basis sets, for example: the Pople basis sets (3-21G, 4-31G, 6-31G, etc) – see References [103, 217] for more details, only the basis sets used in this research are mentioned in detail.

For magnetic properties such as NMR, the AO basis functions described above are altered to include a local gauge:

$$|\chi_\mu(\mathbf{B})\rangle = \exp\left(-\frac{i}{2}(\mathbf{B} \times (\mathbf{R}_\mu - \mathbf{R}_0))\mathbf{r}\right) |\chi_\mu\rangle \quad (1.79)$$

to account for the magnetic field in the molecular Hamiltonian [80, 229].

---

<sup>19</sup>These correlation consistent basis functions may be augmented by adding more tight functions to the description of the core-correlation (cc-pCVNZ) or additional uncontracted diffuse polarization functions for each angular momentum. However, neither of these additions are utilized in this study.

Table 1.1: Description of basis sets used in this work. The primitive Gaussian type orbitals (PGTO) are contracted into  $N$  basis functions of contracted Gaussian type orbitals (CGTO).

	First Row Elements (C,N,O, ...)			Hydrogen		
Basis set	PGTO	CGTO	$N$	PGTO	CGTO	$N$
DZ	$9s5p$	$4s2p$	10	$4s$	$2s$	2
DZP	$9s5p1d$	$4s2p1d$	15	$4s1p$	$2s1p$	5
TZ2P	$11s6p3d$	$5s3p2d$	24	$5s3p$	$3s2p$	9
cc-pVDZ	$9s4p1d$	$3s2p1d$	14	$4s1p$	$2s1p$	5
cc-pVTZ	$10s5p2d1f$	$4s3p2d1f$	30	$5s2p1d$	$3s2p1d$	14
cc-pVQZ	$12s6p3d2f1g$	$5s4p3d2f1g$	55	$6s3p2d1f$	$4s3p2d1f$	30
ANO0	$13s8p6d$	$3s2p1d$	14	$8s6p$	$2s1p$	5
ANO1	$13s8p6d4f$	$4s3p2d1f$	30	$8s6p4d$	$4s2p1d$	15
ANO2	$13s8p6d4f2g$	$5s4p3d2f1g$	55	$8s6p4d3f$	$4s3p2d1f$	30
dzp	$8s4p1d$	$4s2p1d$	15	$4s1p$	$2s1p$	5
tzp	$9s5p1d$	$5s3p1d$	19	$5s1p$	$3s1p$	6
qz2p	$11s7p2d$	$6s4p2d$	28	$6s2p$	$3s2p$	9

## 1.5 Analytic Gradients and Second Derivatives

For the methods described in the previous sections, only computation of the energies has been shown. But, is the energy computed the lowest energy possible of a particular molecule? Can it be used directly to determine the heat of formation of a compound? Since the lowest molecular energy corresponds to a minimum of the potential energy surface (PES)<sup>20</sup>, one of the typical goals in computational chemistry is to optimum geometry to find the equilibrium molecular configuration for a specific isomer (i.e. where the energy is at a minimum<sup>21</sup>. Among the possible strategies needed for a search of the PES, the Newton-Raphson (NR) method is used most often. In this method, the energy,  $E$  is expanded as a Taylor series:

$$E(\mathbf{R}_0) = E(\mathbf{R}) + \mathbf{g}^t(\mathbf{R}_0 - \mathbf{R}) + \frac{1}{2}(\mathbf{R}_0 - \mathbf{R})^t \mathbf{H}(\mathbf{R}_0 - \mathbf{R}) + \dots, \quad (1.80)$$

then the Newton-Raphson step is defined as:

$$(\mathbf{R}_0 - \mathbf{R}) = -\mathbf{H}^{-1} \mathbf{g}. \quad (1.81)$$

Equation 1.81 requires the first and second order changes in energy with respect to changes in the position of the nuclei,  $\Xi$ , i.e. the gradient (first derivative),  $\mathbf{g}$ :

$$\mathbf{g} = \begin{pmatrix} \frac{\partial E}{\partial \xi_1} \\ \frac{\partial E}{\partial \xi_2} \\ \vdots \\ \frac{\partial E}{\partial \xi_N} \end{pmatrix} \quad (1.82)$$

---

<sup>20</sup>A PES often contains several possible structures which correspond to various isomers of a compound. Each of these isomers may correspond to a minimum of the PES.

<sup>21</sup>Transition states and other points are also useful in describing the PES of a molecule and its reactivity.

and the Hessian,  $\mathbf{H}$ , (second derivative):

$$\mathbf{H} = \begin{pmatrix} \frac{\partial^2 E}{\partial \xi_1^2} & \frac{\partial^2 E}{\partial \xi_1 \xi_2} & \cdots & \frac{\partial^2 E}{\partial \xi_1 \xi_N} \\ \frac{\partial^2 E}{\partial \xi_2 \xi_1} & \frac{\partial^2 E}{\partial \xi_2^2} & \cdots & \frac{\partial^2 E}{\partial \xi_2 \xi_N} \\ \vdots & \vdots & \ddots & \vdots \\ \frac{\partial^2 E}{\partial \xi_N \xi_1} & \frac{\partial^2 E}{\partial \xi_N \xi_2} & \cdots & \frac{\partial^2 E}{\partial \xi_N^2} \end{pmatrix}. \quad (1.83)$$

Early methods determined the gradient and Hessian using differences of the energy at finite displacements from a fixed reference. Though effective, these methods scaled with the number of nuclei for the gradient and the number of nuclei squared for the Hessian.

Other properties can be calculated using higher order derivatives of the energy with respect to position ( $\mathbf{R}$ ), nuclear spin ( $\mathbf{I}$ ), magnetic ( $\mathbf{B}$ ) or electric fields ( $\mathbf{E}$ ):

$$\text{Property} \propto \frac{\partial^{n_{\mathbf{E}}+n_{\mathbf{B}}+n_{\mathbf{I}}+n_{\mathbf{R}}} E}{\partial \mathbf{E}^{n_{\mathbf{E}}} \partial \mathbf{B}^{n_{\mathbf{B}}} \partial \mathbf{I}^{n_{\mathbf{I}}} \partial \mathbf{R}^{n_{\mathbf{R}}}}. \quad (1.84)$$

The potential utility of these various derivatives for predicting molecular properties such as vibrational frequencies, infrared and Raman intensities and NMR shieldings is summarized in Table 1.2. The extensive applicability of these derivatives prompted the derivation of analytic forms of the first and second derivatives which will be summarized in the remainder of this section.

### 1.5.1 Coupled-Perturbed Hartree-Fock Equations

The Hartree-Fock approximation serves as the basis of correlated methods. Their analytic derivatives are connected to the analytic derivatives of Hartree-Fock. To determine the analytic gradient for HF, differentiate with

Table 1.2: Properties calculated from derivatives of the energy from Table 10.1 of Reference [103].

$n_{\mathbf{E}}$	$n_{\mathbf{B}}$	$n_{\mathbf{I}}$	$n_{\mathbf{R}}$	Property
0	0	0	0	Energy
1	0	0	0	Electric dipole moment
0	1	0	0	Magnetic dipole moment
0	0	1	0	Hyperfine coupling constant
0	0	0	1	Energy gradient
2	0	0	0	Electric polarizability
0	2	0	0	Magnetizability
0	0	2	0	Spin-spin coupling (for different nuclei)
0	0	0	2	Harmonic vibrational frequencies
1	0	0	1	Infrared absorption intensities
1	1	0	0	Circular dichroism
0	1	1	0	Nuclear magnetic shielding
3	0	0	0	(first) Electric hyperpolarizability
0	3	0	0	(first) Hypermagnetizablity
0	0	0	3	(cubic) Anharmonic corrections to vibrational frequencies
2	0	0	1	Raman intensities
2	1	0	0	Magnetic circular dichroism (Faraday effect)
1	0	0	2	Infrared intensities for two quantum transitions
4	0	0	0	(second) Electric hyperpolarizability
0	4	0	0	(second) Hypermagnetizablity
0	0	0	4	(quartic) Anharmonic corrections to vibrational frequencies
2	0	0	2	Raman intensities for overtone and combination bands
2	2	0	0	Cotton-Mutton effect



Equation 1.31 respect to an arbitrary variable  $\alpha$ <sup>22</sup>:

$$\begin{aligned} \frac{dE_{HF}}{d\alpha} = & \sum_{\mu\nu} D_{\mu\nu}^{SCF} \frac{\partial h_{\mu\nu}}{\partial\alpha} + \frac{1}{2} \sum_{\mu\nu\rho\sigma} D_{\mu\nu}^{SCF} D_{\rho\sigma}^{SCF} \frac{\partial \langle \mu\rho || \nu\sigma \rangle}{\partial\alpha} + \frac{\partial V_{nn}}{\partial\alpha} \\ & + \sum_{\mu\nu} \frac{\partial D_{\mu\nu}^{SCF}}{\partial\alpha} h_{\mu\nu} + \sum_{\mu\nu\rho\sigma} \frac{\partial D_{\mu\nu}^{SCF}}{\partial\alpha} D_{\rho\sigma}^{SCF} \langle \mu\rho || \nu\sigma \rangle. \end{aligned} \quad (1.85)$$

P. Pulay [177, 178] simplified Equation 1.85 by removing the dependence of  $dE/d\alpha$  on  $\partial D_{\mu\nu}/\partial\alpha$ . Using Pulay's separation technique, Pople and co-workers [169] combine the two terms that contain  $\partial D_{\mu\nu}/\partial\alpha$  using Equation 1.26 - ie:

$$\begin{aligned} & \sum_{\mu\nu} \sum_i \left\{ \frac{\partial c_{\mu i}^*}{\partial\alpha} F_{\mu\nu} c_{\nu i} + c_{\mu i}^* F_{\mu\nu} \frac{\partial c_{\nu i}}{\partial\alpha} \right\} \\ = & \sum_{\mu\nu} \sum_i \left\{ \frac{\partial c_{\mu i}^*}{\partial\alpha} \epsilon_i S_{\mu\nu} c_{\nu i} + c_{\mu i}^* \epsilon_i S_{\mu\nu} \frac{\partial c_{\nu i}}{\partial\alpha} \right\}. \end{aligned} \quad (1.86)$$

Since the MO orbitals form an orthonormal basis, the overlap of AO orbitals  $S_{\mu\nu}$  provides:

$$\sum_{\mu\nu} c_{\mu i}^* S_{\mu\nu} c_{\nu j} = \delta_{ij}, \quad (1.87)$$

and its derivative becomes:

$$\sum_{\mu\nu} \sum_i \left\{ \frac{\partial c_{\mu i}^*}{\partial\alpha} S_{\mu\nu} c_{\nu i} + c_{\mu i}^* \frac{\partial S_{\mu\nu}}{\partial\alpha} c_{\nu i} + c_{\mu i}^* S_{\mu\nu} \frac{\partial c_{\nu i}}{\partial\alpha} \right\} = 0. \quad (1.88)$$

Thus, Equation 1.85 becomes:

$$\frac{dE_{HF}}{d\alpha} = \sum_{\mu\nu} D_{\mu\nu}^{SCF} \frac{\partial h_{\mu\nu}}{\partial\alpha} + \frac{1}{2} \sum_{\mu\nu\rho\sigma} D_{\mu\nu}^{SCF} D_{\rho\sigma}^{SCF} \frac{\partial \langle \mu\rho || \nu\sigma \rangle}{\partial\alpha} + \frac{\partial V_{nn}}{\partial\alpha} - \sum_{\mu\nu} I_{\mu\nu} \frac{\partial S_{\mu\nu}}{\partial\alpha}, \quad (1.89)$$

where:

$$I_{\mu\nu} = \sum_i \epsilon_i c_{\mu i}^* c_{\nu i} \quad (1.90)$$

---

<sup>22</sup>Examples of several of these variables are included in Table 1.2

and, the dependence of  $dE_{HF}/d\alpha$  on the derivative of the Hartree-Fock coefficients,  $\partial c_{\mu i}/\partial\alpha$ , has been removed.

However, analytic second derivatives for HF-SCF and analytic derivatives for the correlated methods (Sections 1.5.2 and 1.5.3) require  $\partial c_{\mu i}/\partial\beta$  where  $\beta$  is a second arbitrary variable. If these derivatives can be expressed as a transformation of the Hartree-Fock coefficients:

$$\frac{\partial c_{\mu i}}{\partial\beta} = \sum_q U_{qi}^\beta c_{\mu q}, \quad (1.91)$$

then the orthogonality of the MO orbitals,  $\mathbf{S}$ , provides:

$$S_{qp}^\beta + U_{pq}^\beta + U_{qp}^\beta = 0, \quad (1.92)$$

where:

$$S_{qp}^\beta = \sum_{\mu\nu} c_{\mu p}^* \frac{\partial S_{\mu\nu}}{\partial\beta} c_{\nu q}. \quad (1.93)$$

However, no unique choice of coefficients  $U_{ij}$  and  $U_{ab}$  exists because the energy gradient and perturbed wavefunction are invariant with respect to rotations among the occupied or virtual orbitals [76, 88]. In 1985, Handy *et al.* [88] suggested fixing the occupied-occupied and virtual-virtual block of  $\mathbf{U}$  as follows:

$$U_{ij}^\beta = -\frac{1}{2}S_{ij}^\beta \quad (1.94)$$

and

$$U_{ab}^\beta = -\frac{1}{2}S_{ab}^\beta. \quad (1.95)$$

The remaining virtual-occupied terms are then obtained from solving

the CPHF equations<sup>23</sup>:

$$\sum_b \sum_j \{ \langle ab || ij \rangle + \langle aj || ib \rangle + (\epsilon_a - \epsilon_i) \delta_{ab} \delta_{ij} \} U_{bj}^\beta = B_{ai}^\beta, \quad (1.96)$$

where:

$$B_{ai}^\beta = -F_{ai}^{(\beta)} + \epsilon_i S_{ai}^\beta + \frac{1}{2} \sum_{kl} (\langle ka || li \rangle + \langle ki || la \rangle) S_{kl}^\beta \quad (1.97)$$

and

$$F_{pq}^{(\beta)} = \sum_{\mu\nu} c_{\mu p}^* \left\{ \frac{\partial h_{\mu\nu}}{\partial \beta} + \sum_k \sum_{\rho\sigma} c_{\sigma k}^* c_{\rho k} \frac{\partial \langle \mu\sigma || \nu\rho \rangle}{\partial \beta} \right\} c_{\nu q}. \quad (1.98)$$

### 1.5.2 Second-Order Many-Body Perturbation Theory

For post Hartree-Fock methods, the correction to the Hartree-Fock energy is differentiated. To obtain analytic derivatives for the correction of MP2 to the HF energy, Equation 1.49 may be differentiated with respect to  $\alpha$ <sup>24</sup>:

$$\begin{aligned} \frac{dE_{MP2}}{d\alpha} = & \frac{1}{2} \sum_{ij} \sum_{ab} \frac{\partial \langle ij || ab \rangle}{\partial \alpha} t_{ij}^{ab} - \frac{1}{2} \sum_{ij} \frac{\partial f_{ij}}{\partial \alpha} \sum_k \sum_{ab} t_{ik}^{ab} t_{jk}^{ab} \\ & + \frac{1}{2} \sum_{ab} \frac{\partial f_{ab}}{\partial \alpha} \sum_c \sum_{ij} t_{ij}^{ac} t_{ij}^{bc}. \end{aligned} \quad (1.99)$$

Using Equations 1.92, 1.94 and 1.95, the  $\partial \langle ij || ab \rangle / \partial \alpha$  terms becomes:

$$\begin{aligned} \frac{\partial \langle ij || ab \rangle}{\partial \alpha} = & \langle ij || ab \rangle^{(\alpha)} + U_{ei}^\alpha \langle ej || ab \rangle - \frac{1}{2} S_{mi}^\alpha \langle mj || ab \rangle + U_{ej}^\alpha \langle ie || ab \rangle \\ & - \frac{1}{2} S_{kj}^\alpha \langle im || ab \rangle + \{ U_{am}^\alpha + S_{am}^\alpha \} \langle ij || mb \rangle - \frac{1}{2} S_{ea}^\alpha \langle ij || eb \rangle \\ & + \{ U_{bm}^\alpha + S_{bm}^\alpha \} \langle ij || am \rangle - \frac{1}{2} S_{eb}^\alpha \langle ij || ae \rangle, \end{aligned} \quad (1.100)$$

---

<sup>23</sup>For the details of the derivation of the CPHF equations, the reader is referred to reference [169].

<sup>24</sup>The following derivation is a summary of what was presented J. Gauss and D. Cremer in Reference [76].

where:

$$\langle ij||ab\rangle^{(\alpha)} = \sum_{\mu\nu\sigma\rho} c_{\mu i}^* c_{\nu j}^* \frac{\partial \langle \mu\nu||\sigma\rho\rangle}{\partial \alpha} c_{\sigma a} c_{\rho b}. \quad (1.101)$$

and  $\partial f_{pq}/\partial \alpha$  (the derivative of the Lagrangian multipliers):

$$\begin{aligned} \frac{\partial f_{pq}}{\partial \alpha} = & F_{pq}^{(\alpha)} + U_{em}^\alpha \{ \langle pe||qm\rangle + \langle pm||qe\rangle \} \\ & - \frac{1}{2} S_{mn}^\alpha \{ \langle pm||qn\rangle + \langle pm||qn\rangle \} - \frac{1}{2} S_{pq}^\alpha (f_{pp} + f_{qq}). \end{aligned} \quad (1.102)$$

Substituting Equations 1.100 and 1.102 into Equation 1.99 yields:

$$\begin{aligned} \frac{dE}{d\alpha} = & \sum_{ijab} \Gamma(ij, ab) \langle ij||ab\rangle^{(\alpha)} + \sum_{ij} D_{ij} F_{ij}^{(\alpha)} + \sum_{ab} D_{ab} F_{ab}^{(\alpha)} \\ & + 2 \sum_a \sum_i X_{ai} U_{ai}^\alpha + \sum_{ij} I'_{ij} S_{ij}^\alpha + \sum_{ij} I'_{ab} S_{ab}^\alpha + 2 \sum_{ij} I'_{ai} S_{ai}^\alpha. \end{aligned} \quad (1.103)$$

where the two-particle density matrix elements:

$$\Gamma(ij, ab) = \frac{1}{2} t_{ij}^{ab}, \quad (1.104)$$

the relaxed one-particle density matrix elements for the occupied-occupied and virtual-virtual orbital blocks:

$$D_{ij} = \frac{1}{2} t_{jm}^{ef} t_{mi}^{ef} \quad (1.105)$$

and

$$D_{ab} = -\frac{1}{2} t_{mn}^{ae} t_{mn}^{eb}, \quad (1.106)$$

the gradient of energy with respect to rotations amongst the molecular orbitals:

$$X_{ai} = \Gamma(im, ae) \langle ef||am\rangle - \Gamma(mn, ae) \langle ie||mn\rangle + D_{mn} \langle mi||na\rangle + D_{ef} \langle ei||fa\rangle \quad (1.107)$$

and intermediate matrix elements<sup>25</sup>:

$$I'_{ij} = -\Gamma(jm, ef)\langle im||ef\rangle - \frac{1}{2}(f_{ii} + f_{jj})D_{ij} + D_{mn}\langle im||jn\rangle + D_{ef}\langle ie||jf\rangle, \quad (1.108)$$

$$I'_{ab} = -\Gamma(mn, be)\langle mn||ae\rangle - \frac{1}{2}(f_{aa} + f_{bb})D_{ab}, \quad (1.109)$$

and

$$I'_{ai} = -\Gamma(mn, ae)\langle nm||ie\rangle. \quad (1.110)$$

The Z vector method of Handy and Schaefer [89] allows the  $U_{pq}^\alpha$  terms to be removed from Equation 1.103 provided:

$$D_{em}\{\langle am||ie\rangle + \langle ae||im\rangle\delta_{im} + \delta_{ae}(f_{aa} - f_{ii})\} = -X_{ai}. \quad (1.111)$$

It simplifies to:

$$\begin{aligned} \frac{dE}{d\alpha} = & \sum_{ijkl} \Gamma(ij, kl)\langle ij||ab\rangle^{(\alpha)} + \sum_{ij} D_{ij}F_{ij}^{(\alpha)} + \sum_{ab} D_{ab}F_{ab}^{(\alpha)} \\ & + 2 \sum_{ai} D_{ai}F_{ai}^{(\alpha)} + \sum_{ij} I_{ij}S_{ij}^\alpha + \sum_{ab} I_{ab}S_{ab}^\alpha + 2 \sum_{ai} I_{ai}S_{ai}^\alpha, \end{aligned} \quad (1.112)$$

where the one-particle matrix elements become:

$$\begin{aligned} I_{ij} = & I'_{ij} + \frac{1}{2}\{\langle ei||mj\rangle - \langle ei||mi\rangle\}D_{em} \\ = & -\Gamma(jm, ef)\langle im||ef\rangle - \frac{1}{2}(f_{ii} + f_{jj})D_{ij} + D_{mn}\langle im||jn\rangle \\ & + D_{ef}\langle ie||jf\rangle + \frac{1}{2}\{\langle ei||mj\rangle - \langle ei||mi\rangle\}D_{em}, \end{aligned} \quad (1.113)$$

$$I_{ab} = I'_{ab} = -\Gamma(mn, be)\langle mn||ae\rangle - \frac{1}{2}(f_{aa} + f_{bb})D_{ab}, \quad (1.114)$$

and

$$I_{ai} = I'_{ai} + D_{ai}f_{ii} = -\Gamma(mn, ae)\langle nm||ie\rangle + D_{ai}f_{ii}. \quad (1.115)$$

---

<sup>25</sup>These matrix elements will be part of the energy weighted or one-particle density matrix.

In AO form, Equation 1.112 transforms to:

$$\frac{dE}{d\alpha} = \sum_{\mu\nu\sigma\rho} \Gamma_{\mu\nu\sigma\rho} \frac{\partial \langle \mu\nu || \sigma\rho \rangle}{\partial \alpha} + \sum_{\mu\nu} D_{\mu\nu} F_{\mu\nu}^{(\alpha)} + \sum_{\mu\nu} I_{\mu\nu} S_{\mu\nu}^{\alpha} \quad (1.116)$$

where the intermediates  $\Gamma(pq, rs)$ ,  $D_{pq}$  and  $I_{pq}$  become:

$$\Gamma_{\mu\nu\sigma\rho} = \sum_{pqrs} c_{\mu p}^* c_{\nu q}^* \Gamma(pq, rs) c_{\sigma r} c_{\rho s}, \quad (1.117)$$

$$D_{\mu\nu} = \sum_{pq} c_{\mu p}^* D_{pq} c_{\nu q} \quad (1.118)$$

and

$$I_{\mu\nu} = \sum_{pq} c_{\mu p}^* I_{pq} c_{\nu q}. \quad (1.119)$$

To obtain an analytic form of the second derivative of the MP2 correction to the HF energy, the AO form of the analytic gradient (Equation 1.116) is differentiated:

$$\begin{aligned} \frac{d^2 E}{d\alpha d\beta} = & \sum_{\mu\nu\sigma\rho} \Gamma_{\mu\nu\sigma\rho} \frac{\partial^2 \langle \mu\nu || \sigma\rho \rangle}{\partial \alpha \partial \beta} + \sum_{\mu\nu} F_{\mu\nu}^{(\alpha\beta)} D_{\mu\nu} + \sum_{\mu\nu} S_{\mu\nu}^{\alpha\beta} I_{\mu\nu} \\ & + \sum_{\mu\nu\sigma\rho} \frac{\partial \Gamma_{\mu\nu\sigma\rho}}{\partial \beta} \frac{\partial \langle \mu\nu || \sigma\rho \rangle}{\partial \alpha} + \sum_{\mu\nu} F_{\mu\nu}^{(\alpha)} \frac{\partial D_{\mu\nu}}{\partial \beta} + \sum_{\mu\nu} S_{\mu\nu}^{\alpha} \frac{\partial I_{\mu\nu}}{\partial \beta}. \end{aligned} \quad (1.120)$$

The derivatives of the AO intermediates  $\Gamma_{\mu\nu\sigma\rho}$ ,  $D_{\mu\nu}$ , and  $I_{\mu\nu}$  now depend on the CPHF coefficients,  $U_{pq}^{\beta}$ :

$$\begin{aligned} \frac{\partial \Gamma_{\mu\nu\sigma\rho}}{\partial \beta} = & \sum_{pqrs} c_{\mu p}^* c_{\nu q}^* \frac{\partial \Gamma(pq, rs)}{\partial \beta} c_{\sigma r} c_{\rho s} + \sum_{pqrst} U_{tp}^{\beta*} c_{\mu t}^* c_{\nu q}^* \Gamma(pq, rs) c_{\sigma r} c_{\rho s} \\ & + \sum_{pqrst} c_{\mu p}^* U_{tq}^{\beta*} c_{\nu t}^* \Gamma(pq, rs) c_{\sigma r} c_{\rho s} + \sum_{pqrst} c_{\mu p}^* c_{\nu q}^* \Gamma(pq, rs) U_{tr}^{\beta} c_{\sigma t} c_{\rho s} \\ & + \sum_{pqrst} c_{\mu p}^* c_{\nu q}^* \Gamma(pq, rs) c_{\sigma r} U_{ts}^{\beta} c_{\rho t}, \end{aligned} \quad (1.121)$$

$$\frac{\partial D_{\mu\nu}}{\partial\beta} = \sum_{pq} c_{\mu p}^* \frac{\partial D_{pq}}{\partial\beta} c_{\nu q} + \sum_{pqr} U_{rp}^{\beta*} c_{\mu r}^* D_{pq} c_{\nu q} + \sum_{pqr} c_{\mu p}^* D_{pq} U_{rq}^{\beta} c_{\nu r} \quad (1.122)$$

and

$$\frac{\partial I_{\mu\nu}}{\partial\beta} = \sum_{pq} c_{\mu p}^* \frac{\partial I_{pq}}{\partial\beta} c_{\nu q} + \sum_{pqr} U_{rp}^{\beta*} c_{\mu r}^* I_{pq} c_{\nu q} + \sum_{pqr} c_{\mu p}^* I_{pq} U_{rq}^{\beta} c_{\nu r}. \quad (1.123)$$

Differentiating Equation 1.104 with respect to  $\beta$ , the derivative of the two-particle matrix elements becomes:

$$\frac{\partial \Gamma(ij, ab)}{\partial\beta} = \frac{1}{2} \frac{\partial t_{ij}^{ab}}{\partial\beta}, \quad (1.124)$$

Differentiating Equations 1.113, 1.114 and 1.115, the derivatives of the one-particle density matrix elements become:

$$\begin{aligned} \frac{\partial I_{ij}}{\partial\beta} = & -\frac{\partial \Gamma(jm, ef)}{\partial\beta} \langle im || ef \rangle - \Gamma(jm, ef) \frac{\partial \langle im || ef \rangle}{\partial\beta} - \frac{1}{2} \left( \frac{\partial f_{ii}}{\partial\beta} + \frac{\partial f_{jj}}{\partial\beta} \right) D_{ij} \\ & - \frac{1}{2} (f_{ii} + f_{jj}) \frac{\partial D_{ij}}{\partial\beta} + \frac{\partial D_{mn}}{\partial\beta} \langle im || jn \rangle + D_{mn} \frac{\partial \langle im || jn \rangle}{\partial\beta} \\ & + \frac{\partial D_{ef}}{\partial\beta} \langle ie || jf \rangle + D_{ef} \frac{\partial \langle ie || jf \rangle}{\partial\beta} + \frac{1}{2} \frac{\partial D_{em}}{\partial\beta} \{ \langle ei || mj \rangle - \langle ei || mi \rangle \} \\ & + \frac{1}{2} D_{em} \left\{ \frac{\partial \langle ei || mj \rangle}{\partial\beta} - \frac{\partial \langle ei || mi \rangle}{\partial\beta} \right\}, \end{aligned} \quad (1.125)$$

$$\begin{aligned} \frac{\partial I_{ab}}{\partial\beta} = & -\frac{\partial \Gamma(mn, be)}{\partial\beta} \langle mn || ae \rangle - \Gamma(mn, be) \frac{\partial \langle mn || ae \rangle}{\partial\beta} \\ & - \frac{1}{2} \left\{ \frac{\partial f_{aa}}{\partial\beta} + \frac{\partial f_{bb}}{\partial\beta} \right\} D_{ab} - \frac{1}{2} \{ f_{aa} + f_{bb} \} \frac{\partial D_{ab}}{\partial\beta} \end{aligned} \quad (1.126)$$

and

$$\frac{\partial I_{ai}}{\partial\beta} = -\frac{\partial \Gamma(mn, ae)}{\partial\beta} \langle nm || ie \rangle - \Gamma(mn, ae) \frac{\partial \langle nm || ie \rangle}{\partial\beta} + \frac{\partial D_{ai}}{\partial\beta} f_{ii} + D_{ai} \frac{\partial f_{ii}}{\partial\beta} \quad (1.127)$$

The occupied-occupied and virtual-virtual blocks of the effective or relaxed one-particle density matrix are obtained by differentiating Equations 1.105 and 1.106:

$$\frac{\partial D_{ij}}{\partial \beta} = -\frac{1}{2} \left\{ \frac{\partial t_{im}^{ef}}{\partial \beta} t_{jm}^{ef} + t_{im}^{ef} \frac{\partial t_{jm}^{ef}}{\partial \beta} \right\}, \quad (1.128)$$

and

$$\frac{\partial D_{ab}}{\partial \beta} = -\frac{1}{2} \left\{ \frac{\partial t_{mn}^{ae}}{\partial \beta} t_{mn}^{be} + t_{mn}^{ae} \frac{\partial t_{mn}^{be}}{\partial \beta} \right\}. \quad (1.129)$$

However, to determine the occupied-virtual block, the first-order Z vector equations are solved where:

$$\begin{aligned} & \frac{\partial D_{em}}{\partial \beta} (\langle ei||ma \rangle - \langle mi||ea \rangle + \delta_{im} \delta_{ea} (f_{aa} - f_{ii})) \\ &= -\frac{\partial X_{ai}}{\partial \beta} - D_{em} \left\{ \frac{\partial \langle ei||ma \rangle}{\partial \beta} + \frac{\partial \langle mi||ea \rangle}{\partial \beta} + \delta_{im} \frac{\partial f_{ea}}{\partial \beta} - \delta_{ea} \frac{\partial f_{im}}{\partial \beta} \right\} \end{aligned} \quad (1.130)$$

and

$$\begin{aligned} \frac{\partial X_{ai}}{\partial \beta} &= \frac{\partial \Gamma(im, ef)}{\partial \beta} \langle ef||am \rangle + \Gamma(im, ef) \frac{\partial \langle ef||am \rangle}{\partial \beta} - \frac{\partial \Gamma(mn, ae)}{\partial \beta} \langle ie||mn \rangle \\ &\quad - \Gamma(mn, ae) \frac{\partial \langle ie||mn \rangle}{\partial \beta} + \frac{\partial D_{mn}}{\partial \beta} \langle mi||na \rangle + D_{mn} \frac{\partial \langle mi||na \rangle}{\partial \beta} \\ &\quad + \frac{\partial D_{ef}}{\partial \beta} \langle ei||fa \rangle + D_{ef} \frac{\partial \langle ei||fa \rangle}{\partial \beta}, \end{aligned} \quad (1.131)$$

Finally, the derivative of  $t_{ij}^{ab}$  is obtained via:

$$\frac{\partial t_{ij}^{ab}}{\partial \beta} = \frac{\frac{\partial \langle ab||ij \rangle}{\partial \beta} + \frac{\partial f_{ae}}{\partial \beta} t_{ij}^{eb} + \frac{\partial f_{be}}{\partial \beta} t_{ij}^{ae} - t_{mj}^{ab} \frac{\partial f_{mi}}{\partial \beta} - t_{mj}^{ab} \frac{\partial f_{mi}}{\partial \beta}}{f_{ii} + f_{jj} - f_{aa} - f_{bb}}. \quad (1.132)$$

The implementation of Equation 1.120 will be discussed in Section 1.6.

### 1.5.3 Coupled-Cluster Theory

To determine the coupled-cluster contribution to the gradient, differentiating Equation 1.67 and projecting on the left with  $\langle \Phi_0 |$  or  $\langle \Phi_{ijk\dots}^{abc\dots} |$  yields



the energy gradient:

$$\frac{dE_{cc}}{d\alpha} = \langle \Phi_0 | [\bar{H}, \frac{\partial \hat{T}}{\partial \alpha}] | \Phi_0 \rangle + \langle \Phi_0 | \frac{\partial \bar{H}}{\partial \alpha} | \Phi_0 \rangle \quad (1.133)$$

and

$$0 = \langle \Phi_{ijk\dots}^{abc\dots} | [\bar{H}, \frac{\partial \hat{T}}{\partial \alpha}] | \Phi_0 \rangle + \langle \Phi_{ijk\dots}^{abc\dots} | \frac{\partial \bar{H}}{\partial \alpha} | \Phi_0 \rangle. \quad (1.134)$$

Applying the projection operator:

$$\hat{1} = |P\rangle\langle P| \quad (1.135)$$

where:

$$|P\rangle = |\Phi_0\rangle + |\Phi_{ijk\dots}^{abc\dots}\rangle \quad (1.136)$$

allows Equation 1.133 to be written as:

$$\frac{dE_{cc}}{d\alpha} = \langle \Phi_0 | \frac{\partial \bar{H}}{\partial \alpha} | \Phi_0 \rangle - \langle \Phi_0 | \bar{H} - E_{cc} | \Phi \rangle^{-1} \langle \Phi | \frac{\partial \bar{H}}{\partial \alpha} | \Phi_0 \rangle \quad (1.137)$$

Equation 1.137 is simplified using the “CC response” or  $\Lambda$  equation. If:

$$\hat{\Lambda} = \hat{\Lambda}_1 + \hat{\Lambda}_2 + \hat{\Lambda}_3 + \dots \quad (1.138)$$

where:

$$\hat{\Lambda}_1 = \sum_{ia} \lambda_a^i \{ \hat{a}_i^\dagger \hat{a}_a \} \quad (1.139)$$

and

$$\hat{\Lambda}_2 = \sum_{ijab} \lambda_{ab}^{ij} \{ \hat{a}_i^\dagger \hat{a}_a \hat{a}_j^\dagger \hat{a}_b \}, \quad (1.140)$$

and subject to the constraint:

$$\langle \Phi_0 | \hat{\Lambda} | \Phi_{ijk\dots}^{abc\dots} \rangle = - \langle \Phi_0 | \bar{H} - E_{cc} | \Phi \rangle^{-1} \langle \Phi | \frac{\partial \bar{H}}{\partial \alpha} | \Phi_0 \rangle, \quad (1.141)$$

then, equation 1.137 becomes:

$$\frac{dE_{cc}}{d\alpha} = \langle \Phi_0 | \frac{\partial \bar{H}}{\partial \alpha} | \Phi_0 \rangle + \langle \Phi_0 | \hat{\Lambda} | \Phi_{ijk\dots}^{abc\dots} \rangle. \quad (1.142)$$

For the  $|\Phi_i^a\rangle$  projection, Equation 1.134 becomes:

$$\langle\Phi_0|\bar{H}|\Phi_i^a\rangle + \langle\Phi_0|\hat{\Lambda}\bar{H}|\Phi_i^a\rangle = 0 \quad (1.143)$$

and:

$$\langle\Phi_0|\bar{H}|\Phi_{ij}^{ab}\rangle + \langle\Phi_0|\hat{\Lambda}\bar{H}|\Phi_{ij}^{ab}\rangle + \langle\Phi_0|\bar{H}|\Phi_i^a\rangle\langle\Phi_i^j|\hat{\Lambda}|\Phi_{ij}^{ab}\rangle = 0 \quad (1.144)$$

for the  $|\Phi_{ij}^{ab}\rangle$ . By applying diagrammatic representations [195, 196], Equations 1.143 and 1.144 provide expressions that can be used to solve for  $\lambda_a^i$  and  $\lambda_{ab}^{ij}$  [78]:

$$\begin{aligned} 0 = & \mathcal{F}_{ia} + \lambda_e^i \mathcal{F}_{ea} - \lambda_a^m \mathcal{F}_{im} + \lambda_e^m \mathcal{W}_{ieam} + \frac{1}{2} \lambda_{ef}^{im} \mathcal{W}_{efam} \\ & - \frac{1}{2} \lambda_{ae}^{mn} \mathcal{W}_{iemn} - \mathcal{G}_{ef} \mathcal{W}_{eifa} - \mathcal{G}_{mn} \mathcal{W}_{mina} \end{aligned} \quad (1.145)$$

and

$$\begin{aligned} 0 = & \langle ij||ab\rangle + P_-(ab)\lambda_{ae}^{ij} \mathcal{F}_{eb} - P_-(ij)\lambda_{ab}^{im} \mathcal{F}_{jm} + \frac{1}{2} \lambda_{ab}^{mn} \mathcal{W}_{ijmn} + \frac{1}{2} \mathcal{W}_{efab} \lambda_{ef}^{ij} \\ & + P_-(ij)\lambda_e^i \mathcal{W}_{ejab} - P_-(ab)\lambda_a^m \mathcal{W}_{ijmb} + P_-(ij)P_-(ab)\lambda_{ae}^{im} \mathcal{W}_{jebm} \\ & + P_-(ij)P_-(ab)\lambda_a^i \mathcal{F}_{jb} + P_-\langle ij||ae\rangle \mathcal{G}_{be} - P_-(ij)\langle im||ab\rangle \mathcal{G}_{mj} \end{aligned} \quad (1.146)$$

Expressions for one-body ( $\mathcal{F}_{pq}$ ), two-body ( $\mathcal{W}_{pqrs}$ ) and three-body terms ( $\mathcal{G}_{pq}$ ) intermediates of the effective Hamiltonian,  $\bar{H}$  may be found in Reference [78].

If  $|\Phi_0\rangle$  is used as the reference wavefunction, Equation 1.142 can be simplified to an equation with the same form as the gradient for MP2 (Equation 1.112) for CCSD:

$$\frac{dE}{d\alpha} = \sum_{pqrs} \Gamma_{pqrs} \langle pq||rs\rangle^{(\alpha)} + \sum_{pq} D_{pq} F_{pq}^{(\alpha)} + \sum_{pq} I_{pq} S_{pq}^{\alpha} \quad (1.147)$$

where  $F_{pq}^{(\alpha)}$  are elements of the perturbed Fock matrix given by Equation 1.98,  $\langle pq||rs\rangle^{(\alpha)}$  are derivatives of two electron integrals given by Equation 1.101

and  $S_{pq}^\alpha$  are derivatives of the overlap integrals. The two-particle density matrix elements  $\Gamma(pq, rs)$ , relaxed one-particle density matrix elements  $D_{pq}$ <sup>26</sup> and energy averaged one-particle density matrix elements  $I_{pq}$  are included in References [81] and [78]

To obtain an expression for the second derivative, Equation 1.147 can first be transformed from molecular orbitals to atomic orbitals using Equations 1.117-1.119:

$$\frac{dE}{d\alpha} = \sum_{\mu\nu} D_{\mu\nu} \frac{\partial f_{\mu\nu}}{\partial \alpha} + \sum_{\mu\nu} I_{\mu\nu} \frac{\partial S_{\mu\nu}}{\partial \alpha} + \sum_{\mu\nu\sigma\rho} \Gamma(\mu\nu, \rho\sigma) \frac{\partial \langle \mu\nu || \sigma\rho \rangle}{\partial \alpha} \quad (1.148)$$

Differentiating equation 1.148 yields:

$$\begin{aligned} \frac{d^2 E}{d\alpha d\beta} = & \sum_{\mu\nu} D_{\mu\nu} \frac{\partial^2 f_{\mu\nu}}{\partial \alpha \partial \beta} + \sum_{\mu\nu} I_{\mu\nu} \frac{\partial^2 S_{\mu\nu}}{\partial \alpha \partial \beta} + \sum_{\mu\nu\sigma\rho} \Gamma(\mu\nu, \rho\sigma) \frac{\partial^2 \langle \mu\nu || \sigma\rho \rangle}{\partial \alpha \partial \beta} \\ & + \sum_{\mu\nu} \frac{\partial D_{\mu\nu}}{\partial \beta} \frac{\partial f_{\mu\nu}}{\partial \alpha} + \sum_{\mu\nu} \frac{\partial I_{\mu\nu}}{\partial \beta} \frac{\partial S_{\mu\nu}}{\partial \alpha} + \sum_{\mu\nu\sigma\rho} \frac{\partial \Gamma(\mu\nu, \rho\sigma)}{\partial \beta} \frac{\partial \langle \mu\nu || \sigma\rho \rangle}{\partial \alpha} \end{aligned} \quad (1.149)$$

To use the derivatives of the intermediates in terms of atomic orbitals (Equations 1.121-1.123), the derivatives of the intermediates  $\Gamma(pq, rs)$ ,  $D_{pq}$  (both the response to amplitudes and the orbital relaxation) and  $I_{pq}$  for molecular orbitals are needed. Derivative of two-particle density matrix elements,  $\partial \Gamma(pq, rs) / \partial \beta$ :

To evaluate the intermediates in Equation 1.149, the perturbed  $\lambda$  ( $\partial \lambda_a^i / \partial \beta$ ,  $\partial \lambda_{ab}^{ij} / \partial \beta$ ) and  $t$  amplitudes ( $\partial t_i^a / \partial \beta$ ,  $\partial t_{ij}^{ab} / \partial \beta$ ) are required and may

---

<sup>26</sup>The truncation of the coupled-cluster operator results in two components for  $D_{pq}$ : a term for the response from the cluster amplitudes  $D_{pq}^{(amp)}$  and a term for orbital relaxation  $D_{pq}^{(orb)}$ .

be obtained by solving both the first-order perturbed CCSD equations [78]:

$$\begin{aligned}
0 = & \frac{\partial f_{ai}}{\partial \beta} + \tilde{\mathcal{F}}_{ae}^\beta t_i^a - t_m^a \tilde{\mathcal{F}}_{mi}^\beta + \tilde{\mathcal{F}}_{me}^\beta t_{im}^{ae} + t_m^e \frac{\partial \langle am || ie \rangle}{\partial \beta} - \frac{1}{2} t_{mn}^{ae} \frac{\partial \langle mn || ie \rangle}{\partial \beta} \\
& + \frac{1}{2} \frac{\partial \langle am || ef \rangle}{\partial \beta} t_{im}^{ef} + \mathcal{F}_{ae} \frac{\partial t_i^e}{\partial \beta} - \frac{\partial t_m^a}{\partial \beta} \mathcal{F}_{mi} + \mathcal{F}_{me} \frac{\partial t_{im}^{ae}}{\partial \beta} + \frac{\partial t_m^e}{\partial \beta} \mathcal{W}_{amie} \quad (1.150) \\
& - \frac{1}{2} \frac{\partial t_{mn}^{ae}}{\partial \beta} \mathcal{W}_{mnie} + \frac{1}{2} \mathcal{W}_{amef} \frac{\partial t_{im}^{ef}}{\partial \beta}
\end{aligned}$$

and

$$\begin{aligned}
0 = & \frac{\partial \langle ab || ij \rangle}{\partial \beta} + P_-(ab) t_{ij}^{ae} \left\{ \tilde{\mathcal{F}}_{be}^\beta - \frac{1}{2} t_m^b \tilde{\mathcal{F}}_{me}^\beta \right\} - P_-(ij) t_{im}^{ab} \left\{ \tilde{\mathcal{F}}_{mj}^\beta + \frac{1}{2} t_j^e \tilde{\mathcal{F}}_{me}^\beta \right\} \\
& + \frac{1}{2} \tau_{mn}^{ab} \tilde{\mathcal{W}}_{mni}^\beta + \frac{1}{2} \tilde{\mathcal{W}}_{abef}^\beta \tau_{ij}^{ef} + P_-(ij) P_-(ab) \left\{ t_{im}^{ae} \tilde{\mathcal{W}}_{mbej}^\beta \right. \\
& \left. - t_i^e t_m^a \frac{\partial \langle mb || ej \rangle}{\partial \beta} \right\} + P_-(ij) \frac{\partial \langle ab || ej \rangle}{\partial \beta} t_i^e - P_-(ab) t_m^a \frac{\partial \langle mb || ij \rangle}{\partial \beta} \\
& + P_-(ab) \frac{\partial t_{ij}^{ae}}{\partial \beta} \mathcal{F}_{be} - P_-(ij) \frac{\partial t_{im}^{ab}}{\partial \beta} \mathcal{F}_{mj} + \frac{1}{2} \frac{\partial t_{mn}^{ab}}{\partial \beta} \mathcal{W}_{mni} \\
& + \frac{1}{2} \mathcal{W}_{abef} \frac{\partial t_{ij}^{ef}}{\partial \beta} + P_-(ij) P_-(ab) \frac{\partial t_{im}^{ae}}{\partial \beta} \mathcal{W}_{mbej} - \frac{1}{2} P_-(ab) t_{ij}^{ae} \frac{\partial t_{mn}^{bf}}{\partial \beta} \langle mn || ef \rangle \\
& - \frac{1}{2} P_-(ij) t_{im}^{ab} \frac{\partial t_{jn}^{ef}}{\partial \beta} \langle mn || ef \rangle + P_-(ij) \mathcal{W}_{abej} \frac{\partial t_i^e}{\partial \beta} - P_-(ab) \frac{\partial t_m^a}{\partial \beta} \mathcal{W}_{mbij} \\
& + P_-(ab) \frac{\partial t_m^e}{\partial \beta} \mathcal{W}_{maef} t_{ij}^{fb} - P_-(ij) \frac{\partial t_m^e}{\partial \beta} \mathcal{W}_{mnei} t_{nj}^{ab} \quad (1.151)
\end{aligned}$$

and the first-order perturbed  $\Lambda$  equations:

$$\begin{aligned}
0 = & \frac{\partial F_{ia}}{\partial \beta} + \lambda_e^i \frac{\partial \mathcal{F}_{ea}}{\partial \beta} - \lambda_a^m \frac{\partial \mathcal{F}_{im}}{\partial \beta} + \lambda_e^m \frac{\partial \mathcal{W}_{ieam}}{\partial \beta} + \frac{1}{2} \lambda_{ef}^{im} \frac{\partial \mathcal{W}_{efam}}{\partial \beta} \\
& - \frac{1}{2} \lambda_{ae}^{mn} \frac{\partial \mathcal{W}_{iemn}}{\partial \beta} - \mathcal{G}_{ef} \frac{\partial \mathcal{W}_{eifa}}{\partial \beta} - \tilde{\mathcal{G}}_{ef}^\beta \mathcal{W}_{eifa} - \tilde{\mathcal{G}}_{ef}^\beta \mathcal{W}_{eifa} - \mathcal{G}_{mn} \frac{\partial \mathcal{W}_{mina}}{\partial \beta} \\
& - \tilde{\mathcal{G}}_{mn}^\beta \mathcal{W}_{mina} - \tilde{\mathcal{G}}_{mn}^\beta \mathcal{W}_{mina} + \frac{\partial \lambda_e^i}{\partial \beta} \mathcal{F}_{ea} - \frac{\partial \lambda_a^m}{\partial \beta} \mathcal{F}_{im} \\
& + \frac{\partial \lambda_e^m}{\partial \beta} \mathcal{W}_{ieam} + \frac{1}{2} \frac{\partial \lambda_{ef}^{im}}{\partial \beta} \mathcal{W}_{efam} - \frac{1}{2} \frac{\partial \lambda_{ae}^{mn}}{\partial \beta} \mathcal{W}_{iemn} \quad (1.152)
\end{aligned}$$

and

$$\begin{aligned}
0 = & \frac{\partial \langle ij || ab \rangle}{\partial \beta} + P_-(ab) \lambda_{ae}^{ij} \frac{\partial \mathcal{F}_{eb}}{\partial \beta} - P_-(ij) \lambda_{ab}^{im} \frac{\partial \mathcal{F}_{jm}}{\partial \beta} + \frac{1}{2} \lambda_{ab}^{mn} \frac{\partial \mathcal{W}_{ijmn}}{\partial \beta} \\
& + P_-(ij) \lambda_e^i \frac{\partial \mathcal{W}_{ejab}}{\partial \beta} - P_-(ab) \lambda_a^m \frac{\partial \mathcal{W}_{ijmb}}{\partial \beta} + P_-(ij) P_-(ab) \lambda_{ae}^{im} \frac{\partial \mathcal{W}_{jebm}}{\partial \beta} \\
& + P_-(ij) P_-(ab) \lambda_a^i \frac{\partial \mathcal{F}_{jb}}{\partial \beta} + P_-(ab) \frac{\partial \langle ij || ae \rangle}{\partial \beta} \mathcal{G}_{be} + P_-(ab) \langle ij || ae \rangle \tilde{\mathcal{G}}_{be}^\beta \\
& + P_-(ab) \langle ij || ae \rangle \tilde{\mathcal{G}}_{be}^\beta - P_-(ij) \frac{\partial \langle im || ab \rangle}{\partial \beta} \mathcal{G}_{mj} - P_-(ij) \langle im || ab \rangle \tilde{\mathcal{G}}_{mj}^\beta \\
& + P_-(ij) \langle im || ab \rangle \tilde{\mathcal{G}}_{mj}^\beta + P_-(ab) \frac{\partial \lambda_{ae}^{ij}}{\partial \beta} \mathcal{F}_{eb} - P_-(ij) \frac{\partial \lambda_{ab}^{im}}{\partial \beta} \mathcal{F}_{jm} \\
& + \frac{1}{2} \frac{\partial \lambda_{ab}^{mn}}{\partial \beta} \mathcal{W}_{ijmn} + \frac{1}{2} \mathcal{W}_{efab} \frac{\partial \lambda_{ef}^{ij}}{\partial \beta} + P_-(ij) \frac{\partial \lambda_e^i}{\partial \beta} \mathcal{W}_{ejab} + \frac{1}{2} \frac{\partial \mathcal{W}_{efab}}{\partial \beta} \lambda_{ef}^{ij} \\
& - P_-(ab) \frac{\partial \lambda_a^m}{\partial \beta} \mathcal{W}_{ijmb} + P_-(ij) P_-(ab) \frac{\partial \lambda_{ae}^{im}}{\partial \beta} \mathcal{W}_{jebm} + P_-(ij) P_-(ab) \frac{\partial \lambda_a^i}{\partial \beta} \mathcal{F}_{jb}
\end{aligned} \tag{1.153}$$

The intermediates one-particle ( $\tilde{\mathcal{F}}_{pq}^\beta$ ), two-particle ( $\tilde{\mathcal{W}}_{pqrs}^\beta$ ), and three-body ( $\tilde{\mathcal{G}}_{pq}^\beta$ ) terms and their derivatives are included in Reference [78].

#### 1.5.4 Analytic Derivatives of Perturbative Triples

For the perturbative triples contribution, differentiating Equation 1.5 with respect to an arbitrary variable  $\alpha$  results in terms dependent on the perturbed  $t$  amplitudes ( $\partial t_i^a / \partial \alpha$  and  $\partial t_{ij}^{ab} / \partial \alpha$ ). The gradient theory described in the previous section for CCSD allows this dependency to be removed and results in additional terms in the reduced one particle density matrix and two-particle density matrix. Also, the CCSD  $\Lambda$  equations contain additional terms:

$$\frac{1}{4} t_{imn}^{aef} \langle ef || mn \rangle \tag{1.154}$$

and

$$\frac{1}{2}P_-(ab)\{2t_{ijm}^{aef} + \tilde{t}_{ijm}^{aef}\}\langle ef||bm\rangle - \frac{1}{2}P_-(ij)\{2t_{imn}^{abe} + \tilde{t}_{imn}^{abe}\}\langle je||mn\rangle \quad (1.155)$$

The perturbative triples contribution to the analytic second derivatives are obtained by differentiation of the additional terms with respect to  $\beta$ . The perturbed  $\Lambda$  equations also included additional terms:

$$\frac{1}{4}\left\{\frac{\partial t_{imn}^{aef}}{\partial\beta}\langle ef||mn\rangle + t_{imn}^{aef}\frac{\partial\langle ef||mn\rangle}{\partial\beta}\right\}. \quad (1.156)$$

and

$$\begin{aligned} &\frac{1}{2}P(ab)\left\{\left[2\frac{\partial t_{ijm}^{aef}}{\partial\beta} + \frac{\partial \tilde{t}_{ijm}^{aef}}{\partial\beta}\right]\langle ef||bm\rangle + [2t_{ijm}^{aef} + \tilde{t}_{ijm}^{aef}]\frac{\partial\langle ef||bm\rangle}{\partial\beta}\right\} \\ &-\frac{1}{2}P(ij)\left\{\left[2\frac{\partial t_{imn}^{abe}}{\partial\beta} + \frac{\partial \tilde{t}_{imn}^{abe}}{\partial\beta}\right]\langle je||mn\rangle + [2t_{imn}^{abe} + \tilde{t}_{imn}^{abe}]\frac{\partial\langle je||mn\rangle}{\partial\beta}\right\} \end{aligned} \quad (1.157)$$

The derivatives with respect to  $\beta$  of the connected and disconnected triples are:

$$\begin{aligned} \frac{\partial t_{ijk}^{abc}}{\partial\beta} = &\left[P(abc)P(ijk)\left\{\frac{\partial t_{ij}^{ae}}{\partial\beta}\langle bc||ek\rangle + t_{ij}^{ae}\frac{\partial\langle bc||ek\rangle}{\partial\beta}\right\}\right. \\ &- P(abc)P(ijk)\left\{\frac{\partial t_{im}^{ab}}{\partial\beta}\langle mc||jk\rangle + t_{ij}^{ae}\frac{\partial\langle mc||jk\rangle}{\partial\beta}\right\} \\ &\left.+ P(abc)\frac{\partial f_{ae}}{\partial\beta}t_{ijk}^{ebc} - P(ijk)\frac{\partial f_{mi}}{\partial\beta}t_{mjk}^{abc}\right]/ \\ &(f_{ii} + f_{jj} + f_{kk} - f_{aa} - f_{bb} - f_{cc}) \end{aligned} \quad (1.158)$$

and

$$\begin{aligned} \frac{\partial \tilde{t}_{ijk}^{abc}}{\partial\beta} = &\left[P(abc)P(ijk)\frac{\partial t_i^a}{\partial\beta}\langle bc||jk\rangle + P(abc)P(ijk)t_i^a\frac{\partial\langle bc||jk\rangle}{\partial\beta}\right. \\ &\left.+ P(abc)\frac{\partial f_{ae}}{\partial\beta}\tilde{t}_{ijk}^{ebc} - P(ijk)\frac{\partial f_{mi}}{\partial\beta}\tilde{t}_{mjk}^{abc}\right]/ \\ &(f_{ii} + f_{jj} + f_{kk} - f_{aa} - f_{bb} - f_{cc}). \end{aligned} \quad (1.159)$$

## 1.6 Serial Implementation of Analytic Second Derivatives for MBPT and CC methods

The basic algorithm used to implement the analytic second derivatives for correlated *ab initio* methods (MP2, CCSD and CCSD(T)) was presented in Reference [77], and it is illustrated in Figure 1.1. It consists of the following parts:

Part 1:

1. Calculating unperturbed AO integrals,  $\langle\mu\nu||\sigma\rho\rangle$ .
2. Solving HF equations, Equation 1.27.
3. Transforming integrals from AO to MO basis.
4. Solving unperturbed MP/CC equations. See Sections 1.3.1, 1.3.2.1 and 1.5.4. For CC methods: solve unperturbed  $\Lambda$  equations, discussed in Section 1.5.3.
5. Constructing unperturbed relaxed one-particle density matrix  $\mathbf{D}$ .
6. Calculating integral derivatives,  $\langle\mu\nu||\sigma\rho\rangle/\partial\alpha$  for CPHF equations (Equation 1.96) and  $\partial\langle\mu\nu||\sigma\rho\rangle/\partial\beta$  for  $\beta = 1$ .
7. Solving CPHF equations, Equation 1.96, for each perturbation  $\beta$ .

Part 2:

8. For each perturbation  $\beta$ :
  - (a) Transforming  $\partial\langle\mu\nu||\sigma\rho\rangle/\partial\beta$  from AO to MO representation using the HF coefficients, then add MO derivative contribution to  $\partial\langle pq||rs\rangle/\partial\beta \leftarrow \sum_{\mu\nu\sigma\rho} c_{\mu p}c_{\nu q}\partial\langle\mu\nu||\sigma\rho\rangle/\partial\beta c_{\sigma s}c_{\rho r}$ .

- (b) Solving perturbed MP/CC equations,  $E_{MP}^{(\beta)}/E_{CC}^{(\beta)}$ . Equation 1.132 for MP2, Equations 1.150 and 1.151 for CCSD and Equations 1.158 and 1.159 provide the perturbed triples needed for CCSD(T). For CC methods, solve perturbed  $\Lambda$  equations, Equations 1.152 and 1.153.
- (c) Constructing the perturbed relaxed one-particle density matrix  $\partial D_{pq}/\partial\beta$ .
- (d) Adding MO contribution to  $\partial\Gamma_{pqrs}/\partial\beta$ . Transform perturbed  $\Gamma$  from MO to AO representation via Equation 1.121. Contract  $\partial\Gamma/\partial\beta$  with integral  $\partial\langle\mu\nu||\sigma\rho\rangle/\partial\alpha$ .
- (e) If not last perturbation  $\beta$ : calculating and storing  $\partial\langle\mu\nu||\sigma\rho\rangle/\partial\beta$  for next perturbation.

Part 3:

- 9. Transforming unperturbed  $\Gamma(pq,rs)$  from MO to AO representation using Equation 1.117.
- 10. Contracting relaxed one-particle density matrix,  $D_{\mu\nu}$ , with  $\partial^2 f_{\mu\nu}/\partial\alpha\partial\beta$  formed from second derivatives of one-electron integrals,  $\partial^2 h_{\mu\nu}/\partial\alpha\partial\beta$  and second derivatives of two-electron integrals,  $\partial^2\langle\mu\nu||\sigma\rho\rangle/\partial\alpha\partial\beta$ . Contract one-particle density matrix,  $I_{\mu\nu}$ , with the second derivatives of overlap integrals,  $\partial^2\langle\mu|\nu\rangle/\partial\alpha\partial\beta$ . Contract  $\Gamma_{\mu\nu\sigma\rho}$  with second derivatives of two-electron integrals.

The execution times of the algorithm described above ranges to calculate harmonic frequencies and infrared intensities for molecules like phenol ( $\text{C}_6\text{H}_5\text{OH}$ ) range from 2 hours for MP2/cc-pVDZ to 120 hours for CCSD(T)/



cc-pVDZ while finite difference methods of analytic gradients ranged from 4 hours MP2/cc-pVDZ for to 115 hours for CCSD(T)/cc-pVDZ<sup>27</sup>. Other properties such as NMR shieldings, polarizability, and magnetizability range from 10 minutes for MP2/cc-pVDZ to 12 hours for CCSD(T)/cc-pVDZ.

The algorithm's performance can be improved by a coarse-grained parallelization scheme to be described in Chapter 2. The use of analytic second derivatives in second-order vibrational perturbation theory (VPT2) and its application to spectroscopy is described in Chapter 3 and their application to predicting the vibrational spectrum of benzene and the structure and NMR spectrum of [10]annulene is described in Chapters 4 and 5.

---

<sup>27</sup>These calculation were run locally on a single Pentium 4 3.05 MHz processor with 2 GB of main memory and 134 GB local directly attached disk space.



## Chapter 2

# Coarse-Grained Scheme for Parallel Calculation of Post Hartree-Fock Analytic Second Derivatives

### 2.1 Rationale: Infrared Spectra and Other Observable Properties

The use of coupled-cluster methods to examine and assign spectra has been one of the major focus of quantum chemists [133, 134, 141, 221]. These studies determine either harmonic frequencies calculated from analytic second derivatives via the double harmonic approximation or second-order vibrational perturbation theory (VPT2). Most early techniques calculated second derivatives from finite differences of the energy at small displacements from the equilibrium structure. These methods scaled  $O(N^2)$  where  $N$  is the number of degrees of freedom of the molecule and often required tight convergence of the energy [33]. Developements by P. Pulay [177, 178] became the basis of analytic gradients and analytic second derivatives outlined in the previous chapter. At present, analytic derivatives are routinely used to optimize geometries, compute harmonic and fundamental frequencies, Raman and infrared intensities, NMR shieldings and determine thermal energies. See Table 1.2.

## 2.2 Current Parallelization of Quantum Chemistry Programs

To reduce execution times and increase the size of the system that can be studied, parallel tools such as Array Files (AF) [74], Global Arrays Toolkit (GA) [146, 147] Distributive Data Interface (DDI) [71] and super instruction assembly language (SIAL) [129] are being exploited by quantum chemistry programs like MOLPRO [225], NWChem [36], PQS [170], GAMESS [199] and ACESIII [129]. Early efforts to parallelize correlated methods focused on MP2 and devised effective parallelization of the MP2 energy [199, 206]. However, a desire for the greater accuracy provided by CCSD(T) has recently prompted the parallelization of coupled-cluster methods [21, 93, 102, 151].

Each quantum chemistry program mentioned has incorporated varying degrees of parallelization for calculating the CCSD and CCSD(T) energy; however, M. E. Harding *et al.* has made one of the only attempts to directly parallelize analytic gradients and second derivatives <sup>1</sup>. The parallel routines they implemented in the Mainz-Austin-Budapest version of the ACESII program package (ACESII MAB) [93, 212] focused on: the two electron integrals, SCF energy, CCSD particle-particle ladder term,

$$t_{ij}^{ab} D_{ij}^{ab} \leftarrow \frac{1}{2} \sum_{ef} \tau_{ij}^{ef} \langle ij || ef \rangle \quad (2.1)$$

coupled-cluster perturbative triples contribution, and matrix multiplication. For analytic gradients and second derivatives, they parallelized routines that

---

<sup>1</sup>Other programs determine derivatives primarily through finite difference techniques. Most of the programs (MOLPRO, PQS, NWChem and GAMESS) have implemented analytic gradients for MP2; only ACESIII has implemented analytic gradients for coupled-cluster methods. However, none of them have implemented analytic second derivatives.

computed the perturbed CCSD equations, perturbed  $\Lambda$  equations and  $\Lambda$  particle-particle ladders terms,

$$\frac{\partial t_{ij}^{ab}}{\partial \chi} D_{ij}^{ab} \leftarrow \frac{1}{2} \sum_{ef} \frac{\partial \tau_{ij}^{ef}}{\partial \chi} \langle ij || ef \rangle \quad (2.2)$$

$$\lambda_{ij}^{ab} D_{ij}^{ab} \leftarrow \frac{1}{2} \sum_{ef} \lambda_{ij}^{ef} \langle ef || ab \rangle \quad (2.3)$$

$$\frac{\partial \lambda_{ij}^{ab}}{\partial \chi} D_{ij}^{ab} \leftarrow \frac{1}{2} \sum_{ef} \frac{\partial \lambda_{ij}^{ef}}{\partial \chi} \langle ef || ab \rangle \quad (2.4)$$

and perturbed coupled-cluster perturbative triples contribution. These parallel routines perform best for calculations employing large basis sets.

### 2.3 Coarse Grained Parallelization of the Computation Analytic Second Derivatives

The parallelization of analytic gradients and second derivatives described in the previous section is primarily direct MPI based and focuses on individual terms in the coupled-cluster and  $\Lambda$  equations. However, a coarse-grained scheme suggested by J. Gauss and J. Stanton [77] replaces the loop over  $N$  perturbations described in Section 1.5.4 with the simultaneous calculation of each perturbation (See Figure 2.1). Distributing the perturbations over several different nodes divides the calculation in to three parts. In Part 1, the unperturbed energy and  $\Lambda$  equations are solved followed by the CPHF equations. In Part 2, the perturbed energy and  $\Lambda$  equations are solved. In Part 3, the contribution from each perturbation is added to the second derivative. To implement this scheme, the processors are grouped together if the number of perturbations is less than or equal to the number of processors available,  $N \leq P$ , and executed simultaneously. Or if  $N > P$  then the loop over  $N$

perturbation changes to a loop over  $N/P$  and  $P$  perturbations are calculated simultaneously. Also, the calculation of derivative integrals,  $\partial\langle\mu\nu||\sigma\rho\rangle/\partial\beta$ , is performed before being transformed from AO to MO representation for each perturbation.

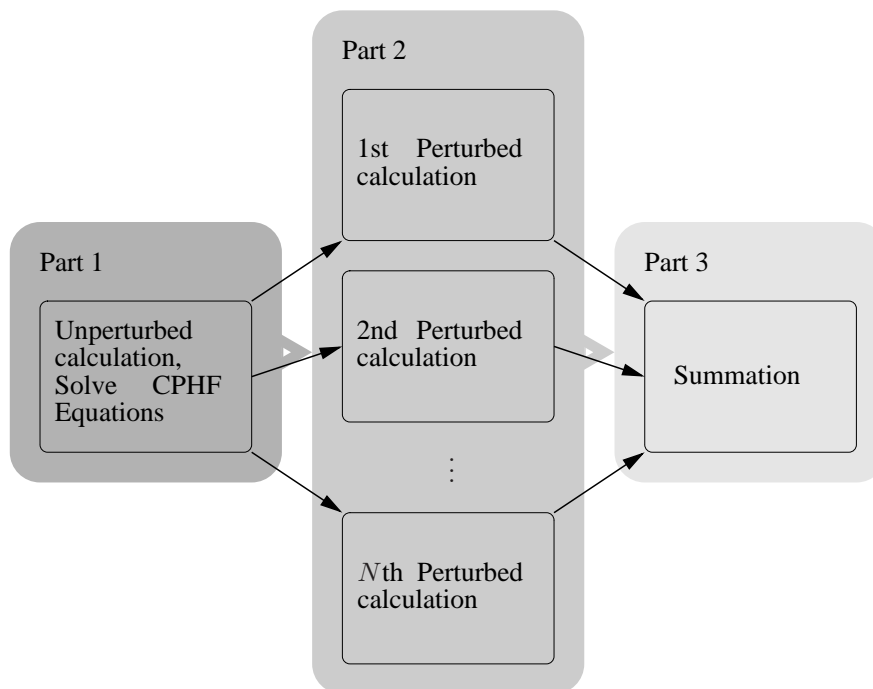


Figure 2.1: General parallel scheme for calculating analytic second derivatives for MP and CC methods. Based on the sequential algorithm outlined in the previous chapter. Part 1: Initial unperturbed calculation. Part 2:  $N$  perturbations, number in parenthesis. Part 3: Final summation.

The scheme will require little communication if  $N \geq P$  since the contribution of each perturbation can be calculated independently then broadcasted upon completion. Communication will be required if  $N < P$  to effectively

utilize the additional nodes. MPI Group communicators [153]<sup>2</sup> are created for each perturbation to handle communication of perturbed CCSD and  $\Lambda$  particle-particle ladder terms and perturbed triples contributions, and may be used in when parallel derivative integrals become available. Additionally, this scheme encompasses each MBPT and CC method where the analytic second derivatives have been implemented particularly the methods uneffected by the earlier parallelization.

## 2.4 Testing

The course grained parallel scheme was tested using three molecules: cyclopropenylidene ( $C_3H_2$ ), cyclopropane ( $C_3H_6$ ) and phenol ( $C_6H_5OH$ )<sup>3</sup>. Calculations of the analytic second derivatives for  $C_3H_2$  included: MP2/cc-pVXZ ( $X=D,T,Q$ ), CCSD/cc-pVXZ ( $X=D,T,Q$ ) and CCSD(T)/cc-pVXZ ( $X=D,T,Q$ ). For  $C_3H_6$ , the calculations included: MP2/cc-pVXZ ( $X=D,T$ ), CCSD/cc-pVXZ ( $X=D,T$ ), and CCSD(T)/cc-pVXZ ( $X=D,T$ ). And, calculations for  $C_6H_5OH$  included: MP2/cc-pVDZ, CCSD/cc-pVDZ and CCSD(T)/cc-pVDZ. Each calculation included all electrons in the correlation treatment. To test the effect of the symmetry on the scheme, the computational point groups  $D_{2h}$ ,  $D_2$ ,  $C_{2h}$ ,  $C_{2v}$ ,  $C_2$ ,  $C_i$ ,  $C_s$ , and  $C_1$  currently available in ACESII MAB were utilized for carbon dioxide  $CO_2$  using CCSD(T)/cc-pVTZ level of theory. An final test using sulfur dichloride,  $SCl_2$ , tested the effect of combining

---

<sup>2</sup>In parallel programs, a communicator contains information about the location of nodes or processors available to the program. The global communicator may be subdivided into groups to allow for communication within a group of processors.

<sup>3</sup>These three molecules were selected because the number of their vibrational and rotational degrees of freedom is a multiple of 12 and allowed for five different number of processors (1,2,4,6,12) to be used.

the coarse grained parallelization scheme with the current parallelization using CCSD(T)/cc-pVQZ(or pVTZ) and upto 12/24 processors. The geometries used in these calculations were optimized for the particular level of theory and basis set using analytic gradients. These calculations were run on Lonestar cluster, a Dell dual-core Linux server, located at Texas Advanced Computing Center consisting of 1300 nodes each equipped with 2 Xeon 5100 series 2.66 GHz dual-core processors, 8 GB of main memory and 73 GB of local directly attached disk space. For communication, Infiniband switch with 1 GB/s P-2-P bandwidth capacity is used.

## 2.5 Performance

To evaluate the performance of the coarse grained parallel scheme, the timings and speed ups will be compared to the current version of ACESII MAB. The effects of method type, basis set size, system size and symmetry will also be discussed with factors effecting the scalability such as the sequential fraction will be estimated and compared.

### 2.5.1 Performance Metrics: Speed up and Sequential Fraction

To evaluate the performance of a parallel program, the speed up is the most common measure of performance. To determine the speed up,  $S$ , from the timing:

$$S(P) = \frac{T(1)}{T(P)} \quad (2.5)$$

is used where  $T(1)$  is the time required for the optimized serial version of the program to be executed and  $T(P)$  is the execution time of the parallel ver-



sion of the program <sup>4</sup>. Ideally, a program scales linearly -  $S = P$  - allowing each processor added to be effectively utilized. However, if some of the routines remain sequential, the speed up diminishes as more processors are added resulting in poor scalability.

Two factors reduce scalability: communication - information passed between processors - and sequential fraction - the portion of the program that is redundantly executed on each processor. For example, the CPHF calculation is not directly parallelized so the same calculation is executed simultaneously on each processor. To estimate the sequential fraction, one assumes using Amdahl's law that all communication is simultaneous [8]. Then, the speed up,  $S(P)$ , may be written as:

$$S(P) = \frac{P}{(P-1)Z + 1} \quad (2.6)$$

where  $Z$  is the sequential fraction of the parallel program. The impact of the sequential fraction can be seen in the following example. If a program has a sequential fraction as little as .01 (99% parallel), then its speed up according to Equation 2.6 will be 24 when 32 processors are used but only 39 when 64 processors are used. Since the sequential fraction provides a good indicator for the scalability of a parallel program, it may be estimated by writing Equation 2.6 as a linear function:

$$\frac{1}{S} = (1 - Z)\frac{1}{P} + Z \quad (2.7)$$

---

<sup>4</sup>Technical limitations of Lonestar's parallel environment systematically added several minutes to distribute files to each node. Due to this significant difference in the system time for parallel verse serial,  $T(1)$  corresponds to the parallel version on one processor instead of the serial code. Also, for  $\text{C}_3\text{H}_6$  CCSD(T)/cc-pVTZ and  $\text{C}_6\text{H}_5\text{OH}$  CCSD(T)/cc-pVDZ tests, the calculation could not be completed in the 12 hour time limit for serial calculations so  $2T(2)$  was used instead to determine  $S(P)$ .

Table 2.1: Comparison of execution times (s) of current parallelization versus coarse grained scheme for harmonic frequency calculations using analytic second derivatives. **Part 1**: Initial unperturbed calculation. **Part 2**:  $N$  perturbations. **Part 3**: Final summation. Numbers in parenthesis are the number of perturbations treated and the number of basis functions.

$P$	Current			New		
	Part 1	Part 2	Part 3	Part 1	Part 2	Part 3
<b>C<sub>3</sub>H<sub>2</sub> CCSD(T)/cc-pVQZ (12, 225)</b>						
2	1366	21709	1373	1464	17898	1354
4	1155	16663	1364	1286	9118	1376
6	1076	14943	1368	1232	6129	1373
12	1000	13365	1376	1178	3091	1366
<b>C<sub>3</sub>H<sub>6</sub> CCSD(T)/cc-pVTZ (24, 174)</b>						
2	518	22186	476	563	19810	482
4	441	15603	479	474	10390	488
6	465	15162	485	453	7029	487
8	393	12460	484	433	5440	493
12	375	11447	483	421	3951	486
<b>C<sub>6</sub>H<sub>5</sub>OH CCSD(T)/cc-pVDZ (36, 128)</b>						
2	1667	114337	564	1704	99320	578
4	1132	71610	570	1177	52077	584
6	962	57835	577	1002	31032	593
12				824	17375	595

The sequential fraction,  $Z$ , may then be estimated from a linear least squares fit of  $1/P$  verses  $1/S$  and an average value,  $\bar{Z}$ , may be obtained from the slope and intercept.

### 2.5.2 Comparison to Current Parallelization

For comparison of the coarse grained scheme with the current parallelization, the overall execution time - the time ACESII MAB required to

complete the calculation and the system time needed to copy files to and from each nodes - is divided into four parts: System, Part 1 (time required for unperturbed calculation), Part 2 (time required to complete  $N$  perturbations) and Part 3 (time required for final summation). The execution times of three cases are tabulated in Table 2.1 while the remaining execution times are included in Appendix A. On average, the system time on Lonestar accounted for an average of 310 s of execution time<sup>5</sup>. The final summation (Part 3 of Table 2.1) accounts for as much as 9% of the total execution time in the calculation using the existing parallelization of ACESII MAB for  $C_3H_2$ ; however, for the larger systems included in Table 2.1 it accounts for 3% or less of the execution time. As a result, little direct parallelization has been incorporated into the routines, and the time required for the final summation lacks any speed up making it roughly the same regardless of how many processors are utilized. Each perturbation in Part 2 requires all the integrals computed in Part 1 to execute independently. As a result, each node computes and stores them locally allowing the initial unperturbed calculation to execute slightly faster using the existing parallelization as indicated in Table 2.1.

In Figure 2.2, the 24 perturbations in Part 2 used the majority of the time ACESII MAB required to calculate the harmonic frequencies of  $C_3H_6$  using CCSD(T)/cc-pVTZ and is echoed by Table 2.1 for  $C_3H_2$  and  $C_6H_5OH$ . The time needed for the current parallelization ACESII MAB decreased steadily as more processors were added; however, the overall speed ups, listed in Table 2.2 remains below 4 for even when 12 processors are used. The new parallel scheme required slightly less computer time using 2 processors. The time for

---

<sup>5</sup>In shorter calculations, it accounts for more than 70% of the execution time. In longer calculations, it accounts for less than 0.5%.

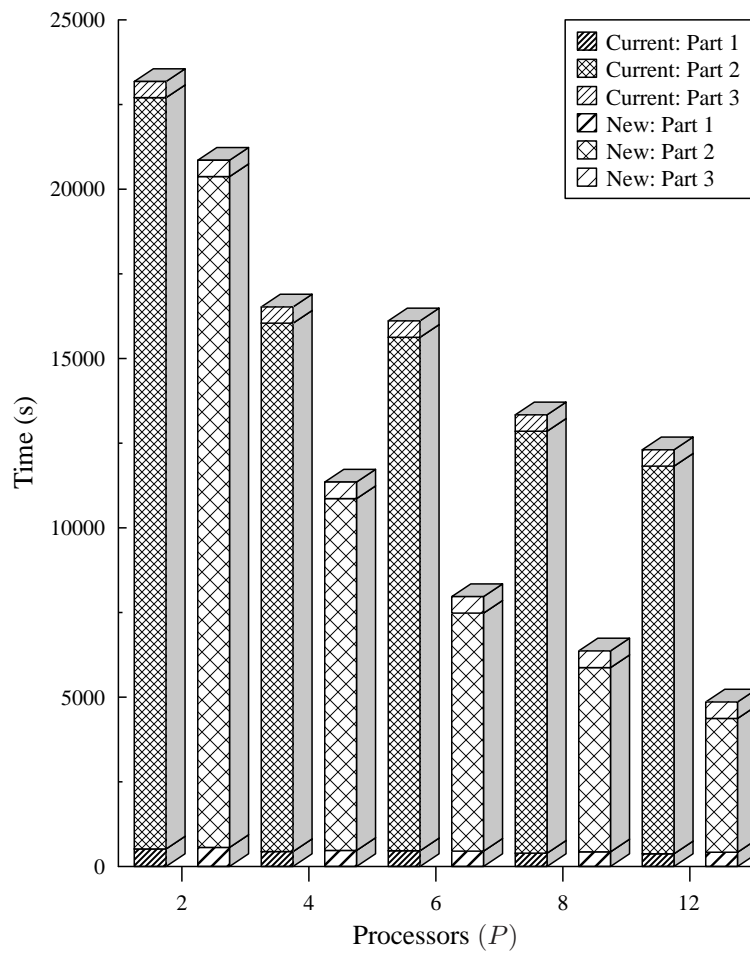


Figure 2.2: Timing of current parallelization versus coarsened grain scheme for  $C_3H_6$  CCSD(T)/cc-pVTZ. Part 1: Initial unperturbed calculation. Part 2: 24 perturbations. Part 3: Final summation.

Table 2.2: Comparison of speed up and sequential fraction ( $\bar{Z}$ ) for the current parallelization versus the coarse grained scheme for harmonic frequency calculations using analytic second derivatives. Part 2:  $N$  perturbations, given in parenthesis.

$P$	Overall		Part 2	
	Current	New	Current	New
<b>C<sub>3</sub>H<sub>2</sub> CCSD(T)/cc-pVQZ (12)</b>				
2	2.0	2.0	2.0	2.0
4	2.5	3.5	2.6	3.9
6	2.8	4.7	2.9	5.8
12	3.1	7.0	3.3	11.6
$\bar{Z}$	0.4	0.1	0.4	0.01
<b>C<sub>3</sub>H<sub>6</sub> CCSD(T)/cc-pVTZ (24)</b>				
2	2.0	2.0	2.0	2.0
4	2.2	3.6	2.2	3.8
6	2.7	5.1	2.7	5.6
8	3.1	6.4	3.1	7.3
12	3.4	8.2	3.5	10.0
$\bar{Z}$	0.4	0.1	0.4	0.04
<b>C<sub>6</sub>H<sub>5</sub>OH CCSD(T)/cc-pVDZ (36)</b>				
2	2.0	2.0	2.0	2.0
4	3.2	3.8	3.2	3.8
6	3.9	6.2	4.0	6.4
12	...	10.7	...	11.4
$\bar{Z}$	0.2	0.01	0.2	0.01

Part 2 decreased almost 50% when 4 processors were used and the overall speed up increased to more than 8 when 12 processors were used (Figure 2.2).

The overall speed up of the coarse grained scheme is almost twice that of the current parallelization as seen in Table 2.2 and Figure 2.3. For the current parallelization, the overall speed up is roughly the same as the speed up for Part 2. The best scaling for the current parallelization is achieved

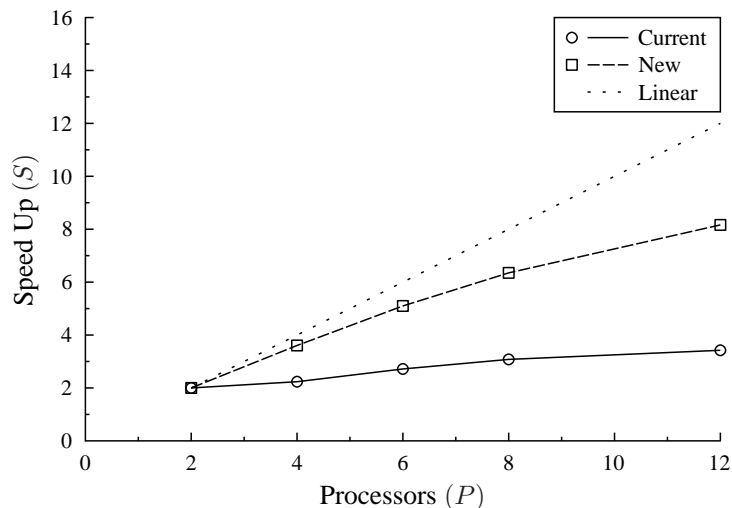


Figure 2.3: Comparison of the overall speed up of ACESII MAB Current parallelization versus the coarse grained scheme for  $C_3H_6$  using CCSD(T)/cc-pVTZ.

for the largest molecule  $C_6H_5OH$  with a speed up of almost 4. However, the overall speed ups of  $C_3H_6$  and  $C_3H_2$  with 12 processors are both smaller than the speed up achieved with the coarse grained scheme with 4 processors. Unlike the current parallelization, the speed up of Part 2 of the coarsened grain scheme improved by as much as 3.5 compared to the scheme's overall speed up demonstrating the effect of the scheme's parallelization. Also, superlinear speed up, when  $S > P$ , is achieved in one case  $C_6H_5OH$  CCSD(T)/cc-pVDZ with 6 processors. However, this speed up seems fortuitous and is not reflected in the speed ups using 4 and 12 processors for the same calculation. However, ideal linear scaling of Part 2 is not achieved and the factors which effect scaling will be discussed in a subsequent section.

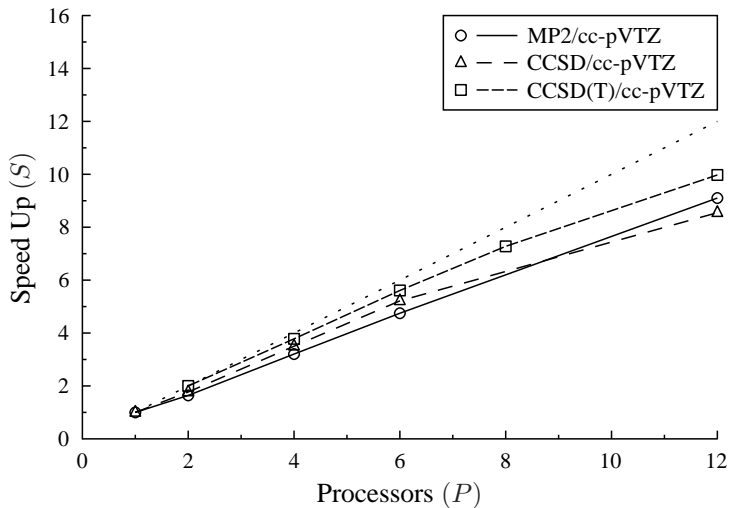


Figure 2.4: Comparison of the speed up of Part 2 using different methods: MP2, CCSD, and CCSD(T) with cc-pVTZ basis set for  $C_3H_6$ .

### 2.5.3 Other Comparisons

One feature of the coarse grained scheme is it may be utilized by any quantum chemical method including electron correlation if the analytic second derivatives are available including many-body methods which presently lacks direct parallelization in ACESII MAB. The overall speed up for MP2 calculations is less than 2 for smaller molecules with small basis sets<sup>6</sup> and more than 5 for larger molecules; however, the speed up of Part 2 increased to between 7 and 11 for 12 processors. Any increase in performance is provided by the coarse grained scheme as MP2 lacks of direct parallelization in ACESII MAB. Thus, no direct comparison between the current scheme and coarse grained

---

<sup>6</sup>Most of the execution time in these cases is spent copying files.

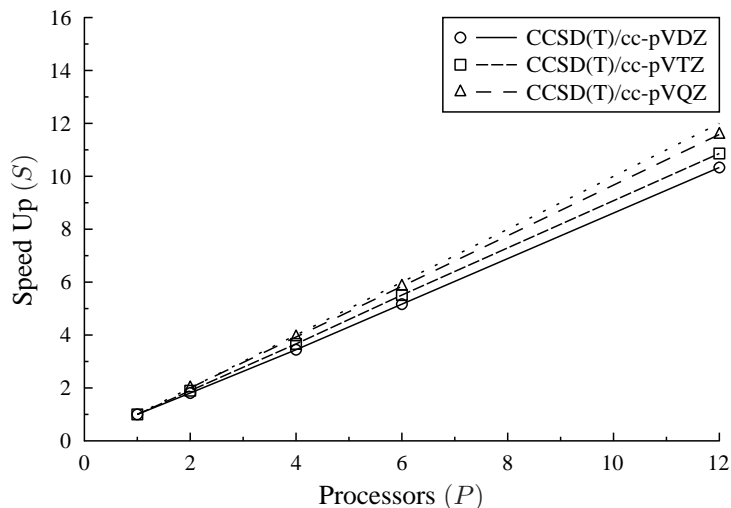


Figure 2.5: Comparison of the speed up of Part 2 using different basis sets in the correlation consistent Dunning series cc-pVXZ ( $X = D, T$  and  $Q$ ) which contain 52, 118 and 225 basis functions for  $C_3H_2$  using CCSD(T).

parallelization could be made.

The speed up for Part 2, illustrated in Figure 2.4, is between 8 and 10 for each method tested (MP2, CCSD, and CCSD(T)) when 12 processors are utilized. CC methods is lower than MP2 due to the time used to solve the perturbed CCSD and  $\Lambda$  equations while computing the derivative integrals required the majority of the time used by MP2.

The speed up of the scheme also did not vary significantly due to the size of the basis set. It remained between 4.8 and 5.8 using 6 processors and 7.9 and 11.6 using 12 processors for  $C_3H_2$  and deviated slightly from linear speed up as shown in Figure 2.5 for CCSD. The overall speed up did improve as the size of the basis set increased since a larger fraction of the time is needed



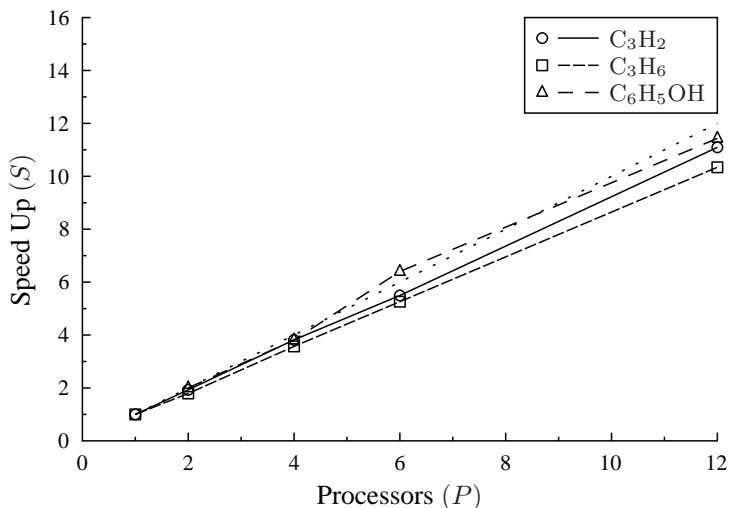


Figure 2.6: Comparison of the speed up of Part 2 using different molecular sizes:  $C_3H_2$ ,  $C_3H_6$  and  $C_6H_5OH$  using CCSD(T)/cc-pVDZ.

to compute the perturbations relative to the system time and unperturbed calculations. The improvements are small for MP2 (from 1.2 for cc-pVDZ to 3.3 for cc-pVQZ using 12 processors) and CCSD (from 1.6 for cc-pVDZ to 4.8 also using 12 processors), but larger for CCSD(T) (1.7 for cc-pVDZ to 7.0 for cc-pVQZ using 12 processors).

Increasing the size of the molecule also did not significantly effect the speed up of the scheme as seen in Figure 2.6. The speed up for 12 processors is between 7.9 and 11.7 for  $C_3H_2$ ,  $C_3H_6$  and  $C_6H_5OH$  whether MP2, CCSD or CCSD(T) is used with cc-pVDZ basis set. The overall speed up did improve as the size of the molecule increased. As with increasing the size of the basis set, the fraction of time needed to compute the perturbations increased (.6 for  $C_3H_2$  CCSD(T)/cc-pVDZ to 1.0 for  $C_6H_5OH$  CCSD(T)/cc-pVDZ). The

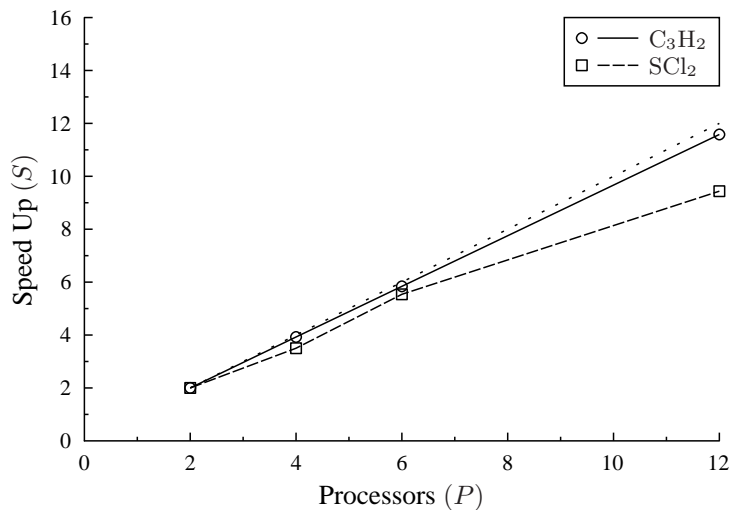


Figure 2.7: Comparison of the speed up of Part 2 of the coarse grained scheme combined with the current parallelization:  $SCl_2$  and  $C_3H_2$  using CCSD(T)/cc-pVQZ.

improvements are larger than the improvements noted increasing the size of the basis set in each case. The speed up for MP2 increased from 1.2 for  $C_3H_2$  to 5.4 for  $C_6H_5OH$  with 12 processors while it increased from 1.6 to 9.8 for CCSD and from 1.7 to 10.7 for CCSD(T).

However, the speed up of Part 2 declines when the number of processors ( $P$ ) exceeds the number of perturbations ( $N$ ) as seen in Figure 2.7. In the case of  $SCl_2$ , once two processors are assigned to each perturbation (when  $P = 12$ ), the speed up of the scheme dropped by 2.1 in comparison to  $C_3H_2$  while the speed up for  $P$  equaling four or six remained similar with a difference of 0.4 or less.

#### 2.5.4 Scalability

The estimated sequential fractions included in Table 2.2 indicate that almost 20% of ACESII MAB is not directly parallelized. One result is poor scalability - modest gains in speed up as more processors are utilized - for some systems. As noted earlier, the overall speed up for the existing parallelization is less than 4 even when 12 processors are used.

The coarse grained scheme decreased the sequential fraction to less than 5% for Part 2 and as a result the overall speed up is over 10 for  $\text{C}_6\text{H}_5\text{OH}$  CCSD(T)/cc-pVDZ with 12 processors. However, the scheme's performance is limited by the number of processors that are factors of the degrees of rotational and vibrational freedom of the molecule. Once the number of processors exceeds the degrees of rotational and vibrational freedom, the increases in performance came from the parallel methods currently included in ACESII MAB.

The primary factor that effects the sequential fraction of the coarse grained parallelization scheme is load balance. The direct methods currently implemented fall into the single data single instruction (SDSI) class of parallelization [72]. By contrast, the scheme used to compute analytic second derivatives belongs to the multiple data single instructions (MDSI) class of parallelization where the same set of instructions are used on  $N$  sets of data. Unlike methods that directly parallelize parts of routines found to require the most computer time whose performance is limited by communication and degree of parallelization, this scheme does not require intermediate communication during processors during Part 2 provided the number of processors used is a factor of the number of perturbations computed <sup>7</sup>. If each pertur-

---

<sup>7</sup>If the number of processors does not correspond to a factor of the perturbations, then some of the performance will be dictated by the direct parallelization currently available.

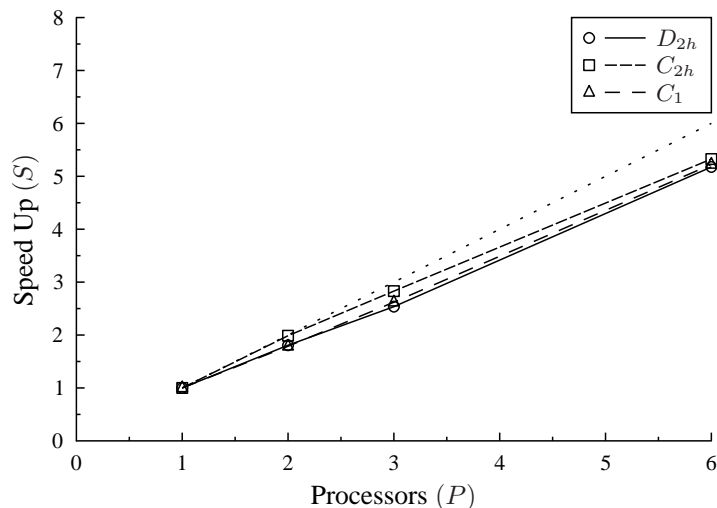


Figure 2.8: Comparison of the speed up of Part 2 using different point groups:  $D_{2h}$ ,  $C_{2h}$  and  $C_1$  for  $\text{CO}_2$  CCSD(T)/cc-pVTZ.

bation required the same execution time, the scheme would scale linearly up to the number of perturbations. However, each perturbation corresponds to a different set of data. Although the terms needed by a processor may be the same for MP2 (See Chapter 1), the time required to evaluate them may vary. For coupled cluster methods, the perturbed coupled-cluster and  $\Lambda$  equations are solved iteratively and may also require differing numbers of iterations to converge. For example,  $\text{C}_3\text{H}_2$  CCSD(T)/cc-pVTZ required between 12 and 18 iterations for the perturbed  $t$  amplitudes and  $\Lambda$  equations to converged to within the desired interval amounting to a difference of almost 200 seconds of computer time<sup>8</sup>. As a result, linear scaling is not achieved.

---

<sup>8</sup>This calculation was executed without using symmetry.

In addition, employing symmetry has been a key for decreasing execution time [81]. For instance, the CCSD(T)/cc-pVQZ energy of CO<sub>2</sub> is computed using  $D_{2h}$  point group (the highest subgroup available in ACESII MAB), the calculation is completed in roughly 1/20 of the time if no symmetry is used. Employing symmetry, groups the perturbations into blocks that require roughly the same computer time; however, the execution times for different symmetry blocks vary and differ by a maximum of 46 seconds for C<sub>3</sub>H<sub>2</sub> CCSD(T)/cc-pVTZ. The difference is more significant for C<sub>3</sub>H<sub>2</sub> CCSD(T)/cc-pVTZ which differs by a maximum of 1088 seconds. Reducing or removing the symmetry removes this variation. But, symmetry also did not alter the speed up as shown in Figure 2.8 and did not effect the effectiveness of the scheme. The speed up for  $D_{2h}$  (5.2) and  $C_1$  (5.2) are roughly the same for CO<sub>2</sub> CCSD(T)/cc-pVTZ using 6 processors.

## 2.6 Summary

The coarse grained parallelization scheme allows for parallel computation of analytic second derivatives for a variety of post Hartree-Fock methods (MP2, MP3, MP4, CC2, CCD, QCISD, CCSD, QCISD(T), CCSD(T), CCSDT-n (n=1-4), CC3, and CCSDT). Comparing it to the current parallelization of ACESII MAB leads to the following conclusions:

1. It achieved significantly better speed ups (See Table 2.2. In the cases compared, the speed up of 12 processors using the current parallelization did not exceed the speed up of 4 processors using this scheme.
2. Testing of MP2, CCSD and CCSD(T) showed this scheme provides roughly the same speed up of Part 2 for each of these methods although

the overall speed up of these methods depends on the fraction of execution time required by Parts 1 and 3.

3. However, when the coarse grained scheme is combined with the current parallelization if  $P > N$ , the gain in speed up decreases, but it is still higher than the speed up of the current parallelization and allows the calculation of harmonic frequencies for fairly extended systems such as benzene and [10]annulene (see Chapters 4 and 5).
4. Similar speed ups occur for different basis sets and system sizes.
5. The speed ups were not adversely effected by symmetry.
6. The overall sequential fraction suggests this scheme is suited for up to 12 processors provided the number of processors is an integer multiple of the number of perturbations.

## Chapter 3

# Vibrational Spectroscopy and Second-Order Vibrational Perturbation Theory

The goal of this chapter is to illustrate how the analytic second derivatives described in the preceding chapters are connected to vibrational spectroscopy. Specifically, the following sections will focus on numerical methods for predicting vibrational frequencies for one quantum and several quantum transitions under the harmonic and anharmonic approximations. Different methods will be presented and compared with especial emphasis on vibrational perturbation theory (VPT).

### 3.1 Systems of Harmonic Oscillators

In the simplest approach, the atoms in a molecule behave as a system of harmonic oscillators [38, 228]<sup>1</sup>. In classical mechanics, a system of harmonic oscillators can be described by the equations of motion:

$$m_i \ddot{\xi}_i + \sum_j k_{ij} \xi_j = 0 \quad (3.1)$$

In this description,  $\xi_i$  represents a small displacement from the equilibrium configuration of the system,  $m_i$ , with  $k_{ij}$  represents the restoring forces ( $k_{ij} =$

---

<sup>1</sup>A system of  $N$  atoms has  $3N$  degrees of freedom: 3 correspond to translational motion, 3 (2 for linear molecules) correspond to rotational motion and the remaining  $3N - 6$  ( $3N - 5$  for linear molecules) correspond to vibrational motion.

$\partial^2 V / \partial \xi_i \partial \xi_j$ ) due to the potential  $V$ . Equation 3.1 may be simplified using mass weighted coordinates:  $s_i = m_i^{\frac{1}{2}} \xi_i$ , and becomes:

$$\ddot{s}_i + \sum f_{ij} s_j = 0 \quad (3.2)$$

where  $f_{ij} = \partial^2 V / \partial s_i \partial s_j$ . There exists a solution to Equation 3.2, defined as:  $s_i = a_i e^{i(\omega t - \delta)}$  where  $a_i$  is the maximum displacement of  $m_i$  (its amplitude of oscillation) and  $\delta$  is the phase of its oscillation. Accordingly, Equation 3.2 can be written as:

$$-\omega^2 m_i a_i + \sum_j f_{ij} a_j = 0. \quad (3.3)$$

For a system of harmonic oscillators, there exists a set of  $\omega$ 's that satisfies Equation 3.3, where  $\omega^2$  is a characteristic or eigenvalue <sup>2</sup>. There also exists an eigenvector,  $\mathbf{l}_i$ , associated with each  $\omega_i^2$  that describes the size of the displacement of  $m_i$  relative to the other displacements. The set of eigenvectors can then be used to form the normal coordinate,  $Q_i = \sum_j l_{ij} s_j$ , such that Equation 3.2 becomes [38, 228]:

$$\ddot{Q}_i - \omega_i^2 Q_i = 0. \quad (3.4)$$

Alternatively, the kinetic ( $T$ ) and potential ( $V$ ) energies may be expressed in terms of  $s_i$ :

$$T = \frac{1}{2} \sum_i \dot{s}_i^2 = \frac{1}{2} \sum_i p_i^2 \quad (3.5)$$

and

$$V = \frac{1}{2} \sum_{i,j} f_{ij} s_i s_j \quad (3.6)$$

---

<sup>2</sup>In a physical sense, the root of a particular eigenvalue corresponds to the frequency of a particular oscillation of the system.



and a LaGrangian treatment of  $T$  and  $V$  yields Equation 3.2. Then, the kinetic and potential energy may be expressed in terms of normal coordinates:

$$T = \frac{1}{2} \sum_i \dot{Q}_i^2 = \frac{1}{2} \sum_i P_i^2 \quad (3.7)$$

and

$$V = \frac{1}{2} \sum_i \omega_i^2 Q_i^2. \quad (3.8)$$

In the classical treatment, the force constants,  $k_{ij}$  or  $\mathbf{K}$ , may be first transformed to mass weighted Cartesian coordinates  $\mathbf{F}$  by a diagonal matrix  $\mathbf{M}$  whose elements are the mass of the system [38]:

$$\mathbf{F} = \mathbf{M}^{1/2} \mathbf{K} \mathbf{M}^{1/2}. \quad (3.9)$$

Then,  $\mathbf{F}$  transformed to normal coordinates using the set of eigenvectors  $\mathbf{L}$  such that  $\mathbf{L}^t \mathbf{F} \mathbf{L} = \mathbf{\Lambda}$ , where  $\mathbf{\Lambda}$  is the set of eigenvalues.

In quantum mechanics, the equation of motion of a harmonic potential energy surface replaces the normal coordinate describing the displacements,  $Q_i$ , in  $\ddot{Q}_i - \omega_i^2 Q_i = 0$  with the wavefunction  $|\phi_v(Q_i)\rangle$  in the Schrödinger equation [38, 202, 228]:

$$\hat{H}_{vib} |\psi_v(Q_i)\rangle = E_v |\psi_v(Q_i)\rangle, \quad (3.10)$$

where the quantum mechanical vibrational Hamiltonian operator,  $\hat{H}$ , is obtained from the classical Hamiltonian function in terms of the normal coordinates,  $Q_i$ :

$$\hat{H} = \hat{T} + \hat{V} = \frac{1}{2} \sum_i \left( \hat{P}_i^2 + \lambda_i Q_i^2 \right). \quad (3.11)$$

Here, the eigenvalues,  $\lambda_i$  (or the vibrational frequencies,  $\omega_i$ ), and normal modes,  $Q_i$ , of the system are determined by transforming the force constant

matrix  $\mathbf{K}$ , or Hessian:

$$\mathbf{K} = \begin{pmatrix} \frac{\partial^2 E}{\partial \xi_1^2} & \frac{\partial^2 E}{\partial \xi_1 \xi_2} & \cdots & \frac{\partial^2 E}{\partial \xi_1 \xi_N} \\ \frac{\partial^2 E}{\partial \xi_2 \xi_1} & \frac{\partial^2 E}{\partial \xi_2^2} & \cdots & \frac{\partial^2 E}{\partial \xi_2 \xi_N} \\ \vdots & \vdots & \ddots & \vdots \\ \frac{\partial^2 E}{\partial \xi_N \xi_1} & \frac{\partial^2 E}{\partial \xi_N \xi_2} & \cdots & \frac{\partial^2 E}{\partial \xi_N^2} \end{pmatrix}, \quad (3.12)$$

where  $\xi_i$  represents Cartesian displacements of an atom in a molecule and may be calculated analytically using the methods described in Chapters 1 and 2, as outlined above.

The wavefunctions,  $|\psi_v(Q_i)\rangle$  or  $|v\rangle$ , that satisfies Equation 3.11 are the product of the  $v$ th order Hermite polynomials,  $H_v$ , a Gaussian function and a normalization constant,  $N_v$ :

$$|\psi_v(\xi)\rangle = N_v H_v(\alpha_i^{\frac{1}{2}} Q_i) e^{-\alpha_i Q^2}, \quad (3.13)$$

where

$$\alpha_i = \frac{2\pi c\omega_i}{\hbar}. \quad (3.14)$$

The corresponding energy of the vibrational state  $v_i$  becomes:

$$E_{v_i} = \hbar\omega \left( v_i + \frac{1}{2} \right) \quad (3.15)$$

and transitions between energy levels of a particular normal mode is defined by:

$$\Delta E = \hbar\omega_i. \quad (3.16)$$

For transitions to occur, the system absorbs energy, often in the form of electromagnetic radiation. This energy can be treated as a time dependent electric field:  $\mathbf{E} = \mathbf{E}_0 \cos 2\pi\omega t$ , that interacts with the molecule. This interaction is incorporated into the Hamiltonian by the time dependent term:

$\boldsymbol{\mu} \cdot \mathbf{E}_0 \cos 2\pi\omega t$  where  $\boldsymbol{\mu}$  is the dipole moment of the molecule. For transitions between vibrational states to occur, the transition moment,  $\langle v+n|\boldsymbol{\mu}(Q_i)|v\rangle$ , must be nonzero<sup>3</sup>. For a first order expansion of the dipole moment:

$$\boldsymbol{\mu}(Q_i) = \boldsymbol{\mu}_0 + \left. \frac{\partial \boldsymbol{\mu}}{\partial Q_i} \right|_{Q_i=0} Q_i, \quad (3.17)$$

the transition moment becomes:

$$\langle v+n|\boldsymbol{\mu}(Q_i)|v\rangle = \boldsymbol{\mu}_0 \langle v+n|v\rangle + \left. \frac{\partial \boldsymbol{\mu}}{\partial Q_i} \right|_{Q_i=0} \langle v+n|Q_i|v\rangle. \quad (3.18)$$

For  $v+n \leftarrow v$  (transition from state  $v$  to  $v+n$ ) to occur,  $\langle v+n|Q_i|v\rangle \neq 0$ <sup>4</sup>. This integral is only nonzero when  $n = \pm 1$ , and only transitions between adjoining states can occur:  $\Delta v = \pm 1$  (the selection rule for harmonic oscillators).

### 3.2 Limitations of the Harmonic Approximation

The harmonic oscillator approximation's predictions<sup>5</sup> are on average less than 5 % different from the experimental vibrational frequencies for the fundamental transition  $1 \leftarrow 0$  and vary between 0 and 16 % different.

Despite this proximity to experiment, the vibrational potential energy surface of a molecule is not adequately described by a quadratic potential ( $V =$

---

<sup>3</sup>This conclusion is reached from time dependent perturbation theory which is typically discussed in textbooks on quantum mechanics and physical chemistry.

<sup>4</sup>The orthonormality of the set of wavefunctions satisfying Equation 3.10 insures that the first integral in Equation 3.18 vanishes for transitions between two states.

<sup>5</sup>The harmonic frequencies of a set of small molecules - hydrogen ( $\text{H}_2$ ), methane ( $\text{CH}_4$ ), acetylene ( $\text{C}_2\text{H}_2$ ), ethylene ( $\text{C}_2\text{H}_4$ ), formaldehyde ( $\text{H}_2\text{CO}$ ), carbon monoxide ( $\text{CO}$ ), carbon dioxide ( $\text{CO}_2$ ), ammonia ( $\text{NH}_3$ ), hydrogen cyanide ( $\text{HCN}$ ), nitrogen ( $\text{N}_2$ ), water ( $\text{H}_2\text{O}$ ), ozone ( $\text{O}_3$ ), hydrogen fluoride ( $\text{HF}$ ) and fluorine ( $\text{F}_2$ ) - were calculated for comparison to the experimental vibrational frequencies using analytic second derivatives at CCSD(T) level of theory using cc-pVQZ(ae) and ANO2(ae) basis sets at geometries optimized using analytic gradients at the same level of theory for the same basis set using ACESII MAB.

$\frac{1}{2} \sum_i \omega_i^2 Q_i^2$ . Bonds between atoms may break<sup>6</sup>, torsion and bending barriers are finite allowing molecules to change conformations<sup>7</sup> and vibrational states may be coupled. These changes to the potential energy surface alter the spacing of vibrational energy levels, vary the energy needed for transitions between adjacent levels and allow overtone and combination bands (i.e. transitions where  $n \neq \pm 1$ ).

### 3.3 Second-Order Vibrational Perturbation Theory

To improve the agreement with experiment, several theoretical approaches have been devised: vibrational self-consistent field (VSCF) [30, 42, 43, 186] and correlated methods (VCI [31, 47, 48], VMPn [46, 47, 105, 148], VCC [48]), quantum Monte Carlo (QMC) [25, 176] and vibrational perturbation theory (VPT) [144]. This section will focus on describing vibrational perturbation theory using Rayleigh-Schrödinger perturbation theory which will be used in Chapter 4. Other perturbative approaches have been used for vibrational problem, such as: canonical van Vleck method (or contact transformation) [142, 155], but only the Rayleigh-Schrödinger approach to VPT2 will be described here. The other theoretical approaches will be described in the next section and compared to VPT2.

---

<sup>6</sup>The dissociation energy,  $D_e$  is between 8 and 42 times the harmonic frequencies for the diatomics considered ( $\text{H}_2$ ,  $\text{CO}$ ,  $\text{N}_2$ ,  $\text{HF}$  and  $\text{F}_2$ ) using CCSD(T)/cc-pVQZ.

<sup>7</sup>For instance, ammonia's umbrella bending mode  $\nu_2(a_1)$  may transition through a planar conformation and the torsion mode  $\omega_{12}(a_{1u})$  of  $\text{C}_2\text{H}_6(D_{3d})$  may transition through a  $D_{3d}$  conformation. The heights of these barriers are  $1958.0 \text{ cm}^{-1}$  for  $\text{NH}_3$  and  $958.9 \text{ cm}^{-1}$  for  $\text{C}_2\text{H}_6$  while the harmonic frequencies of these ground states are  $1081.8$  and  $309.4 \text{ cm}^{-1}$  respectively using CCSD(T)/cc-pVQZ.

Given the nuclear Schrödinger equation for vibrational motion, i.e.:

$$\hat{H}_{vib}|\psi_v\rangle = E_v|\psi_v\rangle \quad (3.19)$$

where  $\hat{H}_{vib}$  is the Hamiltonian describing the motion of the nuclei,  $|\psi_v\rangle$  is the wavefunction of state  $v$  and  $E_v$  is its energy.

According to Rayleigh-Schrödinger perturbation theory the nuclear Hamiltonian can be expanded as a series in terms of a perturbation parameter  $\lambda$ :

$$\hat{H} = \hat{H}_0 + \lambda\hat{H}_1 + \lambda^2\hat{H}_2 + \lambda^3\hat{H}_3 + \dots \quad (3.20)$$

where  $\hat{H}_1$ ,  $\hat{H}_2$ ,  $\hat{H}_3$ , ... are small first-order, second-order, third-order perturbations of the unperturbed Hamiltonian  $\hat{H}_0$ . Similarly, the vibrational energy can be written in terms of  $\lambda$  as:

$$E_i = E_i^{(0)} + \lambda E_i^{(1)} + \lambda^2 E_i^{(2)} + \lambda^3 E_i^{(3)} + \dots \quad (3.21)$$

where  $E_i^{(1)}$ ,  $E_i^{(2)}$ , ... are first-order and second-order corrections to the reference energy. If the nuclear Hamiltonian expansion, Equation 3.20, and the energy expansion, Equation 3.21, are substituted into the nuclear Schrödinger equation, Equation 3.19, expressions for these energy corrections are obtained:

$$E_i^{(1)} = \langle\psi_i|\hat{H}_1|\psi_i\rangle, \quad (3.22)$$

$$E_i^{(2)} = \sum_j \frac{\langle\psi_i|\hat{H}_1|\psi_j\rangle\langle\psi_j|\hat{H}_1|\psi_i\rangle}{E_i^{(0)} - E_j^{(0)}} + \langle\psi_i|\hat{H}_2|\psi_i\rangle, \quad (3.23)$$

etc. where  $|\psi_i\rangle$  and  $|\psi_j\rangle$  are wave functions of the unperturbed Hamiltonian,  $\hat{H}_0$ .

In VPT, the Hamiltonian<sup>8</sup> describing the small amplitude vibrational nuclear motion has the form [222]:

$$\frac{\hat{H}_{vib}}{\hbar c} = \frac{\hbar^2}{2\hbar c} \sum_{\alpha\beta} \mu_{\alpha\beta} \hat{\pi}_\alpha \hat{\pi}_\beta + \frac{1}{2} \sum_i \omega_i \hat{p}_i^2 + \hat{V} + \hat{U}. \quad (3.24)$$

where  $\hat{U}$  is a pseudopotential term defined as:

$$\hat{U} = -\frac{\hbar^2}{8\hbar c} \sum_{\alpha} \mu_{\alpha\alpha} \quad (3.25)$$

which acts as a mass-dependent contribution to the potential energy.  $\hat{V}$ , the potential energy term, is expanded as a Taylor series in terms of the dimensionless normal coordinates,  $q_i$ :

$$\hat{V} = \frac{1}{2} \sum_i \omega_i q_i^2 + \frac{1}{6} \sum_{ijk} \phi_{ijk} q_i q_j q_k + \frac{1}{24} \sum_{ijkl} \phi_{ijkl} q_i q_j q_k q_l + \dots \quad (3.26)$$

where  $q_i$  is related to the normal coordinates  $Q_i$  by  $q_i = (2\pi c \omega_i / \hbar)^{1/2} Q_i$  and  $\hat{p}_i$  is the conjugate vibrational momentum,  $\phi_{ijk}$ ,  $\phi_{ijkl}$ , ... are higher order derivatives of the potential energy surface usually referred to as cubic, quartic, etc force constants. The vibration-rotation interaction term includes the modified reciprocal moment of inertia which is also expanded as a Taylor series in terms of the normal coordinates,  $q$ :

$$\mu_{\alpha\beta} = \mu_{\alpha\beta}^{(e)} \delta_{\alpha\beta} + \sum_k \mu_{\alpha\beta}^{(k)} q_k + \frac{1}{2} \sum_{kl} \mu_{\alpha\beta}^{(kl)} q_k q_l + \dots \quad (3.27)$$

where  $\mu_{\alpha\beta}^{(e)}$  is the equilibrium rotational constant,  $B_e^{(\alpha)}$ , about axis  $\alpha$  and  $\mu_{\alpha\beta}^{(k)}$ ,  $\mu_{\alpha\beta}^{(kl)}$ , ... are the first, second, ... derivatives of  $\mu_{\alpha\beta}$  with respect to  $q_k$ ,  $q_l$ , ...

---

<sup>8</sup>The units of the Hamiltonian have been converted to  $\text{cm}^{-1}$  which are typically used in spectroscopy.

Table 3.1: Elements of Hamiltonian grouped by order of magnitude

---

$\hat{H}_0$	$= \frac{1}{2} \sum_i \omega_i (\hat{p}_i^2 + \hat{q}_i^2)$
$\hat{H}_1$	$= \frac{1}{6} \sum_{ijk} \phi_{ijk} \hat{q}_i \hat{q}_j \hat{q}_k$
$\hat{H}_2$	$= \frac{1}{24} \sum_{ijkl} \phi_{ijkl} \hat{q}_i \hat{q}_j \hat{q}_k \hat{q}_l + \sum_{\alpha} B_e^{(\alpha)} \hat{\pi}_{\alpha} \hat{\pi}_{\alpha}$
$\hat{H}_3$	$= \frac{1}{120} \sum_{ijklm} \phi_{ijklm} \hat{q}_i \hat{q}_j \hat{q}_k \hat{q}_l \hat{q}_m + \frac{\hbar^2}{2hc} \sum_k \sum_{\alpha\beta} \mu_{\alpha\beta}^{(k)} \hat{\pi}_{\alpha} \hat{\pi}_{\beta} \hat{q}_k$
$\vdots$	$\vdots$

---

(the dimensionless normal coordinates) and the effective vibrational angular momentum:

$$\hat{\pi}_{\alpha} = \sum_{kl} \zeta_{kl}^{(\alpha)} \left( \frac{\omega_l}{\omega_k} \right)^{\frac{1}{2}} \hat{q}_k \hat{p}_l. \quad (3.28)$$

where  $\zeta_{kl}^{(\alpha)}$  is the Coriolis constant. The total vibrational Hamiltonian may now be divided into different terms according to the ordering described in Table 3.1<sup>9</sup>.

In second-order vibrational perturbation theory, the first and second-order perturbed Hamiltonians, Table 3.1, and harmonic wave functions, Equation 3.10 are inserted into Equations 3.22 and 3.23. Then, these equations are manipulated and simplified using the values for the integrals:  $\langle v|q|v \rangle$ ,  $\langle v|q|v+1 \rangle$ ,  $\langle v|q|v-1 \rangle$ ,  $\langle v|q^2|v \rangle$ ,  $\langle v|q^2|v+2 \rangle$ ,  $\langle v|q^2|v-2 \rangle$ ,  $\langle v|q^3|v \rangle$ ,  $\langle v|q^3|v+3 \rangle$ ,  $\langle v|q^3|v+1 \rangle$ ,  $\langle v|q^3|v-1 \rangle$ ,  $\langle v|q^3|v-3 \rangle$ , and  $\langle v|q^4|v \rangle$  [38]. Equation 3.22 reduces to zero and algebraic manipulation of Equation 3.23 yields a parametric representation of vibrational energy levels:

$$E(v) = G_0 + \sum_i \omega_i \left( v_i + \frac{1}{2} \right) + \sum_{i \leq j} x_{ij} \left( v_i + \frac{1}{2} \right) \left( v_j + \frac{1}{2} \right) + \dots \quad (3.29)$$

---

<sup>9</sup>Grouping the terms by order of magnitude is actually arbitrary, but traditionally vibration rotation perturbation theory is done using this criteria.

where the anharmonicity constants,  $x_{ii}$  and  $x_{ij}$  [144], are

$$x_{ii} = \frac{1}{16}\phi_{iiii} - \frac{1}{16}\sum_j \phi_{iij}^2 \frac{8\omega_i^2 - 3\omega_j^2}{\omega_i(4\omega_i^2 - \omega_j^2)} \quad (3.30)$$

and

$$\begin{aligned} x_{ij} = & \frac{1}{4}\phi_{iijj} + \sum_{\alpha} B_e^{(\alpha)} \left( \zeta_{ij}^{(\alpha)} \right)^2 \frac{\omega_i}{\omega_j} \frac{\omega_j}{\omega_i} - \frac{1}{4} \sum_k \phi_{iik} \phi_{kjj} \frac{1}{\omega_k} \\ & - \frac{1}{8} \sum_k \phi_{ijk}^2 \left( \frac{1}{\omega_i + \omega_j + \omega_k} - \frac{1}{\omega_i + \omega_j - \omega_k} + \frac{1}{\omega_i - \omega_j + \omega_k} \right. \\ & \left. + \frac{1}{-\omega_i + \omega_j + \omega_k} \right). \end{aligned} \quad (3.31)$$

The cubic and quartic force constants ( $\phi_{ijk}$ ,  $\phi_{iiii}$  and  $\phi_{iijj}$ ) needed may be obtained by a finite difference of second derivatives evaluated at positive ( $+\delta q_i$ ) and negative displacements ( $-\delta q_i$ ) along the normal coordinates:

$$\phi_{ijk} = \frac{\phi_{jk}(+\delta q_i) - \phi_{jk}(-\delta q_i)}{2|\delta q_i|} \quad (3.32)$$

and

$$\phi_{iijj} = \frac{\phi_{jj}(+\delta q_i) + \phi_{jj}(-\delta q_i) - 2\phi_{jj}(0)}{|\delta q_i|^2}. \quad (3.33)$$

where  $\phi_{jk}(+\delta q_i)$  and  $\phi_{jk}(-\delta q_i)$  are quadratic force constants of the displacements - typically obtained using analytic second derivatives - and  $|\delta q_i|$  is the relative size of the displacement used <sup>10</sup>.

### 3.3.1 Resonances

A potential problem with VPT2 is the presence of singularities. VPT2 describes small amplitude vibrations and assumes the perturbation is small

---

<sup>10</sup>ACESII MAB uses a default step size of  $0.0050 \text{ amu}^{1/2} \text{ Bohr}$  for  $|\delta Q_i|$  which is then converted to  $|\delta q_i|$  [33].



relative to the reference. Singularities can arise in Equation 3.31 if  $E_i^{(0)} \approx E_j^{(0)}$  and create a conflict the premise that  $E_i^{(2)}$  is a small correction to  $E_i^{(0)}$ . To treat for this resonance first noted by E. Fermi in the infrared spectrum of CO<sub>2</sub> [70], the singularities are removed from the perturbative treatment and then reintroduced through diagonalizing a matrix which couples the vibrational fundamental effected by resonance with the two quantum transition bands. For  $2\omega_i \approx \omega_j$ , Equation 3.30:

$$\phi_{ij}^2 \frac{8\omega_i^2 - 3\omega_j^2}{\omega_i(4\omega_i^2 - \omega_j^2)} \rightarrow \frac{1}{2}\phi_{ij}^2 \left( \frac{1}{2\omega_i + \omega_j} + \frac{4}{\omega_j} \right). \quad (3.34)$$

For  $\omega_i + \omega_j \approx \omega_k$ , Equation 3.31:

$$\begin{aligned} & \phi_{ijk}^2 \left( \frac{1}{\omega_i + \omega_j + \omega_k} - \frac{1}{\omega_i + \omega_j - \omega_k} + \frac{1}{\omega_i - \omega_j + \omega_k} + \frac{1}{-\omega_i + \omega_j + \omega_k} \right) \rightarrow \\ & \phi_{ijk}^2 \left( \frac{1}{\omega_i + \omega_j + \omega_k} + \frac{1}{\omega_i - \omega_j + \omega_k} + \frac{1}{-\omega_i + \omega_j + \omega_k} \right) \end{aligned} \quad (3.35)$$

The elimination of these terms result in diagonal elements of the effective Hamiltonian matrix such as:

$$\Omega_{k_1} = \langle k_1 | \hat{H}_0 + \hat{H}_2 | k_1 \rangle + \sum_{l \notin (k_1, i_1 j_1)} \frac{\langle k_1 | \hat{H}_1 | l \rangle \langle l | \hat{H}_1 | k_1 \rangle}{\omega_k - \omega_l} \quad (3.36)$$

for  $\omega_i + \omega_j \approx \omega_k$ . The off-diagonal elements are formed from the expectation value of omitted terms:  $\langle v_i + 2, v_j | \phi_{ij} q_i^2 q_j | v_i, v_j + 1 \rangle$  or  $\langle v_i + 1, v_j + 1, v_k | \phi_{ijk} q_i q_j q_k | v_i, v_j, v_k + 1 \rangle$ .

The resulting matrix:

$$H = \begin{bmatrix} \Omega_{k_1} & \frac{1}{8^{1/2}} \phi_{ijk} \\ \frac{1}{8^{1/2}} \phi_{ijk} & \Omega_{i_1 j_1} \end{bmatrix} \quad (3.37)$$

for  $\omega_i + \omega_j \approx \omega_k$  or

$$H = \begin{bmatrix} \Omega_{j_1} & \frac{1}{4} \phi_{ij} \\ \frac{1}{4} \phi_{ij} & \Omega_{i_2} \end{bmatrix} \quad (3.38)$$

for  $2\omega_i \approx \omega_j$  is diagonalize to provide the "dressed" vibrational fundamental and two quantum transition.

Fermi resonance accounts for the coupling between a fundamental and two quantum transitions. However, two quantum predicted by VPT2 may still differ significantly from experiment, particularly in modes that combine two X-H stretches modes [58]. This coupling not accounted for by a second-order treatment can be included by extending to a partial fourth-order of the perturbation approach with the inclusion of terms [120, 141]:

$$E_i^{VPT4} \leftarrow \frac{\langle i|\hat{H}_2|j\rangle\langle j|\hat{H}_2|i\rangle}{\omega_i - \omega_j} + \frac{\langle i|\hat{H}_2|j\rangle\langle j|\hat{H}_1|k\rangle\langle k|\hat{H}_1|i\rangle}{(\omega_i - \omega_j)(\omega_i - \omega_k)} \\ + \frac{\langle i|\hat{H}_1|j\rangle\langle j|\hat{H}_1|k\rangle\langle k|\hat{H}_1|l\rangle\langle l|\hat{H}_1|i\rangle}{(\omega_i - \omega_j)(\omega_i - \omega_k)(\omega_i - \omega_l)} \quad (3.39)$$

These terms may be accounted for using a second order perturbative treatment over VPT2 states. For example, consider the coupling between two quantum transitions of two vibrational modes. The diagonal elements of the vibrational Hamiltonian are the deperturbed VPT2 frequencies for the first overtones ( $\Omega_{a_2}$  and  $\Omega_{b_2}$ ) and combination band ( $\Omega_{a_1b_1}$ ). The off diagonal coupling are determined by algebraically manipulating:

$$\langle a_0, b_2|\hat{H}|a_2, b_0\rangle = \langle a_0, b_2|\hat{H}_2|a_2, b_0\rangle + \sum_k \frac{\langle a_0, b_2|\hat{H}_1|k\rangle\langle k|\hat{H}_1|a_2, b_0\rangle}{(2\omega_a - \omega_k)(2\omega_b - \omega_k)} \quad (3.40)$$

and

$$\langle a_1, b_1|\hat{H}|a_2, b_0\rangle = \langle a_1, b_1|\hat{H}_2|a_2, b_0\rangle + \sum_k \frac{\langle a_1, b_1|\hat{H}_1|k\rangle\langle k|\hat{H}_1|a_2, b_0\rangle}{(\omega_a + \omega_b - \omega_k)(2\omega_a - \omega_k)}. \quad (3.41)$$

Thus,

$$H_{2Q2M} = \begin{pmatrix} \Omega_{a_2}^{VPT2} & \frac{1}{2}K_{aa,bb} & (a) \\ \frac{1}{2}K_{aa,bb} & \Omega_{b_2}^{VPT2} & (b) \\ (a) & (b) & \Omega_{a_1b_1}^{VPT2} \end{pmatrix} \quad (3.42)$$

where:

$$a = \frac{3}{2(2^{1/2})} \left[ 2K_{aa,ab} + K_{bb,ba} + \frac{1}{3} \sum_{c \neq a,b} K_{ac,bc} \right] \quad (3.43)$$

and

$$b = \frac{3}{2(2^{1/2})} \left[ K_{aa,ab} + 2K_{bb,ba} + \frac{1}{3} \sum_{c \neq a,b} K_{ac,bc} \right] \quad (3.44)$$

accounts for the coupling between the two quantum transitions of two vibrational modes where  $K_{aa,bb}$ ,  $K_{aa,ab}$  and  $K_{ac,bc}$  are Darling-Dennison constants [141]:

$$\begin{aligned} K_{aa,bb} = & \frac{1}{4} \phi_{aabb} - \sum_{\alpha} B_{\alpha}^e (\zeta_{ab}^{\alpha})^2 \frac{(\omega_a + \omega_b)^2}{\omega_a \omega_b} + \frac{1}{8} \sum_k \phi_{kaa} \phi_{kbb} \omega_k \left[ \frac{1}{4\omega_a^2 - \omega_k^2} \right. \\ & \left. + \frac{1}{4\omega_b^2 - \omega_k^2} \right] - \frac{1}{2} \sum_k \phi_{kab}^2 \frac{\omega_k}{\omega_k^2 - (\omega_a - \omega_b)^2}, \end{aligned} \quad (3.45)$$

$$\begin{aligned} K_{aa,ab} = & \frac{1}{6} \phi_{aaab} - \frac{1}{12} \sum_k \frac{\phi_{kab} \phi_{kaa}}{\omega_k} \left[ \frac{8\omega_a^2 - 3\omega_k^2}{4\omega_a^2 - \omega_k^2} \right] \\ & - \frac{1}{12} \sum_k \phi_{kab} \phi_{kaa} \omega_k \Omega_{kab}^{-1} (3\omega_a^2 + 3\omega_b^2 + 2\omega_a \omega_b - 3\omega_k^2), \end{aligned} \quad (3.46)$$

and

$$\begin{aligned} K_{ac,bc} = & \frac{1}{2} \phi_{abcc} + 2 \sum_{\alpha} B_{\alpha}^e \zeta_{ac}^{\alpha} \zeta_{bc}^{\alpha} \frac{\omega_a \omega_b + \omega_c^2}{\omega_c (\omega_a \omega_b)^{\frac{1}{2}}} - \frac{1}{4} \sum_k \phi_{kab} \phi_{kcc} \left[ \frac{\omega_k}{\omega_k^2 - (\omega_a - \omega_b)^2} \right. \\ & \left. + \frac{1}{\omega_k} \right] - \frac{1}{2} \sum_k \phi_{kac} \phi_{kbc} \omega_k \left[ \frac{\omega_a^2 + \omega_c^2 - \omega_k^2}{\Omega_{kac}} + \frac{\omega_b^2 + \omega_c^2 - \omega_k^2}{\Omega_{kbc}} \right]. \end{aligned} \quad (3.47)$$

To treat three or more vibrational modes,  $K_{aa,bc}$  and  $K_{ab,cd}$  are needed:

$$\begin{aligned}
K_{aa,bc} = & \frac{1}{2}\phi_{aabc} - 2 \sum_{\alpha} B_{\alpha}^e \zeta_{ab}^{\alpha} \zeta_{ac}^{\alpha} \frac{(\omega_a + \omega_b)(\omega_a + \omega_c)}{\omega_a(\omega_b\omega_c)^{\frac{1}{2}}} \\
& - \frac{1}{4} \sum_k \phi_{kaa} \phi_{kbc} \omega_k \left[ \frac{1}{\omega_k^2 - (\omega_b + \omega_c)^2} + \frac{1}{\omega_k^2 - 4\omega_a^2} \right] \\
& - \frac{1}{2} \sum_k \phi_{kab} \phi_{kac} \omega_k \left[ \frac{1}{\omega_k^2 - (\omega_a - \omega_c)^2} + \frac{1}{\omega_k^2 - (\omega_a - \omega_b)^2} \right]
\end{aligned} \tag{3.48}$$

and

$$\begin{aligned}
K_{ab,cd} = & \phi_{abcd} + 2 \sum_{\alpha} \frac{B_{\alpha}^e}{(\omega_a\omega_b\omega_c\omega_d)^{\frac{1}{2}}} [\zeta_{ab}^{\alpha} \zeta_{cd}^{\alpha} (\omega_a - \omega_b)(\omega_c - \omega_d) \\
& - \zeta_{ac}^{\alpha} \zeta_{bd}^{\alpha} (\omega_a + \omega_c)(\omega_b + \omega_d) - \zeta_{ad}^{\alpha} \zeta_{bc}^{\alpha} (\omega_a + \omega_d)(\omega_b + \omega_c)] \\
& - \frac{1}{2} \sum_k \phi_{kab} \phi_{kcd} \omega_k \left[ \frac{1}{\omega_k^2 - (\omega_a + \omega_b)^2} + \frac{1}{\omega_k^2 - (\omega_c + \omega_d)^2} \right] \\
& - \frac{1}{2} \sum_k \phi_{kac} \phi_{kbd} \omega_k \left[ \frac{1}{\omega_k^2 - (\omega_a - \omega_c)^2} + \frac{1}{\omega_k^2 - (\omega_b - \omega_d)^2} \right] \\
& - \frac{1}{2} \sum_k \phi_{kad} \phi_{kbc} \omega_k \left[ \frac{1}{\omega_k^2 - (\omega_a - \omega_d)^2} + \frac{1}{\omega_k^2 - (\omega_b - \omega_c)^2} \right]
\end{aligned} \tag{3.49}$$

where:  $\Omega_{abc} = (\omega_a + \omega_b + \omega_c)(\omega_a + \omega_b - \omega_c)(\omega_a - \omega_b + \omega_c)(-\omega_a + \omega_b + \omega_c)$ .

### 3.4 Other Methods for Treating the Vibrational Problem

For vibrational self-consistent field theory, the potential energy surface is expanded to include coupling between vibrational states:

$$V(q_1, q_2, \dots, q_n) = \sum_i V_i(q_i) + \sum_{i < j < k < l} V_c(q_i, q_j, q_k, q_l). \tag{3.50}$$

A variational treatment of the normal mode wavefunction,  $|\phi_i(q_i)\rangle$ , results in a self-consistent field:

$$\hat{F}_{i,j} |\phi_{i,j}(q_j)\rangle = \epsilon_{i,j} |\phi_{i,j}(q_j)\rangle \tag{3.51}$$

where

$$\hat{F}_{i,j} = \langle \prod_{j \neq k} \phi_{i,k}(q_k) | \hat{H} | \prod_{j \neq l} \phi_{i,l}(q_l) \rangle, \quad (3.52)$$

if  $|\phi_i(Q_i)\rangle$  is a linear combination of the basis functions,  $|\chi_i(Q_i)\rangle$ :

$$|\phi_i\rangle = \sum_j c_{ij} |\chi_i\rangle. \quad (3.53)$$

The integrals needed for Equation 3.52 can be obtained by effective potentials [30] or by discrete variable representation (DVR)[219]. Programs such as GAMESS [199] and Multimode [42] compute the VSCF energy of vibrational energy for a provided PES.

However, VSCF does not explicitly treat interactions between modes. An exact solution to the many-body problem ( $M$  distinguishable degrees of freedom coupled by the Hamiltonian,  $\hat{H}$ ) can be determined from a sum over all possible states of a complete orthonormal basis for each vibrational mode. A variety of these correlated methods have been devised which utilize VSCF modals  $|\Phi_i\rangle$  as a basis: VMP [46, 47, 105, 148], VCC [48] and VCI [31, 47, 48].

In principle, VMP, VCC and VCI methods form a wavefunction by including modals that are unoccupied VSCF modals. In VMP<sup>11</sup>, the Hamiltonian is divided such that  $\hat{U}$  is the fluctuation potential and corresponds to the difference between the many-mode interaction and VSCF mean field representation [47]. In VCC, the wavefunction:  $|VCC\rangle = e^{\hat{T}}|\Phi_i\rangle$  as in Chapter 1 where the cluster operator,  $\hat{T}$ , excites modals from VSCF ground state  $|\Phi_i\rangle$  to excited states [48]. The energy and amplitudes are found by solving equations

---

<sup>11</sup>The distinction between VPT2 and VMP2 is VPT2 uses the harmonic oscillator as its reference for perturbation while VMP2 use VSCF as its reference similar to the use of SCF as the reference for MP2 described in Chapter 1.

similar to Chapter 1. In VCI, the wavefunction:  $|VCC\rangle = |\Phi_i\rangle + \sum_{\mu} C_{\mu}\tau_{\mu}|\Phi_i\rangle$  is formed subject to the constraint  $1 = \langle\Phi_i|VCI\rangle - C_i$  where  $\tau_{\mu}$  excites modals from the ground state to various excited states [31, 48]. These methods scale poorly and are limited to small molecules.

Several Quantum Monte Carlo methods have been devised to treat vibrational states[45, 87, 175, 176]. In principle, they evaluate multidimensional Hamiltonian through sampling the space. Like variational methods, their proximity to experimental frequencies is limited by the potential energy surface used as a reference.

### 3.4.1 Comparison of Other Methods to VPT2

To illustrate the performance and limitations of these methods versus VPT2 consider formaldehyde for example. Each of these methods have been used to compute the fundamentals and two-quantum transitions of formaldehyde[25, 47, 48, 132, 191, 221] providing a means of comparing these methods to experiment[53]. VPT2 compares favorably with the other methods when treatment for Fermi resonance is included as seen in Table 3.2. The fundamentals for each method had an average absolute difference less than  $20\text{ cm}^{-1}$  from experiment. The largest reported difference,  $\nu_5$  for VPT2 CCSD(T)/cc-pVTZ[132], is effected by Fermi resonance with  $\nu_2 + \nu_6$  and  $\nu_3 + \nu_6$ . The best average absolute difference, VPT2 CCSD(T)/ANO2(fc), is than  $3\text{ cm}^{-1}$  from experiment.

Extending to the two quanta transitions, 17 of the possible 21 transitions have been observed; however, the two quanta transitions are not listed for VCC and VMP2. The mean absolute deviation from experiment ranges from  $5.4\text{ cm}^{-1}$  for VPT2 using CCSD(T)/ANO2(fc) [221] to  $37.4\text{ cm}^{-1}$  for VCI using

Table 3.2: Comparison of methods for treating the vibrational problem: the fundamental vibrational frequencies of formaldehyde

Method	PES	$\nu_1$	$\nu_2$	$\nu_3$	$\nu_4$	$\nu_5$	$\nu_6$
VPT2	CCSD(T)/ cc-pVTZ [132] <sup>a</sup>	2777	1749	1508	1171	2792 <sup>b</sup>	1253
	CCSD(T)/ cc-pVTZ [221] <sup>c</sup>	2777	1749	1508	1172	2845 <sup>d</sup>	1252
	CCSD(T)/ ANO2 [221]	2786	1745	1501	1169	2851 <sup>d</sup>	1249
VSCF	SDQCI/ DZP [191]	2807	1744	1500	1145	2837	1242
VCI	SDQCI/ DZP [191]	2770	1736	1489	1136	2824	1232
	CCSD(T)/ cc-pVTZ [132]	2789	1749	1504	1166	2842	1248
VCC	SDQCI/ DZP [47]	2770	1736	1489	1136	2824	1232
VMP2	SDQCI/ DZP [48]	2768	1736	1490	1136	2819	1232
CFQMC	Exp. [25]	2790	1756	1520	1146	2830	1228
Exp.[53]		2783	1746	1500	1167	2843	1249

<sup>a</sup> Potential energy surface obtained by symmetrized fit of energies obtained for 442 displacements.

<sup>b</sup> VPT2 fundamental frequencies listed in Reference [132] were not treated for Fermi resonance.

<sup>c</sup> Potential energy surface obtained by finite difference of analytic second derivatives obtained for 9 displacements.

<sup>d</sup> VPT2 fundamental frequency for CCSD(T)/cc-pVTZ(fc) and CCSD(T)/ANO2(fc) are 2792 and 2778. Frequencies resulting after diagonalizing the 3x3 resonance Hamiltonian:  $5_1 \approx 2_1 6_1 \approx 3_1 6_1$ .

SDCI/DZP [191]. The largest deviation for VPT2 using CCSD(T)/ANO2(fc) - 15.3 cm<sup>-1</sup> (5<sub>2</sub>(a<sub>1</sub>)) - is roughly twice the largest deviation of the fundamentals. However, 1<sub>1</sub>5<sub>1</sub>(b<sub>2</sub>) combination differed from experiment by more than 100 cm<sup>-1</sup> for variational methods<sup>12</sup>.

VPT2 calculations typically only added a few seconds to the time needed to compute the potential energy surface. By contrast, typical variational and QMC methods add additional computational cost, and poor scaling limits VCI, VCC and VMP to small molecules like formaldehyde. Also, Equations 3.30 and 3.31 only require  $\phi_{iiii}$  and  $\phi_{ijjj}$  unlike the off diagonal terms,  $\phi_{ijkl}$ , typically included in VSCF and QMC. These constants require the analytic second derivative of four displacements as is shown in the next equation:

$$\phi_{ijkl} = \frac{\phi_{kl}(+\delta q_i, +\delta q_j) - \phi_{kl}(+\delta q_i, -\delta q_j) - \phi_{kl}(-\delta q_i, +\delta q_j) + \phi_{kl}(-\delta q_i, -\delta q_j)}{|\delta q_i \delta q_j|} \quad (3.54)$$

where  $\phi_{kl}$  are the quadratic force constants evaluated at displacement of along normal coordinates  $q_i$  and  $q_j$  (i.e.  $\pm\delta q_i$  and  $\pm\delta q_j$ ) and  $|\delta q_i \delta q_j|$  is the size of the displacement<sup>13</sup>. For formaldehyde, it increases the displacements from 9 needed for VPT2 to 36 needed for the full quartic force field. With VPT2+D, only  $\phi_{ijkl}$  require for Darling-Dennison constants  $K_{ij,kl}$  are required. Thus, other methods become impractical for larger molecules while VPT2+D can accurately determine fundamental frequencies and two quantum transitions

---

<sup>12</sup>119 cm<sup>-1</sup> for FCI using a PES calculated using CCSD(T)/cc-pVTZ(fc) [132], 158 cm<sup>-1</sup> for FCI using a PES calculated using SDCI/DZP and 231 cm<sup>-1</sup> for VSCF using with the same PES [191]. This large difference prompted Martin *et al.* [132] to question the experimental assignment made by J. Clouthier and D. A. Ramsay [53].

<sup>13</sup>As with the displacements for cubic force constants, a step size of 0.0050 amu<sup>1/2</sup> Bohr is used for  $|\delta Q_i|$  which is then converted to  $|\delta q_i|$  [33].



[141].

## Chapter 4

### Benzene

#### 4.1 History

Early classification of organic compounds divided them into two groups: aliphatic (or *fatty*) and aromatic (or *fragrant*). Nineteenth century chemists ultimately discovered benzene,  $\text{C}_6\text{H}_6$ , to be the distinguishing feature of all aromatic compounds. But, how were the atoms connected together? The absence of additional hydrogen atoms in its molecular formula suggested benzene had four degrees of unsaturation. The six carbon hexagonal ring (Figure 4.1(b)) proposed by August Kekulé in 1865 did not gain immediate acceptance among other chemists of his day. Benzene did not react with bromine like an ordinary olefin, and they dismissed any proposed structures that contained any double bond between adjacent carbon atoms. One contemporary proposed structure consisted of a triangular prism of carbon atoms with hydrogen atoms attached to each vertex (Figure 4.1(a)). Kekulé's ring finally gained acceptance when efforts to synthesize his structure produced benzene and other proposed structures failed to describe benzene's unique reactivity.

Then, "what made the double bonds of benzene unique?" remained a question for chemists at the start of the twentieth century. Advances in physics in the early twentieth century helped chemists understand atoms and how they bond together, and they concluded that chemical bonds occur when pairs of electrons are shared between atoms. They introduced  $\sigma$  and  $\pi$  bonds

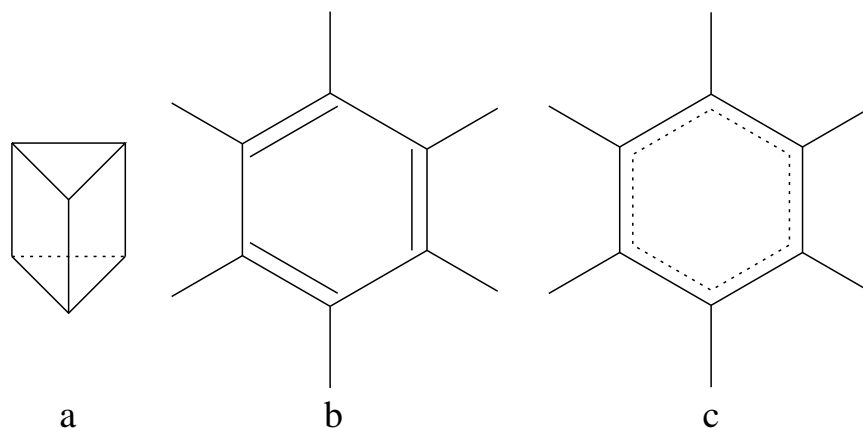


Figure 4.1: Several historic structures of benzene: (a) Landengburg’s prism, (b) Kekulé’s ring and (c) Pauling’s regular hexagon

to describe two different ways the electrons could be shared in different types of bonds.  $\pi$  bonds could describe how conjugation or resonance stabilize molecules and ions by allowing the  $\pi$  electrons to move between different regions of a molecule and become delocalized. Thus, resonance, the rationale proposed by Linus Pauling, described benzene’s unique behavior [156–158] and allowed the  $\pi$  electrons to be shared equally by each carbon atom in the ring. Instead of alternating single and double bonds of different lengths, he concluded that benzene had a regular hexagonal, planar structure (Figure 4.1(c)) -  $D_{6h}$  symmetry - where each of the carbon-carbon bonds had the same length and bond order (one and a half). A symmetric structure with a stable, conjugated  $\pi$  system above and below the ring’s  $\sigma$  framework resulted.

## 4.2 Background

Numerous crystallographic [9, 12, 54, 55], spectroscopic [37, 117, 150, 163, 164, 214] and electron diffraction [18, 19, 106, 112, 201, 218] studies of benzene have been carried out to measure the CH and CC bond lengths. These early studies determined the effective distances,  $r_0$  or  $r_a$ ,<sup>1</sup> between adjacent carbon atoms and between carbon and hydrogen atoms (see Tables 4.3 and B.1). The electron diffraction study by K. Tamagawa, T. Iijima and M. Kimura [218] also determined mean internuclear distances,  $r_g$ , and distances between mean internuclear positions,  $r_z$ .<sup>2</sup> Later experimental studies by J. Plíva *et al.* [163, 164] included a linear vibration-rotation correction to determine the equilibrium bond lengths,  $r_e$ , from the experimental rotational constants of three [163] and five isotopomers [164]. A more recent empirical study by J. Gauss and J. F. Stanton [79] calculated the vibrational corrections and used them to empirically determine the equilibrium bond lengths,  $r_e$ , and mean distances,  $r_g$  and  $r_z$ .

After its basic shape was established, the focus of investigators investigated its spectra. As techniques advanced, they probed deeper into its spectra and learned more about benzene's vibrational modes. E. Bright Wilson provided an early picture of the vibrational modes by applying group theory to

---

<sup>1</sup>The effective bond lengths between two atoms observed in these experiments include rotational and vibrational effects that shift bonds from their equilibrium lengths - or their average distance from each other if the atoms' oscillations are treated as harmonic. The electron diffraction studies determine  $r_a$  while the vibration/rotation studies determine  $r_0$  which differs from  $r_a$ .

<sup>2</sup>The distance average or distance averaged over thermal vibrations,  $r_g$ , is based on corrections to  $r_e$  formed from linear and quadratic average values of the normal coordinates. The position average or distances between nuclear positions averaged over the zero-point vibration,  $r_z$ , is based on corrections to  $r_e$  formed from only the linear average of the normal coordinates. See Ref. [115] for further information.

Pauling’s regular hexagonal structure [227]. He classed benzene’s 30 possible vibrational modes into 10 nondegenerate and 10 doubly degenerate modes; however, the selection rules he derived for benzene’s  $D_{6h}$  symmetry limits the number of these modes that can be observed in the gas phase directly via infrared absorption or Raman scattering<sup>3</sup>. This limitation provides the basis for *ab initio* quantum chemical methods to predict the fundamental frequencies not directly observed spectroscopically<sup>4</sup>.

In the 1930’s, several studies surveyed the infrared spectrum of benzene. Most of these early studies reviewed by C. K. Ingold and coworkers [13] found nine principle bands in the spectrum of benzene vapor in the region from 600 to 3200  $\text{cm}^{-1}$  or 3 to 15  $\mu\text{m}$ . Ingold’s study divided the fifteen absorbance bands observed in their study into six medium to strong bands, three weak bands and six very weak bands. Also during this period, Raman discovered that substances can scatter infrared radiation. In 1928, he and his coworker Krishnan [183] examined this scattering for benzene and observed eight lines absent in the infrared spectrum. Six early Raman studies including one by C. K. Ingold *et al.* [10] showed remarkable consistency with each other with 5  $\text{cm}^{-1}$  being the largest difference<sup>5</sup>. Later studies of the infrared spectrum by S. Brodersen and A. Langseth [35] expanded the region examined earlier, 600 to 3200  $\text{cm}^{-1}$  range, to include combination bands observed between 3000  $\text{cm}^{-1}$  and 7000  $\text{cm}^{-1}$ . They assigned the peaks they observed in this region to vi-

---

<sup>3</sup>The numbering Wilson assigned the vibrational modes will be used throughout this study, and the numbering Herberg assigned will be included when possible for comparison.

<sup>4</sup>For a mode to be IR active, the direct product of its irreducible representation needs to correspond to one of the irreducible representations of the transition dipole moment,  $\mu$ . For a mode to be Raman active, the direct product of its irreducible representation needs to correspond to one of the irreducible representations of the polarizability,  $\alpha$ .

<sup>5</sup>See Ingold’s study [10] for additional references to other early studies.

brational fundamental and combination bands and, were the first to determine values for each of benzene’s twenty fundamental frequencies. As the resolution of infrared and Raman spectroscopy improved via the development of Fourier transform instrumentation, the rotational structure of benzene’s vibrational spectrum could be resolved and analyzed to determine more precisely the experimental fundamentals observed through the infrared absorption or Raman scattering.

#### 4.2.1 Infrared Spectra

The first high resolution infrared study - carried out by A. Cabana *et al.* [37] - focused on the strong absorption band centered at  $674\text{ cm}^{-1}$ . Using Wilson’s numbering [227] to denote individual vibrational modes, this band  $\nu_{11}(a_{2u})$  is one of benzene’s four fundamental vibrations active in the infrared;  $\nu_{18}(e_{1u})$ ,  $\nu_{19}(e_{1u})$  and  $\nu_{20}(e_{1u})$  are the other three. In subsequent studies, J. Kauppinen, P. Jensen and S. Brodersen [107] and J. Lindenmayer, U. Magg and H. Jones [123] obtained the value of  $\nu_{11}$  to higher precision as more rotation-vibration lines were included in the analysis. More recently, H. Hollenstein and co-workers [97] obtained a high resolution spectrum using an interferometric Fourier-transform spectrometer and a tuneable diode-laser spectrometer. They resolved the  $P$ ,  $Q$  and  $R$  parallel band structure to 2641 lines and assigned  $J$  and  $K$  values to each line. Their analysis increased the precision of  $\nu_{11}$  to  $0.00001\text{ cm}^{-1}$  (see Table 4.1).

Despite the success of this analysis with  $\nu_{11}(a_{1u})$ , analysis of  $\nu_{20}(e_{1u})$  centered at  $3048\text{ cm}^{-1}$  has been hindered by its proximity to combination bands:  $\nu_1 + \nu_6 + \nu_{19}$  ( $3079\text{ cm}^{-1}$ ),  $\nu_8 + \nu_{19}$  and  $\nu_3 + \nu_6 + \nu_{15}$  (both near  $3100$

Table 4.1: Observed gas-phase fundamental frequencies ( $\text{cm}^{-1}$ )

Sym.	$\nu^a$	$\nu^b$	$\text{C}_6\text{H}_6^c$	Activity <sup>d</sup>
<b><i>a</i><sub>1g</sub></b>	$\nu_2$	$\nu_1$	3073.942 [104]	R
	$\nu_1$	$\nu_2$	993.071 [104]	R
<b><i>a</i><sub>2g</sub></b>	$\nu_3$	$\nu_3$	1350 [35]	IA
<b><i>b</i><sub>1u</sub></b>	$\nu_{13}$	$\nu_5$	3015 [66]	IA
	$\nu_{12}$	$\nu_6$	1013.74 [39]	IA
<b><i>b</i><sub>2u</sub></b>	$\nu_{14}$	$\nu_9$	1309.4 [83]	TP
	$\nu_{15}$	$\nu_{10}$	1147.675 [166]	TP
<b><i>e</i><sub>2g</sub></b>	$\nu_7$	$\nu_{15}$	3057.04 [39]	R
	$\nu_8$	$\nu_{16}$	1609.518 [68] <sup>e</sup>	R
	$\nu_9$	$\nu_{17}$	1177.776 [99]	R
	$\nu_6$	$\nu_{18}$	608.13 [99]	R
<b><i>e</i><sub>1u</sub></b>	$\nu_{20}$	$\nu_{12}$	3047.908 [167] <sup>f</sup>	IR/TP
	$\nu_{19}$	$\nu_{13}$	1483.9854 [161]	IR/TP
	$\nu_{18}$	$\nu_{14}$	1038.2670 [162]	IR/TP
<b><i>a</i><sub>1u</sub></b>	$\nu_{11}$	$\nu_4$	673.97465 [97]	IR
<b><i>b</i><sub>2g</sub></b>	$\nu_5$	$\nu_7$	992.93 [39]	IA
	$\nu_4$	$\nu_8$	702.24 [39]	IA
<b><i>e</i><sub>1g</sub></b>	$\nu_{10}$	$\nu_{11}$	847.1062 [166]	R
<b><i>e</i><sub>2u</sub></b>	$\nu_{17}$	$\nu_{19}$	967.98 [39]	TP
	$\nu_{16}$	$\nu_{20}$	398.131 [165]	TP

<sup>a</sup> Numbering based on Wilson's criteria [227].

<sup>b</sup> Numbering based on Herzberg's criteria [96].

<sup>c</sup> The citations for the most recent fundamental frequencies are included next to the value listed.

<sup>d</sup> Activity: IR - infrared active, R - Raman active, TP - two photon active and IA - inactive.

<sup>e</sup> This mode is effected by Fermi resonance with  $\nu_{1+6}$ . Its deperturbed value is 1600.9764  $\text{cm}^{-1}$  [160].

<sup>f</sup> This mode is strongly effected by Fermi resonance with  $\nu_{8+19}$ . Its deperturbed value is 3064.367  $\text{cm}^{-1}$  [168].

$\text{cm}^{-1}$ )<sup>6</sup>. In 1982, J. Plíva and A. Pine [167] resolved the dense structure between 3030 and 3065  $\text{cm}^{-1}$  and identified 125 rotation-vibration lines. They assigned them  $J$  and  $K$  numberings and used a polynomial fit to precisely determine its value (see Table 4.1). In a subsequent study [168], they deperturbed  $\nu_{20}$  from its Coriolis and anharmonic interaction with  $\nu_8 + \nu_{19}$ ,  $\nu_1 + \nu_6 + \nu_{19}$  and  $\nu_3 + \nu_6 + \nu_{15}$  which increased the fundamental frequency to 3064.367(3)  $\text{cm}^{-1}$ .

Additional high resolution studies by J. Plíva and J. Johns of  $\nu_{18}(e_{1u})$  [162] and  $\nu_{19}(e_{1u})$  [161] followed shortly after the initial study of  $\nu_{20}$ . Their first study, resolving the rotational structure of  $\nu_{19}$ , identified 125 lines in the  $P$ ,  $Q$  and  $R$  branches. Their next study of  $\nu_{18}$  identified 135 lines in the rotational branches  $P$ ,  $Q$  and  $R$ . In each study, they assigned  $J$  and  $K$  numbering to the lines they resolved and then performed a polynomial fit to accurately determined values for these fundamentals (see Table 4.1).

#### 4.2.2 Raman Spectra

Since Raman spectroscopy provide further insight into the molecular vibrations of benzene (seven additional fundamentals are Raman-active:  $\nu_1(a_{1g})$ ,  $\nu_2(a_{1g})$ ,  $\nu_6(e_{2g})$ ,  $\nu_7(e_{2g})$ ,  $\nu_8(e_{2g})$ ,  $\nu_9(e_{2g})$ , and  $\nu_{10}(e_{1g})$  [227]), the most recent high resolution study by H. B. Jensen and S. Brodersen obtained and analyzed the resolved rotational structure of the totally symmetric,  $a_{1g}$ , Raman bands,  $\nu_1$  and  $\nu_2$  [104]. They assigned 132 lines  $J$  and  $K$  values from the  $O$ ,  $P$ ,  $R$  and  $S$  branches<sup>7</sup> of the spectrum of  $\nu_1$  where  $J$  and  $K$  are the total angular momentum quantum numbers. However, the  $O$  and  $P$  branches of  $\nu_2$  overlapped

---

<sup>6</sup>Assignments here follow those suggested by Plíva and Pine in 1987 [168].

<sup>7</sup>These branches correspond to  $\Delta J = -2, -1, +1$ , and  $+2$ , respectively.



with  $\nu_7$  and only the assignment of  $J$  was possible for 62 lines of the  $R$  and  $S$  branches of  $\nu_2$ 's spectrum (see Table 4.1). Their values for  $\nu_1$  and  $\nu_2$  are similar to the values obtained in an earlier study by A. B. Hollinger and H. L. Welsh [98] who used a different criteria to assign  $J$  and  $K$  to the 146 and 101 lines they analyzed for  $\nu_1$  and  $\nu_2$ .

In additional study, A. B. Hollinger and H. L. Welsh [99] obtained and analyzed the resolved rotational structure of two of the doubly degenerate,  $e_{2g}$ , Raman bands,  $\nu_6$  and  $\nu_9$ . They assigned 153 of 157 peaks  $J$  and  $K$  values from the  $O$ ,  $P$ ,  $R$  and  $S$  branches of  $\nu_9$  and 62 of 69 peaks  $J$  and  $K$  values from  $O$  and  $S$  branches of  $\nu_6$ . However,  $\nu_7$  could not be analyzed conclusively because of its overlap with  $\nu_2$ , but they did estimate its frequency from the  $^oQ_1$  maximum. Also, they did not analyze  $\nu_8$  in a Fermi Diad with  $\nu_{1+6}$  - these two peaks overlapped with each other too closely to be distinguished from each other using ordinary Raman spectroscopy. P. Esherick and co-workers [68] finally succeeded in separating the Fermi Diad using ionization-detected stimulated Raman Spectroscopy. In their analysis, they assigned 1190 peaks  $J$  and  $K$  values and grouped them into two separate bands: states  $|a\rangle$  and  $|b\rangle$  (see Table 4.1). In a subsequent paper with J. Plíva [160], they deperturbed states  $|a\rangle$  and  $|b\rangle$  assigning state  $|a\rangle$  to  $\nu_8$  and  $|b\rangle$  to  $\nu_1 + \nu_6(e_{2g})$  and calculated the coupling constant between the two states.

### 4.2.3 Two Photon Spectroscopy

Several of the remaining fundamentals may be measured using two photon spectroscopy. Its selection rules for benzene allow transitions between the ground state ( $\tilde{X}(^1A_{1g})$ ) and excited state ( $\tilde{A}(^1B_{2u})$ ) to be observed for ungerade vibrations both the  $b_{2u}$  modes ( $\nu_{14}$  and  $\nu_{15}$ ) and the  $e_{2u}$  modes ( $\nu_{16}$

and  $\nu_{17}$ ) not observed using infrared spectroscopy. Two-photon hot bands in the  $\tilde{A}(^1B_{2u}) \leftarrow \tilde{X}(^1A_{1g})$  electronic transition observed by L. Wunsh and co-workers [230] determined values for  $\nu_{14}$ ,  $\nu_{15}$ ,  $\nu_{17}$  and  $\nu_{18}$ . Subsequently, J. Berman and L. Goodman [24] resolved the two photon rotational band contours using fluorescence excitation and examined the R and S branches to extract the rotationless origin frequency for  $\nu_{14}$  and  $\nu_{15}$ .

#### 4.2.4 Combination Bands

The other fundamentals are inactive and are inferred from combination and difference bands. S. Brodersen and A. Langseth [35] calculated values for these fundamentals from peaks in the infrared spectrum between 400 and 7000  $\text{cm}^{-1}$ . By assuming the combinations bands were linear combinations of fundamental bands, i.e.:

$$\nu_{i+j} = \nu_i + \nu_j, \quad (4.1)$$

they assigned 73 of the 90 peaks they observed as either a fundamental or a combination band. Employing both the combination bands and product rules of  $\text{C}_6\text{H}_6$  and symmetric  $\text{C}_6\text{H}_3\text{D}_3$  modes, they determine values for each fundamental. Their values for the fundamentals  $\nu_3(a_{2g})$  1350  $\text{cm}^{-1}$  and  $\nu_{13}(b_{1u})$  3057  $\text{cm}^{-1}$  continue to be cited [28, 84, 143] and  $\nu_3(a_{2g})$  for  $\text{C}_6\text{H}_6$  is included in Table 4.1. Subsequent studies by S. Eppinger *et al.* [65] and E. Cané, A. Miani and A. Trombetti [40] utilized established fundamentals to estimate anharmonic constants from either Raman combination bands and overtones [65] or infrared difference bands [40]. Empirical studies by E. Cané, A. Miani and A. Trombetti [39] and A. Miani *et al.* [143] included anharmonic constants,

$x_{ij}$ , calculated using either *ab initio* or density functional methods<sup>8</sup>:

$$\nu_{i+j} = \nu_i + \nu_j + x_{ij} \quad (4.2)$$

to better estimate several of the remaining fundamentals from the rotationally resolved combination bands. Their studies obtained precise values for  $\nu_4(b_{2g})$ ,  $\nu_5(b_{2g})$ ,  $\nu_7(e_{2g})$ ,  $\nu_{12}(b_{1u})$  and  $\nu_{17}(e_{2u})$  (see Table 4.1).

#### 4.2.5 Other Experiment: $\nu_{13}(b_{1u})$ CH Stretch

The  $b_{1u}$  CH stretch has been difficult to measure. Since it is not IR or Raman active, the  $\nu_{13}$  band is not measured directly. Close proximity of its combination bands to others has limited the effectiveness of E. Cané, A. Miani and A. Trombetti’s technique [39, 143]. The effect of Fermi resonance also limits the reliability of the value obtained by S. Brodersen and A. Langseth since the product rule they used to extrapolate  $\nu_{13}$  from symmetric  $C_6H_3D_3$  fails when states are coupled. The importance of observing the CH stretch region led U. Erlekam and coworkers [66] to exam the region via ion dip spectroscopy of a fifty-fifty mixture of  $C_6H_6/C_6D_6$ . The  $D_{6h}$  symmetry of one of the molecules in a T shaped dimer is broken allowing all four of its CH stretches to become infrared active. They observed ten peaks in the region from 3000 to 3100  $cm^{-1}$  for the  $(C_6H_6)^*(C_6D_6)$  dimer and assigned six of them to the fundamentals  $\nu_2(a_{1g})$ ,  $\nu_7(e_{2g})$ ,  $\nu_{13}(b_{1u})$ , and  $\nu_{20}(e_{1u})$ . They assigned the other bands the combination bands  $\nu_{8+19}$  and  $\nu_{1+6+19}$  which are also observed in this region. After adjusting their value to account for red shift of their measurement, U. Erlekam *et al.* [66] concluded  $\nu_{13} = 3015^{+2}_{-5} cm^{-1}$  (see Table 4.1).

---

<sup>8</sup>Cané’s study used SCF/DZP [140] while Miani’s study used B3LYP/TZ2P.

#### 4.2.6 *Ab Initio* and Density Functional Studies

Since its  $D_{6h}$  symmetry can be exploited by *ab initio* methods to reduce the computational cost, benzene has been studied by a wide variety of methods. Early Hartree-Fock calculations focused on determining benzene’s Hartree-Fock limit for the experimental geometry [67]. Later systematic study by Péter Pulay and others [180, 181] suggested that molecular geometries, force constants, dipole moments and their derivatives could be calculated and compared to experimental values. As a method was developed, benzene was often used to test it. At present, the carbon-carbon and carbon-hydrogen bonds lengths have been calculated for: Hartree Fock or self consistent field theory (SCF) [84, 135]), many-body perturbation theory [84, 90, 135], coupled-cluster theory [34, 79, 135] and several density functional methods [41, 91, 131, 143]. In most of the studies bond lengths ( $r_e$ ) are within 0.02 Å of the empirical values [79] (see Tables B.2 in Appendix).

The harmonic frequencies of a molecule are calculated from the second derivative of its energy with respect to the position of its nuclei. Two basic methods can be employed for these calculations using *ab initio* or density functional methods: (1) finite difference of either the energy or analytic gradients or (2) analytic second derivatives. For benzene, the study by Péter Pulay *et al.* first examined its harmonic frequencies and their connection to its spectrum [180] using Hartree-Fock with 4-31G basis set. Subsequent studies have focused on how newer methods and basis sets reduce the difference between theory and empirical results. To date, harmonic frequencies have been computed for SCF [84, 135, 140], many-body perturbation theory [79, 84, 90, 135], CCSD [34, 108], CCSD(T) [135], and density functional theory [23, 28, 41, 90, 91, 131, 143].

In contrast to the large number of studies which have computed the har-

monic frequencies or measured the fundamental frequencies previously mentioned, only a few studies have determined the third- and fourth-order derivatives needed to calculate the fundamental frequencies using VPT2 (see Chapter 3). An early study by Péter Pulay and others used a correction factor to extrapolate the fundamentals from harmonic frequencies they calculated using SCF/4-31G [180]. A later study by P. E. Maslen and others [140] determined the third and fourth derivatives required from finite differences of analytic second derivatives for SCF/DZP. To date, SCF/DZP [140], B3LYP/TZ2P [28, 143] and B97-1/TZ2P [28] have been used to calculate fundamentals (see Table B.3).

#### **4.2.7 Empirical and Experimental Estimates of Harmonic Frequencies**

The first step in understanding the vibrational spectrum of a compound is to determine how it vibrates and assign each vibration to a peak on the observed spectrum. At its simplest, molecular vibrations can be described by a collection quantum harmonic oscillators, and the observed infrared absorptions correspond to transitions between these vibrational states. The modes of vibration can be described using classical mechanics for multiple harmonic oscillators. However, the selection rules derived from quantum mechanics governed how these transitions occur, and not all of them can be observed directly (see Chapter 3). In 1934, E. Bright Wilson worked out both the modes of oscillation and the infrared and Raman selection rules for the regular hexagonal structure of benzene in 1934 using group theory [227]. First, he found that ten of the normal modes were nondegenerate and the ten remaining were doubly degenerate. Of these twenty vibrational modes, he, then, predicted that only four could be observed in the infrared and seven others could be seen from

Raman scattering<sup>9</sup>.

Although the simplest description confines the vibrations to a harmonic potential, the vibration potentials of molecules deviate from this ideal and the observed vibrational frequencies must be adjusted to account for this anharmonicity before being compared to calculated harmonic frequencies. For benzene, three different approaches have been used:

1. remove measured anharmonic effects directly from the measured fundamental frequencies,
2. construct and diagonalize an  $\mathbb{F}\mathbb{G}$  matrix [228] and
3. use *ab initio* or density functional force fields to account for the anharmonicity in the experimental fundamentals empirically.

L. Goodman, A. G. Ozkabak and S. N. Thakur [84] employed two of these methods to estimate the harmonic frequencies from observations ( $\omega_{obs}$ ). For the first method, they used only nine experimental anharmonic corrections in their estimation. For the second method, they constructed and diagonalized  $\mathbb{F}$  and  $\mathbb{G}$  matrices.

The first use of computed force fields, method (3), to estimate benzene’s harmonic frequencies was part of a Hartree-Fock study by Maslen *et al.* [140]. They estimated them from the experimental values published by Goodman and coworkers [84]. For cases involving Fermi resonance, (i.e.  $\nu_8 \sim \nu_{1+6}$ ,

---

<sup>9</sup>Wilson also numbered the each vibrational mode according to their irreducible representation. Later, G. Herzberg [96] revised Wilson’s numbering. Both of these numberings have been used by others and this study will primarily use Wilson’s numbering for the vibrational normal modes and provide Herzberg’s numbering where possible.

$\nu_2 \sim \nu_{19+19}$  and  $\nu_{13} \sim \nu_{8+19} \sim \nu_{20}$ ), they deperturbed the experimental values using the cubic force constants they had calculated ( $\omega_{emp}$ ). Following Maslen’s study, N. C. Handy and coworkers first decided upon the best value for the harmonic frequency from Maslen’s and Goodman’s values for comparison to future studies [90] then simply averaged them ( $\omega_{ave}$ ) [91]. Later, A. Miani and her colleagues [143] estimated nineteen of the twenty harmonic frequencies (the absence of consistent experimental values and its strong Fermi interaction with  $\nu_{8+19}$  caused them to discard  $\nu_{13}$ ) in a self consistent fashion using the experimental fundamentals and the force field they calculated using B3LYP/TZ2P.

### 4.3 Computational Details

The equilibrium CH and CC bond lengths for benzene,  $r_e$ , were optimized using analytic gradients for HF, MP2, CCSD and CCSD(T) with the correlation consistent Dunning basis sets (cc-pVDZ and cc-pVTZ) (both frozen-core and with all electrons correlated) and the atomic natural orbital basis set contracted as ANO0 and ANO1 (frozen-core). All calculations were performed using the quantum chemistry program ACESII MAB [212, 213]. The geometry and energy convergency criteria of J. Breidung [33] were followed to allow the equilibrium bond lengths to be used in VPT2 calculations<sup>10</sup>. An additional optimization was run using the CCSD(T)/ANO2(fc) level of theory.

---

<sup>10</sup>Convergency of anharmonic calculations is effected by the maximum change in the SCF density matrix ( $\epsilon_1$ ), the CCSD amplitudes ( $\epsilon_2$ ) and the perturbed CC and  $\lambda$  amplitudes ( $\epsilon_3$ ), the norm of the solution space for the CPHF and Z-vector equations ( $\epsilon_4$ ), and the cutoff for inclusion of integrals ( $\epsilon_5$ ). These criteria are expressed as exponentials  $\epsilon_i = 10^{-n_i}$ . For CCSD(T), the  $n_i$  specified are: 12, 10, 10, 12 and 14 for ANO0(fc), 12, 10, 10, 12 and 14 for ANO1(fc), 12, 10, 10, 12 and 14 for cc-pVDZ(fc), 11, 11, 11, 12 and 14 for cc-pVDZ(ae), 10, 11, 11, 12 and 14 for cc-pVTZ(fc) and 10, 11, 11, 12 and 14 for cc-pVTZ(ae).

Then, harmonic frequencies for each geometry were computed using analytic second derivatives by ACESII MAB with coarse-grain parallelization when needed (see Chapter 2).

Calculations were then run using analytic second derivatives at various displacements also using the coarse-grain parallelization scheme discussed in Chapter 2 to determine the cubic and quartic force constants.

These force constants were utilized to calculate vibrational corrections for the mean internuclear distances,  $r_g$ , and distances between mean internuclear positions in the vibrational ground state,  $r_z$  [115]. The effective rotational constants,  $B_0$ , for five isotopomers ( $\text{C}_6\text{H}_6$ ,  $^{13}\text{C}_6\text{H}_6$ ,  $\text{C}_6\text{D}_6$ ,  $^{13}\text{C}_6\text{D}_6$  and  $\text{C}_6\text{H}_3\text{D}_3$   $D_{3h}$ ) were also obtained from the VPT2 calculations for CCSD(T) with the cc-pVDZ(ae), cc-pVTZ(ae), ANO0(fc) and ANO1(fc) basis sets using ACESII MAB. Then, a nonlinear fit yielded the effective CH and CC bond lengths,  $r_0$  for comparison to the experimental gas phase results. Finally, empirical equilibrium rotational constants were also obtained using the experimental rotational constants for the five isotopomers above and corrected using the vibrational corrections,  $B_0 - B_e$ , calculated by ACESII MAB and the empirical equilibrium bond lengths,  $r_e$  were determined by a nonlinear fit [159].

The fundamental frequencies were computed using VPT2 at the SCF, MP2 and CCSD(T) levels of theory using the basis sets cc-pVDZ(ae), cc-pVTZ(ae), ANO0(fc) and ANO1(fc) and Fermi resonance was accounted for using the method outlined in Chapter 3 to obtain “dressed” fundamentals for comparison with experimental values. Fundamental frequencies designated as CCSD(T)/ANO2/1(fc) were also computed using the CCSD(T)/ANO2(fc) harmonic frequencies and the CCSD(T)/ANO1 cubic and quartic force constants. The two quantum transitions were also computed using VPT2 and



treated for Fermi and Darling-Dennison resonance as outlined in Chapter 3.

Finally, empirical harmonic frequencies were obtained by refining the harmonic frequencies until the differences between experimental fundamental and those computed by second order vibrational perturbation theory using cubic and quartic force constants computed from analytic second derivatives converged to within  $0.01\text{ cm}^{-1}$ . For frequencies effected by Fermi resonance with combinations,  $\omega_a \sim \omega_b + \omega_c$ , or overtones,  $\omega_a \sim 2\omega_b$ , the resonant terms:  $1/(\omega_a - \omega_b - \omega_c)$  or  $1/(\omega_a - 2\omega_b)$  were removed from the perturbative treatment and then “dressed” by decoupling the fundamental from the combinations and overtones for two quantum transitions.

Calculations were run on **jfs2** - a Linux cluster with Xeon 32-bit processors at the University of Texas at Austin, **quantum** - a Linux cluster with Xeon 64-bit 3.0 GHz processors at Universität Mainz, or **lonestar** - a Dell Linux cluster of PowerEdge 1955 compute blades with two Xeon 5100 series 64-bit 2.66GHz dual-core processor per blade and InfiniBand interconnection technology at the Texas Advanced Computing Center.

## 4.4 *Ab Initio* and Empirical Geometries

### 4.4.1 Equilibrium Bond Lengths

Each of the *ab initio* equilibrium bond lengths,  $r_e$ , differs by less than two percent or  $0.02\text{ Å}$  from the empirical value found by J. Gauss and J. Stanton [79] (see Table 4.2 and Table B.4 in the appendix). The largest differences ( $0.018\text{ Å}$ ) between the calculated and empirical equilibrium bond lengths occurred for CCSD(T) with the smallest basis sets (ANO0(fc) cc-pVDZ(fc) and cc-pVDZ(ae)). This difference diminished as more basis functions are included in both the ANOn and cc-pVXZ series of basis sets.

Table 4.2: Calculated equilibrium bond lengths,  $r_e$ , mean internuclear distances,  $r_g$  and distances between mean internuclear positions,  $r_z$  (Units: Å). All of these calculations were carried out at CCSD(T) level of theory.

	$r_e$		$r_g^a$		$r_z^a$	
	$r_{CC}$	$r_{CH}$	$r_{CC}$	$r_{CH}$	$r_{CC}$	$r_{CH}$
<b>ANO0(fc)</b>	1.4056	1.0899	1.4138	1.1106	1.4114	1.0943
<b>ANO1(fc)</b>	1.3965	1.0831	1.4045	1.1038	1.4021	1.0875
<b>ANO2(fc)</b>	1.3947	1.0827				
<b>cc-pVDZ(fc)</b>	1.4107	1.0978	1.4187	1.1185	1.4162	1.1021
<b>cc-pVDZ(ae)</b>	1.4095	1.0968	1.4176	1.1175	1.4151	1.1012
<b>cc-pVTZ(fc)</b>	1.3975	1.0831	1.4055	1.1038	1.4030	1.0874
<b>cc-pVTZ(ae)</b>	1.3917	1.0778	1.3996	1.0986	1.3972	1.0824
<b>Emp.</b> <sup>b</sup> [79]	1.3914	1.0802	1.3988	1.1005	1.3964	1.1005
<b>Exp.</b> [218]			1.399(1)	1.101(5)	1.3976(15)	1.085(10)

<sup>a</sup> Calculated using method described in Ref. [115].

<sup>b</sup>  $r_e$  are based on SDQ-MBPT(4)/cc-pVTZ cubic force field used to determine vibrational corrections to experimental rotational constants.  $r_g$  and  $r_z$  are based on a CCSD(T)/cc-pVQZ(ae) geometry ( $r_{CC} = 1.3911$  and  $r_{CH} = 1.0800$ ) with vibrational corrections calculated at the SDQ-MBPT(4)/cc-pVTZ(fc) level.

The lengths of the CH and CC bonds from SCF/cc-pVDZ and SCF/cc-pVTZ are identical to those obtained by J. Martin’s study [135] and bond lengths determined by SCF/ANO0 corresponded with those obtained by L. Goodman and his coworkers [84] who used the 6-311++G\*\* basis set. The CC bond lengths calculated using SCF were at least 0.003 Å and converged to 0.009 Å shorter than the Gauss’s empirical value. SCF’s CH bond lengths were generally shorter than the empirical value with the exception of cc-pVDZ which was only slightly longer. Both classes of basis sets converged to a difference from the empirical length roughly -0.007 Å.

When the correlation energy is included through MP2 and CCSD<sup>11</sup>, the CH and CC bond length increased. The CC and CH bond lengths increased by at least 1 pm for the smaller basis sets (cc-pVDZ(ae) and ANO0(fc)). However, these increases exceeded the empirical bond length used as a reference: 0.006 to 0.018 Å for CC bonds and 0.06 to 0.017 Å for CH bonds. The bond lengths of the larger basis sets (cc-pVTZ(ae) and ANO1(fc)) showed smaller increases due to correlation and were generally closer to the empirical reference. In addition, the MP2 bond lengths from this study are consistent with earlier studies by L. Goodman [84], N. C. Handy [90], and J. M. L. Martin [135]. The only CCSD previous study by Brenner [34] also agrees with the bond lengths calculated in this study using a similar basis set.

While the inclusion of perturbative triples via CCSD(T) followed the same trend for correlation energy as MP2 and CCSD, it also consistently increased the CC and CH bond lengths by roughly 0.005 and 0.002 Å relative to the bonds lengths calculated using CCSD. Relative to earlier studies, the inclu-

---

<sup>11</sup>All the electrons were included in the correlation treatment for MP2, and the core electrons were frozen for CCSD/ANOn.

sion of d-functions in hydrogen (excluded in the studies by Martin *et al.* [135]) did not alter the value of CCSD(T)/ANO1(fc) significantly (less than 0.001 Å). However, the inclusion of core electrons in cc-pVXZ changed the both bond lengths by more than 0.005 Å (see Table 4.2). Also, the bond lengths from the ANOn(fc) basis sets are closer to the reference than the corresponding cc-pVXZ(fc) bond length. However, the differences between CCSD(T)/ANO2(fc) and the empirical bond lengths (.0033 Å for CC and .0025 Å for CH) are more than ten times the difference between CCSD(T)/cc-pVQZ(ae) (obtained by J. Gauss and J. Stanton [79]) and the empirical bond lengths. Thus, their value remains the best *ab initio* estimate of the equilibrium bond length.

Finally, the computed CC bond length for CCSD(T)/cc-pVQZ(ae) lies between 1.5224 Å (the CC length of ethane) and 1.3309 Å (the CC length of ethene) while its CH bond length, 1.0800 Å, is near  $r_{CH} = 1.0798$  Å for ethene. CCSD(T)/ANO2(fc)'s CC bond length, 1.3947 Å, also falls between 1.5452 Å (ethane's CC bond length) and 1.3341 Å (ethene's CC bond length) and its CH bond length is within 0.0003 Å of ethene (1.0827 Å). These comparisons further confirms Pauling's resonance description of the CC bonds in benzene - each bond is equivalent with a bond order of one and a half.

#### 4.4.2 Empirical Equilibrium Bond Lengths

Within each pure vibrational states described in Chapter 3, exists rotational states. For each vibrational state, it is possible to define an effective rotational Hamiltonian (in units of  $\text{cm}^{-1}$ ) defined by:

$$\frac{\hat{H}_{rot}}{hc} = \sum_{\alpha} B_v^{(\alpha)} J_{\alpha}^2 + \frac{1}{4} \sum_{\alpha\beta} (\tau'_{\alpha\alpha\beta\beta})_v J_{\alpha}^2 J_{\beta}^2 + \dots \quad (4.3)$$

where  $B_v^{(\alpha)}$  are the effective rotational constant for the vibrational state  $v$  ( $B_0^{(\alpha)}$ , if  $v = 0$ , may be measured directly using microwave spectroscopy<sup>12</sup>,  $J_\alpha$  are the components of the angular momentum along axis  $\alpha$ , and  $(\tau'_{\alpha\alpha\beta\beta})_v$  are the centrifugal distortion constants also associated with the vibrational state  $v$  [38, 144]. However, the effective rotational constants do not correspond to the equilibrium structure computed using quantum chemistry, but rather a vibrational averaged structure and are connected to the equilibrium structure  $B_e^{(\alpha)}$  via expansion in terms of the rotation-vibration interaction constants  $\alpha_i^{(\alpha)}$ ,  $\gamma_{ij}^{(\alpha)}$ , etc. For the vibrational ground state,  $v = 0$ , this expansion is written as:

$$B_e^{(\alpha)} = B_0^{(\alpha)} + \sum_i \alpha_i^{(\alpha)} \left( v_i + \frac{1}{2} \right) + \sum_{i \geq j} \gamma_{ij}^{(\alpha)} \left( v_i + \frac{1}{2} \right) \left( v_j + \frac{1}{2} \right) + \dots \quad (4.4)$$

where:

$$B_e^\alpha = \frac{\hbar}{2hcI^{(\alpha)}}. \quad (4.5)$$

and  $I^{(\alpha)}$  is the moment of inertia<sup>13</sup> of the molecule about axis  $\alpha$ .

By treating the effective rotational Hamiltonian using second order perturbation theory, the analytic expressions for the first vibration-rotation constant,  $\alpha_i^{(\alpha)}$ , can be derived and has the following form:

$$\begin{aligned} -\alpha_i^{(\alpha)} = & \frac{2 \left( B_e^{(\alpha)} \right)^2}{\omega_i} \left[ \sum_\xi \frac{3 \left( a_i^{(\alpha\xi)} \right)^2}{4I_\xi} + \sum_j \left( \zeta_{ij}^{(\alpha)} \right)^2 \frac{3\omega_i^2 + \omega_j}{\omega_i - \omega_j} \right. \\ & \left. + \pi \left( \frac{c}{h} \right)^{1/2} \sum_j \phi_{ij} a_j^{\alpha\alpha} \left( \frac{\omega_i}{\omega_j^{3/2}} \right) \right] \end{aligned} \quad (4.6)$$

---

<sup>12</sup>In the absence of a dipole moment in molecules like benzene, they may also be deduced from the rotational structure of high resolution vibrational spectra.

<sup>13</sup>The molecule is oriented such that the inertia tensor is diagonal. Then, the diagonal elements correspond to the moments of inertia of the principle axes of rotation.

where  $a_i^{(\alpha\beta)}$  is defined as:

$$a_i^{(\alpha\beta)} = \left( \frac{\partial I_{\alpha\beta}}{\partial Q_i} \right)_e, \quad (4.7)$$

$\phi_{ij}$  is a cubic force constant described in Chapter 3,  $\omega_i$  is the harmonic frequency, and  $\zeta_{ij}^{(\alpha)}$  is the Coriolis constant [38, 144]. An expression for  $\gamma_{ij}$  may be obtained using higher order perturbation theory<sup>14</sup>.

The connection between theory and experiment is two fold. First,  $B_0$  is computed for several isotopomers then used to determine the vibrational averaged structure for comparison with structure obtained from experimental values for  $B_0$ . Alternatively, the computed anharmonic correction  $-\sum_i \alpha_i(v_i + 1/2)$  may be removed from experimental values of  $B_0$  and the empirical values of  $B_e$  used to find an equilibrium structure to compare with *ab initio* predictions. For benzene, effective bond lengths,  $r_0$ , are obtained from a non-linear fit of the experimental rotational constants  $B_0$  for several isotopomers<sup>15</sup> via:

$$[m_C^i r_{CC}^2 + m_H^i (r_{CC} + r_{CH})^2] = h/24\pi^2 c B_0^i. \quad (4.8)$$

where  $m_C^i$  and  $m_H^i$  are the masses of carbon and hydrogen in each isotopomer, and  $r_{CC}$  and  $r_{CH}$  are the effective bond lengths for CC and CH bonds. Empirical equilibrium bond lengths,  $r_e$ , are also obtained from a similar fit of the empirically corrected experimental rotational constants  $B_e$  (See Table 4.3).

The vibrational corrections calculated using CCSD(T) are within 2 MHz of the corrections used previously [79]. The empirical equilibrium bond

---

<sup>14</sup>The higher order derivatives needed to determine  $\gamma_{ij}$  are expensive and not readily available. For benzene, only the first order corrections,  $\alpha_i$ , are used.

<sup>15</sup>The rotational constants for five isotopomers ( $C_6H_6$ ,  $^{13}C_6H_6$ ,  $C_6D_6$ ,  $^{13}C_6D_6$  and  $C_6H_3D_3$   $D_{3h}$ ) are available and used in the fit described above.

Table 4.3: CCSD(T) ground-state rotational constants, calculated vibrational corrections and empirical equilibrium rotational constants of benzene isotopomers in MHz

		$\text{C}_6\text{H}_6$	$\text{C}_6\text{D}_6$	$^{13}\text{C}_6\text{H}_6$	$^{13}\text{C}_6\text{D}_6$	$\text{C}_6\text{H}_3\text{D}_3$ ( $D_{3h}$ )
Exp.	$B_0$	5689.28	4707.31	5337.92	4464.37	5151.91
Ref. [79]	$B_0 - B_e$	-42.45	-32.93	-38.53	-30.23	
	$B_e$	5721.73	4740.24	5376.45	4494.60	
cc-pVDZ(ae)	$B_0 - B_e^a$	-41.98	-32.02	-38.19	-29.45	-36.41
	$B_e$	5731.26	4739.33	5376.11	4493.82	5188.32
	$B_0$	5541.18	4584.06	5198.96	4347.53	5017.36
cc-pVTZ(ae)	$B_0 - B_e^a$	-43.52	-33.60	-39.53	-30.86	-37.97
	$B_e$	5732.80	4740.91	5377.45	4495.23	5189.87
	$B_0$	5689.01	4708.64	5337.44	4465.42	5152.61
ANO0(fc)	$B_0 - B_e^a$	-43.79	-33.48	-39.82	-30.78	-38.03
	$B_e$	5733.07	4740.79	5377.74	4495.15	5189.93
	$B_0$	5574.22	4613.39	5229.80	4375.16	5048.47
ANO1(fc)	$B_0 - B_e^a$	-43.46	-33.34	-39.51	-30.64	-37.81
	$B_e$	5732.74	4740.65	5377.43	4495.01	5189.72
	$B_0$	5648.05	4674.14	5399.08	4432.79	5115.14
Ref. [164]	$B_0 - \beta\rho$	-46.15	-32.85	-42.26	-30.50	-38.61

<sup>a</sup> Calculated from rotation-vibration constants using a cubic force field at CCSD(T) level of theory with the basis set indicated.

Table 4.4: Empirical equilibrium bond lengths  $r_e$  and effective bond lengths  $r_0$  (Å). All calculations were performed using CCSD(T).

	$r_e$		$r_0^a$	
	$r_{CC}$	$r_{CH}$	$r_{CC}$	$r_{CH}$
cc-pVDZ(ae)	1.3914	1.0812	1.3974(2)	1.0781(11)
cc-pVTZ(ae)	1.3913	1.0805	1.4154(2)	1.0964(11)
ANO0(fc)	1.3912	1.0811	1.4116(2)	1.0896(12)
ANO1(fc)	1.3912	1.0811	1.4023(2)	1.0831(11)
Ref. [79]	1.3914	1.0802		
Rot. Raman Spec. [117]			1.397(1)	1.084(5)
Micro. Spec. [150]			1.3950	1.0820
IR Spec. <sup>b</sup> [163]	1.3902	1.0862	1.3970(2)	1.0807(11)

<sup>a</sup> Nonlinear fit of  $[m_C^i r_{CC}^2 + m_H^i (r_{CC} + r_{CH})^2] = h/24\pi^2 c B_0^i$  was performed using ACESII MAB.

<sup>b</sup> Based on nonlinear fit their moments of inertia,  $I_0$ , performed using ACESII MAB.

lengths that result are within 0.001 Å of their lengths (see Table 4.3). In a similar empirical study of 13 small molecules by F. Pawlowski *et al.* [159], the mean absolute difference (0.00020 Å) and maximum absolute difference (0.00113 Å) between CCSD(T)/cc-pVTZ(ae) and CCSD(T)/cc-pVQZ(ae) suggest the CCSD(T)/cc-pVTZ(ae)'s empirical equilibrium bonds lengths provide sufficient comparison to *ab initio* values.

However, the empirical CH lengths still differ significantly (more than .005 Å) from the length determined by Plíva, Johns and Goodman [164]. They based their study on a linear fit to:

$$3(B_0^i - \beta \rho^i)[m_C^i r_{CC}^2 + m_H^i (r_{CC} + r_{CH})^2] = h/8\pi^2 c \quad (4.9)$$

that included a scaling factor,  $\rho^i \sim (B_0^i/B_0)^2 (M^i/M)^{1/2}$  and a fitting parameter  $\beta$  to determine the vibrational correction. The vibrational corrections they



predicted,  $B_0^i - \beta\rho^i$ , exceed the the computed values for  $\text{C}_6\text{H}_6$  and  $^{13}\text{C}_6\text{H}_6$  by 2.7 MHz but are slightly smaller than  $\text{C}_6\text{D}_6$ ,  $^{13}\text{C}_6\text{D}_6$  and  $\text{C}_6\text{H}_3\text{D}_3$  ( $D_{3h}$ )’s values (see Table 4.3). As a result, their CH equilibrium bond length is longer than this and other studies. These findings also suggest that the vibrational correction cannot be described by a scaled parameter as Plíva suggested. This study also confirms the the conclusion of Martin’s study [135] - the experimental value for  $r_{CH}$  is too long. (The average of CCSD(T)/cc-pVTZ(ae) and CCSD(T)/ANO1(fc) empirical equilibrium bond lengths ( $r_{CC} = 1.3912$  and  $r_{CH} = 1.0808$ ) provides the best means of comparison with the current and future computational studies.)

#### 4.4.3 Distance and Position Averages

The vibrational average quantities,  $r_g$  and  $r_z$ , provide another test for the veracity of the results. The differences between mean internuclear distance and the equilibrium bond length,  $r_g - r_e$ , for SCF (0.0071 Å for CC bonds and 0.0193 Å CH bonds) did not vary with basis sets used (see Table B.5). This absence of significant variation persists when correlation energy is included via MP2 or CCSD(T) (see Tables 4.2 and B.5). Correlating the electrons increased this difference slightly (less than 0.0015 Å). The differences between distance between internuclear positions and the equilibrium bond length,  $r_z - r_e$ , also did not vary significantly with either method or basis set (see Tables 4.2 and B.5). The CCSD(T) results are similar the results obtained by Martin *et al.* for acetylene [133] and ethylene [134].

The small variations noted above confirm the method utilized in earlier studies [79]. Most of the difference between the values included in Table 4.2 and those obtained by K. Tamagawa and coworkers results from the

equilibrium bond lengths and these differences are similar to the difference between the *ab initio* and empirical bond lengths already discussed. The agreement of both CCSD(T)/cc-pVTZ(ae) and CCSD(T)/ANO1(fc) with the experimental values of K. Tamagawa is exceptional. For  $r_g$ , the CC distance for CCSD(T)/cc-pVTZ(ae) and the CH distance for both CCSD(T)/cc-pVTZ(ae) and CCSD(T)/ANO1(fc) lie within the range of experimental uncertainty while the value obtained at the CCSD(T)/ANO1(fc) level is 0.004 Å outside this range of uncertainty (see Table 4.2). The results in Table 4.2 are similar for  $r_z$ , except the CC distance for CCSD(T)/ANO1(fc) is within the experimental uncertainty while the value of CCSD(T)/cc-pVTZ(ae) is 0.003 Å outside its uncertainty range.

Finally, these results also conflict with the empirical bond CH length determined by J. Plíva *et al.* Second, the difference between the calculated CH mean internuclear distance and corresponding equilibrium bond length is between 0.019 and 0.021 Å and is close to 0.022 Å ( $r_g - r_e$  for methane) [79] and 0.022 Å ( $r_g - r_e$  for ethylene) [134] for unlike the difference of 0.015 Å obtained when Pliva’s empirical bond length is used. Secondly, the difference also noted above between the compute distance between mean internuclear position of neighboring carbon and hydrogen atoms and the corresponding equilibrium bond length is positive ( $\sim 0.004$  Å) while the difference between the value obtained for  $r_z$  by K. Tamagawa and the value for  $r_e$  by J. Plíva is negative. J. Gauss and J. Stanton noted that a shortening of the CH bond implies the vibrational effect on the totally symmetric CH stretch is negative which inconsistent with typical anharmonic models of stretching modes.

#### 4.4.4 Effective Bond Lengths

Although the computed vibrational corrections are similar to those calculated by Gauss [79], the effective rotational constants for ANO0 and cc-pVDZ differ significantly (more than 100 MHz for cc-pVDZ and more than 90 MHz for ANO0) from the experimental values (see Table 4.3). As a result, the effective bond lengths from nonlinear fit for these smaller basis sets are at least 0.01 Å longer than three of the four experimental values with the exception of ANO0's CH bond which is 0.006 Å longer (see Table 4.4).

In contrast, the most recent experimental effective CC bond lengths are closer to those calculated for CCSD(T)/ANO1(fc) and CCSD(T)/cc-pVTZ(ae) (see Table 4.4). The CC effective lengths for CCSD(T)/ANO1(fc) is 0.006 Å longer than the average of the experimental lengths while CCSD(T)/cc-pVTZ(ae)'s length is only 0.001 Å longer. Unlike the experimental CC bond lengths, the CH bond lengths have greater uncertainty. As a result, CCSD(T)/ANO1(fc)'s CH effective bond length is within the uncertainty of the length obtained by rotational Raman spectroscopy and is within 0.002 Å of infrared spectroscopy's length while the bond length of CCSD(T)/cc-pVTZ(ae) roughly 0.004 Å smaller than the spectroscopic average. Using both the theoretical and experimental, the average effective bond lengths are:  $r_{CC} = 1.3977$  Å and  $r_{CH} = 1.0816$  Å.

Table 4.5: CCSD(T) harmonic frequencies ( $\text{cm}^{-1}$ ) <sup>a</sup>

$\omega^b$	CCSD(T)/ cc-pVTZ(ae)	CCSD(T)/ cc-pVQZ(ae)	CCSD(T)/ ANO1(fc)	CCSD(T)/ ANO2(fc)	Est. [84]
$\omega_1$	1014.6	1013.1	1003.2	1006.0	994.4
$\omega_2$	<b>3227.9</b>	<b>3219.7</b>	3211.7	3208.7	3191
$\omega_3$	1378.3	1378.5	1374.4	1379.4	1367
$\omega_4$	709.2	693.9	708.2	711.9	707
$\omega_5$	993.0	987.5	1007.7	<b>1010.6</b>	990
$\omega_6$	610.7	610.5	610.3	611.1	607.8
$\omega_7$	3187.8	3192.9	3185.1	3182.1	3174
$\omega_8$	<b>1648.6</b>	<b>1646.9</b>	<b>1635.9</b>	<b>1639.5</b>	<b>1607</b>
$\omega_9$	<b>1207.8</b>	1195.8	1191.6	1192.0	1177.8
$\omega_{10}$	<b>872.7</b>	863.4	864.2	863.5	847.1
$\omega_{11}$	<b>704.0</b>	689.7	686.5	684.0	674
$\omega_{12}$	1016.5	1008.2	1019.0	1022.9	1010
$\omega_{13}$	3169.3	3181.7	3175.1	3172.0	3174
$\omega_{14}$	<b>1345.2</b>	<b>1339.3</b>	1325.5	<b>1329.7</b>	1309.4
$\omega_{15}$	<b>1181.4</b>	1163.9	1159.7	1159.0	1149.7
$\omega_{16}$	408.7	404.9	405.7	406.6	398
$\omega_{17}$	981.9	974.9	983.7	985.7	967
$\omega_{18}$	<b>1063.6</b>	<b>1061.0</b>	1054.6	1056.7	1038.3
$\omega_{19}$	<b>1518.4</b>	<b>1514.4</b>	1506.0	1510.5	<b>1494</b>
$\omega_{20}$	<b>3211.6</b>	<b>3209.7</b>	3201.5	3198.5	3181.1

<sup>a</sup> Differences from experimental estimates of more than  $20 \text{ cm}^{-1}$  that are discussed in the text are emphasised in **bold**.

<sup>b</sup> Wilson numbering [227] used. The table has been subdivided by irreducible representations of the molecular symmetry group  $D_{6h}$ . From top to bottom, the symmetry species are:  $a_{1g}$ ,  $a_{2g}$ ,  $b_{2g}$ ,  $e_{2g}$ ,  $e_{1g}$ ,  $a_{1u}$ ,  $b_{1u}$ ,  $b_{2u}$ ,  $e_{2u}$  and  $e_{1u}$ .

## 4.5 Harmonic Frequencies

### 4.5.1 *Ab Initio* Frequencies

Although the *ab initio* harmonic frequencies of benzene can be compared to three different of estimates:  $\omega_{obs}$ <sup>16</sup> [84],  $\omega_{emp}$  [140, 143]<sup>17</sup> and  $\omega_{ave}$  [91]<sup>18</sup>, the discussion in this section will focus on comparing this study to the harmonic frequencies to  $\omega_{obs}$ . The other estimates proposed will be discussed in Section 4.5.2 relative to new empirical estimates.

Beginning with the harmonic frequencies calculated using Hartree-Fock, the average absolute deviation from the harmonic frequencies Goodman *et al.* [84] proposed exceed  $100\text{ cm}^{-1}$  for each basis set (see Table B.6). This average deviation is comparable with the other Hartree-Fock studies of benzene [84, 135, 140]<sup>19</sup> and similar hydrocarbons ( $\text{C}_2\text{H}_2$  [208] and  $\text{C}_2\text{H}_4$  [2, 118]). It also did not improve as the size of the basis set increased, and finally, the absolute percent differences varied from 1.6 to 14.8 %. However, the harmonic frequencies of both the correlation consistent and ANO basis sets of comparable size agree with each other to within  $10\text{ cm}^{-1}$ . The only exception,  $\omega_3(a_{2g})$  for cc-pVDZ verses ANO0, differed by  $13\text{ cm}^{-1}$ . Though basis sets of similar size agreed the harmonic frequencies increased or decreased by more than  $10\text{ cm}^{-1}$  as the size of the basis set increased. The largest changes occur in the

---

<sup>16</sup>Goodman *et al.* estimated harmonic frequencies from experimental fundamentals and anharmonic corrections.

<sup>17</sup>Maslen *et al.* and Miani *et al.* used their computed force field and experimental fundamentals to empirically estimate the harmonic frequencies. They used SCF/DZP and B3LYP/TZ2P respectively.

<sup>18</sup>An average of the experimental and SCF/DZP empirical estimates.

<sup>19</sup>The harmonic frequencies calculated for HF/cc-pVDZ and HF/cc-pVTZ by ACESII are within  $0.5\text{ cm}^{-1}$  of the frequencies Martin *et al.* [135] obtained for the same basis set calculated with MOLPRO 96. This small discrepancy is due to their use of finite difference methods rather than analytic second derivatives used here.

CH stretch modes  $\omega_2(a_{1g})$ ,  $\omega_7(e_{2g})$ ,  $\omega_{13}(b_{1u})$  and  $\omega_{20}(e_{1u})$  which systematically decreased by  $23\text{ cm}^{-1}$  for the correlation consistent basis sets and  $25\text{ cm}^{-1}$  for the ANO basis sets. Several other deviations between cc-pVDZ and cc-pVTZ are also larger than  $10\text{ cm}^{-1}$ :  $\omega_3(a_{2g})$ ,  $\omega_5(b_{1g})$ ,  $\omega_8(e_{2g})$  and  $\omega_{15}(b_{2u})$ , while the only other deviation between ANO0 and ANO1 is  $\omega_{15}(b_{2u})$ .

To reduce the difference between the observed and *ab initio* values, correlation energy is introduced. For MP2, the average absolute deviation dropped to less than  $40\text{ cm}^{-1}$  for each basis set consistent with previous MP2 studies employing various basis sets [84, 91, 135]. See Table B.7. However,  $\omega_{14}(b_{1u})$ , the vibrational mode between Kekulé structures, differed by more than  $160\text{ cm}^{-1}$  for each basis set. Noting the pathological nature of this mode, Martin stated: “Since correctly describing the curvature along this vibration is essentially a two-reference problem at large amplitude, it is not surprising that a low-order perturbation theory method would fail [135].” The average absolute deviation is reduced by at least  $6\text{ cm}^{-1}$  when  $\omega_{14}$  is excluded. Unlike, Hartree-Fock which had relatively small variations ( $30\text{ cm}^{-1}$ ) relating to the size and nature of the basis set, the harmonic frequencies of MP2 are more sensitive to the basis set used. Three frequencies that vary  $50\text{ cm}^{-1}$  or more:  $\omega_4(b_{2g})$ ,  $\omega_5(b_{2g})$  and  $\omega_{17}(e_{2u})$  correspond to out of plane bending modes. The inclusion of *f* functions in cc-pVTZ and ANO1 as suggested by Simandiras *et al.* [208], Goodman *et al.* [84] and Handy *et al.* [90] is a factor. However, the differences between cc-pVDZ(ae) and cc-pVTZ(ae):  $84$ ,  $35$  and  $27\text{ cm}^{-1}$  for  $\omega_4$ ,  $\omega_5$  and  $\omega_{17}$ , are larger than the differences between ANO0(fc) and ANO1(fc):  $24$ ,  $18$  and  $16\text{ cm}^{-1}$ . The additional difference is due to basis set superposition error<sup>20</sup>. In a CCSD(T) study of acetylene by Martin *et al.* [133], cc-pVTZ

---

<sup>20</sup>An artifact of the incompleteness of any basis set. By choice, basis functions are cen-

contained more of this error than ANO1.

If CCSD is used to account for electron correlation, the average absolute deviation are roughly  $25\text{ cm}^{-1}$  for the smaller basis sets cc-pVDZ and ANO0 but higher, almost  $40\text{ cm}^{-1}$ , for cc-pVTZ. See Table B.8 Also, the average absolute deviation of the in-plane modes for CCSD/cc-pVDZ(ae) is larger than Brenner’s study [34]. The differences stems from the inclusion of all electrons in correlation calculations as opposed to the frozen core approximation utilized by Brenner *et al.* and the inclusion of *d* basis functions on the hydrogen atoms. Like their MP2/cc-pVDZ(ae) counterparts, the harmonic frequencies are sensitive to the size and nature of the basis set used and the same out of plane bending modes exhibit basis set superposition error and the need for *f* functions. However, the larger differences,  $60\text{ cm}^{-1}$  and higher, are observed for  $\omega_8$  between CCSD and Goodman’s observed harmonic frequency. Its fundamental,  $\nu_8$ , can be observed using Raman spectroscopy; however, a strong overlap with the Raman active combination band  $\nu_{1+6}$  prevents standard rotation-vibration analysis to obtain the fundamental. This overlap is separated in ionization-detected stimulated Raman spectroscopy [68] and then the fundamental is deperturbed from the Fermi interaction [160]. Goodman *et al.* used liquid Raman studies [149, 233] of the fundamental and first overtone bands to determine the anharmonic correction for  $\nu_8$ . Their correction,  $6\text{ cm}^{-1}$ , is significantly smaller than empirical estimations of both Maslen ( $39\text{ cm}^{-1}$ ) [140] and Miani ( $45\text{ cm}^{-1}$ ) [143]. Smaller differences ( $29\text{ cm}^{-1}$  CCSD/cc-pVDZ(ae) and CCSD/ANO0(fc),  $50\text{ cm}^{-1}$  CCSD/cc-pVTZ(ae) and  $37\text{ cm}^{-1}$  for CCSD/ANO1(fc)) occur for  $\omega_{19}$  which used the fundamental and

---

tered at nuclei and the superposition of a function from a neighboring nuclei will effect the computed electron density.

first overtone bands of liquid Raman of the same studies. The correction Goodman suggests,  $10\text{ cm}^{-1}$ , is smaller than the  $28\text{ cm}^{-1}$  suggested by Maslen or the  $38\text{ cm}^{-1}$  suggested by Miani.

When triples are included via CCSD(T), the average absolute deviation of the calculated harmonic frequencies from Goodman’s is than  $16\text{ cm}^{-1}$  for cc-pVQZ(ae) and  $14\text{ cm}^{-1}$  for ANO2(fc). See Table 4.5. These deviations are slightly higher than the deviations for the harmonic frequencies Martin *et al.* obtained for cc-pVTZ’(fc) ( $11\text{ cm}^{-1}$ ) and ANO1’(fc)<sup>21</sup> ( $13\text{ cm}^{-1}$ ) and are comparable to recent density functional studies ( $18\text{ cm}^{-1}$  for B3LYP/TZ2P and  $14\text{ cm}^{-1}$  for B97-1/TZ2P). The largest differences ( $40\text{ cm}^{-1}$  for cc-pVQZ(ae) and  $33\text{ cm}^{-1}$  for ANO2(fc)) also occur for  $\omega_8(e_{2g})$ . Smaller differences of  $20\text{ cm}^{-1}$  and  $16\text{ cm}^{-1}$  occur for  $\omega_{19}(e_{1u})$  which used the fundamental and first overtone bands of liquid Raman of the same studies. Other deviations of more than  $20\text{ cm}^{-1}$  include:  $\omega_5(b_{2g})$  and  $\omega_{14}(b_{2u})$  for CCSD(T)/ANO2(fc) and  $\omega_2(a_{1g})$ ,  $\omega_{14}(b_{2u})$ ,  $\omega_{18}(e_{1u})$  and  $\omega_{20}(e_{1u})$  for CCSD(T)/cc-pVQZ(ae). Of these frequencies, only  $\omega_{20}(e_{1u})$  contains an anharmonic correction in Goodman’s estimated harmonic frequencies.

Differences between CCSD(T)/ANO2(fc) and CCSD(T)/cc-pVQZ(ae) of more than  $10\text{ cm}^{-1}$  occurred in the C-H stretch modes:  $\omega_2(a_{1g})$ ,  $\omega_7(e_{2g})$  and  $\omega_{20}(e_{1u})$ , the out of plane bending modes:  $\omega_4(b_{2g})$ ,  $\omega_5(b_{2g})$  and  $\omega_{17}(e_{2u})$  and the ring breathing mode:  $\omega_{12}(b_{1u})$ . The systematic difference of  $\sim 11\text{ cm}^{-1}$  for the C-H stretch modes represents a percent difference of less than 0.5% and is not as significant as the other differences. However, the  $b_{2g}$  out of plane bends,  $\omega_4$  and  $\omega_5$ , differ by more than  $15\text{ cm}^{-1}$ . In both cases, the harmonic frequencies

---

<sup>21</sup>They excluded the  $d$  basis functions for each hydrogen atom from standard cc-pVTZ and ANO1 basis sets. Denoted cc-pVTZ’(fc) and ANO1’(fc) respectively.



of decrease from cc-pVTZ(ae) to cc-pVQZ(ae) while increase from ANO1(fc) to ANO2(fc). The ANO2 basis set includes more of each type of function in its primitive set  $13s8p6d4f2g/8s6p4d2f$  than cc-pVQZ  $12s6p3d2f1g/6s3p2d1f$ . The presence of more primitives with higher angular momentum may account for some of the difference. Martin *et al.* [135] suggested the absence basis set superposition error (BSSE) accounted for similar differences he observed between cc-pVTZ'(fc) and ANO1'(fc). ANO1(fc) has less of this error than cc-pVTZ(fc) for acetylene (the augmentation of cc-pVTZ with uncontracted diffuse functions also reduced this error) [133]. The correlation of all electrons (cc-pVQZ(ae)) as opposed to the frozen core approximation (ANO2(fc)) also effected these two frequencies. The average absolute difference between cc-pVTZ(fc) and cc-pVTZ(ae) is  $12\text{ cm}^{-1}$  while differences for  $\omega_4$  and  $\omega_5$  are at least  $25\text{ cm}^{-1}$ . Also, including the core electrons in the correlation increased most of the harmonic frequencies; however, it decreased  $\omega_4$  and  $\omega_5$ .

The harmonic frequencies for cc-pVDZ(fc) computed using analytic second derivatives are almost identical (three frequencies differ by  $0.1\text{ cm}^{-1}$ ) to the frequencies Martin *et al.* obtained using finite difference. See Table B.9. However, differences of as much as  $9\text{ cm}^{-1}$  ( $\omega_3(a_{2g})$ ) occur when  $d$  functions are included in cc-pVTZ and ANO1. Overall, the average difference between the harmonic frequencies obtained by Martin *et al.* [135] and by Goodman *et al.* [84] ( $11\text{ cm}^{-1}$  for CCSD(T)/cc-pVTZ' and  $13\text{ cm}^{-1}$  for CCSD(T)ANO1') is roughly equivalent to the average difference between the harmonic frequencies obtained in this study and by Goodman *et al.*

To summarize:

1. The harmonic frequencies computed using analytic second derivatives differ only slightly from those obtained in earlier studies.

2. The harmonic frequencies computed at the HF level of theory differed systematically from the experimental estimates in the same manner as other hydrocarbons that have been studied.
3. The inclusion of correlation energy with MP2 improved the agreement between the computed harmonic frequencies and experimental estimates, but the MP2 level of theory contained one frequency,  $\omega_{14}(b_{1u})$ , which could not be described by MP2 for reasons discussed in the literature.
4. Harmonic frequencies obtained using CCSD(T) with large basis sets (ANO2(fc) and cc-pVQZ(ae)) deviate on average  $15\text{ cm}^{-1}$  from the experimental estimates and suggest the anharmonic effects not included in all the experimental estimates are significant.

#### 4.5.2 Empirical Estimates

The empirical harmonic frequencies obtained in this study reflect the *ab initio* results discussed in the previous section. For CCSD(T)/cc-pVTZ(ae), the largest deviations from CCSD(T)/ANO2(fc) occur for the out of plane bending modes:  $\omega_4(b_{2g})$ ,  $\omega_5(b_{2g})$  and  $\omega_{17}(e_{2u})$  which displayed basis set superposition error in the *ab initio* harmonic frequencies as seen in Table 4.6. They also have an average absolute difference from the earlier studies by Maslen *et al.* (SCF/DZP) [140] and Miani *et al.* (B3LYP/TZ2P) [143] of more than  $10\text{ cm}^{-1}$  while the CCSD(T)/ANO1(fc) empirical frequencies differ on average  $5\text{ cm}^{-1}$  from those studies. The largest difference between CCSD(T)/ANO1(fc) and earlier studies occurs for  $\omega_7(e_{2g})$  which differs by 25

Table 4.6: Comparison of empirical harmonic frequencies ( $\text{cm}^{-1}$ ) estimated with CCSD(T) to the estimates of other levels of theory and experiment<sup>a</sup>.

$\omega^b$	CCSD(T)/ cc-pVTZ(ae)	CCSD(T)/ ANO1(fc)	Exp. Est. [84]	HF/DZP [140]	B3LYP/ TZ2P [143]
$\omega_1$	1008.7	1009.1	994.4	1008	1003
$\omega_2$	<i>3216.0</i>	<i>3218.5</i>	3191	3208	3218
$\omega_3$	1374.9	1384.0	1367	1390	1392
$\omega_4$	693.8	713.6	707	718	717
$\omega_5$	965.0	1014.3	990	1011	1012
$\omega_6$	610.0	611.9	607.8	613	617
$\omega_7$	<b>3182.2</b>	<b>3184.6</b>	3174	<b>3191</b>	<b>3210</b>
$\omega_8$	<i>1642.8</i>	<i>1643.6</i>	1607	1639	1645
$\omega_9$	<i>1201.7</i>	1193.9	1177.8	1192	1197
$\omega_{10}$	859.7	863.8	847.1	866	861
$\omega_{11}$	692.8	684.9	674	686	683
$\omega_{12}$	1015.9	1027.6	1010	1024	1030
$\omega_{13}$	3172.1	3183.7	3174	3172	
$\omega_{14}$	<i>1332.1</i>	1327.5	1309.4	1318	1338
$\omega_{15}$	<i>1174.8</i>	1161.6	1149.7	1167	1163
$\omega_{16}$	404.6	406.9	398	407	406
$\omega_{17}$	967.4	988.1	967	989	987
$\omega_{18}$	<i>1062.4</i>	<i>1058.8</i>	1038.3	1058	1057
$\omega_{19}$	1513.5	1513.1	1494	1512	1522
$\omega_{20}$	3202.7	3203.2	3181.1	3191	3212

<sup>a</sup> Differences from other empirical estimates of more than  $20 \text{ cm}^{-1}$  that are discussed in the text are emphasised in **bold**. Differences from experimental estimates of more than  $20 \text{ cm}^{-1}$  are emphasised in *italics*.

<sup>b</sup> Wilson numbering [227] used. The table has been subdivided by irreducible representations of the molecular symmetry group  $D_{6h}$ . From top to bottom, the symmetry species are:  $a_{1g}$ ,  $a_{2g}$ ,  $b_{2g}$ ,  $e_{2g}$ ,  $e_{1g}$ ,  $a_{1u}$ ,  $b_{1u}$ ,  $b_{2u}$ ,  $e_{2u}$  and  $e_{1u}$ .

$\text{cm}^{-1}$  from B3LYP/TZ2P<sup>22</sup>. Also, a deviation of  $11 \text{ cm}^{-1}$  from HF/DZP is also seen for  $\omega_{13}(b_{2u})$ . This difference may result from the difference in the experimental fundamental used by Maslen *et al.* [140]. The accepted value:  $3057 \text{ cm}^{-1}$  [35] used in their study is  $42 \text{ cm}^{-1}$  higher than  $3015 \text{ cm}^{-1}$  [66] used in this study. Despite this significant difference the empirical frequencies are remarkably similar.

The absolute average difference between the empirical harmonic frequencies computed using the cubic and quartic force constants obtained using CCSD(T)/ANO1(fc) and CCSD(T)/ANO2(fc)'s the harmonic frequencies is  $3.3 \text{ cm}^{-1}$ . The largest difference,  $11 \text{ cm}^{-1}$ , occurs for  $\omega_{13}(b_{2u})$  whose fundamental,  $3015^{+2}_{-5} \text{ cm}^{-1}$  [66] has the largest uncertainty of any of the fundamentals used to compute the empirical frequencies. Therefore, the uncertainty of  $\omega_{13}(b_{2u})$  is at least  $5 \text{ cm}^{-1}$ , half the difference between the *ab initio* frequency and empirical estimate.

The *ab initio* harmonic frequencies varied significantly, by as much as  $40 \text{ cm}^{-1}$  in one case, from those estimated by Goodman and coworkers [84]. Other estimates by Maslen *et al.* [140] and Miani *et al.* [143] used the cubic and quartic force constants they calculated to determine the anharmonic correction. In these case, the harmonic frequencies increased: an average of  $16 \text{ cm}^{-1}$  for SCF/DZP and an average  $20 \text{ cm}^{-1}$  for B3LYP/TZ2P. The absolute deviation of harmonic frequencies from CCSD(T)/cc-pVQZ(ae) and CCSD(T)/ANO2(fc) averages  $9 \text{ cm}^{-1}$  and  $4 \text{ cm}^{-1}$  when SCF/DZP force constants are used and  $8 \text{ cm}^{-1}$  and  $7 \text{ cm}^{-1}$  for B3LYP/TZ2P force constants.

---

<sup>22</sup>The estimated frequency obtained by Miani *et al.* [143] also differed by  $42 \text{ cm}^{-1}$  from the frequency they computed using B3LYP/TZ2P and differs by  $28 \text{ cm}^{-1}$  from the frequency computed in this study using CCSD(T)/ANO2(fc).

The empirical frequencies calculated in this study from CCSD(T)/ANO1(fc)'s cubic and quartic force constants also differ from the experimental estimates Goodman *et al.* used to construct their harmonic force field. The average difference of  $17 \text{ cm}^{-1}$  suggests the anharmonic corrections they derived from experiment do not account for the anharmonicity present in the vibrational modes and do not provide a close comparison with *ab initio* harmonic frequencies.

In summary, most of the empirical harmonic frequencies estimated at the CCSD(T) level of theory agree with the earlier empirical estimates to within  $10 \text{ cm}^{-1}$  -  $\nu_7(e_{2g})$  being the most notable exception. However, these frequencies deviate significantly from the experimental estimates determined by Goodman *et al.* These sets of frequencies also include an estimate for  $\omega_{13}(b_{1u})$  not included earlier by Miani *et al.* and provide a reasonable standard of comparison for the harmonic frequencies computed using *ab initio* methods.

## 4.6 Spectral Predictions

As discussed in Chapter 3, the vibrational frequencies contain anharmonic effects and are not adequately described by harmonic frequencies. Second-order vibrational perturbation theory, outlined in Chapter 3, is one technique used to compute *ab initio* vibrational frequencies. The vibrational energy level may be expanded in terms of vibrational quantum numbers,  $v_i$ :

$$E(v) = G_0 + \sum_i \omega_i \left( v_i + \frac{1}{2} \right) + \sum_{i \leq j} x_{ij} \left( v_i + \frac{1}{2} \right) \left( v_j + \frac{1}{2} \right) + \dots \quad (4.10)$$

where  $G_0$  is a constant independent of the vibrational quantum numbers which arises from VPT2 and  $x_{ij}$  are the anharmonicity constants defined in Chapter

3. The energy of a transition from the vibrational ground state to the first excited vibrational state of a particular vibrational mode  $i$ , i.e. the fundamental frequency ( $\nu_i$  or  $i_1$ ), may then be obtained using:

$$\nu_i = \omega_i + 2x_{ii} + \frac{1}{2} \sum_{j \neq i} x_{ij}. \quad (4.11)$$

Two quantum transitions such as combination bands, a transition from the ground state to a vibrational excited state where two modes have been excited to their first excited state, or first overtones, a transition from the ground state to the second excited state of a particular vibrational mode, may be obtained using<sup>23</sup>:

$$\nu_i + \nu_j = \omega_i + \omega_j + x_{ij}. \quad (4.12)$$

To highlight the agreement of the spectral predictions of VPT2 with experimental spectra, the following points will be discussed in this section:

1. Agreement between the fundamental frequencies computed with VPT2 and measured by experiment for benzene,
2. Effects of Fermi resonance and how to account for them in fundamental frequencies,
3. Agreement of VPT2 infrared active two quantum transitions with experiment, and
4. Effects of Darling-Dennison and Fermi resonances and how to account for them in infrared active two quantum transitions.

---

<sup>23</sup>The abelian treatment utilized in this study incorporates the  $g_{ij}$  terms describe in the nonabelian treatment by Reference [144] into the anharmonicity constants  $x_{ij}$  directly. As a result, two quantum transitions involving degenerate states split because the anharmonic constants are not identical, i.e.  $x_{7a8a} \neq x_{7a8b}$ .

### 4.6.1 Fundamental Frequencies

The absolute mean deviation straight forward between VPT2 fundamentals determined using SCF and experimental frequencies as seen in Table B.10 ranged from 93.8 to 98.3  $\text{cm}^{-1}$ <sup>24</sup>. The fundamentals' absolute mean deviation is also similar to the frequencies obtained by Maslen *et al.* [140] (96.1  $\text{cm}^{-1}$ ) and Willets and Handy [226] (100.2  $\text{cm}^{-1}$ ) who used DZP as their basis set<sup>25</sup>.

Straight forward VPT2 fundamentals computed from MP2 harmonic frequencies, cubic and quartic force constants and rotational constants deviated from the current experimental fundamentals on average from 23.7 to 32.4  $\text{cm}^{-1}$  depending on the basis set as seen in Table B.12. Each correlation consistent Dunning and atomic natural orbital basis set deviated significantly (more than 120  $\text{cm}^{-1}$ ) from the experimental fundamental  $\nu_{14}(b_{2u})$ . As noted in Section 4.5.1, this vibrational mode is between Kekulé structures and is poorly described by perturbation theory. However, the deviation is not as acute as the harmonic deviation discussed earlier.

Using the CCSD(T) level of theory, the absolute mean deviation from experiment of the fundamentals computed using straight forward VPT2 is between 10 (CCSD(T)/ANO1(fc) and CCSD(T)/ANO2/1(fc)<sup>26</sup> and 50  $\text{cm}^{-1}$

---

<sup>24</sup>For  $\nu_{20}(e_{2u})$ , the original [167] and not the deperturbed frequency [168] is used comparisons.

<sup>25</sup>Maslen *et al.* [140] initial study in 1992 accounted for Fermi resonance by diagonalizing a matrix of fundamentals coupled with combinations while Willets and Handy used the symmetric top formalism described earlier to compute the anharmonic constants from the cubic and quartic force constants Maslen *et al.* computed and treated for Fermi resonance by excluding denominators with differences between  $\omega_i$  and  $\omega_j + \omega_k$  smaller than 100  $\text{cm}^{-1}$ .

<sup>26</sup>Fundamentals and two quantum transitions computed using the harmonic frequencies at the CCSD(T)/ANO2(fc) level of theory and the cubic and quartic force constants calculated at the CCSD(T)/ANO1(fc) level of theory are designated as CCSD(T)/ANO2/1(fc).

Table 4.7: CCSD(T) fundamental frequencies: VPT2 ( $\text{cm}^{-1}$ )

Sym.		CCSD(T)/ ANO1(fc)	CCSD(T)/ ANO2/1(fc) <sup>a</sup>	CCSD(T)// B97-1 [28]	Exp. <sup>b</sup>
<i>a<sub>1g</sub></i>	$\nu_1$	987.1	989.9	987	993.1
	$\nu_2$ <sup>c</sup>	<b>3070.4</b>	<b>3070.2</b>	3069	3073.9
<i>a<sub>2g</sub></i>	$\nu_3$	1340.3	1344.0	1348	1350.0
<i>b<sub>2g</sub></i>	$\nu_4$	697.0	700.7	698	702.2
	$\nu_5$	986.5	989.3	984	992.9
<i>e<sub>2g</sub></i>	$\nu_6$	604.4	605.3	607	608.1
	$\nu_7$	3055.0	3053.6	3050	3057.0
	$\nu_8$ <sup>c</sup>	<b>1601.8</b>	<b>1605.5</b>	1620	1609.5
	$\nu_9$	1175.4	1175.8	1177	1177.8
<i>e<sub>1g</sub></i>	$\nu_{10}$	847.5	846.8	843	847.1
<i>a<sub>1u</sub></i>	$\nu_{11}$	675.8	673.3	673	674.0
<i>b<sub>1u</sub></i>	$\nu_{12}$	1005.2	1009.1	1004	1013.7
	$\nu_{13}$ <sup>c</sup>	<b>3006.1</b>	<b>3006.3</b>	3022	3015.0
<i>b<sub>2u</sub></i>	$\nu_{14}$	1307.4	1310.6	1305	1309.4
	$\nu_{15}$	1145.6	1145.0	1149	1147.7
<i>e<sub>2u</sub></i>	$\nu_{16}$	397.0	397.8	398	398.1
	$\nu_{17}$	963.5	965.5	962	968.0
<i>e<sub>1u</sub></i>	$\nu_{18}$	1033.9	1036.2	1046	1038.3
	$\nu_{19}$	1476.8	1481.3	1486	1484.0
	$\nu_{20}$ <sup>c</sup>	<b>3040.7</b>	<b>3043.2</b>	3051	3047.9

<sup>a</sup> ANO2/1(fc) utilized the harmonic frequencies computed at the CCSD(T)/ANO2(fc) level of theory with cubic and quartic force constants determined using CCSD(T)/ANO1(fc) to compute vibrational fundamental frequencies.

<sup>b</sup> See Table 4.1 for experimental references. Frequencies which have been treated for Fermi resonance will be emphasized using **bold**. Frequencies which deviate more than 10  $\text{cm}^{-1}$  from experiment will be emphasized using *italics*.

<sup>c</sup>  $\nu_2$  in Fermi resonance with  $2\nu_{19}$  overtone. VPT2 results are: 3065.5 and 3064.7  $\text{cm}^{-1}$  CCSD(T)/ANO1(fc) and CCSD(T)/ANO2/1(fc), respectively.  $\nu_8$  in Fermi resonance with  $\nu_1 + \nu_6$  combination band. VPT2 results are: 1598.1 and 1601.8  $\text{cm}^{-1}$  for CCSD(T)/ANO1(fc) and CCSD(T)/ANO2/1(fc), respectively.  $\nu_{13}$  and  $\nu_{20}$  in Fermi resonance with  $\nu_8 + \nu_{19}$  combination band. VPT2 results are: 3089.3 and 3115.0  $\text{cm}^{-1}$  for  $\nu_{13}(b_{1u})$  and 3085.3 and 3086.3  $\text{cm}^{-1}$  for  $\nu_{20}(e_{1u})$  for CCSD(T)/ANO1(fc) and CCSD(T)/ANO2/1(fc), respectively.



(CCSD(T)/cc-pVTZ(ae)) as seen in Table B.14. The largest deviation 780  $\text{cm}^{-1}$  for  $\nu_{13}(b_{1u})$  CCSD(T)/cc-pVTZ(ae) results from strong Fermi resonance with  $\nu_{8+19}$ . However, other significant not resulting from Fermi resonance. For cc-pVDZ(ae),  $\nu_5(b_{2g})$ ,  $\nu_{12}(b_{1u})$  and  $\nu_{17}(e_{1u})$  differ by more than 20  $\text{cm}^{-1}$ . These differences are consistent with significant differences noted earlier in Section 4.5.1; however, the difference for  $\nu_4(b_{2g})$  coincidentally improved significantly (more than 70  $\text{cm}^{-1}$ ) once the anharmonic correction is included. For cc-pVTZ(ae),  $\nu_5(b_{2g})$  differs more than any other frequency computed using CCSD(T), 28  $\text{cm}^{-1}$ . See Table B.14. Several less significant differences larger than 10  $\text{cm}^{-1}$  occur for  $\nu_2(a_{1g})$ ,  $\nu_4(b_{2g})$ ,  $\nu_{10}(e_{1g})$ ,  $\nu_{11}(a_{2u})$ ,  $\nu_{14}(b_{1u})$  and  $\nu_{17}(e_{2u})$ . These differences coincide with the differences noted in Section 4.5.1. For ANO0(fc),  $\nu_4(b_{2g})$ ,  $\nu_5(b_{2g})$  and  $\nu_{17}(e_{2u})$  also differ by more than 20  $\text{cm}^{-1}$  from experiment. Seven other frequencies differ by 10  $\text{cm}^{-1}$  or more; however, each of the fundamentals of ANO1(fc) and ANO2/1(fc) fundamental are less than 10  $\text{cm}^{-1}$  if they are not effected by Fermi resonance. with a mean absolute deviation of 4.2 and 2.5  $\text{cm}^{-1}$ , respectively. This average deviation is similar to the mean absolute deviation of 4.6  $\text{cm}^{-1}$  for CCSD(T)//B97-1<sup>27</sup>. The largest difference,  $\nu_3(a_{2g})$  (9.7  $\text{cm}^{-1}$ ) has the most experimental uncertainty since it was determined from combination bands without anharmonic corrections<sup>28</sup>

As described in Chapter 3, Fermi resonance is a limitation of VPT2<sup>29</sup> VPT2 fails to account for Fermi resonances (i.e. when  $\omega_i \sim \omega_j + \omega_k$ ). To

---

<sup>27</sup>In this method, the anharmonicity constants obtained using B97-1/TZ2P are added to the harmonic frequencies of CCSD(T)/ANO1' [28, 135].

<sup>28</sup>The anharmonic effect ought to be small since the anharmonic constants computed by VPT2 are small for the combination bands Brodersen and Langseth [35] used to determine  $\nu_3$ . Also, the combination frequencies they computed as a consistency check are 5  $\text{cm}^{-1}$  or less than what they observed.

<sup>29</sup>A difference from experiment of more than 50  $\text{cm}^{-1}$  occurs in  $\nu_5$  of formaldehyde for straight forward VPT2. See Table 3.2.

account for this resonance,

$$\phi_{ijk}^2 \left( \frac{1}{\omega_i + \omega_j + \omega_k} + \frac{1}{\omega_i - \omega_j - \omega_k} - \frac{1}{-\omega_i + \omega_j - \omega_k} - \frac{1}{-\omega_i - \omega_j + \omega_k} \right) \quad (4.13)$$

is replaced with

$$\phi_{ijk}^2 \left( \frac{1}{\omega_i + \omega_j + \omega_k} - \frac{1}{-\omega_i + \omega_j - \omega_k} - \frac{1}{-\omega_i - \omega_j + \omega_k} \right) \quad (4.14)$$

in the anharmonicity constants  $x_{ij}$  if  $\omega_i \sim \omega_j + \omega_k$ . The resulting fundamentals are dressed by diagonalizing a matrix containing the deperturbed fundamental and combination bands in Fermi resonance and the cubic force constant which couples the states:

$$\begin{bmatrix} \Omega_i & \frac{1}{2\sqrt{2}}\phi_{ijk} \\ \frac{1}{2\sqrt{2}}\phi_{ijk} & \Omega_{j_1 k_1} \end{bmatrix} \quad (4.15)$$

where:

$$\Omega_i = \langle i_1 | \hat{H}_0 + \hat{H}_2 | i_1 \rangle + \sum_{m \neq [i_1, j_1, k_1]} \frac{\langle i_1 | \hat{H}_1 | m \rangle \langle m | \hat{H}_1 | i_1 \rangle}{\omega_i - \omega_m}. \quad (4.16)$$

For benzene, Fermi resonance occurs between  $\nu_8$  and  $\nu_{1+6}$ :

$$\begin{bmatrix} \Omega_{8(a_g)} & \frac{1}{2\sqrt{2}}\phi_{1,6a,8a} & 0 & 0 \\ \frac{1}{2\sqrt{2}}\phi_{1,6a,8a} & \Omega_{1_1 6_1(a_g)} & 0 & 0 \\ 0 & 0 & \Omega_{8(b_{1g})} & \frac{1}{2\sqrt{2}}\phi_{1,6b,8b} \\ 0 & 0 & \frac{1}{2\sqrt{2}}\phi_{1,6b,8b} & \Omega_{1_1 6_1(b_{1g})} \end{bmatrix}, \quad (4.17)$$

$\nu_2$  and  $2\nu_{19}$ :

$$\begin{bmatrix} \Omega_2 & \frac{1}{2}\phi_{2,19a,19a} & \frac{1}{2}\phi_{2,19b,19b} \\ \frac{1}{2}\phi_{2,19a,19a} & \Omega_{19_2(b_{2u})} & 0 \\ \frac{1}{2}\phi_{2,19b,19b} & 0 & \Omega_{19_2(b_{3u})} \end{bmatrix} \quad (4.18)$$

and  $\nu_{13}$ ,  $\nu_{20}$ , and  $\nu_{8+19}$ :

$$\begin{bmatrix} \Omega_{20(b_{2u})} & \frac{1}{2\sqrt{2}}\phi_{8a,19a,20a} & \frac{1}{2\sqrt{2}}\phi_{8b,19b,20a} \\ \frac{1}{2\sqrt{2}}\phi_{8a,19a,20a} & \Omega_{8_1(a_g)19_1(b_{2u})} & 0 \\ \frac{1}{2\sqrt{2}}\phi_{8b,19b,20a} & 0 & \Omega_{8_1(b_{1g})19_1(b_{3u})} \end{bmatrix} \begin{bmatrix} \Omega_{13} & 0 & \frac{1}{2\sqrt{2}}\phi_{8a,13,19b} & \frac{1}{2\sqrt{2}}\phi_{8b,13,19a} \\ 0 & \Omega_{20(b_{3u})} & \frac{1}{2\sqrt{2}}\phi_{8a,19b,20b} & \frac{1}{2\sqrt{2}}\phi_{8b,19a,20b} \\ \frac{1}{2\sqrt{2}}\phi_{8a,13,19b} & \frac{1}{2\sqrt{2}}\phi_{8a,19b,20b} & \Omega_{8_1(a_g)19_1(b_{3u})} & 0 \\ \frac{1}{2\sqrt{2}}\phi_{8b,13,19a} & \frac{1}{2\sqrt{2}}\phi_{8b,19a,20b} & 0 & \Omega_{8_1(b_{1g})19_1(b_{2u})} \end{bmatrix}. \quad (4.19)$$

Other resonances also include:  $\nu_3 \sim \nu_{16} + \nu_{17}$  and  $\nu_{18} \sim \nu_4 + \nu_{16}$ <sup>30</sup>.

Dressing the fundamentals as outlined above had little effect on the difference between fundamentals calculated using SCF and fundamentals obtained from experiment. See Table B.11. The mean absolute deviation remained high ranging from 95.6 to 100.3 cm<sup>-1</sup>. Fermi resonance accounts for most of the deviations in other fundamentals. Deviations larger than 50 cm<sup>-1</sup> are seen in MP2 for  $\nu_3$ ,  $\nu_8$ ,  $\nu_{13}$  and  $\nu_{20}$  which are coupled to combinations  $\nu_{16+17}$ ,  $\nu_{1+6}$ ,  $\nu_{8+19}$  and  $\nu_{8+19}$  respectively. Dressing the frequencies, as outlined above, reduces these deviations significantly. The absolute mean deviations between the dressed fundamentals and experimental frequencies are between 11.5 and 19.0 cm<sup>-1</sup> if the deviation of  $\nu_{14}$  is excluded. See Table B.13. Once the fundamentals for CCSD(T) have been dressed (see Table 4.8 for an example), the mean absolute deviation from experiment of the fundamental frequencies is between 3.2 (CCSD(T)/ANO2/1(fc)) and 10.0 cm<sup>-1</sup> (CCSD(T)/ANO0(fc)) for each level of theory. The largest deviations for CCSD(T)/ANO2/1(fc) (10

---

<sup>30</sup>The doubly degenerate irreducible representations of  $D_{6h}$  ( $e_{1g}$ ,  $e_{2g}$ ,  $e_{1u}$  and  $e_{2u}$ ) split into two singly degenerate irreducible representations in the subgroup  $D_{2h}$  (for example  $e_{2g} \rightarrow a_g + b_{1g}$ ). These subgroups will be used to distinguish the degenerate vibrational levels, particularly those effected by resonance.

Table 4.8: Comparison of CCSD(T)/ANO2/1(fc) straight forward VPT2 fundamental frequencies with deperturbed and diagonalized or dressed frequencies ( $\text{cm}^{-1}$ ).

	VPT2 CCSD(T)/ ANO2/1(fc) <sup>a</sup>	Deperturbed <sup>b</sup> CCSD(T)/ ANO2/1(fc)	Diagonalized CCSD(T)/ ANO2/1(fc)	Exp. <sup>c</sup>
2 <sub>1</sub>	3064.7	3057.3	3070.2	3073.9
19 <sub>2</sub> (b <sub>2u</sub> )	2956.2	2959.9	2949.1	
19 <sub>2</sub> (b <sub>3u</sub> )	2956.2	2959.9	2957.9	
8 <sub>1</sub> (a <sub>g</sub> )	1601.8	1598.3	1605.5	1609.5
1 <sub>1</sub> 6 <sub>1</sub> (a <sub>g</sub> )	1590.9	1594.5	1587.2	
20 <sub>1</sub> (b <sub>2u</sub> )	3086.3	3068.3	3043.7	3047.9
8 <sub>1</sub> (a <sub>g</sub> )19 <sub>1</sub> (b <sub>2u</sub> )	3070.1	3079.2	3079.0	
8 <sub>1</sub> (b <sub>1g</sub> )19 <sub>1</sub> (b <sub>3u</sub> )	3070.1	3079.2	3103.9	
13 <sub>1</sub>	3115.1	3031.0	3006.3	3015.0
20 <sub>1</sub> (b <sub>2u</sub> )	3086.3	3068.3	3043.2	3047.9
8 <sub>1</sub> (a <sub>g</sub> )19 <sub>1</sub> (b <sub>2u</sub> )	3028.4	3079.5	3103.1	
8 <sub>1</sub> (b <sub>1g</sub> )19 <sub>1</sub> (b <sub>3u</sub> )	3028.4	3079.5	3105.6	

<sup>a</sup> ANO2/1(fc) utilized the harmonic frequencies computed at the CCSD(T)/ANO2(fc) level of theory with cubic and quartic force constants determined using CCSD(T)/ANO1(fc) to compute vibrational fundamental frequencies.

<sup>b</sup> Deperturbed frequencies obtained using Equation 4.16.

<sup>c</sup> See Table 4.1 for experimental references.

$\text{cm}^{-1}$ ) occurs for  $\nu_{13}(b_{1u})$  whose experimental fundamental has the largest degree of uncertainty. However, its closer proximity to the experimental value of U. Erlekam *et al.* [66] confirms their findings.

To summarize, CCSD(T) accurately predicts the fundamental frequencies using VPT2 when treated for Fermi resonance obtained by the variety of experiments described earlier. In particular, the frequencies obtained for  $\nu_{13}(b_{1u})$  are closer to the value of  $3015^{+2}_{-5} \text{ cm}^{-1}$  measured by U. Erlekam *et al.* [66] than the more established value of  $3057 \text{ cm}^{-1}$  obtained by S. Brodersen and A. Langseth [35]. Finally, the fundamental frequencies determined by using the harmonic frequencies of a larger basis set like ANO2(fc) with the cubic and quartic force constants of a smaller basis set like ANO1(fc) (i.e. ANO2/1(fc)) improve the agreement of theory with experiment without significantly increasing the computational cost.

#### 4.6.2 Combination Bands and Overtones

In addition to the fundamental frequencies determined in the previous section, VPT2 may be applied to the two quantum transitions in the infrared spectrum of benzene. Several difficulties arise in two quantum transitions. First, the number of states to be considered increased by nearly  $N^2/2$  where  $N$  is the number of vibrational degrees of freedom. For a molecule like formaldehyde, the number of possible two quantum transitions totals 21 combination bands and first overtones, but for benzene, this number is more than 250 of which only some are infrared active. Second, some transitions are effected by Fermi resonance if one of their vibrational modes is coupled to a two quantum transition, but some transitions may also be effected by Darling-Dennison resonance if they couple with another two quantum transi-

tion as described in Chapter 3. Third, the precise vibrational frequencies are obscured by the rotational branches which can span  $100\text{ cm}^{-1}$  or more [190].

The spectrum assigned and published by S. Brodersen and A. Langseth [35] in 1956 is one of the few spectra available that spans the region from 600 to  $6200\text{ cm}^{-1}$  for benzene in the vapor phase. One recent studies by J. E. Bertiea and C. D. Keefe [27] measured the spectrum of liquid benzene for this region, and another by C. P. Rinsland *et al.* [190] reported integrated intensities of the stronger bands in this region rather than identifying new ones. A third study by Page *et al.* [154] only examined the  $5800$  to  $6200\text{ cm}^{-1}$  region of the spectrum associated the two quantum C-H stretch transitions. As a result, the two quantum transitions determined using VPT2 will be compared first to the experimental values of the spectrum measured by S. Brodersen and A. Langseth, then the  $5800$  to  $6200\text{ cm}^{-1}$  transitions will be compared to the spectrum measured by Page *et al.* The goal of this comparison will be to verify the two quantum assignments, clarify the  $5800$  to  $6200\text{ cm}^{-1}$  region of the spectrum<sup>31</sup> and demonstrate the utility of using VPT2 to analyze spectra.

Table 4.9: CCSD(T) two quantum transitions: VPT2 ( $\text{cm}^{-1}$ )

	CCSD(T)/ ANO2/1(fc)	Exp. [35]
$6_1(a_g)16_1(b_{1u}), 6_1(b_{1g})16_1(a_u)$	1003.4	1003
$4_116_1(a_u), 4_116_1(b_{1u})$	1101.4	1106
$10_1(b_{2g})16_1(b_{1u}), 10_1(b_{3g})16_1(a_u)$	1235.4	1242
$10_1(b_{2g})16_1(a_u), 10_1(b_{3g})16_1(b_{1u})$	1243.9	

---

<sup>31</sup>This region was difficult for S. Brodersen and A. Langseth to assign. They assigned four peaks in this region to two quantum C-H stretches, but their experimental values differed by  $100\text{ cm}^{-1}$  from the values determined from the fundamental frequencies.

$5_1 16_1(a_u), 5_1 16_1(b_{1u})$	1385.4	1388
$10_1(b_{2g}) 11_1, 10_1(b_{3g}) 11_1$	1519.1	1522
$6_1(a_g) 17_1(b_{1u}), 6_1(b_{1g}) 17_1(a_u)$	1570.6	
$9_1(a_g) 16_1(b_{1u}), 9_1(b_{1g}) 16_1(a_u)$	1574.1	
$6_1(a_g) 12_1, 6_1(b_{1g}) 12_1$	1614.3	1622
$6_1(a_g) 18_1(b_{3u}), 6_1(b_{1g}) 18_1(b_{2u})$	1640.9	
$6_1(a_g) 18_1(b_{2u}), 6_1(b_{1g}) 18_1(b_{3u})$	1641.6	
$1_1 11_1$	1662.7	1667
$4_1 17_1(a_u), 4_1 17_1(b_{1u})$	1666.1	1673
$4_1 12_1$	1709.6	1716
$6_1(a_g) 15_1, 6_1(b_{1g}) 15_1$	1750.5	1755
$10_1(b_{2g}) 17_1(a_u), 10_1(b_{3g}) 17_1(b_{1u})$	1809.1	
$10_1(b_{2g}) 17_1(b_{1u}), 10_1(b_{3g}) 17_1(a_u)$	1811.4	1811
$10_1(b_{2g}) 18_1(b_{3u}), 10_1(b_{3g}) 18_1(b_{2u})$	1882.2	1888
$6_1(a_g) 14_1, 6_1(b_{1g}) 14_1$	1913.5	1917
$5_1 17_1(a_u), 5_1 17_1(b_{1u})$	1953.6	1958
$5_1 12_1$	1998.1	2005
$8_1(a_g) 16_1(b_{1u}), 8_1(b_{1g}) 16_1(a_u)$ <sup>32</sup>	1985.6	1989
$1_1 18_1(b_{2u})$	2024.9	
$6_1(a_g) 19_1(b_{3u}), 6_1(b_{1g}) 19_1(b_{2u})$	2085.0	2077
$6_1(a_g) 19_1(b_{2u}), 6_1(b_{1g}) 19_1(b_{3u})$	2085.6	
$9_1(a_g) 17_1(b_{1u}), 9_1(b_{1g}) 17_1(a_u)$	2141.4	2144
$9_1(a_g) 12_1, 9_1(b_{1g}) 12_1$	2184.6	
$9_1(a_g) 18_1(b_{3u}), 9_1(b_{1g}) 18_1(b_{2u})$	2209.9	2214
$9_1(a_g) 18_1(b_{2u}), 9_1(b_{1g}) 18_1(b_{3u})$	2212.7	
$9_1(a_g) 15_1, 9_1(b_{1g}) 15_1$	2323.1	2326
$10_1(b_{2g}) 19_1(b_{3u}), 10_1(b_{3g}) 19_1(b_{2u})$	2327.1	2328
$3_1 18_1(b_{3u}), 3_1 18_1(b_{2u})$	2379.0	2386
$1_1 19_1(b_{2u}), 1_1 19_1(b_{3u})$	2469.2	
$9_1(a_g) 14_1, 9_1(b_{1g}) 14_1$	2484.3	2486
$8_1(a_g) 17_1(b_{1u}), 8_1(b_{1g}) 17_1(a_u)$ <sup>33</sup>	2552.1	2556
$8_1(a_g) 12_1, 8_1(b_{1g}) 12_1$ <sup>34</sup>	2612.4	2611

---

<sup>32</sup>Treated for Fermi resonance of  $1_1 6_1(a_g)$  with  $8_1(a_g)$  and  $1_1 6_1(b_{1g})$  with  $8_1(b_{1g})$ .

<sup>33</sup>Treated for Fermi resonance of  $1_1 6_1(a_g)$  with  $8_1(a_g)$  and  $1_1 6_1(b_{1g})$  with  $8_1(b_{1g})$ .

<sup>34</sup>Treated for Fermi resonance of  $1_1 6_1(a_g)$  with  $8_1(a_g)$  and  $1_1 6_1(b_{1g})$  with  $8_1(b_{1g})$ .

$8_1(a_g)18_1(b_{2u}), 8_1(b_{1g})18_1(b_{3u})$ <sup>35</sup>	2619.6	
$8_1(a_g)18_1(b_{3u}), 8_1(b_{1g})18_1(b_{2u})$ <sup>36</sup>	2619.6	
$9_1(a_g)19_1(b_{3u}), 9_1(b_{1g})19_1(b_{2u})$	2652.4	2659
$9_1(a_g)19_1(b_{2u}), 9_1(b_{1g})19_1(b_{3u})$	2657.2	
$8_1(a_g)15_1, 8_1(b_{1g})15_1$ <sup>37</sup>	2748.3	2751
$3_119_1(b_{3u}), 3_119_1(b_{2u})$	2820.3	2827
$8_1(a_g)14_1, 8_1(b_{1g})14_1$ <sup>38</sup>	2905.7	2898
$8_1(a_g)19_1(b_{2u}), 8_1(b_{1g})19_1(b_{3u})$ <sup>39</sup>	3083.2	3083
$8_1(a_g)19_1(b_{3u}), 8_1(b_{1g})19_1(b_{2u})$ <sup>40</sup>	3072.5	
$7_1(a_g)16_1(b_{1u}), 7_1(b_{1g})16_1(a_u)$	3451.3	3455
$6_1(a_g)13_1, 6_1(b_{1g})13_1$ <sup>41</sup>	3608.7	
$6_1(a_g)20_1(b_{2u}), 6_1(b_{1g})20_1(b_{3u})$ <sup>42</sup>	3644.7	3654
$6_1(a_g)20_1(b_{3u}), 6_1(b_{1g})20_1(b_{2u})$ <sup>43</sup>	3644.0	
$2_111_1$ <sup>44</sup>	3741.1	3743
$4_113_1$ <sup>45</sup>	3704.3	
$10_1(b_{2g})20_1(b_{3u}), 10_1(b_{3g})20_1(b_{2u})$ <sup>46</sup>	3893.4	3889
$7_1(a_g)17_1(b_{1u}), 7_1(b_{1g})17_1(a_u)$	4014.2	
$7_1(a_g)12_1, 7_1(b_{1g})12_1$	4061.5	4070

---

<sup>35</sup>Treated for Fermi resonance of  $1_16_1(a_g)$  with  $8_1(a_g)$  and  $1_16_1(b_{1g})$  with  $8_1(b_{1g})$ .

<sup>36</sup>Treated for Fermi resonance of  $1_16_1(a_g)$  with  $8_1(a_g)$  and  $1_16_1(b_{1g})$  with  $8_1(b_{1g})$ .

<sup>37</sup>Treated for Fermi resonance of  $1_16_1(a_g)$  with  $8_1(a_g)$  and  $1_16_1(b_{1g})$  with  $8_1(b_{1g})$ .

<sup>38</sup>Treated for Fermi resonance of  $1_16_1(a_g)$  with  $8_1(a_g)$  and  $1_16_1(b_{1g})$  with  $8_1(b_{1g})$ .

<sup>39</sup>Treated for Fermi resonance of  $1_16_1(a_g)$  with  $8_1(a_g)$  and  $1_16_1(b_{1g})$  with  $8_1(b_{1g})$ .

<sup>40</sup>Treated for Fermi resonance of  $1_16_1(a_g)$  with  $8_1(a_g)$  and  $1_16_1(b_{1g})$  with  $8_1(b_{1g})$ .

<sup>41</sup>Treated for Fermi resonance of  $20_1(b_{3u}), 8_1(a_g)19_1(b_{3u}), 8_1(b_{1g})19_1(b_{2u}), 1_16_1(a_g)19_1(b_{3u})$  and  $1_16_1(b_{1g})19_1(b_{2u})$  with  $13_1$ .

<sup>42</sup>Treated for Fermi resonance of  $8_1(a_g)19_1(b_{2u}), 8_1(b_{1g})19_1(b_{3u}), 1_16_1(a_g)19_1(b_{2u})$  and  $1_16_1(b_{1g})19_1(b_{3u})$  with  $20_1(b_{2u})$ , and  $13_1, 8_1(a_g)19_1(b_{3u}), 8_1(b_{1g})19_1(b_{2u}), 1_16_1(a_g)19_1(b_{3u})$  and  $1_16_1(b_{1g})19_1(b_{2u})$  with  $20_1(b_{3u})$

<sup>43</sup>Treated for Fermi resonance of  $8_1(a_g)19_1(b_{2u}), 8_1(b_{1g})19_1(b_{3u}), 1_16_1(a_g)19_1(b_{2u})$  and  $1_16_1(b_{1g})19_1(b_{3u})$  with  $20_1(b_{2u})$ , and  $13_1, 8_1(a_g)19_1(b_{3u}), 8_1(b_{1g})19_1(b_{2u}), 1_16_1(a_g)19_1(b_{3u})$  and  $1_16_1(b_{1g})19_1(b_{2u})$  with  $20_1(b_{3u})$

<sup>44</sup>Treated for Fermi resonance of  $2_1, 19_2(b_{2u})$  and  $19_2(b_{3u})$ .

<sup>45</sup>Treated for Fermi resonance of  $20_1(b_{3u}), 8_1(a_g)19_1(b_{3u}), 8_1(b_{1g})19_1(b_{2u}), 1_16_1(a_g)19_1(b_{3u})$  and  $1_16_1(b_{1g})19_1(b_{2u})$  with  $13_1$ .

<sup>46</sup>Treated for Fermi resonance of  $8_1(a_g)19_1(b_{2u}), 8_1(b_{1g})19_1(b_{3u}), 1_16_1(a_g)19_1(b_{2u})$  and  $1_16_1(b_{1g})19_1(b_{3u})$  with  $20_1(b_{2u})$ , and  $13_1, 8_1(a_g)19_1(b_{3u}), 8_1(b_{1g})19_1(b_{2u}), 1_16_1(a_g)19_1(b_{3u})$  and  $1_16_1(b_{1g})19_1(b_{2u})$  with  $20_1(b_{3u})$



$1_1 20_1(b_{2u}), 1_1 20_1(b_{3u})$ <sup>47</sup>	4026.8	4030
$7_1(a_g)18_1(b_{2u}), 7_1(b_{1g})18_1(b_{3u})$	4087.3	
$7_1(a_g)18_1(b_{3u}), 7_1(b_{1g})18_1(b_{2u})$	4088.7	
$2_1 18_1(b_{2u}), 2_1 18_1(b_{3u})$ <sup>48</sup>	4104.3	4107
$5_1 13_1$ <sup>49</sup>	3991.2	
$9_1(a_g)13_1, 9_1(b_{1g})13_1$ <sup>50</sup>	4212.8	4220
$9_1(a_g)20_1(b_{3u}), 9_1(b_{1g})20_1(b_{2u})$ <sup>51</sup>	4211.5	4198
$9_1(a_g)20_1(b_{2u}), 9_1(b_{1g})20_1(b_{3u})$ <sup>52</sup>	4210.2	
$7_1(a_g)14_1, 7_1(b_{1g})14_1$	4366.6	
$3_1 20_1(b_{2u})$ <sup>53</sup>	4408.2	4394
$3_1 20_1(b_{3u})$ <sup>54</sup>	4399.5	
$7_1(a_g)19_1(b_{3u}), 7_1(b_{1g})19_1(b_{2u})$	4535.9	
$7_1(a_g)19_1(b_{2u}), 7_1(b_{1g})19_1(b_{3u})$	4537.1	
$2_1 19_1(b_{2u}), 2_1 19_1(b_{3u})$ <sup>55</sup>	4556.1	4556
$8_1(a_g)13_1, 8_1(b_{1g})13_1$ <sup>56</sup>	4605.6	4600
$8_1(a_g)20_1(b_{3u}), 8_1(b_{1g})20_1(b_{2u})$ <sup>57</sup>	4683.6	

---

<sup>47</sup>Treated for Fermi resonance of  $8_1(a_g)19_1(b_{2u}), 8_1(b_{1g})19_1(b_{3u}), 1_1 6_1(a_g)19_1(b_{2u})$  and  $1_1 6_1(b_{1g})19_1(b_{3u})$  with  $20_1(b_{2u})$ , and  $13_1, 8_1(a_g)19_1(b_{3u}), 8_1(b_{1g})19_1(b_{2u}), 1_1 6_1(a_g)19_1(b_{3u})$  and  $1_1 6_1(b_{1g})19_1(b_{2u})$  with  $20_1(b_{3u})$

<sup>48</sup>Treated for Fermi resonance of  $2_1, 19_2(b_{2u}), 19_1(b_{2u})19_1(b_{3u})$ , and  $19_2(b_{3u})$ .

<sup>49</sup>Treated for Fermi resonance of  $20_1(b_{3u}), 8_1(a_g)19_1(b_{3u}), 8_1(b_{1g})19_1(b_{2u}), 1_1 6_1(a_g)19_1(b_{3u})$  and  $1_1 6_1(b_{1g})19_1(b_{2u})$  with  $13_1$ .

<sup>50</sup>Treated for Fermi resonance of  $20_1(b_{3u}), 8_1(a_g)19_1(b_{3u}), 8_1(b_{1g})19_1(b_{2u}), 1_1 6_1(a_g)19_1(b_{3u})$  and  $1_1 6_1(b_{1g})19_1(b_{2u})$  with  $13_1$ .

<sup>51</sup>Treated for Fermi resonance of  $8_1(a_g)19_1(b_{2u}), 8_1(b_{1g})19_1(b_{3u}), 1_1 6_1(a_g)19_1(b_{2u})$  and  $1_1 6_1(b_{1g})19_1(b_{3u})$  with  $20_1(b_{2u})$ , and  $13_1, 8_1(a_g)19_1(b_{3u}), 8_1(b_{1g})19_1(b_{2u}), 1_1 6_1(a_g)19_1(b_{3u})$  and  $1_1 6_1(b_{1g})19_1(b_{2u})$  with  $20_1(b_{3u})$

<sup>52</sup>Treated for Fermi resonance of  $8_1(a_g)19_1(b_{2u}), 8_1(b_{1g})19_1(b_{3u}), 1_1 6_1(a_g)19_1(b_{2u})$  and  $1_1 6_1(b_{1g})19_1(b_{3u})$  with  $20_1(b_{2u})$ , and  $13_1, 8_1(a_g)19_1(b_{3u}), 8_1(b_{1g})19_1(b_{2u}), 1_1 6_1(a_g)19_1(b_{3u})$  and  $1_1 6_1(b_{1g})19_1(b_{2u})$  with  $20_1(b_{3u})$

<sup>53</sup>Treated for Fermi resonance of  $8_1(a_g)19_1(b_{2u}), 8_1(b_{1g})19_1(b_{3u}), 1_1 6_1(a_g)19_1(b_{2u})$  and  $1_1 6_1(b_{1g})19_1(b_{3u})$  with  $20_1(b_{2u})$ , and  $13_1, 8_1(a_g)19_1(b_{3u}), 8_1(b_{1g})19_1(b_{2u}), 1_1 6_1(a_g)19_1(b_{3u})$  and  $1_1 6_1(b_{1g})19_1(b_{2u})$  with  $20_1(b_{3u})$

<sup>54</sup>Treated for Fermi resonance of  $8_1(a_g)19_1(b_{2u}), 8_1(b_{1g})19_1(b_{3u}), 1_1 6_1(a_g)19_1(b_{2u})$  and  $1_1 6_1(b_{1g})19_1(b_{3u})$  with  $20_1(b_{2u})$ , and  $13_1, 8_1(a_g)19_1(b_{3u}), 8_1(b_{1g})19_1(b_{2u}), 1_1 6_1(a_g)19_1(b_{3u})$  and  $1_1 6_1(b_{1g})19_1(b_{2u})$  with  $20_1(b_{3u})$

<sup>55</sup>Treated for Fermi resonance of  $2_1, 19_2(b_{2u}), 19_1(b_{2u})19_1(b_{3u})$ , and  $19_2(b_{3u})$ .

<sup>56</sup>Treated for Fermi resonance of  $20_1(b_{3u}), 8_1(a_g)19_1(b_{3u}), 8_1(b_{1g})19_1(b_{2u}), 1_1 6_1(a_g)19_1(b_{3u})$  and  $1_1 6_1(b_{1g})19_1(b_{2u})$  with  $13_1$ .

<sup>57</sup>Treated for Fermi resonance of  $8_1(a_g)19_1(b_{2u}), 8_1(b_{1g})19_1(b_{3u}), 1_1 6_1(a_g)19_1(b_{2u})$  and

$8_1(a_g)20_1(b_{2u}), 8_1(b_{1g})20_1(b_{3u})$ <sup>58</sup>	4683.0	
$2_120_1(b_{2u}), 2_120_1(b_{3u})$ <sup>59</sup>	5923.7	5936
$7_1(a_g)13_1, 7_1(b_{1g})13_1$ <sup>60</sup>	5994.7	6003
$7_1(a_g)20_1(b_{3u}), 7_1(b_{1g})20_1(b_{2u})$ <sup>61</sup>	6121.8	6130
$7_1(a_g)20_1(b_{2u}), 7_1(b_{1g})20_1(b_{3u})$ <sup>62</sup>	6129.7	

The mean average deviation of the two quantum transitions from experiment is between  $21.3 \text{ cm}^{-1}$  for CCSD(T)/ANO2/1(fc) and  $30.0 \text{ cm}^{-1}$  for

---

$1_16_1(b_{1g})19_1(b_{3u})$  with  $20_1(b_{2u})$ , and  $13_1, 8_1(a_g)19_1(b_{3u}), 8_1(b_{1g})19_1(b_{2u}), 1_16_1(a_g)19_1(b_{3u})$  and  $1_16_1(b_{1g})19_1(b_{2u})$  with  $20_1(b_{3u})$

<sup>58</sup>Treated for Fermi resonance of  $8_1(a_g)19_1(b_{2u}), 8_1(b_{1g})19_1(b_{3u}), 1_16_1(a_g)19_1(b_{2u})$  and  $1_16_1(b_{1g})19_1(b_{3u})$  with  $20_1(b_{2u})$ , and  $13_1, 8_1(a_g)19_1(b_{3u}), 8_1(b_{1g})19_1(b_{2u}), 1_16_1(a_g)19_1(b_{3u})$  and  $1_16_1(b_{1g})19_1(b_{2u})$  with  $20_1(b_{3u})$

<sup>59</sup>Treated for Darling-Dennison resonance of  $2_1$  with  $19_2(b_{2u}), 19_2(b_{3u})$ , and  $19_1(b_{2u})19_1(b_{3u}), 20_1(b_{2u})$  with  $8_1(a_g)19_1(b_{2u}), 8_1(b_{1g})19_1(b_{3u}), 1_16_1(a_g)19_1(b_{2u})$  and  $1_16_1(b_{1g})19_1(b_{3u})$ , and  $13_1$  and  $20_1(b_{2u})$  with  $8_1(a_g)19_1(b_{3u}), 8_1(b_{1g})19_1(b_{2u}), 1_16_1(a_g)19_1(b_{3u})$  and  $1_16_1(b_{1g})19_1(b_{2u})$ . The quartic force constants  $\Phi_{2,7a,13,20b}$  and  $\Phi_{2,7a,13,20b}$  were determined at the CCSD(T)/ANO0(fc) level of theory using finite difference scheme for analytic second derivatives described in Chapter 3.

<sup>60</sup>Treated for Darling-Dennison resonance of  $2_1$  with  $19_2(b_{2u}), 19_2(b_{3u})$ , and  $19_1(b_{2u})19_1(b_{3u}), 20_1(b_{2u})$  with  $8_1(a_g)19_1(b_{2u}), 8_1(b_{1g})19_1(b_{3u}), 1_16_1(a_g)19_1(b_{2u})$  and  $1_16_1(b_{1g})19_1(b_{3u})$ , and  $13_1$  and  $20_1(b_{2u})$  with  $8_1(a_g)19_1(b_{3u}), 8_1(b_{1g})19_1(b_{2u}), 1_16_1(a_g)19_1(b_{3u})$  and  $1_16_1(b_{1g})19_1(b_{2u})$ . The quartic force constants  $\Phi_{2,7a,13,20b}$  and  $\Phi_{2,7a,13,20b}$  were determined at the CCSD(T)/ANO0(fc) level of theory using finite difference scheme for analytic second derivatives described in Chapter 3.

<sup>61</sup>Treated for Darling-Dennison resonance of  $2_1$  with  $19_2(b_{2u}), 19_2(b_{3u})$ , and  $19_1(b_{2u})19_1(b_{3u}), 20_1(b_{2u})$  with  $8_1(a_g)19_1(b_{2u}), 8_1(b_{1g})19_1(b_{3u}), 1_16_1(a_g)19_1(b_{2u})$  and  $1_16_1(b_{1g})19_1(b_{3u})$ , and  $13_1$  and  $20_1(b_{2u})$  with  $8_1(a_g)19_1(b_{3u}), 8_1(b_{1g})19_1(b_{2u}), 1_16_1(a_g)19_1(b_{3u})$  and  $1_16_1(b_{1g})19_1(b_{2u})$ . The quartic force constants  $\Phi_{2,7a,13,20b}$  and  $\Phi_{2,7a,13,20b}$  were determined at the CCSD(T)/ANO0(fc) level of theory using finite difference scheme for analytic second derivatives described in Chapter 3.

<sup>62</sup>Treated for Darling-Dennison resonance of  $2_1$  with  $19_2(b_{2u}), 19_2(b_{3u})$ , and  $19_1(b_{2u})19_1(b_{3u}), 20_1(b_{2u})$  with  $8_1(a_g)19_1(b_{2u}), 8_1(b_{1g})19_1(b_{3u}), 1_16_1(a_g)19_1(b_{2u})$  and  $1_16_1(b_{1g})19_1(b_{3u})$ , and  $13_1$  and  $20_1(b_{2u})$  with  $8_1(a_g)19_1(b_{3u}), 8_1(b_{1g})19_1(b_{2u}), 1_16_1(a_g)19_1(b_{3u})$  and  $1_16_1(b_{1g})19_1(b_{2u})$ . The quartic force constants  $\Phi_{2,7a,13,20b}$  and  $\Phi_{2,7a,13,20b}$  were determined at the CCSD(T)/ANO0(fc) level of theory using finite difference scheme for analytic second derivatives described in Chapter 3.

CCSD(T)/ANO0(fc). Differences from experiment are particularly significant for combinations containing  $20_1$  or  $13_1$  which are effected by Fermi resonance with  $8_119_1$  (for CCSD(T)/ANO2/1(fc) the average difference for the two quantum transitions is  $63.5\text{ cm}^{-1}$ ). The Fermi resonance effect of  $8_1$  and  $1_16_1$  is not as dramatic and the largest deviation from experiment ranges from  $10.5\text{ cm}^{-1}$  for CCSD(T)/ANO2/1(fc) to  $25.4\text{ cm}^{-1}$  for CCSD(T)/ANO0(fc).

To treat for resonance in the two quantum transitions, the VPT2 frequencies are deperturbed and form the diagonal of the matrix. The coupling between two quantum transitions is accounted for by  $K_{ij,kl}$  defined in Chapter 3 and a partial coupling between two and three quantum states is accounted for by a combination of  $K_{ij,kl}$  constants<sup>63</sup>. This coupling constant lacks the quintic force constants required for a full treatment, but the results indicate that these higher order force constants may not be needed. The doubly degenerate vibrational states were also divided by into symmetric subgroups ( $b_{2u}$  and  $b_{3u}$ ) to partition of the matrix into two parts. Once the matrix has been diagonalized, the eigenvalue closest to the observed transition was selected<sup>64</sup>. The mean absolute deviation of the VPT2+D for the two quantum transitions dropped to  $5.2\text{ cm}^{-1}$  with the largest difference being  $17.7\text{ cm}^{-1}$  as seen in Tables 4.9 and B.16. The experimental assignments made by S. Brodersen and A. Langseth are a combination of states - particularly states effected by the resonance of  $13_1$  and  $20_1$ . For example,  $6_1(a_g)13_1$  is the principle state

---

<sup>63</sup>The quartic force constants  $\Phi_{2,7a,13,20b}$  and  $\Phi_{2,7a,13,20b}$  were determined at the CCSD(T)/ANO0(fc) level of theory using finite difference scheme for analytic second derivatives described in Chapter 3.

<sup>64</sup>Coupled vibrational states in close proximity to each other mix together and an eigenvalue may correspond to a combination of several states. Without knowing the infrared intensities which were not computed for three quantum transitions, the eigenvector of the closest eigenvalue to experiment is used to see if the computed vibrational frequencies agree with the experimental assignments.

of  $3608.7\text{ cm}^{-1}$ , but  $6_1(a_g)20_1(b_{2u})$  is in combination with  $6_1(a_g)8_1(a_g)19_1(b_{2u})$  and  $6_1(a_g)8_1(b_{1g})19_1(b_{3u})$  in  $3644.7\text{ cm}^{-1}$ .

Of particular interest is the infrared spectrum from  $5800$  to  $6200\text{ cm}^{-1}$  obtained more recently by R. H. Page, Y. R. Shen and Y. T. Lee [154]. Of the 30 peaks they measured in the two quantum C-H stretch region, eight correspond to  $2_120_1(b_{2u})$ ,  $2_120_1(b_{3u})$ ,  $7_1(a_g)13_1$ ,  $7_1(b_{1g})13_1$ ,  $7_1(a_g)20_1(b_{2u})$ ,  $7_1(b_{1g})20_1(b_{3u})$ ,  $7_1(a_g)20_1(b_{3u})$  and  $7_1(b_{1g})20_1(b_{2u})$ <sup>65</sup>. The higher energy section of their spectrum is reproduced by the Darling-Dennison resonance treatment highlighted above. However, the lower section of the spectra between  $5900$  and  $6000\text{ cm}^{-1}$  is poorly described by the two quantum C-H stretches and their resonance with  $8_119_1$ ,  $1_16_119_1$  and  $19_2$  (see Figure 4.2).

Additional three quantum transitions:  $3_17_119_1$ ,  $2_13_119_1$ ,  $8_19_113_1$ ,  $8_19_120_1$ ,  $13_114_119_1$ ,  $14_119_120_1$ ,  $7_18_114_1$ ,  $2_18_114_1$ ,  $3_18_113_1$ ,  $3_18_120_1$  and  $13_119_2$  are infrared active in this region and may be included in the resonance treatment. The agreement in the region from  $5920\text{ cm}^{-1}$  to  $6040\text{ cm}^{-1}$  improves as seen in Figures 4.3 and 4.4. However, only one of the assignments ( $7_1(a_g)13_1$ ) corresponded to a two quantum transition.

In summary, VPT2+D at the CCSD(T)/ANO2/1(fc) level of theory determined the two quantum transitions of benzene to within an average of  $5.2\text{ cm}^{-1}$ . This level of accuracy was achieved by including the coupling of resonance states via diagonalization of the Hamiltonian corresponding to these vibrational states. A draw back to this approach is the eigenvalues correspond to a combination of two and three quantum states rather than a uniquely

---

<sup>65</sup>The Fermi resonance treatment splits the doubly degenerate VPT2 states into two separate states.

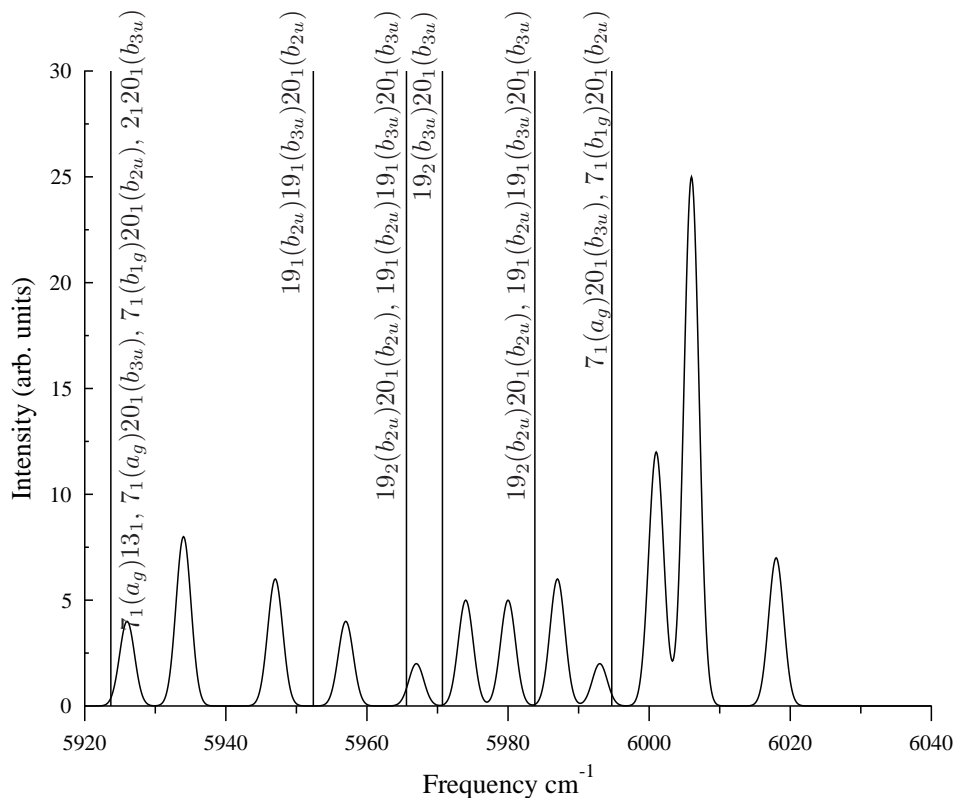


Figure 4.2: The experimental infrared spectrum of benzene  $5920\text{ cm}^{-1}$  to  $6040\text{ cm}^{-1}$  obtained by reference [154]. The experimental peaks are based on Gaussian functions of with a width of  $1.5\text{ cm}^{-1}$  centered at the transition frequency and the height scaled relative intensities provided in reference [154]. The vertical lines and assignments listed are based on a resonance treatment of the vibrational states utilizing the CCSD(T)/ANO2/1(fc) level of theory. Vibrational states:  $2_120_1(b_{2u})$ ,  $2_120_1(b_{3u})$ ,  $7_1(a_g)13_1$ ,  $7_1(b_{1g})13_1$ ,  $7_1(a_g)20_1(b_{2u})$ ,  $7_1(b_{1g})20_1(b_{3u})$ ,  $7_1(a_g)20_1(b_{3u})$  and  $7_1(b_{1g})20_1(b_{2u})$  and their associated Fermi resonance states have been included in the resonance treatment.

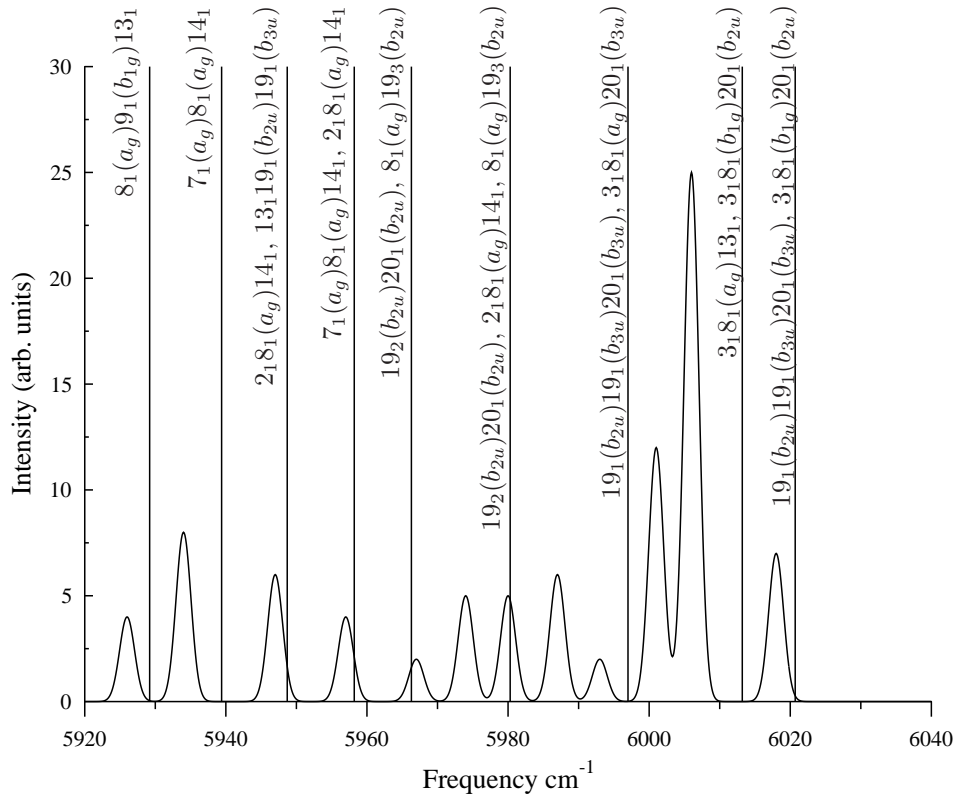


Figure 4.3: The experimental infrared spectrum of benzene 5920  $\text{cm}^{-1}$  to 6040  $\text{cm}^{-1}$  obtained by reference [154]. The experimental peaks are based on Gaussian functions of with a width of 1.5  $\text{cm}^{-1}$  centered at the transition frequency and the height scaled relative intensities provided in reference [154]. The vertical lines and assignments listed are based on a resonance treatment of the vibrational states utilizing the CCSD(T)/ANO2/1(fc) level of theory. Vibrational states corresponding to the  $b_{2u}$  symmetry subgroup:  $2_120_1(b_{2u})$ ,  $7_1(b_{1g})13_1$ ,  $7_1(a_g)20_1(b_{2u})$ , and  $7_1(b_{1g})20_1(b_{3u})$  with additional states  $3_17_119_1$ ,  $2_13_119_1$ ,  $8_19_113_1$ ,  $8_19_120_1$ ,  $13_114_119_1$ ,  $14_119_120_1$ ,  $7_18_114_1$ ,  $2_18_114_1$ ,  $3_18_113_1$ ,  $3_18_120_1$  and  $13_119_2$  and Fermi resonance states  $8_119_1$ ,  $1_16_119_1$  and  $19_2$  are included in the resonance treatment.

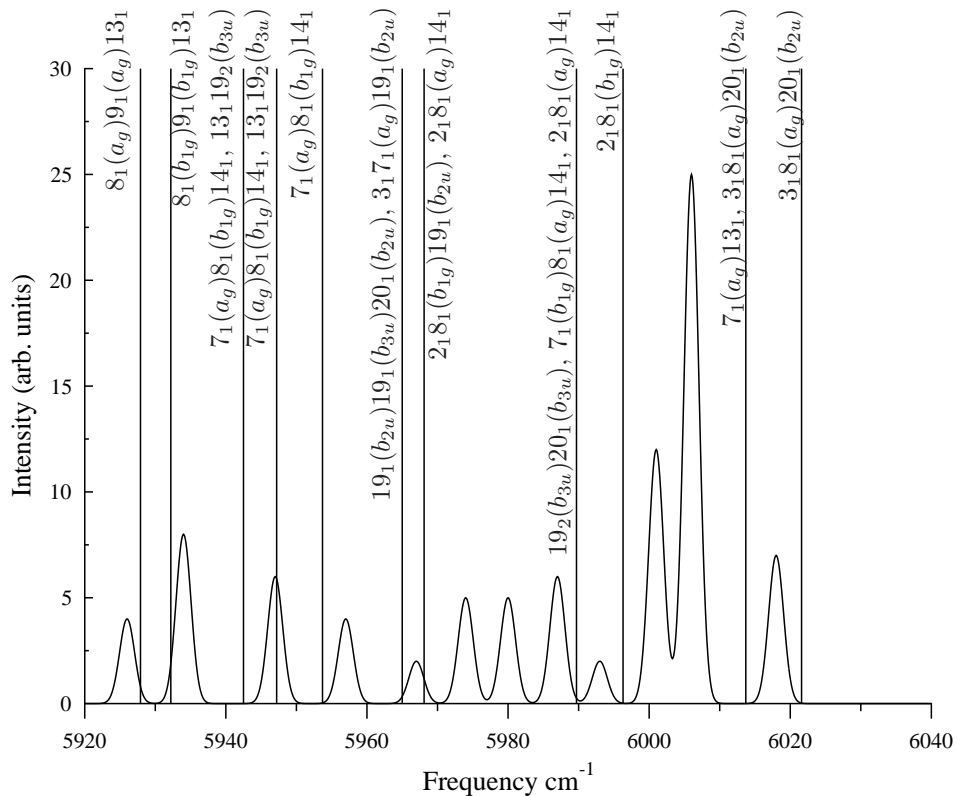


Figure 4.4: The experimental infrared spectrum of benzene 5920  $\text{cm}^{-1}$  to 6040  $\text{cm}^{-1}$  obtained by reference [154]. The experimental peaks are based on Gaussian functions of with a width of 1.5  $\text{cm}^{-1}$  centered at the transition frequency and the height scaled relative intensities provided in reference [154]. The vertical lines and assignments listed are based on a resonance treatment of the vibrational states utilizing the CCSD(T)/ANO2/1(fc) level of theory. Vibrational states corresponding to the  $b_{3u}$  symmetry subgroup:  $2_1 20_1(b_{3u})$ ,  $7_1(a_g)13_1$ ,  $7_1(a_g)20_1(b_{3u})$ , and  $7_1(b_{1g})20_1(b_{2u})$  with additional states  $3_1 7_1 19_1$ ,  $2_1 3_1 19_1$ ,  $8_1 9_1 13_1$ ,  $8_1 9_1 20_1$ ,  $13_1 14_1 19_1$ ,  $14_1 19_1 20_1$ ,  $7_1 8_1 14_1$ ,  $2_1 8_1 14_1$ ,  $3_1 8_1 13_1$ ,  $3_1 8_1 20_1$  and  $13_1 19_2$  and Fermi resonance states  $8_1 19_1$ ,  $1_1 6_1 19_1$  and  $19_2$  are included in the resonance treatment.

defined state VPT2 transition. As a result, the peaks in this region may be associated with several transitions making some assignments ambiguous.

## 4.7 Summary

The high accuracy *ab initio* methods used in the past to accurately predict experimental spectra and structures of smaller molecules [132–134, 159, 221] agree with experimental values for benzene. The effective bond lengths,  $r_0$ , determined using CCSD(T)/ANO1(fc) (1.4023(2) for  $r_{CC}$  and 1.0831(11) for  $r_{CH}$ ) are within 0.006 Å of the experimental value (1.3970(2) for  $r_{CC}$  and 1.0807(11) for  $r_{CH}$ ). The fundamental frequencies calculated using VPT2 are within 10 cm<sup>-1</sup> at the CCSD(T)/ANO2/1(fc) level of theory when vibrational states effected by Fermi resonance are treated as described above. In particular, the “dressed” value of  $\nu_{13}(b_{2u})$  favors the experimental frequency obtained by U. Erlekam *et al.* [66] over the value obtained early by S. Brodersen and A. Langseth [35]. The two quantum frequencies are within 20 cm<sup>-1</sup> of the experimental results with an absolute mean deviation of 5 cm<sup>-1</sup>. However, those vibrational states effected by resonance mix together and the peaks observed may be combinations of several two, three and four quantum states. The coupling of these states may be approximated using Darling-Dennison constants described in Chapter 3 if quintic and sextic force constants are unavailable.

Also, the force constants needed for VPT2 may be used to empirically determine equilibrium bond lengths ( $r_e$ ) and estimate harmonic frequencies from experimental fundamentals. The empirical bond lengths obtained using CCSD(T)/ANO1(fc) are with 0.004 Å of the equilibrium bond lengths at the CCSD(T)/ANO2(fc) level of theory. The estimated harmonic frequencies provide a better basis for comparison than the strictly experimental estimates



obtained by Goodman *et al* since they incorporate the anharmonicity from each vibrational mode. In some instances, the difference is as much as 36  $\text{cm}^{-1}$  between the empirical estimates based on CCSD(T)/ANO1(fc) force field and experimental estimates of Goodman *et al* [84] while the difference between the empirical estimate at the CCSD(T)/ANO1(fc) level of theory and the harmonic frequencies for CCSD(T)/ANO2(fc) is less than 12  $\text{cm}^{-1}$ .

## Chapter 5

### [10]Annulene

#### 5.1 Introduction

Hückel proposed that any cyclic compound with  $4n + 2$   $\pi$  electrons in a conjugated system would be aromatic and have similar properties as benzene: planar, low reactivity and low heat of formation. Members of the annulene family of compounds meet this criteria - [14]annulene and [18]annulene<sup>1</sup>; however, [10]annulene lacks stability and a planar configuration. If the carbon atoms are arranged in a ring with either  $D_{5h}$  or  $D_{10h}$  symmetry, the bond angle between hydrogen and carbon is closer to ethane than benzene and the ring is destabilized by eclipsing interactions between adjacent hydrogen atoms. If the carbon atoms are arranged instead in a ring with two *trans* double bonds like naphthalene, two hydrogen atoms overlap and prevent the molecule from becoming planar. This inherent instability prevented the isolation and characterization of [10]annulene until 1969 when S. Masamune and R. T. Seidner [138] identified it from two of the NMR signals they observed in photolyzed samples of *cis*-9,10-dihydronaphthalene<sup>2</sup>. In a subsequent paper, S. Masamune *et al.* [137] reported the NMR spectra and reactivity for two isomers of [10]annulene. Compound 1(B) reformed *cis*-9,10-dihydronaphthalene

---

<sup>1</sup>The family of annulene compounds is reviewed by R. D. Kennedy, D. Lloyd and H. McNab [110].

<sup>2</sup>To confirm their identification of [10]annulene, they hydrogenated the isolated compounds and produced cyclodecane.

upon warming while compound 2(A) formed *trans*-9,10-dihydronaphthalene. The structures they proposed have been explored through several theoretical methods. These structures are shown in Figures 5.1 through 5.9 and will be referred to as conformations **1a** to **6**.

The first study by Leška and Loos in 1974 and 1980 investigated these geometries using MINDO2 [121] and MINDO3 [128]. Since this initial studies, self-consistent field theory [69, 113, 232], second-order perturbation theory [113, 232], density functional theory [44, 113, 152, 216], and coupled cluster theory [44, 113, 215], have been utilized to determine the relative energies and geometries of the conformations proposed:  $D_{5h}$  (**1a**),  $D_{10h}$  (**1b**),  $C_s$  “boat” (**2a**),  $C_2$  “boat” (**2b**),  $C_2$  “azulene-like” (**3a**),  $C_1$  “azulene-like” (**3b**),  $C_s$  “heart” (**4**),  $C_2$  “naphthalene-like” (**5**) and  $C_2$  “twist” (**6**) (see Figures 5.1 through 5.9). However, determining the geometry of the ground state based on the energy of these conformations is problematic. The ordering of the relative energies from the previous studies is ambiguous as highlighted by the study of King *et al* [113]. In their study, the relative energies for CCSD(T) suggest conformation **6** (“twist”) is the ground state while the relative energies for B3LYP and MP2 suggest instead that conformation **4** (“heart”) is the ground state.

In their study, Sulzbach and coworkers address this issue by determining the NMR shifts of three conformations relative to benzene using SCF only to find the energies they calculated using B3LYP conflicted with their NMR shifts [216]. An additional study by Orlova and Goddard [152] used various density functional methods to reproduce the CCSD(T) obtained by King *et al* [113]. Subsequently, C. Castro *et al.* [44] explored the conformational space identifying the transitions between various conformations using

the density functional method suggested by Orlova and Goddard [152]. As part of their study, they computed vibrational frequencies using BH&HLYP/6-311+G\*\*. However, they omitted the transition of [10]annulene to either *cis*-9,10-dihydronaphthalene or *trans*-9,10-dihydronaphthalene from their study.

The purpose of this study is to resolve the conflict Sulzbach encountered and confirm and expand Castro’s findings.

## 5.2 Computational Details

The equilibrium geometry of the conformations of [10]annulene were optimized using analytic gradients for SCF, MP2, CCSD and CCSD(T) with the standard Dunning-Hay double set augmented by a set of polarization functions on all atoms (DZP) using ACESII MAB [212, 213]. The default geometry and energy convergency criteria was followed <sup>3</sup>.

Then, harmonic frequencies for each geometry were computed using analytic second derivatives by using ACESII MAB with coarse-grain parallelization when needed.

Chemical shielding for conformations **4**, **5** and **6** were computed for the CCSD(T)/DZd optimized geometries obtained from the literature [113] with SCF/DZP, MP2/DZP, CCSD/DZP and CCSD(T)/DZP using gauge-included atomic orbital. Additional chemical shielding for these conformations were computed with SCF/tzp and MP2/tzp [197]. The NMR shift rela-

---

<sup>3</sup>Settings for: the maximum change in the SCF density matrix ( $\epsilon_1$ ), the CCSD amplitudes ( $\epsilon_2$ ) and the perturbed CC and  $\lambda$  amplitudes ( $\epsilon_3$ ), the norm of the solution space for the CPHF and Z-vector equations ( $\epsilon_4$ ), and the cutoff for inclusion of integrals ( $\epsilon_5$ ). These criteria are expressed as exponentials  $\epsilon_i = 10^{-n_i}$ . Default settings for the  $n_i$  specified are: 7, 7, 7, 12, and 14

tive to TMS standard were then determined from the difference between the chemical shielding of the conformation and the chemical shielding of TMS calculated using equivalent theory and basis set at a geometry optimized using CCSD(T)/DZd.

Additional chemical shielding for conformations **2b**, **4**, **5** and **6** were computed for the CCSD(T)/DZP optimized geometries obtained in this study at the CCSD(T)/tzp level of theory to determine NMR shifts. Finally, NMR shifts of conformation **6** were determined using CCSD(T)/qz2p and the vibrational effects were computed using SCF/tzp [11, 92].

Calculations were run on **jfs2** - a Linux cluster with Xeon 32-bit processors at the University of Texas at Austin, **quantum** - a Linux cluster with Xeon 64-bit 3.0 GHz processors at Universität Mainz, or **lonestar** - a Dell Linux cluster of PowerEdge 1955 compute blades with two Xeon 5100 series 64-bit 2.66GHz dual-core processor per blade and InfiniBand interconnection technology.

### 5.3 Structures of Conformations

The two planar conformations **1a**( $D_{5h}$ ) and **1b**( $D_{10h}$ ) (shown in Figures 5.1 and 5.2) assume a decagon shape. In **1a**( $D_{5h}$ ), the  $\pi$  bonds are localized such that the CC bond lengths alternates between 1.3714 and 1.4262 Å for SCF/DZP as opposed to delocalized throughout the ring in **1b**( $D_{10h}$ ) where CC bond lengths are 1.3969 Å for SCF/DZP and 1.4121 Å for MP2/DZP<sup>4</sup>. The larger ring angle (144°) induces strain on the conformation. For *cis*-1,3-dibutene, a bond angle between carbons of 145° added 20 kcal mol<sup>-1</sup> using

---

<sup>4</sup>Conformation **1a**( $D_{5h}$ ) optimized to conformation **1b**( $D_{10h}$ ).

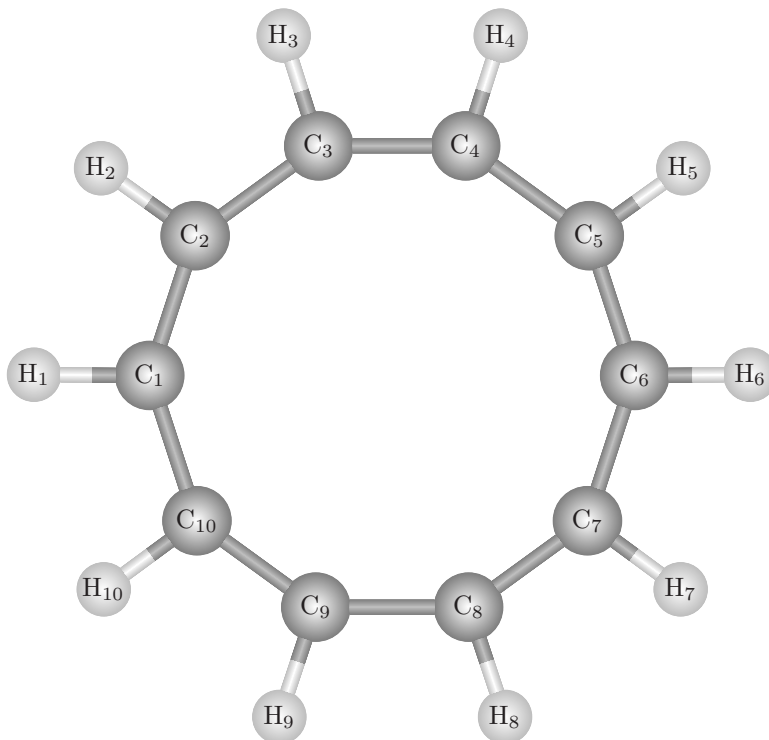


Figure 5.1: Conformation **1a**( $D_{5h}$ ) of [10]annulene

CCSD(T)/DZP and the planar cyclooctene ( $D_{4h}$ ) with a bond angle of  $135^\circ$  is  $13 \text{ kcal mol}^{-1}$  higher than the ground state ( $D_{2d}$ ) at CCSD(T)/DZP.

To relieve the ring strain, the conformation contorts out of a planar conformation like cyclooctene. Conformation **2a**( $C_s$ ), Figure 5.3, also localizes the  $\pi$  bonds between alternating carbons ( $C_1C_3$ ,  $C_2C_4$ ,  $C_5C_7$ ,  $C_6C_8$  and  $C_9C_{10}$ ). Like **1a**( $D_{5h}$ ), the average CC bond length alternates from an average of  $1.3608 \text{ \AA}$  to  $1.4881 \text{ \AA}$  for CCSD(T)/DZP similar to cyclooctene which alternates between  $1.3600 \text{ \AA}$  and  $1.4876 \text{ \AA}$  for the same level of theory. The shorter CC double bonds are longer than ethylene ( $1.3541 \text{ \AA}$ ) but shorter than

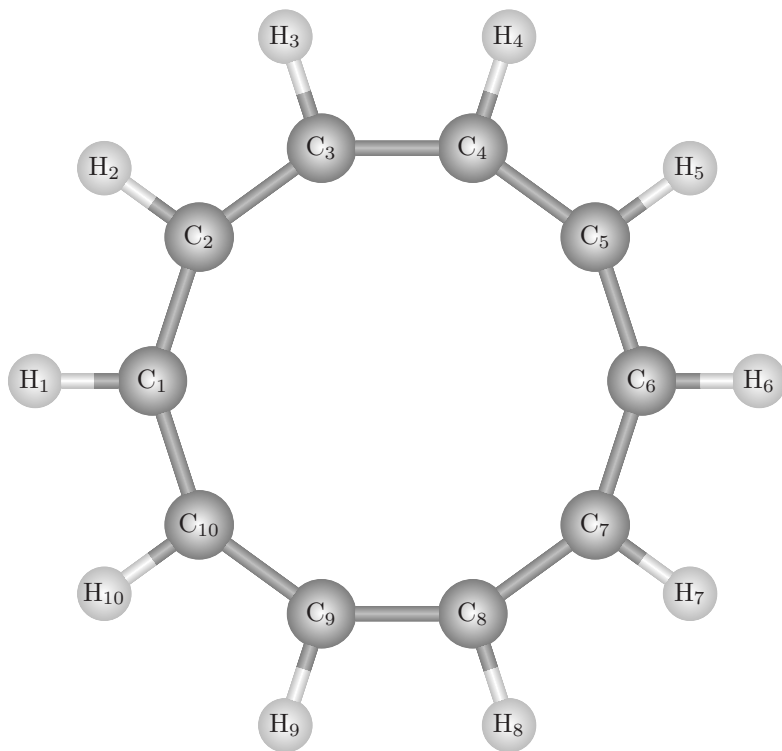


Figure 5.2: Conformation **1b**( $D_{10h}$ ) of [10]annulene

benzene (1.4111 Å) at CCSD(T)/DZP while the longer CC single bonds are shorter than ethane (1.5375 Å). Some of the ring strain is also relieved by decreasing the bond angle between carbon atoms for CCSD(T)/DZP which range from 120.8° to 138.2° and average of 128.5°. For *cis*-1,3-dibutene, bond angles between carbons of 130° and 140° only added 1 and 11 kcal mol<sup>-1</sup> to the ground state using CCSD(T)/DZP as opposed to 20 kcal mol<sup>-1</sup> added by 145°. Also, the dihedral angle of the  $\pi$  bonds are between 10° and -10°. Ideally, this angle ought to be either 0° or 180°; however, twisting the dihedral angle of ethylene 10° only increased its energy 1 kcal mol<sup>-1</sup> for CCSD(T)/DZP. The

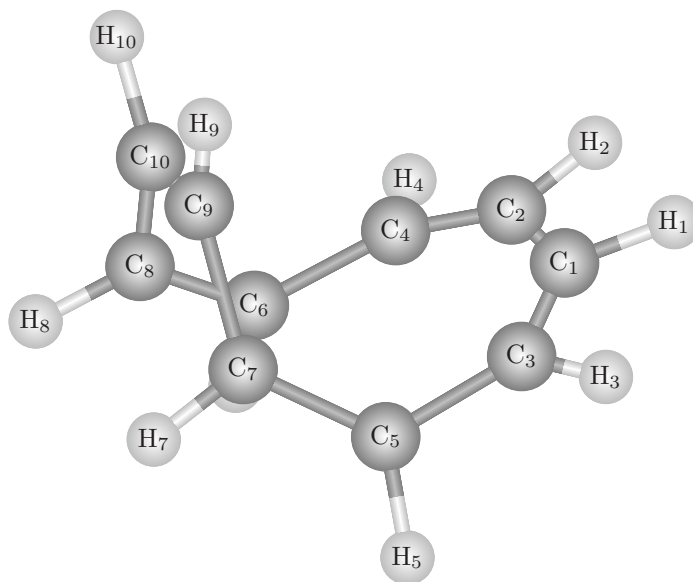


Figure 5.3: Conformation **2a**( $C_s$ ) of [10]annulene

other dihedral angles range from  $0^\circ$  to  $90^\circ$ . Finally, a dihedral angle approximately  $0^\circ$  suggest a *cis* arrangement for each of the double bonds.

However, it was discovered by L. Farnell and others [69] that conformation **2a**( $C_s$ ) is not a ground state (the reason will be discussed in the next section). C. Castro *et al.* [44] proposed a similar conformation with  $C_2$  symmetry conformation **2b**( $C_2$ ), Figure 5.4. The  $\pi$  bonds are localized between alternating carbons similar to conformation **2a**( $C_s$ ) alternating from an average of  $1.3633 \text{ \AA}$  to  $1.4905 \text{ \AA}$ . The bond angles between carbon atoms also mirror conformation **2a**( $C_s$ ) ranging from  $121.6^\circ$  to  $138.9^\circ$  and average of  $128.7^\circ$ . The



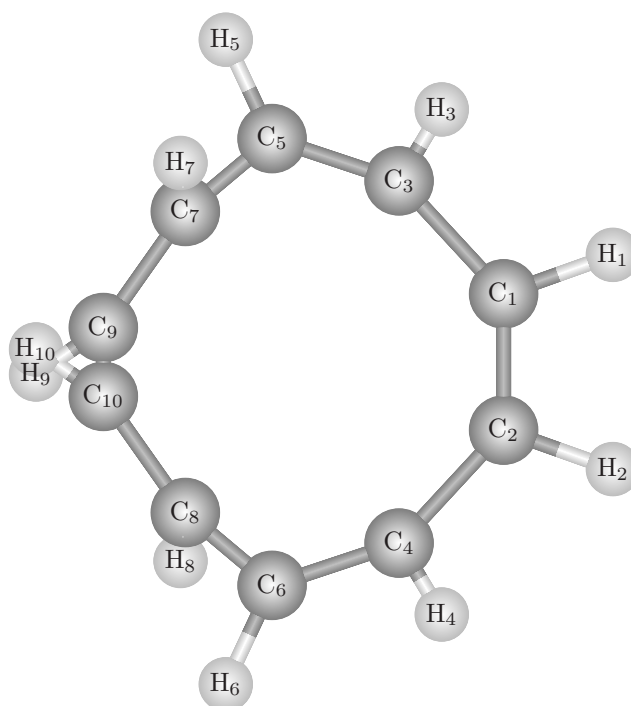


Figure 5.4: Conformation **2b**( $C_2$ ) of [10]annulene

dihedral angles of the  $\pi$  bonds are between  $4.7^\circ$  and  $11.1^\circ$  also suggesting a *cis* arrangement for each of the double bonds. The remaining dihedral angles range from  $36.1^\circ$  to  $96.5^\circ$  a narrower range than conformation **2a**( $C_s$ ). However, the primary difference between **2a**( $C_s$ ) and **2b**( $C_2$ ) is symmetry.

Unlike conformations **2a**( $C_s$ ) and **2b**( $C_2$ ), the  $\pi$  electrons of conformation **3a**( $C_2$ ) are more delocalized as reflected by CC bonds average that average  $1.4215 \text{ \AA}$  in length and range from  $1.4056$  to  $1.4343 \text{ \AA}$  similar to benzene. Like conformations **2a**( $C_s$ ) and **2b**( $C_2$ ), the ring strain has been reduced since the average bond angle between carbon atoms is  $126.67^\circ$  and ranges from  $118.33^\circ$

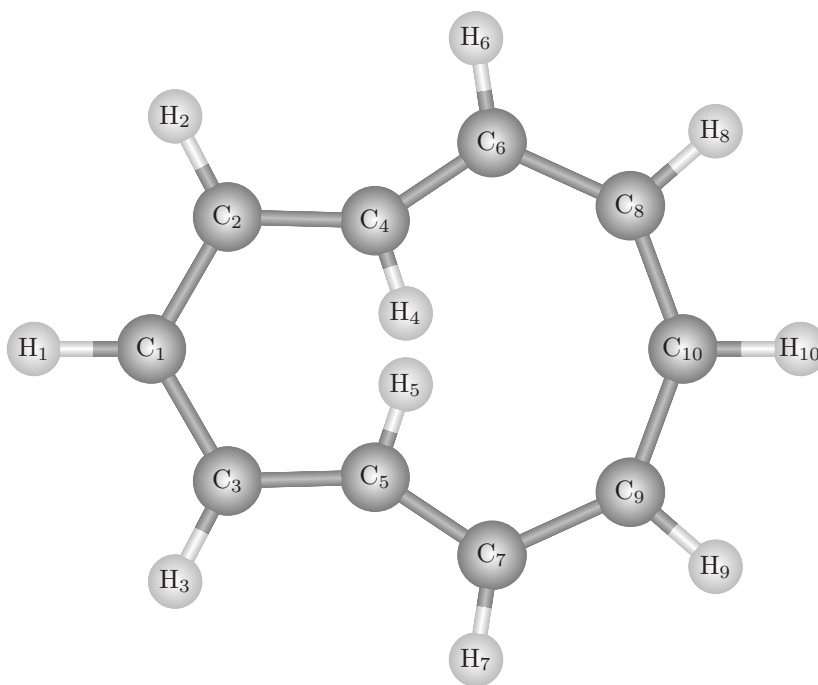


Figure 5.5: Conformation **3a**( $C_2$ ) of [10]annulene

to  $139.91^\circ$ ; however,  $\theta(C_9C_{10}C_8)$  is close to  $140^\circ$  which added  $10 \text{ kcal mol}^{-1}$  to *cis*-1,3-dibutene. Finally, the dihedral angles between the carbon atoms are twisted between  $8^\circ$  and  $40^\circ$  out of the plane adding torsional strain on  $\pi$  system.

By contrast, the  $\pi$  electron density of conformation **3b**( $C_1$ ) (see Figure 5.6) is localized such that the CC bond lengths alternates between 1.3784 and 1.4736 Å for CCSD(T)/DZP and vary between 1.3664 and 1.3895 Å for the double bonds and 1.4569 and 1.4818 Å for the single bonds. The ring strain is comparable to **3a** as the average bond angle between carbon atoms is  $122.8^\circ$

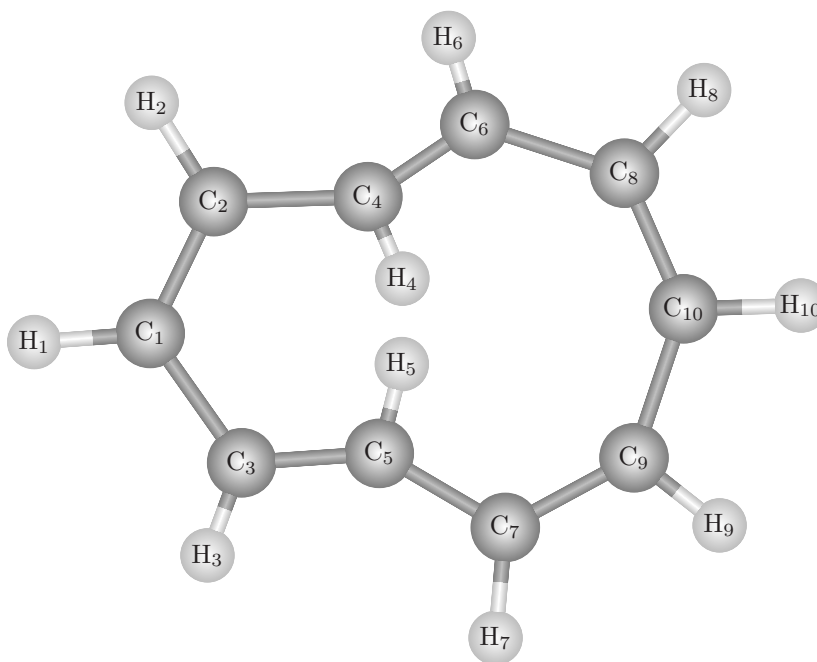


Figure 5.6: Conformation **3b**( $C_1$ ) of [10]annulene

and ranges from  $117.5^\circ$  to  $138.3^\circ$ . But, some of the torsional strain on the  $\pi$  system has diminished since the dihedral angles of the double bonds are twisted between  $1^\circ$  and  $37^\circ$  out of the plane. Also, two of the double bonds, between  $C_3C_5$  and  $C_4C_6$ , have dihedral angles closer to  $180^\circ$  and assume a *trans* configuration.

Like conformation **3a**( $C_2$ ), the  $\pi$  electrons of conformation **4** (see Figure 5.7) are more delocalized and the CC bond lengths also do not alternate and average  $1.4188 \text{ \AA}$ , but vary over a broader range ( $1.3957$  to  $1.4420 \text{ \AA}$ ). However, on pair of bond angles,  $\theta(C_6C_8C_{10})$  and  $\theta(C_7C_9C_{10})$  exceeds  $145^\circ$  lowering the

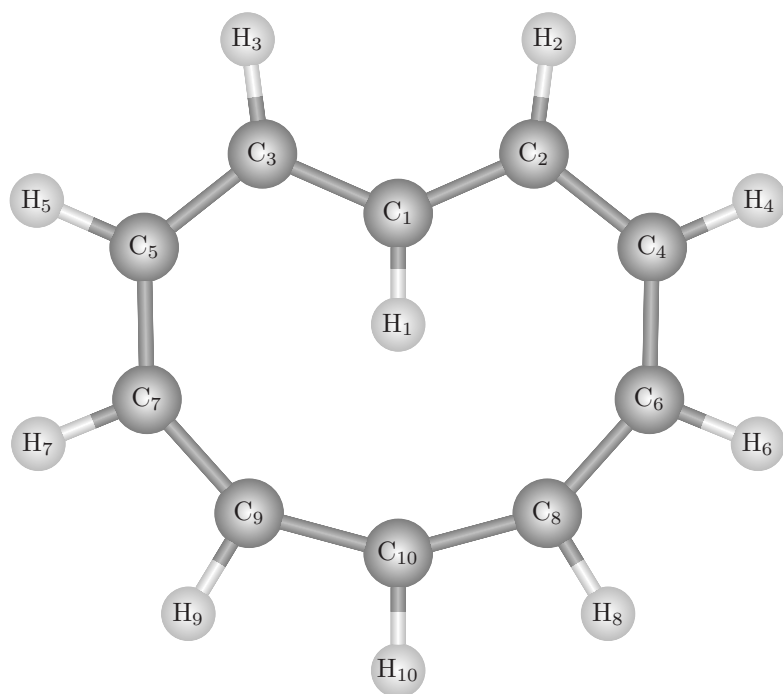


Figure 5.7: Conformation **4** of [10]annulene

stability of the conformation while the remaining angles range from  $117.5^\circ$  to  $139.0^\circ$ . Also, one of pair of dihedral angles  $\tau(\text{C}_2\text{C}_1\text{C}_3\text{C}_5)$  and  $\tau(\text{C}_3\text{C}_1\text{C}_2\text{C}_4)$  are closer to  $180^\circ$  than  $0^\circ$  suggesting a conformation with a *trans* double bond as opposed to a conformation with all *cis* double bonds in similar to conformations **2b** and **2b**.

Like conformation **2b**( $C_2$ ), the CC bond lengths alternate on average from  $1.3710 \text{ \AA}$  to  $1.4835 \text{ \AA}$  indicating that the CC bonds alternate between double ( $\text{C}_1\text{C}_3$ ,  $\text{C}_2\text{C}_4$ ,  $\text{C}_5\text{C}_7$ ,  $\text{C}_6\text{C}_8$  and  $\text{C}_9\text{C}_{10}$ ) and single bonds (see Figure 5.8). The ring strain still present in conformation **2b**( $C_2$ ) is reduced further as

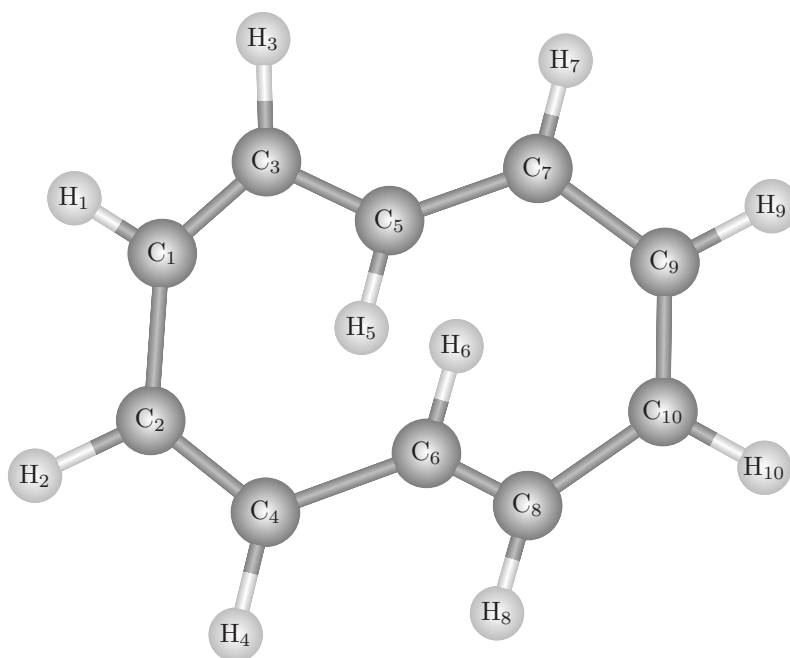


Figure 5.8: Conformation **5** of [10]annulene

the average bond angle between carbon atoms averages  $124.4^\circ$  and only ranges from  $122.7$  to  $128.4^\circ$ . However, one pair of dihedral angles ( $\tau(\text{C}_3\text{C}_5\text{C}_7\text{C}_9)$  and  $\tau(\text{C}_4\text{C}_6\text{C}_8\text{C}_{10})$  each equalling  $150.4^\circ$ ) is twisted more than  $30^\circ$  from a planar configuration which added  $10 \text{ kcal mol}^{-1}$  to ethylene. This pair of angles is also closer to  $180^\circ$  suggesting a conformation with two *trans* double bonds similar to conformation **3b**.

Finally, the  $\pi$  density of conformation **6**( $C_2$ ) (see Figure 5.9) is localized as indicated by the CC bonds alternating in length on average from  $1.3638$  to  $1.4897 \text{ \AA}$  like conformations **2b**( $C_2$ ) and **5**( $C_2$ ). The ring strain is comparable

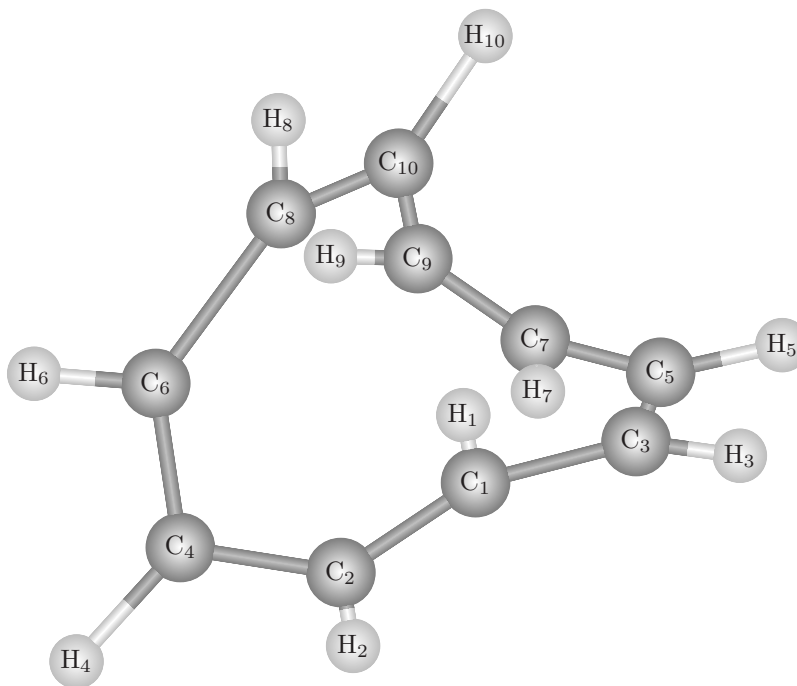


Figure 5.9: Conformation **6** of [10]annulene

to **5** as the average bond angle between carbon atoms is  $125.0^\circ$  and ranges from  $121.3^\circ$  to  $128.0^\circ$ . However, only one dihedral angle  $\tau(\text{C}_3\text{C}_1\text{C}_2\text{C}_4)$  is twisted almost than  $30^\circ$  out of a planar configuration also corresponds to a *trans* conformation similar to **4**.

#### 5.4 *Ab Initio* Energies of the Studied Conformations

The relative energies in Table 5.1 follow the trends found in the literature which are summarized in Table C.1 in the appendix.

The minor differences ( $< 1 \text{ kcal mol}^{-1}$ ) between the relative energies

Table 5.1: Relative energies of conformations and transition states for [10]-annulene (in kcal mol<sup>-1</sup>)

	MP2/DZP		CCSD/DZP		CCSD(T)/DZP	CCSD(T)/TZ2P// CCSD(T)/DZP
	Rel. <i>E</i>	IF <sup><i>a</i></sup>	Rel. <i>E</i>	IF <sup><i>a</i></sup>		
<b>1a</b> <i>D</i> <sub>5h</sub>	<sup><i>b</i></sup>		<sup><i>c</i></sup>		<sup><i>c</i></sup>	<sup><i>c</i></sup>
<b>1b</b> <i>D</i> <sub>10h</sub>	15.91	2	<sup><i>c</i></sup>		<sup><i>c</i></sup>	<sup><i>c</i></sup>
<b>2a</b> <i>C</i> <sub>s</sub>	7.08	1	5.08	1	5.73	4.91
<b>2b</b> <i>C</i> <sub>2</sub>	6.93	0	4.88	0	5.58	4.77
<b>3a</b> <i>C</i> <sub>2</sub>	-3.75	0	12.70	1	6.74	5.65
<b>3b</b> <i>C</i> <sub>1</sub>	<sup><i>d</i></sup>		6.85	0	5.31	
<b>4</b> <i>C</i> <sub>s</sub>	-7.42	0	8.53	0	3.56	3.33
<b>5</b> <i>C</i> <sub>2</sub>	-3.90	0	1.87	0	1.05	0.17
<b>6</b> <i>C</i> <sub>2</sub>	0.00	0	0.00	0	0.00	0.00

<sup>*a*</sup>IF = number of imaginary vibrational frequencies.

<sup>*b*</sup>Geometry optimization converged to conformation **1b** *D*<sub>10h</sub>.

<sup>*c*</sup>Geometry optimization of conformations **1a** and **1b** were not calculated due to two or more imaginary vibrational frequencies in SCF/DZP and MP2/DZP calculations.

<sup>*d*</sup>Geometry optimization converged to conformation **3a** *C*<sub>2</sub>.

from Xie *et al.* [232] and this study for SCF/DZP result from small differences in the polarization functions added to the Huzinaga-Dunning double- $\zeta$  basis set (DZ). In the present study, polarization functions with  $\alpha_d(C) = 0.654$  and  $\alpha_p(H) = 0.7$  have been used to augment the basis set while previous studies [216, 232] used  $\alpha_d(C) = 0.75$  and  $\alpha_p(H) = 0.75$ . As a result, the relative energy of conformations **3a** and **5** is slightly smaller in this study while conformations **1a**, **1b**, **2a** and **4** are somewhat larger.

One major difference between this study and the previous study by King *et al.* occurs for conformation **5** whose MP2/DZP relative energy from this study is 4.43 kcal mol<sup>-1</sup> smaller than the MP2/DZd relative energy [113]. The presence of polarization functions on hydrogen atoms in this study and a difference in polarization functions on carbon atoms  $\alpha_d(C) = 0.654$  verses  $\alpha_d(C) = 0.75$  may account for this difference; however, only minor differences between the relative energies of MP2/DZP and MP2/DZd occurred for other conformations (**2a**, **3a** and **4**).

Table 5.1 also illustrates the limit of arranging the relative stability of conformations based solely on energy. MP2/DZP suggests that **4** is the lowest energy structure conflicting with CCSD/DZP and CCSD(T)/DZP which each suggest **6** in the lowest energy structure. Additionally, each method arranges the conformation in a different order: **4** < **5** < **3a** < **6** < **2b** < **2a** for MP2/DZP, **6** < **5** < **2b** < **2a** < **3b** < **4** < **3a** for CCSD/DZP and **6** < **5** < **4** < **3b** < **2b** < **2a** < **3a** for CCSD(T)/DZP. The accuracy of CCSD(T) improves as more basis functions are included [119, 217] and CCSD(T)/DZP and CCSD(T)/TZ2P//CCSD(T)/DZP are within 3 kcal mol<sup>-1</sup> for isomers of C<sub>4</sub>H<sub>6</sub><sup>5</sup>. However, this uncertainty is larger than the differences in energy

---

<sup>5</sup>The relative energy of 8 isomers of C<sub>4</sub>H<sub>6</sub> are known experimentally [22, 103] and mean



of the conformations preventing conclusive identification of the structure of compound **A** or **B** based solely on the energy of the structure.

## 5.5 Harmonic Frequencies

The harmonic frequencies calculated for the conformations of [10]annulene serve three main purposes. First, they allow conformations to be excluded if harmonic frequency is imaginary<sup>6</sup>. Second, the zero point energy will adjust the relative energy to account for vibrational effects. Third, the harmonic frequencies and their infrared absorption intensities between 600 and 1200  $\text{cm}^{-1}$  may suggest spectral features that could distinguish conformations and determine the identity of compounds **A** and **B** in an Argon matrix study.

Conformations **1a**( $D_{5h}$ ) and **1b**( $D_{10h}$ ) each have multiple imaginary harmonic frequencies for HF/DZP and MP2/DZP and may easily be excluded as a ground state. An imaginary harmonic frequency for conformation **2a** using both MP2/DZP and CCSD/DZP levels of theory also exclude it as a possible ground state. However, an imaginary frequency using CCSD/DZP excludes **3a** as a possible ground state and suggest a  $C_1$  conformation is preferred while no imaginary harmonic frequencies are obtained using MP2/DZP. These results mirror what C. Castro *et al.* obtained using BH&HLYP/6-311+G\*\* [44].

The vibrational zero point energy had a minor effect on the relative energy of the possible ground state structures (**2b**, **3b**, **4**, **5** and **6**). Differences as much as 2.4  $\text{kcal mol}^{-1}$  (the difference between conformations **4** and

---

absolute deviations from experiment of the energy computed using CCSD(T)/DZP and CCSD(T)/TZ2P are 0.88 and 0.90  $\text{kcal mol}^{-1}$  at CCSD(T)/DZP optimized geometry, and deviations between 2 and 3  $\text{kcal mol}^{-1}$  occurred in only two cases.

<sup>6</sup>A negative second derivative or imaginary harmonic frequency indicates the conformation is a local maximum or transition state and not a local minimum or ground state.

**6**) occur for MP2/DZP. By contrast, the differences between other possible ground states and conformation **6** are less than 1 kcal/mol for CCSD/DZP. The lowest harmonic frequency of **2b** is only  $25\text{ cm}^{-1}$  - one fourth the size of the lowest harmonic frequency of the other conformations which suggests that conformation **2b**. The vibrational normal mode associated with this frequency corresponds to torsional bending of the dihedral angle and suggest a relatively flat part of the potential energy surface that allows the conformation to rearrange. One result is the  $^{13}\text{C}$  NMR shieldings observed for each carbon would be an average of each arrangement even at low temperatures.

In addition to the factors related to the relative energy and stability of the conformations, the pattern of harmonic frequencies and infrared intensities between the  $1250$  to  $600\text{ cm}^{-1}$  provide a finger print for a particular molecule<sup>7</sup>. The predicted absorbances in this region are classed as medium for an infrared intensity between  $10$  and  $25\text{ km mol}^{-1}$  and strong for an infrared intensity between  $25$  to  $100\text{ km mol}^{-1}$ . Conformation **2b** has two strong absorbance between  $620$  and  $630\text{ cm}^{-1}$ , another strong absorbance near  $710$  and a medium absorbance near  $790\text{ cm}^{-1}$ , but only weak absorbance between  $800$  and  $1200\text{ cm}^{-1}$ . See Figure 5.10. Conformation **3b** has one very strong absorbance near  $750\text{ cm}^{-1}$ , another strong absorbance near  $1000\text{ cm}^{-1}$ , but only weak absorbance between  $1000$  and  $1200\text{ cm}^{-1}$ . See Figure 5.11. Conformation **4** has two strong absorbances near  $660$  and  $670\text{ cm}^{-1}$ , and another medium absorbance near  $700\text{ cm}^{-1}$ . It also has a medium absorbance near  $840$  and a strong absorbance near  $1000\text{ cm}^{-1}$ . See Figure 5.12. Conformation **5** only has weak absorbance between  $600\text{ cm}^{-1}$  and a strong absorbance at  $740\text{ cm}^{-1}$ . This

---

<sup>7</sup>In general infrared spectroscopy, the finger print region is between  $1200$  and  $600\text{ cm}^{-1}$ . But this range has been extended to account for anharmonic effects up to  $50\text{ cm}^{-1}$ .

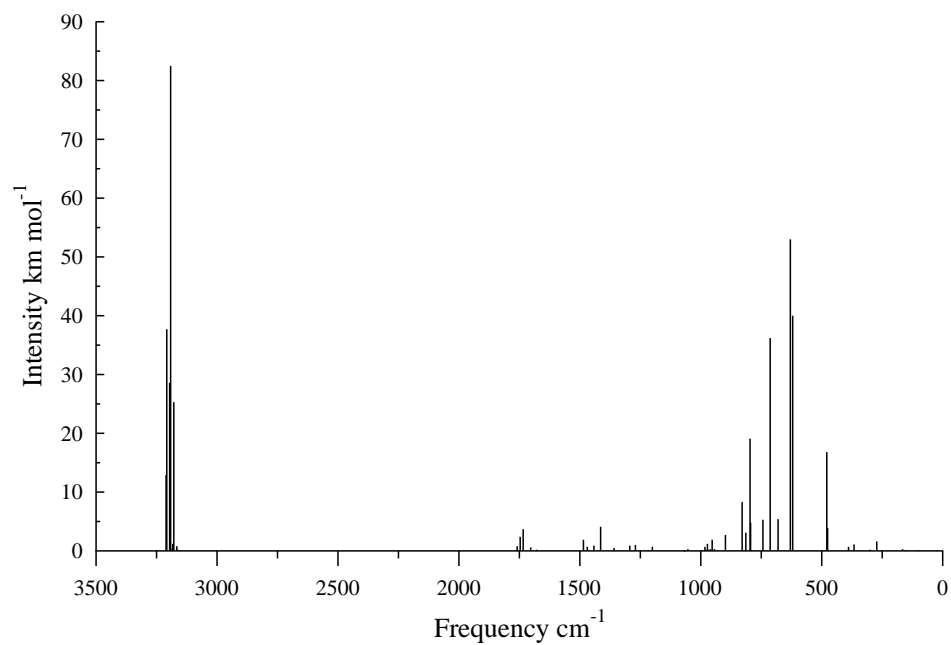


Figure 5.10: Infrared spectra of Conformation **2b** based on harmonic frequencies and IR intensities calculated using CCSD/DZP.

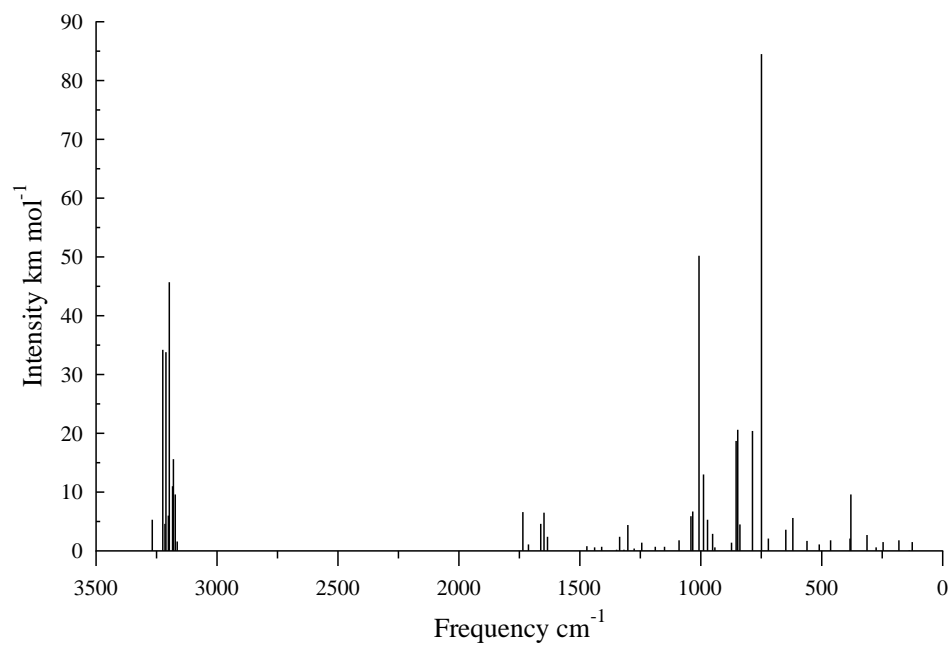


Figure 5.11: Infrared spectra of Conformation **3b** based on harmonic frequencies and IR intensities calculated using CCSD/DZP.

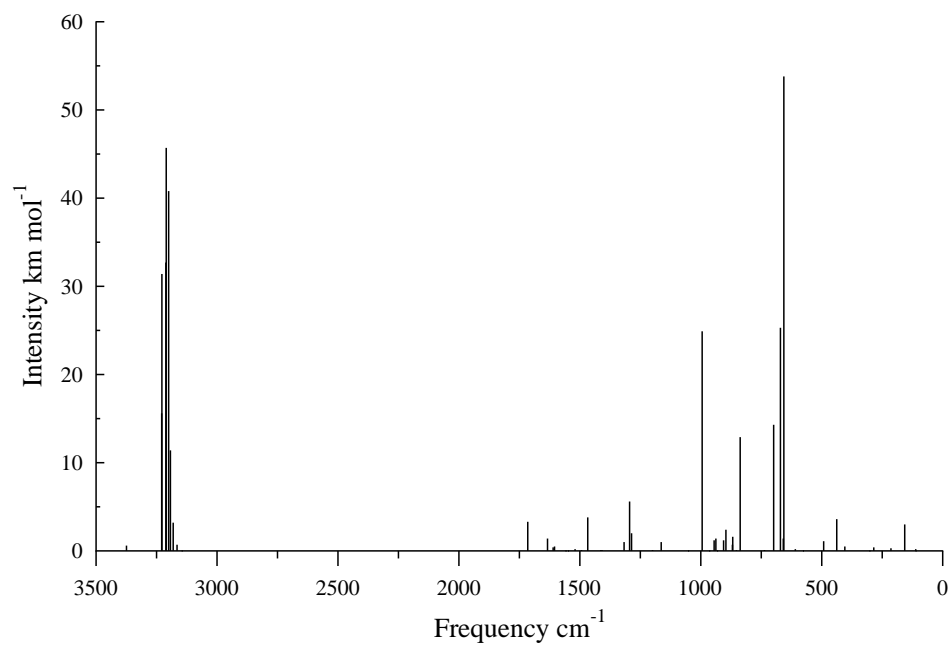


Figure 5.12: Infrared spectra of Conformation **4** based on harmonic frequencies and IR intensities calculated using CCSD/DZP.

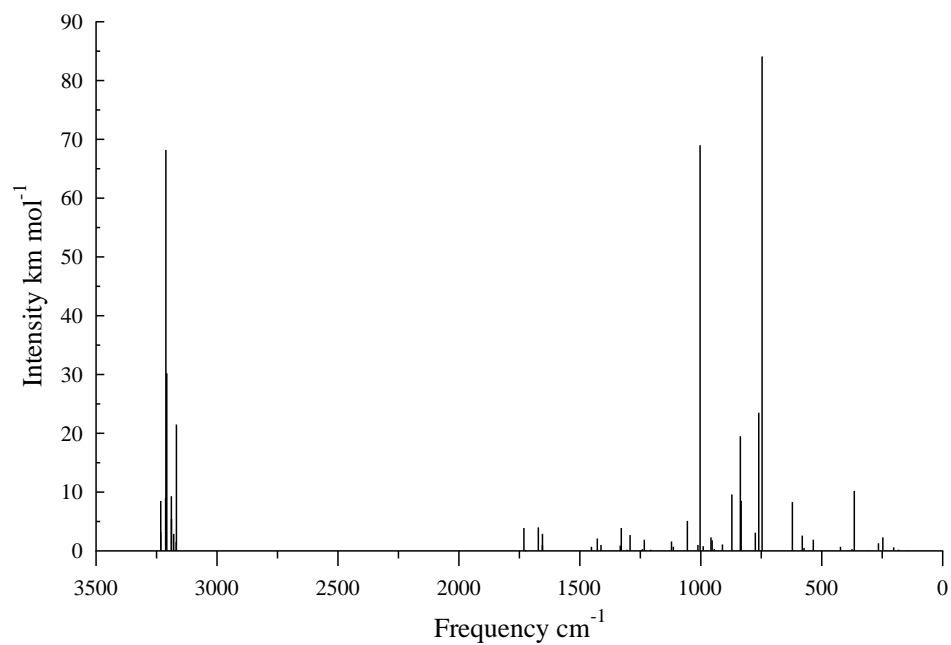


Figure 5.13: Infrared spectra of Conformation **5** based on harmonic frequencies and IR intensities calculated using CCSD/DZP.

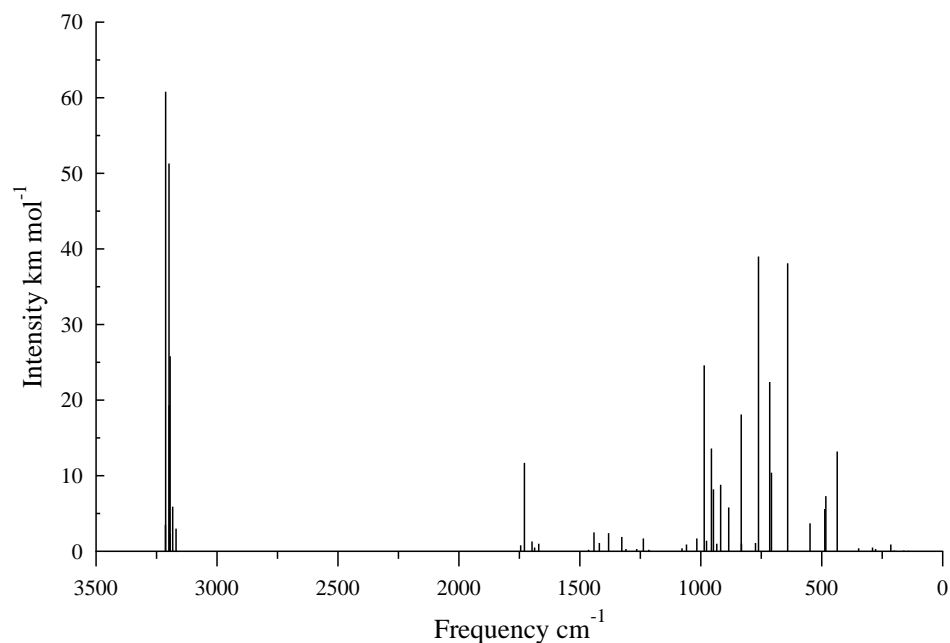


Figure 5.14: Infrared spectra of Conformation **6** based on harmonic frequencies and IR intensities calculated using CCSD/DZP.

absorbance has a medium absorbance neighboring at  $760\text{ cm}^{-1}$ , and similar absorbances as conformation **4** - a medium absorbance near  $840\text{ cm}^{-1}$  and a strong absorbance near  $1000\text{ cm}^{-1}$ . See Figure 5.13. Finally, conformation **6** has seven peaks scattered between  $640$  and  $990\text{ cm}^{-1}$  - two strong absorbances at  $640$  and  $760\text{ cm}^{-1}$  and five medium absorbances at  $700$ ,  $710$ ,  $830$ ,  $960$  and  $990\text{ cm}^{-1}$ . See Figure 5.14.

Conformation **2b** may be distinguished by its absorbance at lower vibrational frequencies between  $620$  and  $630\text{ cm}^{-1}$ , but also the absence of absorbance above  $800\text{ cm}^{-1}$ . Conformation **5** may be distinguished primarily by

its strong absorbance near  $740\text{ cm}^{-1}$  and the absence of medium and strong absorbance between  $600$  and  $740\text{ cm}^{-1}$  and secondarily by an absorbance near  $1000\text{ cm}^{-1}$  stronger than predicted for absorbances of conformations **4** and **6** in the same vicinity. Conformation **4** may be distinguished primarily by three strong and medium absorbance bands between  $650$  and  $700\text{ cm}^{-1}$  coupled with absorbances near  $840$  and  $1000\text{ cm}^{-1}$  and the absence of medium and strong absorbances between  $700$  and  $840\text{ cm}^{-1}$ . Conformation **6** lacks major features that would distinguish it from the other conformations. A medium peak at  $960\text{ cm}^{-1}$  might be used to identify it in an experimental spectrum.

## 5.6 NMR Shifts

The initial investigation of the NMR shifts measured by Masamune and coworkers [137] suggested that conformation **6** corresponded to their compound **B**. The NMR shifts shown in Figure 5.15 were based on CCSD(T)/DZP NMR shifts calculated at the CCSD(T)/DZd geometry obtained by King *et al.* [113] then corrected to account for basis set effect by:

$$\sigma = \sigma_{MP2}^{tzip} + \sigma_{CCSD(T)}^{DZP} - \sigma_{MP2}^{DZP} \quad (5.1)$$

where  $\sigma$  refers to the NMR shifts following standard notation. The resulting NMR shifts allowed conformation **4** to be excluded by the presence of six NMR shifts including two with half the intensity of the other four shifts instead of five shifts of equal intensity. Conformation **5** was also excluded due a difference of  $12.4\text{ ppm}$  for one of its shifts from experiment and the relative spacing of one of its remaining shifts ( $2.1$ ,  $0.3$  and  $4.6\text{ ppm}$ ) deviated significantly from experiment ( $3.1$ ,  $0.2$ ,  $0.6$  and  $0.2\text{ ppm}$ ). Conformation **6** was identified as the likeliest structure for compound **B** due to both an average difference from



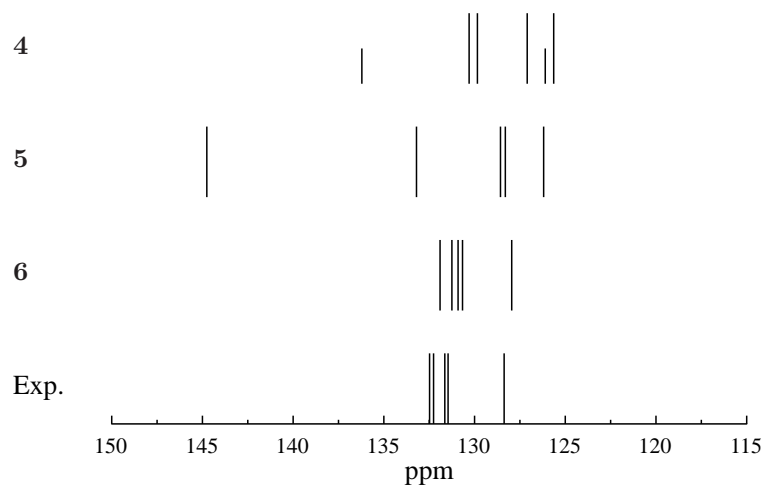


Figure 5.15:  $^{13}\text{C}$  NMR shifts relative to TMS computed using CCSD(T)/DZP at geometries optimized at the CCSD(T)/DZd level from Ref. [113]. The NMR shifts have been corrected to account for the basis set effect as described in the text.

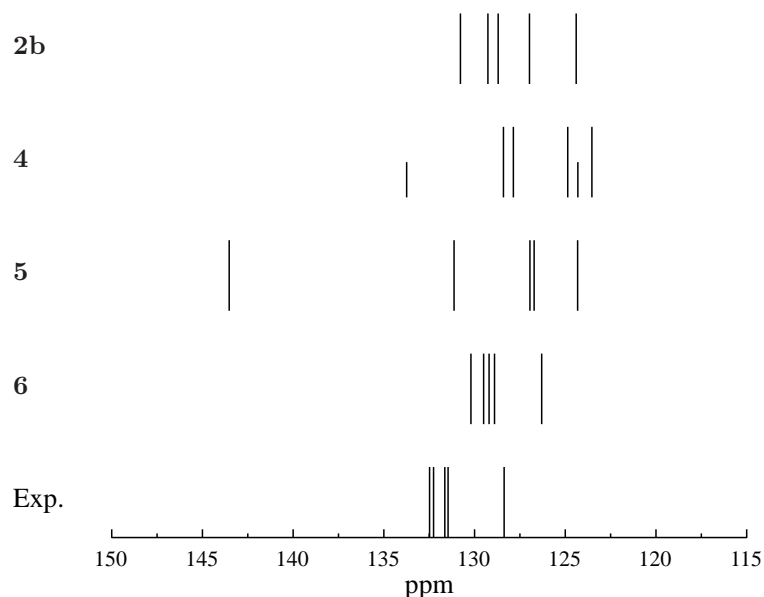


Figure 5.16:  $^{13}\text{C}$  NMR shifts relative to TMS computed using CCSD(T)/tzip at geometries optimized at the CCSD(T)/DZP level.

experiment of less than 1 ppm and the relative spacing (2.7, 0.2, 0.3 and 0.7 ppm) are within 0.5 ppm of experiment.

However, the basis set correction gave fortuitous results. Subsequent  $^{13}\text{C}$  NMR shifts were calculated using CCSD(T)/tzip at CCSD(T)/DZP geometry computed in this study deviated more on average from experiment as seen in Figure 5.16. Conformation **2b** deviated on average 3.2 ppm from experiment, but its relative spacing (2.6, 1.7, 0.6 and 1.5) deviate significantly from experiment in two cases. Conformation **5** deviated more on average (5.1 ppm) from experiment than conformation **2b** and a significant difference of 11.0 ppm persists. One of the relative spacing of its remaining shifts (2.4,

0.2 and 4.2 ppm) still deviates significantly from experiment. Conformation **6** deviated on average 2.4 ppm from experiment - more than three times the average deviation of CCSD(T)/DZP with basis set correction. However, the relative spacing (2.6, 0.3, 0.3 and 0.7 ppm) remains similar. To improve the agreement between theory and experiment,  $^{13}\text{C}$  NMR shifts calculated using CCSD(T)/qz2p for conformation **6**. The chemical shifts for CCSD(T)/qz2p were on average 2.3 ppm more than experiment in contrast to the average of 2.4 ppm less than experiment for CCSD(T)/tzp. Also, the relative spacing (2.9, 0.2, 0.1 and 1.0 ppm) remains similar to CCSD(T)/tzp. See Figure 5.17.

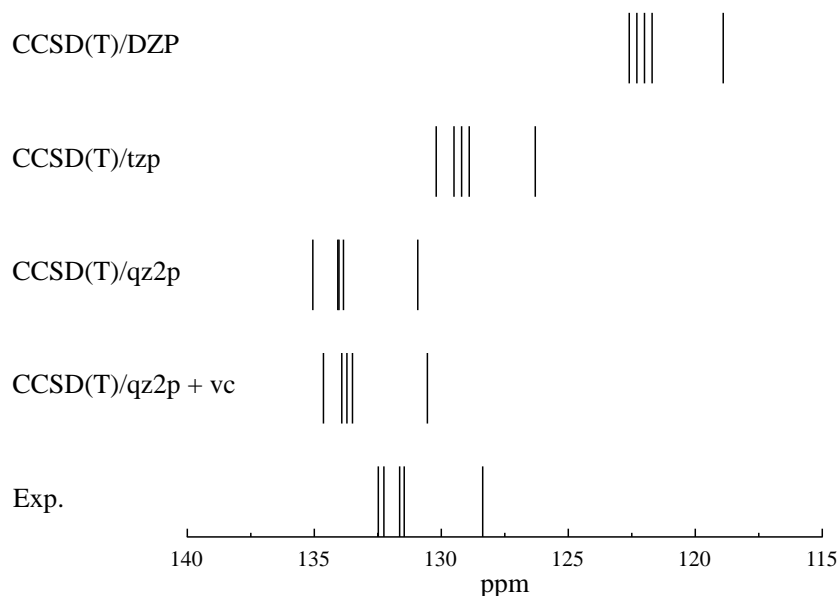


Figure 5.17:  $^{13}\text{C}$  NMR shifts relative to TMS computed using CCSD(T)/DZP, CCSD(T)/tzp and CCSD(T)/qz2p at geometries optimized using CCSD(T)/DZP. The vibrational corrections (vc) for conformation **6** and TMS were computed using SCF/tzp and then added to the  $^{13}\text{C}$  NMR shifts.

To account for this systematic shift in conformation **6**, the vibrational correction [11, 92] to the NMR shielding,  $\sigma$ , is expanded in a Taylor series:

$$\langle \sigma \rangle = \sigma_0 + \sum_r \left( \frac{\partial \sigma}{\partial Q_r} \right)_{Q_r=0} \langle Q_r \rangle + \frac{1}{2} \sum_{rs} \left( \frac{\partial^2 \sigma}{\partial Q_r \partial Q_s} \right)_{Q_r, Q_s=0} \langle Q_r Q_s \rangle. \quad (5.2)$$

The first- and second-order vibrational average of the normal coordinates in the expansion,  $Q_i$  are:

$$\langle Q_r \rangle = -\frac{\hbar}{4\omega_r^2} \sum_s \frac{k_{rss}}{\omega_s} \quad (5.3)$$

and

$$\langle Q_r Q_s \rangle = \delta_{rs} \frac{\hbar}{2\omega_r}. \quad (5.4)$$

where  $k_{rss}$  is a cubic force constant (see Chapter 3) proportional to  $\phi_{rss}$  used earlier. For [10]annulene, this correction is computed for HF/tzp. However, the vibrational correction decreased the systematic shift (see Figure 5.17) slightly from an average of 2.3 ppm to 2.0 ppm while maintaining similar relative spacing (2.9, 0.2, 0.2 and 0.7 ppm). Including a temperature effect in the first- and second-order vibrational average [92]:

$$\langle Q_r \rangle = -\frac{\hbar}{4\omega_r^2} \left[ \sum_s \frac{k_{rss}}{\omega_s} \coth \left( \frac{\hbar\omega_s}{2k_bT} \right) - 2k_bT \sum_{\alpha} \frac{a_r^{(\alpha\alpha)}}{I_{\alpha\alpha}} \right] \quad (5.5)$$

and

$$\langle Q_r Q_s \rangle = \delta_{rs} \frac{\hbar}{2\omega_r} \coth \left( \frac{\hbar\omega_r}{2k_bT} \right), \quad (5.6)$$

did not alter the relative shifts at  $T = 170$  K (the temperature where the NMR signal split into 5 peaks) more than 0.1 ppm..

The other compound isolated by Masumune *et al.* with  $^{13}\text{C}$  NMR shift 130.4 ppm from TMS is believed to a conformational average where carbon atoms shift position within the ring. The average  $^{13}\text{C}$  NMR shifts of conformations **2b** (128.0 ppm), **4**, **5** (130.5 ppm) and **6** (128.8 ppm) using CCSD(T)/tzp

at the CCSD(T)/DZP geometry are each within 3 ppm of the experimental  $^{13}\text{C}$  shift for Compound **A**. The systematic 2 ppm error noted above suggests conformation **2b** may be the structure for Compound **A**.

## 5.7 Summary

By examining nine of the conformations proposed for the structure of the two compounds Masumune and coworkers isolated in 1971, the structures of compound **A** and **B** are conformation **2b** and **6**. Of the nine structures, five are vibrational ground states based on the harmonic frequency calculations performed using CCSD/DZP. However, relative energy of these conformations are within 6 kcal mol $^{-1}$  of each other preventing conclusive determinations of compound **A** and **B** based solely on relative energy. Conformation **2b** is a plausible candidate for the structure of compound **A**. A harmonic frequency (25 cm $^{-1}$ ) significantly smaller than the other conformations, and a possible transition state, conformation **2a**, within 0.14 kcal mol $^{-1}$  suggest tautomerization of conformation **2b** accounts for the  $^{13}\text{C}$  NMR shift observed for compound **A**, and the average  $^{13}\text{C}$  NMR shifts at CCSD(T)/tzp and CCSD(T)/DZP with basis set correction support this conclusion. By contrast, the structure of compound **B** may be more conclusively be identified by  $^{13}\text{C}$  NMR shifts computed using CCSD(T)/tzp and CCSD(T)/DZP with basis set correction as conformation **6**. The proposed structures may be examined further by argon matrix IR studies. The fingerprint region of the vibrational spectra predicted using harmonic frequencies suggest the location of several that may help confirm the structures proposed.

## Chapter 6

### Conclusion

The high accuracy *ab initio* methods used in the past to accurately predict experimental spectra and structures of smaller molecules [132–134, 159, 221] can be extended to larger molecules like benzene and [10]annulene through parallelization of analytic second derivatives. The coarse grained parallelization scheme described in Chapter 2 allows for parallel computation of analytic second derivatives for a variety of post Hartree-Fock methods (MP2, MP3, MP4, CC2, CCD, QCISD, CCSD, QCISD(T), CCSD(T), CCSDT-n (n=1-4), CC3, and CCSDT). As a result, the fundamental frequencies of benzenes calculated using VPT2 (see Chapter 3) are within 10 cm<sup>-1</sup> at the CCSD(T)/ANO2/1(fc) level of theory when vibrational states effected by Fermi resonance are treated as described above. In particular, the “dressed” value of  $\nu_{13}(b_{2u})$  for benzene favors the experimental frequency obtained by U. Erlekam *et al.* [66] over the value obtained early by S. Brodersen and A. Langseth [35]. Benzene’s two quantum frequencies are within 20 cm<sup>-1</sup> of the experimental results with an absolute mean deviation of 5 cm<sup>-1</sup>. The NMR shifts and harmonic frequencies of nine conformations proposed previously suggest that conformation **2b** and **6** are plausible candidates for the structures of the two compounds Masumune and coworkers isolated in 1971, compound **A** and **B**.

## Appendices

# Appendix A

## Parallel Timings

Table A.1: Timing (s) and Speed Up

	Timing					Speed Up		
$P$	Over.	ACESII	I	II	III	Over.	ACESII	II
CO <sub>2</sub> CCSD(T)/cc-pVTZ $D_{2h}$ Current								
1	703	446	75	347	24	1.0	1.0	1.0
2	706	402	83	291	28	1.0	1.1	1.2
3	667	366	77	262	27	1.1	1.2	1.3
6	652	349	77	243	29	1.1	1.3	1.4
CO <sub>2</sub> CCSD(T)/cc-pVTZ $D_{2h}$ New								
1	745	488	76	383	29	1.0	1.0	1.0
2	656	328	83	212	33	1.1	1.5	1.8
3	595	272	83	151	38	1.3	1.8	2.5
6	488	183	76	74	33	1.5	2.7	5.2
CO <sub>2</sub> CCSD(T)/cc-pVTZ $D_2$ Current								
1	1073	813	93	696	24	1.0	1.0	1.0
2	834	576	79	473	24	1.3	1.4	1.5
3	761	501	74	402	25	1.4	1.6	1.7
6	768	461	83	351	27	1.4	1.8	2.0
CO <sub>2</sub> CCSD(T)/cc-pVTZ $D_2$ New								
1	1112	861	102	729	30	1.0	1.0	1.0
2	819	513	90	389	34	1.4	1.7	1.9
3	685	393	86	273	34	1.6	2.2	2.7
6	571	267	82	151	34	2.0	3.2	4.8



Table A.1: Continue

	Timing					Speed Up		
$P$	Over.	ACESII	I	II	III	Over.	ACESII	II
CO <sub>2</sub> CCSD(T)/cc-pVTZ $C_{2v}$ Current								
1	1166	855	104	723	28	1.0	1.0	1.0
2	929	622	89	505	28	1.3	1.4	1.4
3	778	522	76	421	25	1.5	1.6	1.7
6	790	480	84	368	28	1.5	1.8	2.0
CO <sub>2</sub> CCSD(T)/cc-pVTZ $C_{2v}$ New								
1	1101	858	96	734	28	1.0	1.0	1.0
2	810	505	89	384	32	1.4	1.7	1.9
3	706	400	88	278	34	1.6	2.2	2.6
6	564	257	83	141	33	2.0	3.3	5.2
CO <sub>2</sub> CCSD(T)/cc-pVTZ $C_{2h}$ Current								
1	1167	862	106	728	28	1.0	1.0	1.0
2	948	629	93	508	28	1.2	1.4	1.4
3	888	563	89	446	28	1.3	1.5	1.6
6	779	469	81	360	28	1.5	1.8	2.0
CO <sub>2</sub> CCSD(T)/cc-pVTZ $C_{2h}$ New								
1	1209	905	105	767	33	1.0	1.0	1.0
2	818	511	93	386	32	1.5	1.8	2.0
3	713	394	89	271	34	1.7	2.3	2.8
6	570	264	86	144	34	2.1	3.4	5.3
CO <sub>2</sub> CCSD(T)/cc-pVTZ $C_2$ Current								
1	2492	2230	163	2039	28	1.0	1.0	1.0
2	1765	1463	135	1295	33	1.4	1.5	1.6
3	1509	1187	118	1039	30	1.7	1.9	2.0
6	1234	923	108	783	32	2.0	2.4	2.6
CO <sub>2</sub> CCSD(T)/cc-pVTZ $C_2$ New								
1	2520	2268	165	2070	33	1.0	1.0	1.0
2	1550	1259	131	1092	36	1.6	1.8	1.9
3	1179	880	122	722	36	2.1	2.6	2.9
6	870	564	110	415	39	2.9	4.0	5.0

Table A.1: Continue

	Timing					Speed Up		
$P$	Over.	ACESII	I	II	III	Over.	ACESII	II
CO <sub>2</sub> CCSD(T)/cc-pVTZ $C_i$ Current								
1	2606	2301	183	2085	33	1.0	1.0	1.0
2	1892	1563	141	1390	32	1.4	1.5	1.5
3	1617	1267	123	1113	31	1.6	1.8	1.9
6	1363	1004	114	855	35	1.9	2.3	2.4
CO <sub>2</sub> CCSD(T)/cc-pVTZ $C_i$ New								
1	2612	2303	174	2092	37	1.0	1.0	1.0
2	1692	1390	150	1198	42	1.5	1.7	1.8
3	1255	950	128	784	38	2.1	2.4	2.7
6	890	582	124	417	41	2.9	4.0	5.0
CO <sub>2</sub> CCSD(T)/cc-pVTZ $C_s$ Current								
1	2689	2424	189	2199	36	1.0	1.0	1.0
2	2032	1733	155	1536	42	1.3	1.4	1.4
3	1741	1438	140	1256	42	1.5	1.7	1.8
6	1447	1132	126	963	43	1.9	2.1	2.3
CO <sub>2</sub> CCSD(T)/cc-pVTZ $C_s$ New								
1	2806	2503	193	2266	44	1.0	1.0	1.0
2	1825	1479	160	1272	47	1.5	1.7	1.6
3	1369	1053	145	859	49	2.1	2.4	2.4
6	908	608	127	434	47	3.1	4.1	4.8
CO <sub>2</sub> CCSD(T)/cc-pVTZ $C_1$ Current								
1	9540	9287	560	8686	41	1.0	1.0	1.0
2	6834	6529	462	6020	47	1.4	1.4	1.4
3	6800	6498	502	5938	58	1.4	1.4	1.5
6	4508	4207	369	3788	50	2.1	2.2	2.3
CO <sub>2</sub> CCSD(T)/cc-pVTZ $C_1$ New								
1	9671	9364	569	8745	50	1.0	1.0	1.0
2	5716	5411	466	4890	55	1.7	1.7	1.8
3	4110	3801	413	3336	52	2.4	2.5	2.6
6	2403	2096	366	1674	56	4.0	4.5	5.2

Table A.1: Continue

	Timing					Speed Up		
$P$	Over.	ACESII	I	II	III	Over.	ACESII	II
SCl <sub>2</sub> CCSD(T)/cc-pVQZ $C_{2v}$ Current								
2	49559	49516	2992	46139	385	2.0	2.0	2.0
4	29595	29554	1909	27256	389	3.3	3.4	3.4
6	23012	22965	1556	21019	390	4.3	4.3	4.4
12	16508	16465	1198	14877	390	6.0	6.0	6.2
SCl <sub>2</sub> CCSD(T)/cc-pVQZ $C_{2v}$ New								
2	49898	49854	3346	46114	394	2.0	2.0	2.0
4	29205	29159	2429	26340	390	3.4	3.4	3.5
6	19237	19189	2143	16650	396	5.2	5.2	5.5
12	12057	12007	1841	9773	393	8.3	8.3	9.4
C <sub>3</sub> H <sub>2</sub> MP2/cc-pVDZ $C_{2v}$ Current								
1	573	316	53	239	24			
C <sub>3</sub> H <sub>2</sub> MP2/cc-pVDZ $C_{2v}$ New								
1	617	376	57	291	28	1.0	1.0	1.0
2	567	266	60	174	32	1.1	1.4	1.7
4	484	187	65	89	33	1.3	2.0	3.3
6	462	156	65	61	30	1.3	2.4	4.8
12	508	147	75	37	35	1.2	2.6	7.9
C <sub>3</sub> H <sub>2</sub> MP2/cc-pVDZ $C_s$ Current								
1	682	376	65	284	27			
C <sub>3</sub> H <sub>2</sub> MP2/cc-pVDZ $C_s$ New								
1	742	438	63	345	30	1.0	1.0	1.0
2	485	231	52	152	27	1.5	1.9	2.3
4	485	188	66	89	33	1.5	2.3	3.9
6	462	160	65	62	33	1.6	2.7	5.6
12	447	131	65	31	35	1.7	3.3	11.1
C <sub>3</sub> H <sub>2</sub> MP2/cc-pVDZ $C_1$ Current								
1	694	393	68	295	30			

Table A.1: Continue

	Timing					Speed Up		
$P$	Over.	ACESII	I	II	III	Over.	ACESII	II
C <sub>3</sub> H <sub>2</sub> MP2/cc-pVDZ $C_1$ New								
1	782	476	68	371	37	1.0	1.0	1.0
2	604	293	66	192	35	1.3	1.6	1.9
4	503	199	66	97	36	1.6	2.4	3.8
6	475	170	67	67	36	1.7	2.8	5.5
12	444	138	66	34	38	1.8	3.5	10.9
C <sub>3</sub> H <sub>2</sub> MP2/cc-pVTZ $C_{2v}$ Current								
1	1194	885	116	657	112			
C <sub>3</sub> H <sub>2</sub> MP2/cc-pVTZ $C_{2v}$ New								
1	1393	1144	102	947	95	1.0	1.0	1.0
2	1056	748	115	516	117	1.3	1.5	1.8
4	791	487	110	259	118	1.8	2.4	3.7
6	736	428	118	187	123	1.9	2.7	5.1
12	654	343	123	95	125	2.1	3.3	10.0
C <sub>3</sub> H <sub>2</sub> MP2/cc-pVTZ $C_s$ Current								
1	1296	992	130	748	114			
C <sub>3</sub> H <sub>2</sub> MP2/cc-pVTZ $C_s$ New								
1	1547	1242	109	1033	100	1.0	1.0	1.0
2	1070	763	113	533	117	1.5	1.6	1.9
4	816	515	109	286	120	1.9	2.4	3.6
6	733	434	117	194	123	2.1	2.9	5.3
12	648	343	117	101	125	2.4	3.6	10.2
C <sub>3</sub> H <sub>2</sub> MP2/cc-pVTZ $C_1$ Current								
1	1946	1673	214	1267	192			
C <sub>3</sub> H <sub>2</sub> MP2/cc-pVTZ $C_1$ New								
1	2554	2246	147	1892	207	1.0	1.0	1.0
2	1615	1311	153	959	199	1.6	1.7	2.0
4	1142	840	152	489	199	2.2	2.7	3.9
6	1065	764	164	380	220	2.4	2.9	5.0
12	884	579	163	204	212	2.9	3.9	9.3
C <sub>3</sub> H <sub>2</sub> MP2/cc-pVQZ $C_{2v}$ Current								
1	8042	7737	982	5504	1251			

Table A.1: Continue

	Timing					Speed Up		
$P$	Over.	ACESII	I	II	III	Over.	ACESII	II
C <sub>3</sub> H <sub>2</sub> MP2/cc-pVQZ $C_{2v}$ New								
1	11578	11303	797	9246	1260	1.0	1.0	1.0
2	8352	8057	907	5807	1343	1.4	1.4	1.6
4	5291	4993	911	2745	1337	2.2	2.3	3.4
6	4463	4162	921	1909	1332	2.6	2.7	4.8
12	3551	3252	919	987	1346	3.3	3.5	9.4
C <sub>3</sub> H <sub>2</sub> CCSD/cc-pVDZ $C_{2v}$ Current								
1	744	439	67	345	27			
C <sub>3</sub> H <sub>2</sub> CCSD/cc-pVDZ $C_{2v}$ New								
1	701	444	56	362	26	1.0	1.0	1.0
2	510	266	53	185	28	1.4	1.7	2.0
4	498	202	65	104	33	1.4	2.2	3.5
6	478	172	65	74	33	1.5	2.6	4.9
12	444	139	69	38	32	1.6	3.2	9.5
C <sub>3</sub> H <sub>2</sub> CCSD/cc-pVDZ $C_s$ Current								
1	660	410	55	335	20			
C <sub>3</sub> H <sub>2</sub> CCSD/cc-pVDZ $C_s$ New								
1	858	556	69	454	33	1.0	1.0	1.0
2	546	293	55	210	28	1.6	1.9	2.2
4	526	223	67	125	31	1.6	2.5	3.6
6	488	182	67	82	33	1.8	3.1	5.5
12	451	144	67	43	34	1.9	3.9	10.6
C <sub>3</sub> H <sub>2</sub> CCSD/cc-pVDZ $C_1$ Current								
1	888	625	66	534	25			
C <sub>3</sub> H <sub>2</sub> CCSD/cc-pVDZ $C_1$ New								
1	1072	768	77	655	36	1.0	1.0	1.0
2	669	415	64	320	31	1.6	1.9	2.1
4	620	300	76	187	37	1.7	2.6	3.5
6	533	230	74	120	36	2.0	3.3	5.5
12	528	188	80	67	41	2.0	4.1	9.8
C <sub>3</sub> H <sub>2</sub> CCSD/cc-pVTZ $C_{2v}$ Current								
1	2336	2030	163	1751	116			

Table A.1: Continue

	Timing					Speed Up		
$P$	Over.	ACESII	I	II	III	Over.	ACESII	II
C <sub>3</sub> H <sub>2</sub> CCSD/cc-pVTZ $C'_{2v}$ New								
1	2529	2278	145	2018	115	1.0	1.0	1.0
2	1697	1404	157	1122	125	1.5	1.6	1.8
4	1161	852	150	576	126	2.2	2.7	3.5
6	963	656	146	386	124	2.6	3.5	5.2
12	772	468	146	196	126	3.3	4.9	10.3
C <sub>3</sub> H <sub>2</sub> CCSD/cc-pVTZ $C_s$ Current								
1	3068	2827	184	2543	100			
C <sub>3</sub> H <sub>2</sub> CCSD/cc-pVTZ $C_s$ New								
1	3375	3119	181	2833	105	1.0	1.0	1.0
2	2103	1852	171	1572	109	1.6	1.7	1.8
4	1415	1121	171	821	129	2.4	2.8	3.5
6	1159	857	171	555	131	2.9	3.6	5.1
12	895	590	172	286	132	3.8	5.3	9.9
C <sub>3</sub> H <sub>2</sub> CCSD/cc-pVTZ $C_1$ Current								
1	8270	7968	373	7328	267			
C <sub>3</sub> H <sub>2</sub> CCSD/cc-pVTZ $C_1$ New								
1	9062	8756	376	8103	277	1.0	1.0	1.0
2	5327	5014	332	4426	256	1.7	1.8	1.8
4	3208	2901	300	2317	284	2.8	3.0	3.5
6	2425	2123	294	1545	284	3.7	4.1	5.2
12	1679	1368	283	793	292	5.4	6.4	10.2
C <sub>3</sub> H <sub>2</sub> CCSD/cc-pVQZ $C_{2v}$ Current								
1	20358	20050	1356	17411	1283	1.0	1.0	1.0
2	18272	17985	1201	15429	1355	1.1	1.1	1.1
4	16030	15727	1056	13304	1367	1.3	1.3	1.3
C <sub>3</sub> H <sub>2</sub> CCSD/cc-pVQZ $C_{2v}$ New								
1	23565	23313	1333	20691	1289	1.0	1.0	1.0
2	14521	14216	1291	11561	1364	1.6	1.6	1.8
4	8798	8488	1192	5932	1364	2.7	2.8	3.5
6	6905	6612	1156	4082	1374	3.4	3.5	5.1
12	4879	4565	1140	2050	1375	4.8	5.1	10.1

Table A.1: Continue

	Timing					Speed Up		
$P$	Over.	ACESII	I	II	III	Over.	ACESII	II
C <sub>3</sub> H <sub>2</sub> CCSD(T)/cc-pVDZ $C'_{2v}$ Current								
1	811	502	67	410	25	1.0	1.0	1.0
2	766	461	69	366	26	1.1	1.1	1.1
4	734	433	64	343	26	1.1	1.2	1.2
C <sub>3</sub> H <sub>2</sub> CCSD(T)/cc-pVDZ $C'_{2v}$ New								
1	770	516	55	434	27	1.0	1.0	1.0
2	638	338	66	240	32	1.2	1.5	1.8
4	521	221	64	126	31	1.5	2.3	3.4
6	486	182	66	84	32	1.6	2.8	5.2
12	442	144	67	42	35	1.7	3.6	10.3
C <sub>3</sub> H <sub>2</sub> CCSD(T)/cc-pVDZ $C_s$ Current								
1	808	557	61	473	23	1.0	1.0	1.0
2	830	536	65	444	27	1.0	1.0	1.1
4	806	503	67	410	26	1.0	1.1	1.2
C <sub>3</sub> H <sub>2</sub> CCSD(T)/cc-pVDZ $C_s$ New								
1	1005	693	73	588	32	1.0	1.0	1.0
2	711	407	70	305	32	1.4	1.7	1.9
4	555	256	71	154	31	1.8	2.7	3.8
6	514	208	68	107	33	2.0	3.3	5.5
12	474	157	70	53	34	2.1	4.4	11.1
C <sub>3</sub> H <sub>2</sub> CCSD(T)/cc-pVDZ $C_1$ Current								
1	1153	902	74	800	28	1.0	1.0	1.0
2	972	723	68	629	26	1.2	1.3	1.3
4	1004	702	77	595	30	1.2	1.3	1.3
C <sub>3</sub> H <sub>2</sub> CCSD(T)/cc-pVDZ $C_1$ New								
1	1243	987	76	881	30	1.0	1.0	1.0
2	913	609	82	490	37	1.4	1.6	1.8
4	661	365	79	249	37	1.9	2.7	3.5
6	597	283	77	172	34	2.1	3.5	5.1
12	509	203	78	87	38	2.4	4.9	10.1

Table A.1: Continue

	Timing					Speed Up		
$P$	Over.	ACESII	I	II	III	Over.	ACESII	II
C <sub>3</sub> H <sub>2</sub> CCSD(T)/cc-pVTZ $C_{2v}$ Current								
1	3622	3325	201	3010	114	1.0	1.0	1.0
2	2829	2518	168	2231	119	1.3	1.3	1.4
4	2343	2045	149	1777	119	1.6	1.6	1.7
C <sub>3</sub> H <sub>2</sub> CCSD(T)/cc-pVTZ $C_{2v}$ New								
1	4044	3701	202	3378	121	1.0	1.0	1.0
2	2314	2063	162	1782	119	1.8	1.8	1.9
4	1512	1213	163	922	128	2.7	3.1	3.7
6	1193	890	154	613	123	3.4	4.2	5.5
12	901	592	155	311	126	4.5	6.3	10.9
C <sub>3</sub> H <sub>2</sub> CCSD(T)/cc-pVTZ $C_s$ Current								
1	6220	5971	273	5597	101	1.0	1.0	1.0
2	4514	4275	215	3938	122	1.4	1.4	1.4
4	3608	3305	194	2985	126	1.7	1.8	1.9
C <sub>3</sub> H <sub>2</sub> CCSD(T)/cc-pVTZ $C_s$ New								
1	6581	6279	279	5893	107	1.0	1.0	1.0
2	3859	3550	235	3183	132	1.7	1.8	1.9
4	2222	1925	197	1600	128	3.0	3.3	3.7
6	1713	1411	192	1088	131	3.8	4.5	5.4
12	1162	860	179	550	131	5.7	7.3	10.7
C <sub>3</sub> H <sub>2</sub> CCSD(T)/cc-pVTZ $C_1$ Current								
1	14861	14603	546	13792	265	1.0	1.0	1.0
2	10891	10579	422	9881	276	1.4	1.4	1.4
4	8507	8209	336	7594	279	1.8	1.8	1.8
C <sub>3</sub> H <sub>2</sub> CCSD(T)/cc-pVTZ $C_1$ New								
1	15415	15154	553	14331	270	1.0	1.0	1.0
2	8695	8443	422	7738	283	1.8	1.8	1.9
4	4909	4609	353	3970	286	3.1	3.3	3.6
6	3628	3275	340	2647	288	4.3	4.6	5.4
12	2258	1950	310	1353	287	6.8	7.8	10.6
C <sub>3</sub> H <sub>6</sub> MP2/cc-pVDZ $C_{2v}$ Current								
1	919	661	60	567	34			



Table A.1: Continue

	Timing					Speed Up		
$P$	Over.	ACESII	I	II	III	Over.	ACESII	II
C <sub>3</sub> H <sub>6</sub> MP2/cc-pVDZ $C_{2v}$ New								
1	1308	1008	69	892	47	1.0	1.0	1.0
2	880	577	70	459	48	1.5	1.8	1.9
4	643	346	72	228	46	2.0	2.9	3.9
6	570	275	70	157	48	2.3	3.7	5.7
12	503	196	70	78	48	2.6	5.1	11.4
C <sub>3</sub> H <sub>6</sub> MP2/cc-pVDZ $C_s$ Current								
1	1036	782	63	666	53			
C <sub>3</sub> H <sub>6</sub> MP2/cc-pVDZ $C_s$ New								
1	1367	1109	65	986	58	1.0	1.0	1.0
2	1009	702	73	568	61	1.4	1.6	1.7
4	717	416	71	282	63	1.9	2.7	3.5
6	638	336	77	195	64	2.1	3.3	5.1
12	555	242	77	100	65	2.5	4.6	9.9
C <sub>3</sub> H <sub>6</sub> MP2/cc-pVDZ $C_1$ Current								
1	1381	1120	84	953	83			
C <sub>3</sub> H <sub>6</sub> MP2/cc-pVDZ $C_1$ New								
1	1992	1694	89	1523	82	1.0	1.0	1.0
2	1267	967	86	789	92	1.6	1.8	1.9
4	894	598	88	414	96	2.2	2.8	3.7
6	764	466	89	280	97	2.6	3.6	5.4
12	632	327	88	143	96	3.2	5.2	10.7
C <sub>3</sub> H <sub>6</sub> MP2/cc-pVTZ $C_{2v}$ Current								
1	3074	2826	220	2435	171			
C <sub>3</sub> H <sub>6</sub> MP2/cc-pVTZ $C_{2v}$ New								
1	3918	3650	177	3295	178	1.0	1.0	1.0
2	2715	2408	203	2006	199	1.4	1.5	1.6
4	1747	1440	211	1028	201	2.2	2.5	3.2
6	1416	1109	213	694	202	2.8	3.3	4.8
12	1153	787	221	362	204	3.4	4.6	9.1
C <sub>3</sub> H <sub>6</sub> MP2/cc-pVTZ $C_s$ Current								
1	9090	8781	387	7744	650			

Table A.1: Continue

	Timing					Speed Up		
$P$	Over.	ACESII	I	II	III	Over.	ACESII	II
C <sub>3</sub> H <sub>6</sub> MP2/cc-pVTZ $C_s$ New								
1	13809	13548	417	12467	664	1.0	1.0	1.0
2	8360	8056	451	6735	870	1.7	1.7	1.9
4	5129	4823	464	3494	865	2.7	2.8	3.6
6	3998	3689	454	2364	871	3.5	3.7	5.3
12	2894	2565	466	1227	872	4.8	5.3	10.2
C <sub>3</sub> H <sub>6</sub> MP2/cc-pVTZ $C_1$ Current								
1	19015	18748	1738	16450	560			
C <sub>3</sub> H <sub>6</sub> MP2/cc-pVTZ $C_1$ New								
1	20598	20286	445	19273	568	1.0	1.0	1.0
2	14532	14183	516	13027	640	1.4	1.4	1.5
4	7917	7579	501	6438	640	2.6	2.7	3.0
6	5906	5557	512	4409	636	3.5	3.7	4.4
12	3670	3320	512	2163	645	5.6	6.1	8.9
C <sub>3</sub> H <sub>6</sub> CCSD/cc-pVDZ $C_{2v}$ Current								
1	1349	1077	65	974	38			
C <sub>3</sub> H <sub>6</sub> CCSD/cc-pVDZ $C'_{2v}$ New								
1	1674	1376	71	1263	42	1.0	1.0	1.0
2	1067	759	72	641	46	1.6	1.8	2.0
4	777	470	78	345	47	2.2	2.9	3.7
6	656	356	77	231	48	2.6	3.9	5.5
12	534	240	76	116	48	3.1	5.7	10.9
C <sub>3</sub> H <sub>6</sub> CCSD/cc-pVDZ $C_s$ Current								
1	2111	1809	89	1665	55			
C <sub>3</sub> H <sub>6</sub> CCSD/cc-pVDZ $C_s$ New								
1	2242	1985	80	1855	50	1.0	1.0	1.0
2	1490	1191	89	1040	62	1.5	1.7	1.8
4	1012	707	88	555	64	2.2	2.8	3.3
6	829	527	89	374	64	2.7	3.8	5.0
12	675	346	89	190	67	3.3	5.7	9.8
C <sub>3</sub> H <sub>6</sub> CCSD/cc-pVDZ $C_1$ Current								
1	4288	4033	131	3825	77			

Table A.1: Continue

	Timing					Speed Up		
$P$	Over.	ACESII	I	II	III	Over.	ACESII	II
C <sub>3</sub> H <sub>6</sub> CCSD/cc-pVDZ $C_1$ Current								
1	4974	4643	137	4420	86	1.0	1.0	1.0
2	2923	2620	129	2390	101	1.7	1.8	1.9
4	1762	1460	127	1227	106	2.8	3.2	3.6
6	1345	1044	125	812	107	3.7	4.5	5.4
12	947	641	121	414	106	5.3	7.2	10.7
C <sub>3</sub> H <sub>6</sub> CCSD/cc-pVTZ $C_{2v}$ Current								
1	14665	14359	436	13728	195	1.0	1.0	1.0
2	12768	12472	382	11868	222	1.2	1.2	1.2
4	11015	10714	324	10171	219	1.3	1.3	1.4
C <sub>3</sub> H <sub>6</sub> CCSD/cc-pVTZ $C_{2v}$ New								
1	15504	15200	430	14568	202	1.0	1.0	1.0
2	9164	8854	404	8223	227	1.7	1.7	1.8
4	5059	4746	359	4160	227	3.1	3.2	3.5
6	3675	3367	348	2793	226	4.2	4.5	5.2
12	2772	2399	406	1704	289	5.6	6.3	8.6
C <sub>3</sub> H <sub>6</sub> CCSD(T)/cc-pVDZ $C_{2v}$ Current								
1	2187	1888	86	1774	28	1.0	1.0	1.0
2	1622	1363	65	1273	25	1.4	1.4	1.4
4	1527	1227	72	1127	28	1.4	1.5	1.6
C <sub>3</sub> H <sub>6</sub> CCSD(T)/cc-pVDZ $C_{2v}$ New								
1	2114	1857	70	1760	27	1.0	1.0	1.0
2	1401	1088	75	981	32	1.5	1.7	1.8
4	905	603	69	503	31	2.3	3.1	3.5
6	825	532	78	418	36	2.6	3.5	4.2
12	620	321	78	206	37	3.4	5.8	8.5
C <sub>3</sub> H <sub>6</sub> CCSD(T)/cc-pVDZ $C_s$ Current								
1	3687	3433	102	3280	51	1.0	1.0	1.0
2	2901	2606	94	2455	57	1.3	1.3	1.3
4	2456	2135	96	1981	58	1.5	1.6	1.7

Table A.1: Continue

	Timing					Speed Up		
$P$	Over.	ACESII	I	II	III	Over.	ACESII	II
C <sub>3</sub> H <sub>6</sub> CCSD(T)/cc-pVDZ $C_s$ New								
1	3957	3740	101	3588	51	1.0	1.0	1.0
2	2474	2167	101	2003	63	1.6	1.7	1.8
4	1516	1162	94	1005	63	2.6	3.2	3.6
6	1148	843	97	682	64	3.5	4.4	5.3
12	841	506	93	347	66	4.7	7.4	10.3
C <sub>3</sub> H <sub>6</sub> CCSD(T)/cc-pVDZ $C_1$ Current								
1	16979	16722	257	16409	56	1.0	1.0	1.0
2	11542	11237	205	10967	65	1.5	1.5	1.5
4	7953	7648	165	7418	65	2.1	2.2	2.2
C <sub>3</sub> H <sub>6</sub> CCSD(T)/cc-pVDZ $C_1$ New								
1	17440	17133	271	16795	67	1.0	1.0	1.0
2	9707	9401	205	9128	68	1.8	1.8	1.8
4	5130	4821	167	4583	71	3.4	3.6	3.7
6	3586	3284	157	3056	71	4.9	5.2	5.5
12	2094	1750	142	1537	71	8.3	9.8	10.9
C <sub>6</sub> H <sub>5</sub> OH MP2/cc-pVDZ $C_s$ Current								
1	7155	6849	279	6108	462			
C <sub>6</sub> H <sub>5</sub> OH MP2/cc-pVDZ $C_s$ New								
1	11251	10999	248	10267	484	1.0	1.0	1.0
2	6481	6235	261	5566	408	1.7	1.8	1.8
4	3889	3635	262	2880	493	2.9	3.0	3.6
6	3095	2750	284	1966	500	3.6	4.0	5.2
12	2084	1773	276	991	506	5.4	6.2	10.4
C <sub>6</sub> H <sub>5</sub> OH MP2/cc-pVDZ $C_1$ Current								
1	9938	9635	519	8644	472			
C <sub>6</sub> H <sub>5</sub> OH MP2/cc-pVDZ $C_1$ New								
1	14223	13930	301	13145	484	1.0	1.0	1.0
2	8259	8007	311	7201	495	1.7	1.7	1.8
4	4826	4521	328	3683	510	3.0	3.1	3.6
6	3628	3328	328	2488	512	3.9	4.2	5.3
12	2441	2132	327	1297	508	5.8	6.5	10.1

Table A.1: Continue

	Timing					Speed Up		
$P$	Over.	ACESII	I	II	III	Over.	ACESII	II
C <sub>6</sub> H <sub>5</sub> OH CCSD/cc-pVDZ $C_s$ New								
2	38226	37932	1077	36282	573	2.0	2.0	2.0
4	20049	19728	850	18294	584	3.8	3.9	4.0
6	13971	13652	771	12295	586	5.5	5.6	5.9
9	10256	9902	735	8583	584	7.5	7.7	8.5
12	7818	7481	709	6184	588	9.8	10.1	11.7

# Appendix B

## Benzene Supporting Information

### B.1 Literature Values

Table B.1: Previous experimental effective bond lengths ( $r_0$ ) and electron diffraction ( $r_a$ ) (Å)

			$r_{CC}$	$r_{CH}$
$r_0$	Rotational Raman	Ref. [214]	1.397(1)	1.084(6)
	Spectroscopy	Ref. [117]	1.397(1)	1.084(5)
	Microwave Spectroscopy	Ref. [150]	1.3950	1.0820
	Infrared Spectroscopy	Ref. [37]	1.3964(2)	1.0831(13)
		Ref. [163]	1.3969	1.0815
		Ref. [164]	1.3935(2)	1.0839(3)
	X-Ray Diffraction	Ref. [55]	1.392(4)	
	Neutron Diffraction	Ref. [12]	1.398	1.090
	NMR Crystal	Ref. [9]	1.3971	1.1018
$r_a$	Electron Diffraction	Ref. [201]	1.39(2)	1.08(4)
		Ref. [106]	1.393(5)	1.08(2)
		Ref. [112]	1.397(4)	1.08(2)
		Ref. [19]	1.3979	1.094
		Ref. [218]	1.3971(18)	1.102(11)

Table B.2: Bond distances from previous studies

	Ref.	$r_{CC}$	$r_{CH}$
HF/6-311++G**	[84]	1.397	1.084
HF/cc-pVDZ	[135]	1.3886	1.3827
HF/cc-pVTZ	[135]	1.3827	1.0734
MP2/6-311G**	[84]	1.398	1.086

Table B.2: Cont.

	Ref.	$r_{CC}$	$r_{CH}$
MP2/cc-pVDZ	[135]	1.4057	1.0952
MP2/TZ2P+f	[90]	1.3896	1.0804
CCSD/6-31G	[108]	1.4131	1.0939
CCSD/6-31+G	[108]	1.4151	1.0944
CCSD/6-31++G	[108]	1.4151	1.0945
CCSD/6-311G	[108]	1.4088	1.0899
CCSD/6-311+G	[108]	1.4097	1.0904
CCSD/6-311++G	[108]	1.4097	1.0908
CCSD/cc-pVDZ	[108]	1.4060	1.0959
CCSD/cc-pVTZ'	[34]	1.393	1.082
CCSD(T)/cc-pVDZ	[135]	1.4107	1.0978
CCSD(T)/cc-pVTZ'	[135]	1.3976	1.0840
CCSD(T)/cc-pVTZ	[135]	1.3975	1.0831
CCSD(T)/cc-pVQZ	[79]	1.3911	1.0800
CCSD(T)/ANO1'	[135]	1.3967	1.0834
LDF/STO	[23]	1.388	1.094
LDA/DZP	[91]	1.398	1.099
LDA/TZ2P	[91]	1.386	1.093
LDA/TZ2P+f	[91]	1.386	1.094
BLYP/DZP	[91]	1.422	1.106
BLYP/TZ2P	[91]	1.401	1.088
BLYP/TZ2P+f	[91]	1.401	1.088
B3LYP/DZP	[143]	1.4031	1.0888
B3LYP/TZ2P	[143]	1.3914	1.0818
B3LYP/cc-pVDZ	[134]	1.3986	1.0927
B3LYP/cc-pVTZ	[134]	1.3908	1.0820
B3LYP/cc-pVQZ	[41]	1.3906	1.0815
B3PW91/cc-pVQZ	[41]	1.3886	1.0829
B3P86/cc-pVQZ	[41]	1.3870	1.0820
mPW1PW/cc-pVQZ	[41]	1.3870	1.0820

Table B.3: Fundamental frequencies: Literature ( $\text{cm}^{-1}$ )

$\nu$ <sup>1</sup>	HF/ 4-31G [180]	HF/ DZP [140]	B3LYP/ TZ2P [143] [28]		B97-1/ TZ2P [28]	CCSD(T)/ B97-1 <sup>2</sup> [28]
$\nu_1$	983	1057.1	995	995	992	987
$\nu_2$	3095	3224.8 <sup>3</sup>	3051 <sup>3</sup>	3051	3048	3069
$\nu_3$	1365	1456.4	1351 <sup>3</sup>	1350 <sup>3</sup>	1348	1348
$\nu_4$	701	758.2	708	708	707	698
$\nu_5$	996	1109.4	997	997	987	984
$\nu_6$	607	654.9 <sup>3</sup>	615 <sup>3</sup>	615 <sup>3</sup>	613	607
$\nu_7$	3061	3199.6	3028	3028	3032 <sup>3</sup>	3050
$\nu_8$	1607	1748.5 <sup>3</sup>	1613 <sup>3</sup>	1613 <sup>3</sup>	1611 <sup>3</sup>	1620
$\nu_9$	1183	1272.9	1181	1181	1178	1177
$\nu_{10}$	843	949.5	846	846	841	843
$\nu_{11}$	667	764.2	677	677	672	673
$\nu_{12}$	997	1069.8	1015	1015	1006	1004
$\nu_{13}$	3051	3182.6 <sup>3</sup>	2988 <sup>3</sup>	2988 <sup>3</sup>	3004 <sup>3</sup>	3022
$\nu_{14}$	1297	1347.5	1305	1305	1309	1305
$\nu_{15}$	1162	1171.0	1163	1163	1156	1149
$\nu_{16}$	402	441.0	403	403	400	398
$\nu_{17}$	969	1085.6	972	972	964	962
$\nu_{18}$	1036	1115.1	1038	1038	1045	1046
$\nu_{19}$	1482	1606.8 <sup>3</sup>	1484	1484	1486	1486
$\nu_{20}$	3080	3215.5 <sup>3</sup>	3023 <sup>3</sup>	3023 <sup>3</sup>	3031 <sup>3</sup>	3051

## B.2 Geometry

<sup>1</sup>Numbering based on Wilson's criteria [227].

<sup>2</sup>Formed from the cubic and quartic force constants of B97-1/TZ2P and CCSD(T)/ANO1's harmonic frequencies.

<sup>3</sup>Terms effect by Fermi resonance. See each reference for how terms were adjusted.



Table B.4: Bond distances  $r_e$  for other levels of theory (Å)

	SCF/		MP2/		CCSD/	
	$r_{CC}$	$r_{CH}$	$r_{CC}$	$r_{CH}$	$r_{CC}$	$r_{CH}$
ANO0(fc)	1.3825	1.0732	1.3977	1.0868	1.4007	1.0879
ANO1(fc)	1.3853	1.0758	1.3843	1.0769	1.3914	1.0810
cc-pVDZ(ae)	1.3886	1.0822	1.4046	1.0942	1.4049	1.0949
cc-pVTZ(ae)	1.3827	1.0734	1.3880	1.0766	1.3868	1.0758

Table B.5: Bond distances  $r_g$  and  $r_z$  for other levels of theory (Å)

	$r_g$		$r_z$	
	$r_{CC}$	$r_{CH}$	$r_{CC}$	$r_{CH}$
SCF/cc-pVDZ	1.3957	1.1015	1.3935	1.0866
SCF/cc-pVTZ	1.3898	1.0927	1.3875	1.0778
SCF/ANO0	1.3925	1.0951	1.3903	1.0802
SCF/ANO1	1.3895	1.0925	1.3873	1.0776
MP2/cc-pVDZ(ae)	1.4124	1.1145	1.4099	1.0983
MP2/cc-pVTZ(ae)	1.3920	1.0971	1.3897	1.0809
MP2/ANO0(fc)	1.4057	1.1071	1.4033	1.0910
MP2/ANO1(fc)	1.3920	1.0971	1.3897	1.0809

### B.3 Harmonic Frequencies

Table B.6: Harmonic frequencies for SCF level of theory ( $\text{cm}^{-1}$ )

$\omega^1$	SCF/			
	cc-pVDZ	cc-pVTZ	ANO0	ANO1
$\omega_1$	1081.1	1072.7	1077.0	1072.1
$\omega_2$	3371.0	3347.8	3378.0	3352.1
$\omega_3$	1477.6	1498.2	1490.9	1498.7
$\omega_4$	771.2	776.0	773.4	779.0
$\omega_5$	1116.9	1127.4	1126.9	1135.9

Table B.6: Cont.

$\omega^1$	SCF/			
	cc-pVDZ	cc-pVTZ	ANO0	ANO1
$\omega_6$	660.9	663.0	661.2	664.1
$\omega_7$	3339.7	3316.9	3347.5	3322.1
$\omega_8$	1787.8	1775.0	1784.4	1776.4
$\omega_9$	1273.2	1281.8	1282.1	1282.2
$\omega_{10}$	948.8	956.1	953.8	959.6
$\omega_{11}$	752.8	758.8	756.3	760.6
$\omega_{12}$	1085.8	1095.4	1090.0	1097.0
$\omega_{13}$	3328.0	3305.1	3335.5	3310.6
$\omega_{14}$	1341.6	1336.9	1341.7	1337.9
$\omega_{15}$	1188.7	1171.3	1190.2	1171.9
$\omega_{16}$	449.7	451.6	450.5	452.1
$\omega_{17}$	1090.3	1100.2	1100.2	1109.2
$\omega_{18}$	1131.0	1129.7	1132.1	1129.2
$\omega_{19}$	1627.3	1635.1	1632.8	1635.1
$\omega_{20}$	3359.0	3336.1	3366.6	3340.6

Table B.7: Harmonic frequencies for MP2 level of theory ( $\text{cm}^{-1}$ )

$\omega^1$	MP2/			
	cc-pVDZ(ae)	cc-pVTZ(ae)	ANO0(ae)	ANO1(ae)
$\omega_1$	1019.0	1023.5	1016.1	1029.3
$\omega_2$	3252.6	3256.0	3253.8	3254.7
$\omega_3$	1358.8	1378.4	1371.3	1376.8
$\omega_4$	637.6	721.2	723.0	747.0
$\omega_5$	966.3	1001.4	1019.2	1037.6
$\omega_6$	606.3	610.8	612.9	615.4
$\omega_7$	3226.1	3219.0	3228.3	3220.6
$\omega_8$	1652.7	1651.7	1647.4	1646.1
$\omega_9$	1191.9	1212.6	1202.2	1200.2

<sup>1</sup>Wilson numbering [227]

Table B.7: Cont.

$\omega^1$	MP2/			
	cc-pVDZ(ae)	cc-pVTZ(ae)	ANO0(ae)	ANO1(ae)
$\omega_{10}$	861.8	878.2	875.2	885.2
$\omega_{11}$	688.3	707.9	696.9	704.9
$\omega_{12}$	1007.3	1024.2	1030.5	1036.5
$\omega_{13}$	3214.8	3201.0	3217.8	3209.5
$\omega_{14}$	1476.5	1472.2	1478.3	1473.4
$\omega_{15}$	1164.3	1191.3	1175.5	1168.0
$\omega_{16}$	402.0	412.3	413.7	419.7
$\omega_{17}$	957.7	984.7	992.1	1008.5
$\omega_{18}$	1062.7	1070.8	1065.1	1070.1
$\omega_{19}$	1506.6	1518.3	1505.8	1514.5
$\omega_{20}$	3242.6	3241.2	3244.2	3239.0

Table B.8: Harmonic Frequencies for CCSD level of theory ( $\text{cm}^{-1}$ )

$\omega^1$	CCSD/			
	cc-pVDZ(ae)	cc-pVTZ(ae)	ANO0(fc)	ANO1(fc)
$\omega_1$	1024.9	1034.4	1018.0	1023.6
$\omega_2$	3240.5	3253.1	3244.3	3237.2
$\omega_3$	1371.6	1399.4	1383.1	1394.6
$\omega_4$	657.6	732.0	706.4	724.3
$\omega_5$	982.6	1028.3	1013.2	1034.1
$\omega_6$	612.6	621.3	615.2	620.8
$\omega_7$	3211.8	3212.6	3216.8	3210.3
$\omega_8$	1674.9	1683.2	1666.9	1671.3
$\omega_9$	1196.5	1224.5	1205.1	1208.3
$\omega_{10}$	870.7	894.3	874.7	884.6
$\omega_{11}$	693.6	719.3	695.0	701.6
$\omega_{12}$	1008.3	1031.6	1022.1	1033.0
$\omega_{13}$	3200.8	3194.0	3206.3	3200.2

<sup>1</sup>Wilson numbering [227]

Table B.8: Cont.

$\omega^1$	CCSD/			
	cc-pVDZ(ae)	cc-pVTZ(ae)	ANO0(fc)	ANO1(fc)
$\omega_{14}$	1322.7	1328.2	1313.4	1306.7
$\omega_{15}$	1158.9	1185.4	1166.1	1164.8
$\omega_{16}$	405.8	419.5	410.7	415.7
$\omega_{17}$	977.4	1012.8	992.7	1010.1
$\omega_{18}$	1067.1	1080.9	1067.4	1072.0
$\omega_{19}$	1523.4	1543.7	1522.9	1531.3
$\omega_{20}$	3229.4	3236.6	3233.9	3226.8

Table B.9: CCSD(T) Harmonic Frequencies for Other Basis Sets ( $\text{cm}^{-1}$ )

$\omega^1$	CCSD(T)/			
	cc-pVDZ(fc)	cc-pVTZ(fc)	cc-pVDZ(ae)	ANO0(fc)
$\omega_1$	1003.9	1004.5	1005.8	997.8
$\omega_2$	3212.1	3209.1	3217.8	3220.1
$\omega_3$	1353.6	1370.2	1353.8	1364.4
$\omega_4$	624.9	674.7	628.6	689.5
$\omega_5$	947.5	966.7	952.1	986.4
$\omega_6$	602.8	607.1	603.5	605.6
$\omega_7$	3183.8	3180.7	3189.3	3192.8
$\omega_8$	1640.5	1637.2	1643.4	1633.6
$\omega_9$	1181.0	1190.6	1182.3	1189.7
$\omega_{10}$	847.2	856.4	850.2	854.4
$\omega_{11}$	676.7	685.3	679.0	680.1
$\omega_{12}$	994.6	1010.3	995.0	1009.2
$\omega_{13}$	3172.9	3169.4	3178.4	3182.3
$\omega_{14}$	1340.4	1328.2	1344.5	1333.0
$\omega_{15}$	1151.5	1158.9	1153.0	1160.3
$\omega_{16}$	394.6	401.3	395.8	401.4
$\omega_{17}$	943.7	959.1	947.9	965.9

<sup>1</sup>Wilson numbering [227]

Table B.9: Cont.

$\omega^1$	CCSD(T)/			
	cc-pVDZ(fc)	cc-pVTZ(fc)	cc-pVDZ(ae)	ANO0(fc)
$\omega_{18}$	1050.0	1054.4	1051.4	1050.4
$\omega_{19}$	1499.9	1506.9	1501.6	1499.6
$\omega_{20}$	3201.2	3198.3	3206.9	3209.9

## B.4 Fundamental Frequencies

Table B.10: VPT2 Fundamental Frequencies for SCF level of theory ( $\text{cm}^{-1}$ )

$\nu$	SCF/			
	cc-pVDZ	cc-pVTZ	ANO0	ANO1
$\nu_1$	1066.4	1058.2	1062.3	1057.7
$\nu_2$	3248.3	3237.1	3257.3	3239.6
$\nu_3$	1450.5	1470.6	1463.4	1470.6
$\nu_4$	758.9	771.3	761.7	767.1
$\nu_5$	1092.5	1122.0	1103.9	1113.5
$\nu_6$	655.8	658.2	656.3	659.2
$\nu_7$	3235.8	3236.1	3246.4	3237.0
$\nu_8$	1751.2	1738.9	1748.0	1740.5
$\nu_9$	1260.8	1268.6	1268.9	1269.4
$\nu_{10}$	931.4	941.5	936.7	942.5
$\nu_{11}$	742.7	749.8	746.1	750.5
$\nu_{12}$	1072.1	1082.0	1075.8	1082.7
$\nu_{13}$	3178.9	3165.9	3185.2	3168.4
$\nu_{14}$	1308.3	1310.8	1311.4	1312.2
$\nu_{15}$	1175.6	1156.7	1175.3	1157.5
$\nu_{16}$	441.2	444.2	442.1	443.7
$\nu_{17}$	1069.5	1091.5	1078.7	1087.8
$\nu_{18}$	1113.7	1111.9	1114.1	1111.7
$\nu_{19}$	1600.9	1608.1	1606.3	1608.7
$\nu_{20}$	3227.4	3215.9	3234.4	3218.3

Table B.11: Dressed VPT2 Fundamental Frequencies for SCF level of theory ( $\text{cm}^{-1}$ )

$\nu$	SCF/			
	cc-pVDZ	cc-pVTZ	ANO0	ANO1
$\nu_2$	3258.2	3251.0	3267.8	3253.8
$\nu_7$	3244.9	3242.1	3255.2	3244.3
$\nu_8$	1752.1	1740.1	1748.9	1741.7
$\nu_{13}$	3187.9	3172.3	3195.5	3175.5
$\nu_{20}$	3234.6	3220.3	3243.2	3223.2

Table B.12: VPT2 Fundamental Frequencies for MP2 level of theory ( $\text{cm}^{-1}$ )

$\nu$	MP2/			
	cc-pVDZ(ae)	cc-pVTZ(ae)	ANO0(ae)	ANO1(ae)
$\nu_1$	1003.3	1009.0	1000.2	1014.3
$\nu_2$	3106.7	3112.1	3107.3	3109.0
$\nu_3$	1208.1	1354.1	1342.0	1351.8
$\nu_4$	724.0	733.1	709.2	732.0
$\nu_5$	984.6	1031.4	989.2	1014.3
$\nu_6$	601.3	606.8	606.4	610.6
$\nu_7$	3097.0	3100.6	3101.3	3099.6
$\nu_8$	1615.2	1616.7	1610.8	1672.1
$\nu_9$	1177.2	1189.2	1186.7	1188.3
$\nu_{10}$	848.5	863.1	856.2	869.4
$\nu_{11}$	679.3	691.1	684.1	694.6
$\nu_{12}$	1002.5	1022.1	1015.3	1023.6
$\nu_{13}$	3109.4	3137.0	3110.6	3113.0
$\nu_{14}$	1435.1	1430.6	1434.5	1431.9
$\nu_{15}$	1151.3	1165.3	1162.0	1159.9
$\nu_{16}$	398.9	405.9	404.6	410.1
$\nu_{17}$	956.0	988.8	966.7	988.0
$\nu_{18}$	1054.3	1049.7	1045.2	1052.8
$\nu_{19}$	1477.1	1490.4	1478.3	1489.7
$\nu_{20}$	3126.1	3133.2	3130.1	3131.6

Table B.13: Dressed VPT2 Fundamental Frequencies for MP2 level of theory ( $\text{cm}^{-1}$ )

$\nu$	MP2/			
	cc-pVDZ(ae)	cc-pVTZ(ae)	ANO0(ae)	ANO1(ae)
$\nu_2$	3109.7	3116.0	3110.7	3113.1
$\nu_3$	1332.5			
$\nu_8$	1618.1	1604.4	1615.1	1605.7
$\nu_{13}$	3038.5	3044.9	3038.3	3046.0
$\nu_{18}$	1044.5			
$\nu_{20}$	3067.5	3078.5	3064.9	3140.3

Table B.14: VPT2 Fundamental Frequencies for CCSD(T) level of theory ( $\text{cm}^{-1}$ )

Sym.		CCSD(T)/		
		cc-pVDZ(ae)	cc-pVTZ(ae)	ANO0(fc)
$a_{1g}$	$\nu_1$	989.0	999.2	980.9
	$\nu_2$	3067.9	3081.2	3068.1
$a_{2g}$	$\nu_3$	1345.3	1351.5	1295.8
$b_{2g}$	$\nu_4$	697.0	717.6	681.1
	$\nu_5$	966.4	1021.0	966.6
$e_{2g}$	$\nu_6$	598.4	606.8	599.6
	$\nu_7$	3054.7	3064.5	3059.0
	$\nu_8$	1604.3	1612.2	1593.4
	$\nu_9$	1167.1	1183.8	1172.8
$e_{1g}$	$\nu_{10}$	840.7	860.3	837.6
$a_{1u}$	$\nu_{11}$	669.0	685.4	669.0
$b_{1u}$	$\nu_{12}$	988.9	1014.4	995.2
	$\nu_{13}$	3086.8	3795.8	3076.7
$b_{2u}$	$\nu_{14}$	1319.2	1323.5	1309.1
	$\nu_{15}$	1139.6	1154.4	1145.8
$e_{2u}$	$\nu_{16}$	397.0	402.3	398.1
	$\nu_{17}$	945.4	982.5	946.4
$e_{1u}$	$\nu_{18}$	1040.2	1040.9	1028.1
	$\nu_{19}$	1470.2	1489.2	1470.1
	$\nu_{20}$	3084.7	3101.4	3087.9

Table B.15: Dressed VPT2 Fundamental Frequencies for CCSD(T) level of theory ( $\text{cm}^{-1}$ )

$\nu$	CCSD(T)/		
	cc-pVDZ(ae)	cc-pVTZ(ae)	ANO0(fc)
$\nu_2$	3071.7	3086.3	3072.3
$\nu_3$	1324.0	1356.6	1350.0
$\nu_8$	1606.1	1616.1	1595.7
$\nu_{13}$	3005.6	3018.3	3004.1
$\nu_{18}$	1031.1		
$\nu_{20}$	3040.5	3060.0	3035.4

## B.5 Two Quantum Transitions

Table B.16: CCSD(T) two quantum transitions: VPT2 ( $\text{cm}^{-1}$ )

	CCSD(T)/ ANO0(fc)	CCSD(T)/ ANO1(fc)
$6_1(a_g)16_1(b_{1u}), 6_1(b_{1g})16_1(a_u)$	992.8	1001.7
$4_116_1(a_u), 4_116_1(b_{1u})$	1078.6	1096.9
$10_1(b_{2g})16_1(b_{1u}), 10_1(b_{3g})16_1(a_u)$	1222.9	1234.7
$10_1(b_{2g})16_1(a_u), 10_1(b_{3g})16_1(b_{1u})$	1229.8	1243.7
$5_116_1(a_u), 5_116_1(b_{1u})$	1358.1	1381.7
$10_1(b_{2g})11_1, 10_1(b_{3g})11_1$	1505.5	1522.3
$6_1(a_g)17_1(b_{1u}), 6_1(b_{1g})17_1(a_u)$	1545.7	1567.8
$9_1(a_g)16_1(b_{1u}), 9_1(b_{1g})16_1(a_u)$	1566.1	1572.9
$6_1(a_g)12_1, 6_1(b_{1g})12_1$	1594.6	1609.5
$6_1(a_g)18_1(b_{3u}), 6_1(b_{1g})18_1(b_{2u})$	1627.0	1637.8
$6_1(a_g)18_1(b_{2u}), 6_1(b_{1g})18_1(b_{3u})$	1627.7	1638.5
$1_111_1$	1649.4	1662.4
$4_117_1(a_u), 4_117_1(b_{1u})$	1627.8	1660.3
$4_112_1$	1675.9	1701.9
$6_1(a_g)15_1, 6_1(b_{1g})15_1$	1745.5	1750.3
$10_1(b_{2g})17_1(a_u), 10_1(b_{3g})17_1(b_{1u})$	1780.7	1807.8
$10_1(b_{2g})17_1(b_{1u}), 10_1(b_{3g})17_1(a_u)$	1783.1	1810.1
$10_1(b_{2g})18_1(b_{3u}), 10_1(b_{3g})18_1(b_{2u})$	1864.8	1880.6



Table B.16: Cont.

	CCSD(T)/ ANO0(fc)	CCSD(T)/ ANO1(fc)
$6_1(a_g)14_1, 6_1(b_{1g})14_1$	1906.1	1909.5
$5_117_1(a_u), 5_117_1(b_{1u})$	1912.3	1948.8
$5_112_1$	1961.4	1991.3
$8_1(a_g)16_1(b_{1u}), 8_1(b_{1g})16_1(a_u)$ <sup>1</sup>	1968.7	1981.0
$1_118_1(b_{2u})$	2007.8	2019.9
$6_1(a_g)19_1(b_{3u}), 6_1(b_{1g})19_1(b_{2u})$	2068.1	2079.7
$6_1(a_g)19_1(b_{2u}), 6_1(b_{1g})19_1(b_{3u})$	2068.8	2080.3
$9_1(a_g)17_1(b_{1u}), 9_1(b_{1g})17_1(a_u)$	2119.2	2139.0
$9_1(a_g)12_1, 9_1(b_{1g})12_1$	2167.6	2180.3
$9_1(a_g)18_1(b_{3u}), 9_1(b_{1g})18_1(b_{2u})$	2198.7	2207.3
$9_1(a_g)18_1(b_{2u}), 9_1(b_{1g})18_1(b_{3u})$	2201.5	2210.1
$9_1(a_g)15_1, 9_1(b_{1g})15_1$	2320.6	2323.4
$10_1(b_{2g})19_1(b_{3u}), 10_1(b_{3g})19_1(b_{2u})$	2306.6	2323.2
$3_118_1(b_{3u}), 3_118_1(b_{2u})$	2322.8	2373.1
$1_119_1(b_{2u}), 1_119_1(b_{3u})$	2448.9	2461.8
$9_1(a_g)14_1, 9_1(b_{1g})14_1$	2479.5	2480.7
$8_1(a_g)17_1(b_{1u}), 8_1(b_{1g})17_1(a_u)$ <sup>2</sup>	2520.3	2546.4
$8_1(a_g)12_1, 8_1(b_{1g})12_1$ <sup>3</sup>	2588.3	2604.8
$8_1(a_g)18_1(b_{2u}), 8_1(b_{1g})18_1(b_{3u})$ <sup>4</sup>	2618.5	2613.6
$8_1(a_g)18_1(b_{3u}), 8_1(b_{1g})18_1(b_{2u})$ <sup>5</sup>	2618.5	2613.7
$9_1(a_g)19_1(b_{3u}), 9_1(b_{1g})19_1(b_{2u})$	2638.5	2647.6
$9_1(a_g)19_1(b_{2u}), 9_1(b_{1g})19_1(b_{3u})$	2643.1	2652.3
$8_1(a_g)15_1, 8_1(b_{1g})15_1$ <sup>6</sup>	2739.0	2745.3
$3_119_1(b_{3u}), 3_119_1(b_{2u})$	2761.6	2812.4
$8_1(a_g)14_1, 8_1(b_{1g})14_1$ <sup>7</sup>	2893.6	2898.9

<sup>1</sup>Treated for Fermi resonance of  $1_16_1(a_g)$  with  $8_1(a_g)$  and  $1_16_1(b_{1g})$  with  $8_1(b_{1g})$ .

<sup>2</sup>Treated for Fermi resonance of  $1_16_1(a_g)$  with  $8_1(a_g)$  and  $1_16_1(b_{1g})$  with  $8_1(b_{1g})$ .

<sup>3</sup>Treated for Fermi resonance of  $1_16_1(a_g)$  with  $8_1(a_g)$  and  $1_16_1(b_{1g})$  with  $8_1(b_{1g})$ .

<sup>4</sup>Treated for Fermi resonance of  $1_16_1(a_g)$  with  $8_1(a_g)$  and  $1_16_1(b_{1g})$  with  $8_1(b_{1g})$ .

<sup>5</sup>Treated for Fermi resonance of  $1_16_1(a_g)$  with  $8_1(a_g)$  and  $1_16_1(b_{1g})$  with  $8_1(b_{1g})$ .

<sup>6</sup>Treated for Fermi resonance of  $1_16_1(a_g)$  with  $8_1(a_g)$  and  $1_16_1(b_{1g})$  with  $8_1(b_{1g})$ .

<sup>7</sup>Treated for Fermi resonance of  $1_16_1(a_g)$  with  $8_1(a_g)$  and  $1_16_1(b_{1g})$  with  $8_1(b_{1g})$ .

Table B.16: Cont.

	CCSD(T)/ ANO0(fc)	CCSD(T)/ ANO1(fc)
$8_1(a_g)19_1(b_{2u}), 8_1(b_{1g})19_1(b_{3u})$ <sup>8</sup>	3061.9	3074.9
$8_1(a_g)19_1(b_{3u}), 8_1(b_{1g})19_1(b_{2u})$ <sup>9</sup>	3093.9	3065.2
$7_1(a_g)16_1(b_{1u}), 7_1(b_{1g})16_1(a_u)$	3451.9	3451.9
$6_1(a_g)13_1, 6_1(b_{1g})13_1$ <sup>10</sup>	3601.2	3607.2
$6_1(a_g)20_1(b_{2u}), 6_1(b_{1g})20_1(b_{3u})$ <sup>11</sup>	3661.0	3659.9
$6_1(a_g)20_1(b_{3u}), 6_1(b_{1g})20_1(b_{2u})$ <sup>12</sup>	3650.7	3657.4
$2_111_1$ <sup>13</sup>	3739.0	3743.8
$4_113_1$ <sup>14</sup>	3683.1	3700.0
$10_1(b_{2g})20_1(b_{3u}), 10_1(b_{3g})20_1(b_{2u})$ <sup>15</sup>	3882.6	3888.8
$7_1(a_g)17_1(b_{1u}), 7_1(b_{1g})17_1(a_u)$	4000.4	4013.6
$7_1(a_g)12_1, 7_1(b_{1g})12_1$	4053.0	4059.1
$1_120_1(b_{2u}), 1_120_1(b_{3u})$ <sup>16</sup>	4029.6	4035.5
$7_1(a_g)18_1(b_{2u}), 7_1(b_{1g})18_1(b_{3u})$	4084.5	4086.4
$7_1(a_g)18_1(b_{3u}), 7_1(b_{1g})18_1(b_{2u})$	4085.9	4087.8
$2_118_1(b_{2u}), 2_118_1(b_{3u})$ <sup>17</sup>	4098.4	4102.3

<sup>8</sup>Treated for Fermi resonance of  $1_16_1(a_g)$  with  $8_1(a_g)$  and  $1_16_1(b_{1g})$  with  $8_1(b_{1g})$ .

<sup>9</sup>Treated for Fermi resonance of  $1_16_1(a_g)$  with  $8_1(a_g)$  and  $1_16_1(b_{1g})$  with  $8_1(b_{1g})$ .

<sup>10</sup>Treated for Fermi resonance of  $20_1(b_{3u}), 8_1(a_g)19_1(b_{3u}), 8_1(b_{1g})19_1(b_{2u}), 1_16_1(a_g)19_1(b_{3u})$  and  $1_16_1(b_{1g})19_1(b_{2u})$  with  $13_1$ .

<sup>11</sup>Treated for Fermi resonance of  $8_1(a_g)19_1(b_{2u}), 8_1(b_{1g})19_1(b_{3u}), 1_16_1(a_g)19_1(b_{2u})$  and  $1_16_1(b_{1g})19_1(b_{3u})$  with  $20_1(b_{2u})$ , and  $13_1, 8_1(a_g)19_1(b_{3u}), 8_1(b_{1g})19_1(b_{2u}), 1_16_1(a_g)19_1(b_{3u})$  and  $1_16_1(b_{1g})19_1(b_{2u})$  with  $20_1(b_{3u})$

<sup>12</sup>Treated for Fermi resonance of  $8_1(a_g)19_1(b_{2u}), 8_1(b_{1g})19_1(b_{3u}), 1_16_1(a_g)19_1(b_{2u})$  and  $1_16_1(b_{1g})19_1(b_{3u})$  with  $20_1(b_{2u})$ , and  $13_1, 8_1(a_g)19_1(b_{3u}), 8_1(b_{1g})19_1(b_{2u}), 1_16_1(a_g)19_1(b_{3u})$  and  $1_16_1(b_{1g})19_1(b_{2u})$  with  $20_1(b_{3u})$

<sup>13</sup>Treated for Fermi resonance of  $2_1, 19_2(b_{2u})$  and  $19_2(b_{3u})$ .

<sup>14</sup>Treated for Fermi resonance of  $20_1(b_{3u}), 8_1(a_g)19_1(b_{3u}), 8_1(b_{1g})19_1(b_{2u}), 1_16_1(a_g)19_1(b_{3u})$  and  $1_16_1(b_{1g})19_1(b_{2u})$  with  $13_1$ .

<sup>15</sup>Treated for Fermi resonance of  $8_1(a_g)19_1(b_{2u}), 8_1(b_{1g})19_1(b_{3u}), 1_16_1(a_g)19_1(b_{2u})$  and  $1_16_1(b_{1g})19_1(b_{3u})$  with  $20_1(b_{2u})$ , and  $13_1, 8_1(a_g)19_1(b_{3u}), 8_1(b_{1g})19_1(b_{2u}), 1_16_1(a_g)19_1(b_{3u})$  and  $1_16_1(b_{1g})19_1(b_{2u})$  with  $20_1(b_{3u})$

<sup>16</sup>Treated for Fermi resonance of  $8_1(a_g)19_1(b_{2u}), 8_1(b_{1g})19_1(b_{3u}), 1_16_1(a_g)19_1(b_{2u})$  and  $1_16_1(b_{1g})19_1(b_{3u})$  with  $20_1(b_{2u})$ , and  $13_1, 8_1(a_g)19_1(b_{3u}), 8_1(b_{1g})19_1(b_{2u}), 1_16_1(a_g)19_1(b_{3u})$  and  $1_16_1(b_{1g})19_1(b_{2u})$  with  $20_1(b_{3u})$

<sup>17</sup>Treated for Fermi resonance of  $2_1, 19_2(b_{2u}), 19_1(b_{2u})19_1(b_{3u})$ , and  $19_2(b_{3u})$ .

Table B.16: Cont.

	CCSD(T)/ ANO0(fc)	CCSD(T)/ ANO1(fc)
$5_1 13_1$ <sup>18</sup>	3967.4	3988.0
$9_1(a_g)13_1, 9_1(b_{1g})13_1$ <sup>19</sup>	4219.9	4227.7
$9_1(a_g)20_1(b_{3u}), 9_1(b_{1g})20_1(b_{2u})$ <sup>20</sup>	4199.2	4207.8
$9_1(a_g)20_1(b_{2u}), 9_1(b_{1g})20_1(b_{3u})$ <sup>21</sup>	4197.6	4206.3
$7_1(a_g)14_1, 7_1(b_{1g})14_1$	4370.0	4364.6
$3_1 20_1(b_{2u})$ <sup>22</sup>	4388.4	4397.1
$3_1 20_1(b_{3u})$ <sup>23</sup>	4388.8	4399.9
$7_1(a_g)19_1(b_{3u}), 7_1(b_{1g})19_1(b_{2u})$	4529.3	4532.5
$7_1(a_g)19_1(b_{2u}), 7_1(b_{1g})19_1(b_{3u})$	4530.2	4533.5
$2_1 19_1(b_{2u}), 2_1 19_1(b_{3u})$ <sup>24</sup>	4545.8	4551.3
$8_1(a_g)13_1, 8_1(b_{1g})13_1$ <sup>25</sup>	4603.5	4601.4
$8_1(a_g)20_1(b_{3u}), 8_1(b_{1g})20_1(b_{2u})$ <sup>26</sup>	4675.0	4686.8

<sup>18</sup>Treated for Fermi resonance of  $20_1(b_{3u}), 8_1(a_g)19_1(b_{3u}), 8_1(b_{1g})19_1(b_{2u}), 1_1 6_1(a_g)19_1(b_{3u})$  and  $1_1 6_1(b_{1g})19_1(b_{2u})$  with  $13_1$ .

<sup>19</sup>Treated for Fermi resonance of  $20_1(b_{3u}), 8_1(a_g)19_1(b_{3u}), 8_1(b_{1g})19_1(b_{2u}), 1_1 6_1(a_g)19_1(b_{3u})$  and  $1_1 6_1(b_{1g})19_1(b_{2u})$  with  $13_1$ .

<sup>20</sup>Treated for Fermi resonance of  $8_1(a_g)19_1(b_{2u}), 8_1(b_{1g})19_1(b_{3u}), 1_1 6_1(a_g)19_1(b_{2u})$  and  $1_1 6_1(b_{1g})19_1(b_{3u})$  with  $20_1(b_{2u})$ , and  $13_1, 8_1(a_g)19_1(b_{3u}), 8_1(b_{1g})19_1(b_{2u}), 1_1 6_1(a_g)19_1(b_{3u})$  and  $1_1 6_1(b_{1g})19_1(b_{2u})$  with  $20_1(b_{3u})$

<sup>21</sup>Treated for Fermi resonance of  $8_1(a_g)19_1(b_{2u}), 8_1(b_{1g})19_1(b_{3u}), 1_1 6_1(a_g)19_1(b_{2u})$  and  $1_1 6_1(b_{1g})19_1(b_{3u})$  with  $20_1(b_{2u})$ , and  $13_1, 8_1(a_g)19_1(b_{3u}), 8_1(b_{1g})19_1(b_{2u}), 1_1 6_1(a_g)19_1(b_{3u})$  and  $1_1 6_1(b_{1g})19_1(b_{2u})$  with  $20_1(b_{3u})$

<sup>22</sup>Treated for Fermi resonance of  $8_1(a_g)19_1(b_{2u}), 8_1(b_{1g})19_1(b_{3u}), 1_1 6_1(a_g)19_1(b_{2u})$  and  $1_1 6_1(b_{1g})19_1(b_{3u})$  with  $20_1(b_{2u})$ , and  $13_1, 8_1(a_g)19_1(b_{3u}), 8_1(b_{1g})19_1(b_{2u}), 1_1 6_1(a_g)19_1(b_{3u})$  and  $1_1 6_1(b_{1g})19_1(b_{2u})$  with  $20_1(b_{3u})$

<sup>23</sup>Treated for Fermi resonance of  $8_1(a_g)19_1(b_{2u}), 8_1(b_{1g})19_1(b_{3u}), 1_1 6_1(a_g)19_1(b_{2u})$  and  $1_1 6_1(b_{1g})19_1(b_{3u})$  with  $20_1(b_{2u})$ , and  $13_1, 8_1(a_g)19_1(b_{3u}), 8_1(b_{1g})19_1(b_{2u}), 1_1 6_1(a_g)19_1(b_{3u})$  and  $1_1 6_1(b_{1g})19_1(b_{2u})$  with  $20_1(b_{3u})$

<sup>24</sup>Treated for Fermi resonance of  $2_1, 19_2(b_{2u}), 19_1(b_{2u})19_1(b_{3u})$ , and  $19_2(b_{3u})$ .

<sup>25</sup>Treated for Fermi resonance of  $20_1(b_{3u}), 8_1(a_g)19_1(b_{3u}), 8_1(b_{1g})19_1(b_{2u}), 1_1 6_1(a_g)19_1(b_{3u})$  and  $1_1 6_1(b_{1g})19_1(b_{2u})$  with  $13_1$ .

<sup>26</sup>Treated for Fermi resonance of  $8_1(a_g)19_1(b_{2u}), 8_1(b_{1g})19_1(b_{3u}), 1_1 6_1(a_g)19_1(b_{2u})$  and  $1_1 6_1(b_{1g})19_1(b_{3u})$  with  $20_1(b_{2u})$ , and  $13_1, 8_1(a_g)19_1(b_{3u}), 8_1(b_{1g})19_1(b_{2u}), 1_1 6_1(a_g)19_1(b_{3u})$  and  $1_1 6_1(b_{1g})19_1(b_{2u})$  with  $20_1(b_{3u})$

Table B.16: Cont.

	CCSD(T)/ ANO0(fc)	CCSD(T)/ ANO1(fc)
$8_1(a_g)20_1(b_{2u}), 8_1(b_{1g})20_1(b_{3u})$ <sup>27</sup>	4674.8	4688.5
$2_120_1(b_{2u}), 2_120_1(b_{3u})$ <sup>28</sup>	5937.6	5947.1
$7_1(a_g)13_1, 7_1(b_{1g})13_1$ <sup>29</sup>	5996.3	5996.0
$7_1(a_g)20_1(b_{3u}), 7_1(b_{1g})20_1(b_{2u})$ <sup>30</sup>	6128.4	6124.2
$7_1(a_g)20_1(b_{2u}), 7_1(b_{1g})20_1(b_{3u})$ <sup>31</sup>	6130.0	6127.1

<sup>27</sup>Treated for Fermi resonance of  $8_1(a_g)19_1(b_{2u}), 8_1(b_{1g})19_1(b_{3u}), 1_16_1(a_g)19_1(b_{2u})$  and  $1_16_1(b_{1g})19_1(b_{3u})$  with  $20_1(b_{2u})$ , and  $13_1, 8_1(a_g)19_1(b_{3u}), 8_1(b_{1g})19_1(b_{2u}), 1_16_1(a_g)19_1(b_{3u})$  and  $1_16_1(b_{1g})19_1(b_{2u})$  with  $20_1(b_{3u})$

<sup>28</sup>Treated for Fermi resonance of  $2_1$  with  $19_2(b_{2u}), 19_2(b_{3u}),$  and  $19_1(b_{2u})19_1(b_{3u}), 20_1(b_{2u})$  with  $8_1(a_g)19_1(b_{2u}), 8_1(b_{1g})19_1(b_{3u}), 1_16_1(a_g)19_1(b_{2u})$  and  $1_16_1(b_{1g})19_1(b_{3u}),$  and  $13_1$  and  $20_1(b_{2u})$  with  $8_1(a_g)19_1(b_{3u}), 8_1(b_{1g})19_1(b_{2u}), 1_16_1(a_g)19_1(b_{3u})$  and  $1_16_1(b_{1g})19_1(b_{2u}).$

<sup>29</sup>Treated for Fermi resonance of  $2_1$  with  $19_2(b_{2u}), 19_2(b_{3u}),$  and  $19_1(b_{2u})19_1(b_{3u}), 20_1(b_{2u})$  with  $8_1(a_g)19_1(b_{2u}), 8_1(b_{1g})19_1(b_{3u}), 1_16_1(a_g)19_1(b_{2u})$  and  $1_16_1(b_{1g})19_1(b_{3u}),$  and  $13_1$  and  $20_1(b_{2u})$  with  $8_1(a_g)19_1(b_{3u}), 8_1(b_{1g})19_1(b_{2u}), 1_16_1(a_g)19_1(b_{3u})$  and  $1_16_1(b_{1g})19_1(b_{2u}).$

<sup>30</sup>Treated for Fermi resonance of  $2_1$  with  $19_2(b_{2u}), 19_2(b_{3u}),$  and  $19_1(b_{2u})19_1(b_{3u}), 20_1(b_{2u})$  with  $8_1(a_g)19_1(b_{2u}), 8_1(b_{1g})19_1(b_{3u}), 1_16_1(a_g)19_1(b_{2u})$  and  $1_16_1(b_{1g})19_1(b_{3u}),$  and  $13_1$  and  $20_1(b_{2u})$  with  $8_1(a_g)19_1(b_{3u}), 8_1(b_{1g})19_1(b_{2u}), 1_16_1(a_g)19_1(b_{3u})$  and  $1_16_1(b_{1g})19_1(b_{2u}).$

<sup>31</sup>Treated for Fermi resonance of  $2_1$  with  $19_2(b_{2u}), 19_2(b_{3u}),$  and  $19_1(b_{2u})19_1(b_{3u}), 20_1(b_{2u})$  with  $8_1(a_g)19_1(b_{2u}), 8_1(b_{1g})19_1(b_{3u}), 1_16_1(a_g)19_1(b_{2u})$  and  $1_16_1(b_{1g})19_1(b_{3u}),$  and  $13_1$  and  $20_1(b_{2u})$  with  $8_1(a_g)19_1(b_{3u}), 8_1(b_{1g})19_1(b_{2u}), 1_16_1(a_g)19_1(b_{3u})$  and  $1_16_1(b_{1g})19_1(b_{2u}).$

# Appendix C

## [10]Annulene Supporting Information

### C.1 Literature Values

Table C.1: Previously reported relative energy for conformations of [10]annulene relative to conformation **6** (kcal mol<sup>-1</sup>)

	<b>2a</b> $C_s$	<b>2b</b> $C_2$	<b>3a</b> $C_2$	<b>3b</b> $C_1$	<b>4</b> $C_s$	<b>5</b> $C_2$
MINDO2 [121]	-10.3	–	–	–	24.7	9.4
MINDO3 [128]	-36.1	–	–	–	–	-6.0
MM3 [232]	15.53	–	–	7.41	–	-3.55
AM1 [232]	2.40	–	–	–	23.95	-0.68
HF/DZP [232]	1.88	–	–	8.14	11.47	2.91
HF/TZ2P//						
HF/DZd [113]	1.61	–	8.59	–	12.93	3.29
MP2/DZd [113]	7.12	–	-1.14	–	-4.22	1.23
MP2/TZ2P//						
MP2/DZd [113]	6.81	–	-4.15	–	-7.06	0.53
CCSD/6-31G [44]	4.28	4.13	17.22	8.18	13.75	2.92
CCSD(T)/pVDZ//						
CCSD/6-31G [44]	5.48	5.38	6.10	6.80	3.43	1.32
CCSD(T)/pVDZ//						
BH&HLYP/	5.89	5.79	5.66	4.63	3.17	0.54
6-311+G** [44]						
CCSD(T)/DZd [113]	–	–	–	–	6.29	1.74
CCSD(T)/TZ2P//						
CCSD(T)/DZd [113]	–	–	–	–	4.10	1.27
B3LYP/DZd [113]	2.47	–	-2.96	–	-9.11	-2.89
B3LYP/TZ2P//						

Table C.1: Cont.

	<b>2a</b> $C_s$	<b>2b</b> $C_2$	<b>3a</b> $C_2$	<b>3b</b> $C_1$	<b>4</b> $C_s$	<b>5</b> $C_2$
B3LYP/DZd [113]	1.99	–	-1.17	–	-6.92	-1.24
BH&HLYP/ 6-311G(d)[152]	2.90	–	–	5.10	1.29	1.22
BH&HLYP/ 6-311+G** [44]	2.81	2.71	5.42	4.28	-0.63	0.89

## C.2 Structures of Conformations

Table C.2: Geometry of conformation **1a** ( $D_{5h}$ ) and **1b** ( $D_{10h}$ ) (Å)

	<b>1a</b> $D_{5h}$ SCF/DZP	<b>1b</b> $D_{10h}$ SCF/DZP    MP2/DZP	
$r(C_1C_2)$	1.3714	1.3969	1.4121
$r(C_2C_3)$	1.4262		
$r(C_1H_1)$	1.0801	1.0801	1.0943

Table C.3: Geometry of conformation **2a** ( $C_s$ ) (Å)

	SCF/DZP	MP2/DZP	CCSD/DZP	CCSD(T)/DZP
$r(C_1C_2)$	1.4857	1.4730	1.4871	1.4848
$r(C_1C_3)$	1.3364	1.3679	1.3606	1.3687
$r(C_3C_5)$	1.4821	1.4740	1.4849	1.4849
$r(C_5C_7)$	1.3263	1.3554	1.3501	1.3569
$r(C_7C_9)$	1.4891	1.4846	1.4940	1.4948
$r(C_9C_{10})$	1.3260	1.3551	1.3504	1.3568
$r(H_1C_1)$	1.0811	1.0942	1.0949	1.0968
$r(H_3C_3)$	1.0832	1.0959	1.0961	1.0981
$r(H_5C_5)$	1.0822	1.0946	1.0947	1.0966
$r(H_7C_7)$	1.0820	1.0945	1.0946	1.0965
$r(H_9C_9)$	1.0811	1.0934	1.0937	1.0955
$\theta(C_2C_1C_3)$	138.48	138.01	138.30	138.19
$\theta(C_1C_3C_5)$	135.71	134.63	134.49	134.43

Table C.3: Cont.

	SCF/DZP	MP2/DZP	CCSD/DZP	CCSD(T)/DZP
$\theta(C_3C_5C_7)$	128.06	125.50	125.32	125.24
$\theta(C_5C_7C_9)$	126.12	123.65	123.72	123.58
$\theta(C_7C_9C_{10})$	122.61	120.67	120.95	120.79
$\theta(H_1C_1C_2)$	109.17	110.00	109.45	109.59
$\theta(H_3C_3C_1)$	113.40	113.09	113.50	113.40
$\theta(H_5C_5C_3)$	113.92	115.82	115.56	115.66
$\theta(H_7C_7C_5)$	117.76	118.24	118.62	118.57
$\theta(H_9C_9C_7)$	117.71	119.34	118.83	118.99
$\tau(C_4C_2C_1C_3)$	0.00	0.00	0.00	0.00
$\tau(C_2C_1C_3C_5)$	3.90	9.17	8.41	9.18
$\tau(C_1C_3C_5C_7)$	61.91	60.56	60.97	60.65
$\tau(C_3C_5C_7C_9)$	-8.59	-9.45	-9.62	-9.72
$\tau(C_5C_7C_9C_{10})$	-87.87	-90.71	-90.61	-90.70
$\tau(C_7C_9C_{10}C_8)$	0.00	0.00	0.00	0.00
$\tau(H_1C_1C_2C_4)$	-176.51	-173.17	-173.98	-173.40
$\tau(H_3C_3C_1C_2)$	-174.44	-170.48	-172.04	-171.18
$\tau(H_5C_5C_3C_1)$	-126.98	-129.95	-128.65	-129.45
$\tau(H_7C_7C_5C_3)$	172.44	172.89	173.18	173.16
$\tau(H_9C_9C_7C_5)$	94.85	90.54	90.50	90.31

Table C.4: Geometry of conformation **2b** ( $C_2$ ) (Å)

	SCF/DZP	MP2/DZP	CCSD/DZP	CCSD(T)/DZP
$r(C_1C_2)$	1.3391	1.3715	1.3635	1.3716
$r(C_1C_3)$	1.4837	1.4738	1.4857	1.4845
$r(C_3C_5)$	1.3302	1.3603	1.3542	1.3615
$r(C_5C_7)$	1.4847	1.4777	1.4892	1.4895
$r(C_7C_9)$	1.3258	1.3547	1.3504	1.3568
$r(C_9C_{10})$	1.4918	1.4874	1.4968	1.4975
$r(H_1C_1)$	1.0823	1.0954	1.0958	1.0978
$r(H_3C_3)$	1.0818	1.0947	1.0952	1.0971
$r(H_5C_5)$	1.0827	1.0950	1.0955	1.0973
$r(H_7C_7)$	1.0815	1.0936	1.0940	1.0959
$r(H_9C_9)$	1.0813	1.0937	1.0941	1.0959

Table C.4: Cont.

	SCF/DZP	MP2/DZP	CCSD/DZP	CCSD(T)/DZP
$\theta(C_2C_1C_3)$	139.06	139.44	138.75	138.85
$\theta(C_1C_3C_5)$	134.07	132.23	132.96	132.71
$\theta(C_3C_5C_7)$	130.22	127.31	128.77	128.37
$\theta(C_5C_7C_9)$	123.60	121.10	121.86	121.62
$\theta(C_7C_9C_{10})$	123.68	122.07	122.27	122.09
$\theta(H_1C_1C_2)$	111.95	111.08	111.80	111.63
$\theta(H_3C_3C_1)$	110.86	112.16	111.59	111.76
$\theta(H_5C_5C_3)$	115.75	116.21	116.02	116.06
$\theta(H_7C_7C_5)$	116.91	119.03	118.12	118.34
$\theta(H_9C_9C_7)$	119.10	119.37	119.55	119.55
$\tau(C_4C_2C_1C_3)$	-1.16	-8.43	-3.86	-5.78
$\tau(C_2C_1C_3C_5)$	-36.03	-35.73	-36.59	-36.05
$\tau(C_1C_3C_5C_7)$	8.29	12.38	10.36	11.06
$\tau(C_3C_5C_7C_9)$	77.58	74.00	77.92	77.13
$\tau(C_5C_7C_9C_{10})$	-4.69	-2.77	-5.04	-4.74
$\tau(C_7C_9C_{10}C_8)$	-92.59	-101.50	-95.26	-96.50
$\tau(H_1C_1C_2C_4)$	178.05	173.89	176.64	175.45
$\tau(H_3C_3C_1C_2)$	151.62	155.55	152.53	153.93
$\tau(H_5C_5C_3C_1)$	-172.17	-169.35	-171.49	-170.82
$\tau(H_7C_7C_5C_3)$	-108.51	-111.06	-108.02	-108.76
$\tau(H_9C_9C_7C_5)$	175.04	177.49	176.05	176.40

Table C.5: Geometry of conformation **3a** ( $C_2$ ) (Å)

	SCF/DZP	MP2/DZP	CCSD/DZP	CCSD(T)/DZP
$r(C_1C_3)$	1.4054	1.4203	1.4200	1.4249
$r(C_3C_5)$	1.4015	1.4145	1.4158	1.4212
$r(C_5C_7)$	1.3885	1.3985	1.4010	1.4056
$r(C_7C_9)$	1.4017	1.4173	1.4163	1.4215
$r(C_9C_{10})$	1.4176	1.4288	1.4296	1.4343
$r(H_1C_1)$	1.0805	1.0935	1.0934	1.0954
$r(H_3C_3)$	1.0809	1.0953	1.0942	1.0962
$r(H_5C_5)$	1.0705	1.0893	1.0866	1.0897
$r(H_7C_7)$	1.0804	1.0946	1.0937	1.0958



Table C.5: Cont.

	SCF/DZP	MP2/DZP	CCSD/DZP	CCSD(T)/DZP
$r(H_9C_9)$	1.0817	1.0952	1.0951	1.0971
$r(H_{10}C_{10})$	1.0812	1.0956	1.0952	1.0973
$\theta(C_2C_1C_3)$	120.63	119.60	120.08	120.04
$\theta(C_1C_3C_5)$	118.24	118.52	118.33	118.33
$\theta(C_3C_5C_7)$	131.42	130.30	130.74	130.54
$\theta(C_5C_7C_9)$	120.49	120.91	120.73	120.83
$\theta(C_7C_9C_{10})$	134.33	133.16	133.74	133.66
$\theta(C_8C_{10}C_9)$	139.75	140.46	139.98	139.91
$\theta(H_1C_1C_2)$	119.69	120.20	119.96	119.98
$\theta(H_3C_3C_1)$	120.06	120.20	120.25	120.28
$\theta(H_5C_5C_3)$	114.04	114.26	114.21	114.24
$\theta(H_7C_7C_5)$	121.19	120.70	120.83	120.75
$\theta(H_9C_9C_7)$	114.02	114.58	114.30	114.34
$\theta(H_{10}C_{10}C_9)$	110.12	109.77	110.01	110.04
$\tau(C_4C_2C_1C_3)$	-16.34	-16.59	-16.44	-16.54
$\tau(C_1C_3C_5C_7)$	140.57	139.68	140.03	139.73
$\tau(C_3C_5C_7C_9)$	-145.99	-146.43	-146.23	-146.07
$\tau(C_5C_7C_9C_{10})$	9.84	10.72	10.06	9.98
$\tau(C_7C_9C_{10}C_8)$	8.30	8.33	8.52	8.73
$\tau(H_1C_1C_2C_4)$	163.66	163.41	163.56	163.46
$\tau(H_3C_3C_1C_2)$	159.27	159.65	159.41	159.21
$\tau(H_5C_5C_3C_1)$	-26.83	-24.62	-25.88	-25.66
$\tau(H_7C_7C_5C_3)$	24.26	24.34	24.13	24.19
$\tau(H_9C_9C_7C_5)$	-173.96	-172.78	-173.38	-173.31
$\tau(H_{10}C_{10}C_9C_7)$	-171.70	-171.66	-171.48	-171.26

Table C.6: Geometry of conformation **3b** ( $C_1$ ) (Å)

	SCF/DZP	CCSD/DZP	CCSD(T)/DZP
$r(C_1C_2)$	1.3393	1.3648	1.3794
$r(C_1C_3)$	1.4894	1.4905	1.4798
$r(C_2C_4)$	1.4950	1.4947	1.4805
$r(C_3C_5)$	1.3345	1.3610	1.3762
$r(C_4C_6)$	1.3269	1.3528	1.3663

Table C.6: Cont.

	SCF/DZP	CCSD/DZP	CCSD(T)/DZP
$r(C_5C_7)$	1.4684	1.4685	1.4568
$r(C_6C_8)$	1.4787	1.4786	1.4691
$r(C_7C_9)$	1.3420	1.3668	1.3805
$r(C_8C_{10})$	1.3479	1.3733	1.3895
$r(C_9C_{10})$	1.4926	1.4901	1.4818
$r(H_1C_1)$	1.0802	1.0930	1.0950
$r(H_2C_2)$	1.0800	1.0932	1.0952
$r(H_3C_3)$	1.0827	1.0954	1.0971
$r(H_4C_4)$	1.0785	1.0919	1.0927
$r(H_5C_5)$	1.0729	1.0870	1.0883
$r(H_6C_6)$	1.0834	1.0958	1.0969
$r(H_7C_7)$	1.0802	1.0935	1.0954
$r(H_8C_8)$	1.0817	1.0949	1.0969
$r(H_9C_9)$	1.0810	1.0945	1.0966
$r(H_{10}C_{10})$	1.0817	1.0953	1.0972
$\theta(C_2C_1C_3)$	118.08	117.50	118.28
$\theta(C_1C_2C_4)$	118.54	118.40	118.59
$\theta(C_1C_3C_5)$	119.22	118.72	118.12
$\theta(C_2C_4C_6)$	125.82	125.77	127.84
$\theta(C_3C_5C_7)$	125.55	125.26	126.82
$\theta(C_4C_6C_8)$	124.10	123.69	122.40
$\theta(C_5C_7C_9)$	123.12	122.92	122.03
$\theta(C_6C_8C_{10})$	129.98	130.16	131.38
$\theta(C_8C_{10}C_9)$	137.25	137.27	138.31
$\theta(H_1C_1C_2)$	120.75	120.94	120.58
$\theta(H_2C_2C_1)$	120.87	120.89	120.62
$\theta(H_3C_3C_1)$	118.20	119.08	119.80
$\theta(H_4C_4C_2)$	115.10	115.65	114.69
$\theta(H_5C_5C_3)$	117.68	117.34	116.49
$\theta(H_6C_6C_4)$	119.87	119.54	120.20
$\theta(H_7C_7C_5)$	119.04	119.09	115.07
$\theta(H_8C_8C_6)$	115.31	115.48	115.07
$\theta(H_9C_9C_7)$	114.90	114.82	114.65
$\theta(H_{10}C_{10}C_9)$	112.86	112.48	111.69

Table C.6: Cont.

	SCF/DZP	CCSD/DZP	CCSD(T)/DZP
$\tau(C_4C_2C_1C_3)$	-0.41	-1.13	-4.05
$\tau(C_2C_1C_3C_5)$	-46.80	-43.60	-35.50
$\tau(C_1C_2C_4C_6)$	110.95	115.36	124.58
$\tau(C_1C_3C_5C_7)$	148.00	147.50	145.91
$\tau(C_2C_4C_6C_8)$	-154.18	-154.31	-151.94
$\tau(C_3C_5C_7C_9)$	-125.15	-128.29	-134.17
$\tau(C_5C_7C_9C_{10})$	42.95	37.22	26.93
$\tau(C_6C_8C_{10}C_9)$	-3.76	-2.62	-1.15
$\tau(C_7C_9C_{10}C_8)$	19.69	20.74	20.37
$\tau(H_1C_1C_2C_4)$	175.86	175.02	172.64
$\tau(H_2C_2C_1C_3)$	179.69	178.79	175.34
$\tau(H_3C_3C_1C_2)$	118.97	121.97	132.42
$\tau(H_4C_4C_2C_1)$	-55.10	-50.72	-40.55
$\tau(H_5C_5C_3C_1)$	-16.71	-17.28	-18.41
$\tau(H_6C_6C_4C_2)$	15.16	15.17	17.30
$\tau(H_7C_7C_5C_3)$	48.66	44.67	37.82
$\tau(H_8C_8C_6C_4)$	-143.57	-148.67	-158.47
$\tau(H_9C_9C_7C_5)$	177.46	177.66	178.79
$\tau(H_{10}C_{10}C_9C_7)$	177.88	178.96	-179.21

Table C.7: Geometry of conformation 4 ( $C_s$ ) (Å)

	SCF/DZP	MP2/DZP	CCSD/DZP	CCSD(T)/DZP
$r(C_1C_3)$	1.3771	1.3896	1.3912	1.3957
$r(C_3C_5)$	1.3885	1.4042	1.4033	1.0481
$r(C_5C_7)$	1.4019	1.4133	1.4145	1.4190
$r(C_7C_9)$	1.4096	1.4254	1.4240	1.4293
$r(C_9C_{10})$	1.4226	1.4369	1.4367	1.4420
$r(H_1C_1)$	1.0638	1.0835	1.0800	1.0836
$r(H_3C_3)$	1.0792	1.0927	1.0920	1.0941
$r(H_5C_5)$	1.0798	1.0933	1.0930	1.0950
$r(H_7C_7)$	1.0798	1.0941	1.0938	1.0959
$r(H_9C_9)$	1.0798	1.0944	1.0943	1.0965
$r(H_{10}C_{10})$	1.0794	1.0946	1.0942	1.0965

Table C.7: Cont.

	SCF/DZP	MP2/DZP	CCSD/DZP	CCSD(T)/DZP
$\theta(C_2C_1C_3)$	131.36	130.56	130.65	130.43
$\theta(C_1C_3C_5)$	117.46	117.50	117.45	117.49
$\theta(C_3C_5C_7)$	128.09	127.14	127.42	127.31
$\theta(C_5C_7C_9)$	139.05	139.22	139.00	138.98
$\theta(C_6C_8C_{10})$	146.90	146.84	146.95	146.96
$\theta(C_8C_{10}C_9)$	149.42	149.68	149.59	149.57
$\theta(H_1C_1C_{10})$	21.79	18.45	20.54	20.63
$\theta(H_3C_3C_1)$	122.21	121.79	121.90	120.63
$\theta(H_5C_5C_3)$	117.47	117.95	117.81	117.88
$\theta(H_7C_7C_5)$	111.17	111.17	111.23	111.27
$\theta(H_9C_9C_7)$	106.95	106.99	106.94	106.07
$\theta(H_{10}C_{10}C_9)$	105.26	105.13	105.17	105.17
$\tau(C_2C_1C_3C_5)$	-167.26	-170.14	-169.14	-168.92
$\tau(C_1C_3C_5C_7)$	7.62	6.83	7.42	7.42
$\tau(C_3C_5C_7C_9)$	5.59	4.62	5.31	5.38
$\tau(C_5C_7C_9C_{10})$	-4.33	-4.05	-4.59	-4.53
$\tau(C_7C_9C_{10}C_8)$	-7.37	-6.60	-7.62	-7.61
$\tau(H_1C_1C_3C_5)$	10.87	8.84	9.99	9.99
$\tau(H_3C_3C_1C_2)$	10.11	7.71	8.57	8.68
$\tau(H_5C_5C_3C_1)$	-175.72	-175.94	-175.62	-175.55
$\tau(H_7C_7C_5C_3)$	-178.69	-178.83	-178.77	-178.64
$\tau(H_9C_9C_7C_5)$	174.51	175.38	174.60	174.69
$\tau(H_{10}C_{10}C_9C_7)$	-176.29	-177.03	-176.51	-176.55

Table C.8: Geometry of conformation **5** ( $C_2$ ) (Å)

	SCF/DZP	MP2/DZP	CCSD/DZP	CCSD(T)/DZP
$r(C_1C_2)$	1.4897	1.4222	1.4891	1.4856
$r(C_1C_3)$	1.3406	1.4262	1.3644	1.3739
$r(C_3C_5)$	1.4784	1.4018	1.4804	1.4760
$r(C_5C_7)$	1.3296	1.4018	1.3551	1.3643
$r(C_7C_9)$	1.4889	1.4262	1.4907	1.4887
$r(C_9C_{10})$	1.3420	1.4222	1.3659	1.3747
$r(H_1C_1)$	1.0815	1.0956	1.0946	1.0964

Table C.8: Cont.

	SCF/DZP	MP2/DZP	CCSD/DZP	CCSD(T)/DZP
$r(H_3C_3)$	1.0805	1.0954	1.0938	1.0957
$r(H_5C_5)$	1.0763	1.0881	1.0903	1.0919
$r(H_7C_7)$	1.0834	1.0954	1.0962	1.0982
$r(H_9C_9)$	1.0811	1.0956	1.0942	1.0962
$\theta(C_2C_1C_3)$	129.63	129.84	128.69	128.34
$\theta(C_1C_3C_5)$	122.98	121.35	122.88	122.68
$\theta(C_3C_5C_7)$	123.52	129.16	122.81	122.92
$\theta(C_5C_7C_9)$	123.77	121.35	123.76	123.65
$\theta(C_7C_9C_{10})$	124.32	129.84	124.01	124.50
$\theta(H_1C_1C_2)$	113.76	115.75	114.60	116.70
$\theta(H_3C_3C_1)$	118.08	117.88	118.17	118.22
$\theta(H_5C_5C_3)$	115.66	114.25	116.46	118.85
$\theta(H_7C_7C_5)$	119.39	120.36	118.77	118.69
$\theta(H_9C_9C_7)$	117.65	115.75	118.00	117.30
$\tau(C_4C_2C_1C_3)$	-37.98	-12.17	-38.04	-37.04
$\tau(C_2C_1C_3C_5)$	1.66	-14.02	1.32	0.35
$\tau(C_1C_3C_5C_7)$	121.13	143.20	123.50	126.31
$\tau(C_3C_5C_7C_9)$	-150.82	-143.20	-151.37	-150.42
$\tau(C_5C_7C_9C_{10})$	42.82	14.01	41.80	39.45
$\tau(C_7C_9C_{10}C_8)$	-8.33	12.16	-8.24	-7.44
$\tau(H_1C_1C_2C_4)$	143.42	165.43	143.46	144.26
$\tau(H_3C_3C_1C_2)$	177.12	158.72	176.44	175.06
$\tau(H_5C_5C_3C_1)$	-43.40	-18.20	-41.56	-37.98
$\tau(H_7C_7C_5C_3)$	15.45	29.36	14.73	15.92
$\tau(H_9C_9C_7C_5)$	-143.68	-168.41	-144.94	-147.36

Table C.9: Geometry of conformation **6** ( $C_2$ ) (Å)

	SCF/DZP	MP2/DZP	CCSD/DZP	CCSD(T)/DZP
$r(C_1C_2)$	1.3258	1.3606	1.3517	1.3204
$r(C_1C_3)$	1.4784	1.4681	1.4820	1.4718
$r(C_3C_5)$	1.3359	1.3691	1.3605	1.3296
$r(C_5C_7)$	1.4911	1.4807	1.4932	1.4847
$r(C_7C_9)$	1.3319	1.3626	1.3561	1.3257

Table C.9: Cont.

	SCF/DZP	MP2/DZP	CCSD/DZP	CCSD(T)/DZP
$r(C_9C_{10})$	1.4943	1.4812	1.4957	1.4879
$r(H_1C_1)$	1.0806	1.0937	1.0936	1.0837
$r(H_3C_3)$	1.0807	1.0935	1.0936	1.0831
$r(H_5C_5)$	1.0820	1.0947	1.0948	1.0845
$r(H_7C_7)$	1.0823	1.0950	1.0954	1.0847
$r(H_9C_9)$	1.0821	1.0947	1.0950	1.0850
$\theta(C_2C_1C_3)$	123.07	122.52	122.70	123.27
$\theta(C_1C_3C_5)$	121.82	121.08	121.34	121.86
$\theta(C_3C_5C_7)$	127.86	125.67	126.56	127.93
$\theta(C_5C_7C_9)$	130.57	126.78	128.68	130.62
$\theta(C_7C_9C_{10})$	129.31	125.92	127.53	129.41
$\theta(H_1C_1C_2)$	119.45	118.39	118.97	119.40
$\theta(H_3C_3C_1)$	119.41	120.40	119.83	119.32
$\theta(H_5C_5C_3)$	117.64	117.56	117.80	117.66
$\theta(H_7C_7C_5)$	113.33	115.89	114.57	113.22
$\theta(H_9C_9C_7)$	116.33	117.35	116.87	116.28
$\tau(C_4C_2C_1C_3)$	151.36	150.74	151.68	151.06
$\tau(C_2C_1C_3C_5)$	-50.83	-45.56	-48.59	-50.71
$\tau(C_1C_3C_5C_7)$	5.30	2.97	4.67	5.19
$\tau(C_3C_5C_7C_9)$	-48.39	-47.88	-48.73	-48.34
$\tau(C_5C_7C_9C_{10})$	-6.29	-8.58	-7.25	-6.23
$\tau(C_7C_9C_{10}C_8)$	103.28	114.64	109.11	103.04
$\tau(H_1C_1C_2C_4)$	-15.66	-16.93	-15.51	-16.00
$\tau(H_3C_3C_1C_2)$	134.75	139.66	136.76	134.82
$\tau(H_5C_5C_3C_1)$	-178.66	178.96	-179.55	-178.72
$\tau(H_7C_7C_5C_3)$	131.58	130.21	130.16	131.72
$\tau(H_9C_9C_7C_5)$	178.41	173.37	176.67	178.36

### C.3 Relative Energies

Table C.10: Relative energies of conformations and transition states for [10]annulene (kcal mol<sup>-1</sup>)

	SCF/DZP	
	Rel. <i>E</i>	IF
<b>1a</b> <i>D</i> <sub>5h</sub>	32.03	2
<b>1b</b> <i>D</i> <sub>10h</sub>	32.33	3
<b>2a</b> <i>C</i> <sub>s</sub>	1.95	1
<b>2b</b> <i>C</i> <sub>2</sub>	1.84	0
<b>3a</b> <i>C</i> <sub>2</sub>	19.36	1
<b>3b</b> <i>C</i> <sub>1</sub>	8.08	0
<b>4</b> <i>C</i> <sub>s</sub>	11.77	1
<b>5</b> <i>C</i> <sub>2</sub>	2.88	0
<b>6</b> <i>C</i> <sub>2</sub>	0.00	0

## C.4 Harmonic Frequencies

Table C.11: Harmonic frequencies for conformation **2a** in cm<sup>-1</sup>. Infrared intensities in parenthesis (km mol<sup>-1</sup>).

Sym		SCF/DZP	MP2/DZP	CCSD/DZP
$\omega_1$	<i>a'</i>	3340.0 (22.1)	3224.6 (15.5)	3214.3 (18.8)
$\omega_2$	<i>a'</i>	3333.0 (50.2)	3212.8 (14.8)	3202.4 (22.2)
$\omega_3$	<i>a'</i>	3324.7 (71.1)	3209.1 (60.7)	3195.9 (79.9)
$\omega_4$	<i>a'</i>	3301.3 (5.4)	3186.0 (1.2)	3177.0 (2.8)
$\omega_5$	<i>a'</i>	3286.1 (1.0)	3171.1 (1.5)	3159.0 (0.6)
$\omega_6$	<i>a'</i>	1893.1 (0.1)	1706.3 (0.0)	1758.6 (0.2)
$\omega_7$	<i>a'</i>	1857.5 (12.9)	1685.0 (4.0)	1730.9 (5.2)
$\omega_8$	<i>a'</i>	1816.5 (0.2)	1639.5 (0.0)	1678.1 (0.0)
$\omega_9$	<i>a'</i>	1598.3 (2.0)	1476.2 (2.0)	1490.1 (2.2)
$\omega_{10}$	<i>a'</i>	1526.6 (4.2)	1399.6 (1.6)	1414.2 (3.1)
$\omega_{11}$	<i>a'</i>	1467.5 (1.5)	1352.2 (1.2)	1361.7 (1.4)
$\omega_{12}$	<i>a'</i>	1338.7 (0.5)	1225.4 (0.3)	1233.0 (0.2)
$\omega_{13}$	<i>a'</i>	1298.0 (0.8)	1188.8 (0.4)	1199.6 (0.4)
$\omega_{14}$	<i>a'</i>	1132.5 (0.0)	1075.6 (0.3)	1068.6 (0.1)
$\omega_{15}$	<i>a'</i>	1121.7 (0.2)	980.7 (2.3)	987.2 (1.1)
$\omega_{16}$	<i>a'</i>	1094.9 (0.2)	957.5 (0.1)	973.7 (1.2)

Table C.11: Cont.

Cont.	Sym	SCF/DZP	MP2/DZP	CCSD/DZP
$\omega_{17}$	$a'$	1020.4 (5.3)	935.4 (0.3)	949.3 (0.2)
$\omega_{18}$	$a'$	906.2 (5.0)	831.8 (8.5)	834.9 (9.1)
$\omega_{19}$	$a'$	853.2 (16.0)	795.9 (16.8)	797.9 (13.4)
$\omega_{20}$	$a'$	792.8 (32.2)	737.7 (2.7)	740.0 (4.7)
$\omega_{21}$	$a'$	745.4 (29.1)	679.5 (39.5)	689.4 (35.5)
$\omega_{22}$	$a'$	689.2 (62.9)	620.8 (53.3)	626.8 (51.7)
$\omega_{23}$	$a'$	522.7 (13.9)	465.7 (19.6)	476.8 (14.9)
$\omega_{24}$	$a'$	429.3 (1.0)	383.1 (0.7)	387.3 (0.4)
$\omega_{25}$	$a'$	307.2 (1.6)	256.3 (3.4)	274.9 (1.9)
$\omega_{26}$	$a'$	191.6 (0.3)	166.3 (0.1)	172.7 (0.1)
$\omega_{27}$	$a'$	156.9 (0.2)	140.1 (0.7)	151.2 (0.3)
$\omega_{28}$	$a''$	28.7i	24.3i	19.8i
$\omega_{29}$	$a''$	3325.9 (52.9)	3210.2 (28.9)	3201.2 (35.6)
$\omega_{30}$	$a''$	3315.3 (0.0)	3199.3 (0.3)	3188.9 (0.0)
$\omega_{31}$	$a''$	3310.8 (30.7)	3193.9 (21.4)	3180.0 (24.1)
$\omega_{32}$	$a''$	3300.0 (0.0)	3184.8 (0.2)	3174.5 (5.0)
$\omega_{33}$	$a''$	3281.4 (3.2)	3166.0 (0.1)	3152.4 (0.4)
$\omega_{34}$	$a''$	1880.3 (3.8)	1703.1 (0.7)	1746.1 (1.2)
$\omega_{35}$	$a''$	1840.8 (6.5)	1664.9 (2.0)	1705.0 (2.5)
$\omega_{36}$	$a''$	1583.1 (0.4)	1459.9 (0.4)	1474.6 (0.7)
$\omega_{37}$	$a''$	1547.9 (1.0)	1421.6 (0.4)	1437.2 (1.1)
$\omega_{38}$	$a''$	1469.3 (0.4)	1340.6 (0.2)	1356.5 (0.4)
$\omega_{39}$	$a''$	1421.2 (0.0)	1306.5 (0.0)	1316.5 (0.0)
$\omega_{40}$	$a''$	1334.4 (2.2)	1216.3 (1.1)	1224.8 (1.1)
$\omega_{41}$	$a''$	1130.9 (0.5)	1055.9 (0.5)	1056.0 (0.4)
$\omega_{42}$	$a''$	1124.0 (0.0)	961.4 (0.9)	967.8 (0.3)
$\omega_{43}$	$a''$	1107.5 (0.1)	942.0 (0.4)	958.3 (0.2)
$\omega_{44}$	$a''$	1072.5 (0.6)	931.0 (0.4)	947.9 (0.8)
$\omega_{45}$	$a''$	1010.0 (1.7)	909.5 (0.3)	926.2 (0.3)
$\omega_{46}$	$a''$	973.6 (6.0)	894.8 (0.7)	896.3 (1.5)
$\omega_{47}$	$a''$	884.1 (2.8)	802.0 (9.3)	807.3 (7.5)
$\omega_{48}$	$a''$	860.8 (16.0)	787.9 (15.7)	794.4 (12.9)
$\omega_{49}$	$a''$	771.8 (15.2)	693.5 (9.7)	700.8 (10.4)
$\omega_{50}$	$a''$	696.1 (40.5)	620.7 (33.8)	626.6 (32.6)



Table C.11: Cont.

Cont.	Sym	SCF/DZP	MP2/DZP	CCSD/DZP
$\omega_{51}$	$a''$	531.1 (4.9)	477.9 (7.2)	481.5 (4.6)
$\omega_{52}$	$a''$	410.7 (1.1)	364.0 (2.0)	368.7 (1.4)
$\omega_{53}$	$a''$	333.4 (0.5)	294.8 (0.3)	298.8 (0.3)
$\omega_{54}$	$a''$	131.7 (0.2)	79.9 (0.2)	100.7 (0.2)

Table C.12: Harmonic frequencies for conformation **2b** in  $\text{cm}^{-1}$ . Infrared intensities in parenthesis in  $\text{km mol}^{-1}$ .

	Sym	SCF/DZP	MP2/DZP	CCSD/DZP
$\omega_1$	$a$	3337.3 (13.4)	3221.9 (10.4)	3210.7 (12.9)
$\omega_2$	$a$	3327.7 (47.7)	3208.5 (18.0)	3195.9 (28.6)
$\omega_3$	$a$	3312.0 (3.0)	3196.8 (1.2)	3185.0 (0.4)
$\omega_4$	$a$	3308.4 (22.4)	3191.8 (20.0)	3178.7 (25.3)
$\omega_5$	$a$	3291.0 (0.0)	3177.6 (1.0)	3163.1 (0.2)
$\omega_6$	$a$	1892.5 (0.1)	1706.2 (0.3)	1759.2 (0.8)
$\omega_7$	$a$	1861.9 (12.2)	1690.6 (3.6)	1734.4 (3.7)
$\omega_8$	$a$	1838.3 (0.8)	1661.5 (0.1)	1703.2 (0.6)
$\omega_9$	$a$	1578.4 (0.6)	1456.5 (0.3)	1469.4 (0.7)
$\omega_{10}$	$a$	1524.5 (4.4)	1398.0 (2.3)	1414.2 (4.1)
$\omega_{11}$	$a$	1471.3 (0.0)	1359.7 (0.1)	1362.8 (0.1)
$\omega_{12}$	$a$	1374.8 (1.5)	1252.7 (0.9)	1270.4 (1.0)
$\omega_{13}$	$a$	1314.4 (0.3)	1210.7 (0.0)	1218.9 (0.1)
$\omega_{14}$	$a$	1130.9 (0.3)	1054.7 (0.2)	1053.3 (0.3)
$\omega_{15}$	$a$	1128.4 (0.1)	977.7 (1.8)	983.0 (0.7)
$\omega_{16}$	$a$	1115.6 (0.0)	955.1 (0.0)	972.6 (1.2)
$\omega_{17}$	$a$	1070.6 (0.8)	944.5 (0.1)	960.2 (0.3)
$\omega_{18}$	$a$	1017.5 (3.5)	920.5 (0.0)	931.8 (0.1)
$\omega_{19}$	$a$	899.5 (6.7)	824.9 (10.8)	829.1 (8.3)
$\omega_{20}$	$a$	848.6 (4.5)	793.5 (5.6)	794.2 (4.8)
$\omega_{21}$	$a$	788.3 (12.1)	746.3 (4.0)	743.2 (5.3)
$\omega_{22}$	$a$	739.9 (2.1)	672.0 (3.9)	680.5 (5.4)
$\omega_{23}$	$a$	687.8 (48.1)	617.2 (49.9)	620.1 (40.0)
$\omega_{24}$	$a$	527.6 (3.6)	468.7 (6.5)	475.8 (3.9)
$\omega_{25}$	$a$	410.0 (0.8)	364.1 (1.9)	366.6 (1.1)

Table C.12: Cont.

Cont.	Sym	SCF/DZP	MP2/DZP	CCSD/DZP
$\omega_{26}$	<i>a</i>	305.9 (1.5)	256.7 (3.1)	272.5 (1.6)
$\omega_{27}$	<i>a</i>	166.5 (0.1)	153.0 (0.1)	155.4 (0.1)
$\omega_{28}$	<i>a</i>	127.1 (0.1)	72.3 (0.2)	98.7 (0.1)
$\omega_{29}$	<i>b</i>	3333.8 (44.1)	3220.0 (27.0)	3207.7 (37.7)
$\omega_{30}$	<i>b</i>	3322.1 (99.5)	3205.5 (64.4)	3191.8 (82.5)
$\omega_{31}$	<i>b</i>	3310.4 (2.5)	3195.3 (0.4)	3183.3 (1.2)
$\omega_{32}$	<i>b</i>	3295.1 (1.8)	3180.2 (0.4)	3166.3 (0.8)
$\omega_{33}$	<i>b</i>	3281.2 (0.7)	3163.7 (0.1)	3151.6 (0.1)
$\omega_{34}$	<i>b</i>	1878.4 (5.6)	1699.7 (1.5)	1746.7 (2.4)
$\omega_{35}$	<i>b</i>	1817.5 (0.9)	1642.6 (0.2)	1678.7 (0.2)
$\omega_{36}$	<i>b</i>	1594.9 (1.6)	1471.3 (1.9)	1485.2 (1.9)
$\omega_{37}$	<i>b</i>	1552.6 (0.7)	1427.3 (0.2)	1441.8 (0.9)
$\omega_{38}$	<i>b</i>	1469.4 (0.5)	1342.0 (0.1)	1358.7 (0.5)
$\omega_{39}$	<i>b</i>	1398.3 (1.3)	1278.6 (0.9)	1293.4 (0.9)
$\omega_{40}$	<i>b</i>	1300.2 (1.5)	1185.7 (0.8)	1200.2 (0.7)
$\omega_{41}$	<i>b</i>	1129.3 (0.0)	1075.5 (0.1)	1068.8 (0.0)
$\omega_{42}$	<i>b</i>	1117.1 (0.0)	965.0 (1.5)	972.1 (0.3)
$\omega_{43}$	<i>b</i>	1093.4 (0.4)	949.2 (0.8)	953.0 (1.9)
$\omega_{44}$	<i>b</i>	1013.6 (3.0)	929.4 (0.2)	943.5 (0.3)
$\omega_{45}$	<i>b</i>	974.3 (6.8)	896.6 (2.3)	898.2 (2.7)
$\omega_{46}$	<i>b</i>	894.9 (0.6)	805.8 (4.0)	813.8 (3.1)
$\omega_{47}$	<i>b</i>	860.0 (20.3)	789.4 (23.1)	796.4 (19.1)
$\omega_{48}$	<i>b</i>	788.8 (53.5)	702.8 (33.6)	713.2 (36.2)
$\omega_{49}$	<i>b</i>	694.5 (68.7)	630.8 (55.1)	629.8 (53.0)
$\omega_{50}$	<i>b</i>	524.2 (18.1)	469.2 (22.1)	479.1 (16.8)
$\omega_{51}$	<i>b</i>	430.3 (1.1)	386.8 (1.0)	389.3 (0.7)
$\omega_{52}$	<i>b</i>	335.0 (0.4)	294.2 (0.2)	299.5 (0.2)
$\omega_{53}$	<i>b</i>	185.8 (0.4)	161.3 (0.4)	166.0 (0.3)
$\omega_{54}$	<i>b</i>	28.9 (0.2)	26.8 (0.1)	25.1 (0.1)

Table C.13: Harmonic frequencies for conformation **3a** in  $\text{cm}^{-1}$ . Infrared intensities in parenthesis in  $\text{km mol}^{-1}$ .

	Sym	SCF/DZP	MP2/DZP	CCSD/DZP
$\omega_1$	<i>a</i>	3433.3 (1.3)	3237.1 (0.5)	3265.3 (0.1)
$\omega_2$	<i>a</i>	3350.1 (32.5)	3220.8 (22.2)	3218.0 (29.0)
$\omega_3$	<i>a</i>	3340.8 (31.2)	3207.5 (20.1)	3206.6 (20.0)
$\omega_4$	<i>a</i>	3326.2 (0.4)	3193.5 (21.8)	3192.4 (0.0)
$\omega_5$	<i>a</i>	3324.7 (45.7)	3190.9 (1.6)	3190.3 (34.1)
$\omega_6$	<i>a</i>	3293.6 (0.1)	3169.1 (0.0)	3162.2 (0.1)
$\omega_7$	<i>a</i>	1768.9 (64.7)	1658.8 (0.1)	1667.4 (17.6)
$\omega_8$	<i>a</i>	1682.0 (0.3)	1554.0 (0.3)	1576.8 (0.0)
$\omega_9$	<i>a</i>	1591.1 (3.4)	1477.5 (6.9)	1491.9 (2.2)
$\omega_{10}$	<i>a</i>	1456.6 (10.4)	1336.8 (0.2)	1355.8 (2.8)
$\omega_{11}$	<i>a</i>	1372.9 (0.1)	1279.2 (2.0)	1290.8 (0.5)
$\omega_{12}$	<i>a</i>	1357.3 (7.3)	1260.5 (4.7)	1272.1 (3.9)
$\omega_{13}$	<i>a</i>	1286.6 (0.4)	1194.6 (11.9)	1204.9 (2.5)
$\omega_{14}$	<i>a</i>	1180.5 (56.5)	1078.1 (32.2)	1085.7 (27.7)
$\omega_{15}$	<i>a</i>	1117.1 (5.1)	1044.0 (11.6)	1052.1 (7.9)
$\omega_{16}$	<i>a</i>	1069.8 (0.0)	911.0 (0.1)	938.7 (0.0)
$\omega_{17}$	<i>a</i>	983.4 (9.7)	894.3 (7.7)	886.0 (8.4)
$\omega_{18}$	<i>a</i>	921.4 (1.6)	859.7 (4.5)	864.1 (1.0)
$\omega_{19}$	<i>a</i>	910.5 (1.0)	850.2 (0.0)	854.1 (1.0)
$\omega_{20}$	<i>a</i>	891.0 (3.2)	803.7 (19.2)	804.1 (8.1)
$\omega_{21}$	<i>a</i>	771.2 (2.9)	722.0 (0.0)	725.3 (0.3)
$\omega_{22}$	<i>a</i>	586.1 (13.0)	547.0 (11.6)	544.7 (10.5)
$\omega_{23}$	<i>a</i>	499.4 (1.4)	459.2 (3.3)	462.1 (1.7)
$\omega_{24}$	<i>a</i>	372.9 (0.5)	341.4 (2.0)	342.0 (0.1)
$\omega_{25}$	<i>a</i>	324.0 (4.6)	303.6 (1.7)	303.8 (2.2)
$\omega_{26}$	<i>a</i>	218.9 (0.2)	196.0 (0.1)	198.4 (0.1)
$\omega_{27}$	<i>b</i>	1089.1i (24.6)	3234.6 (8.9)	754.8i
$\omega_{28}$	<i>b</i>	3428.1 (3.8)	3202.9 (35.0)	3261.5 (6.6)
$\omega_{29}$	<i>b</i>	3338.4 (76.3)	3196.1 (16.0)	3203.5 (52.4)
$\omega_{30}$	<i>b</i>	3336.0 (0.3)	3182.7 (1.9)	3200.2 (10.1)
$\omega_{31}$	<i>b</i>	3311.3 (8.8)	1982.8 (6.4)	3178.7 (5.2)
$\omega_{32}$	<i>b</i>	1720.8 (19.0)	1599.9 (5.1)	1621.4 (2.5)
$\omega_{33}$	<i>b</i>	1649.1 (1.4)	1534.1 (32.0)	1552.1 (5.9)

Table C.13: Cont.

Cont.	Sym	SCF/DZP	MP2/DZP	CCSD/DZP
$\omega_{34}$	<i>b</i>	1611.9 (0.4)	1476.3 (0.9)	1500.9 (0.3)
$\omega_{35}$	<i>b</i>	1551.0 (4.1)	1422.6 (7.2)	1445.3 (2.0)
$\omega_{36}$	<i>b</i>	1510.4 (4.3)	1346.2 (0.9)	1413.3 (3.1)
$\omega_{37}$	<i>b</i>	1413.8 (6.1)	1306.0 (0.3)	1322.4 (1.2)
$\omega_{38}$	<i>b</i>	1362.1 (2.8)	1262.3 (5.4)	1275.6 (3.1)
$\omega_{39}$	<i>b</i>	1333.7 (6.2)	1220.6 (3.1)	1251.5 (3.8)
$\omega_{40}$	<i>b</i>	1227.9 (5.7)	1121.8 (1.6)	1172.9 (6.5)
$\omega_{41}$	<i>b</i>	1188.4 (12.8)	1058.0 (3.5)	1120.8 (3.1)
$\omega_{42}$	<i>b</i>	1146.5 (33.2)	992.9 (56.3)	1069.3 (4.6)
$\omega_{43}$	<i>b</i>	1122.7 (38.2)	927.0 (0.5)	1006.5 (59.8)
$\omega_{44}$	<i>b</i>	1071.0 (8.3)	904.6 (16.2)	939.6 (7.0)
$\omega_{45}$	<i>b</i>	992.7 (23.0)	865.8 (14.6)	887.0 (11.4)
$\omega_{46}$	<i>b</i>	901.6 (51.7)	780.1 (58.1)	815.2 (25.6)
$\omega_{47}$	<i>b</i>	843.4 (60.0)	697.9 (27.0)	769.5 (55.8)
$\omega_{48}$	<i>b</i>	747.3 (16.8)	646.1 (1.6)	683.8 (13.5)
$\omega_{49}$	<i>b</i>	691.0 (2.2)	556.7 (3.2)	646.2 (1.6)
$\omega_{50}$	<i>b</i>	576.6 (1.1)	490.1 (5.2)	522.7 (0.2)
$\omega_{51}$	<i>b</i>	472.5 (20.7)	420.3 (11.0)	436.1 (15.2)
$\omega_{52}$	<i>b</i>	322.4 (2.1)	292.3 (1.7)	296.2 (1.7)
$\omega_{53}$	<i>b</i>	266.4 (0.6)	231.7 (0.9)	241.5 (0.4)
$\omega_{54}$	<i>b</i>	188.0 (1.1)	166.1 (1.8)	169.9 (1.3)

Table C.14: Harmonic frequencies for conformation **3b** in  $\text{cm}^{-1}$ . Infrared intensities in parenthesis in  $\text{km mol}^{-1}$ .

	Sym	SCF/DZP	CCSD/DZP
$\omega_1$	<i>a</i>	3413.5 (5.1)	3267.7 (5.3)
$\omega_2$	<i>a</i>	3354.6 (38.2)	3224.2 (34.2)
$\omega_3$	<i>a</i>	3351.9 (4.3)	3215.2 (4.6)
$\omega_4$	<i>a</i>	3345.3 (43.4)	3211.2 (33.8)
$\omega_5$	<i>a</i>	3331.4 (11.0)	3201.2 (6.0)
$\omega_6$	<i>a</i>	3328.9 (51.6)	3197.3 (45.7)
$\omega_7$	<i>a</i>	3315.2 (16.7)	3183.8 (11.0)
$\omega_8$	<i>a</i>	3308.2 (18.9)	3180.3 (15.6)

Table C.14: Cont.

Cont.	Sym	SCF/DZP	CCSD/DZP
$\omega_9$	$a$	3299.2 (8.4)	3172.7 (9.6)
$\omega_{10}$	$a$	3292.5 (6.3)	3164.6 (1.6)
$\omega_{11}$	$a$	1869.0 (15.0)	1735.6 (6.6)
$\omega_{12}$	$a$	1845.2 (1.1)	1712.5 (1.1)
$\omega_{13}$	$a$	1789.1 (1.2)	1661.7 (4.6)
$\omega_{14}$	$a$	1774.3 (21.3)	1648.2 (6.5)
$\omega_{15}$	$a$	1765.1 (4.4)	1633.8 (2.4)
$\omega_{16}$	$a$	1575.1 (1.1)	1471.0 (0.8)
$\omega_{17}$	$a$	1542.7 (0.9)	1439.0 (0.6)
$\omega_{18}$	$a$	1509.6 (1.2)	1409.8 (0.7)
$\omega_{19}$	$a$	1446.5 (0.4)	1348.1 (0.2)
$\omega_{20}$	$a$	1436.5 (4.4)	1335.6 (2.4)
$\omega_{21}$	$a$	1416.0 (0.2)	1317.7 (0.2)
$\omega_{22}$	$a$	1394.9 (4.5)	1301.6 (4.4)
$\omega_{23}$	$a$	1368.9 (0.6)	1275.5 (0.4)
$\omega_{24}$	$a$	1335.6 (1.3)	1244.1 (1.4)
$\omega_{25}$	$a$	1269.4 (0.6)	1188.2 (0.7)
$\omega_{26}$	$a$	1205.8 (1.6)	1150.0 (0.7)
$\omega_{27}$	$a$	1144.7 (6.4)	1089.9 (1.8)
$\omega_{28}$	$a$	1138.9 (43.8)	1040.8 (5.9)
$\omega_{29}$	$a$	1124.3 (0.9)	1033.3 (6.7)
$\omega_{30}$	$a$	1118.6 (16.5)	1007.4 (50.2)
$\omega_{31}$	$a$	1099.3 (1.9)	988.8 (13.0)
$\omega_{32}$	$a$	1093.6 (8.2)	972.2 (5.3)
$\omega_{33}$	$a$	1068.5 (11.9)	951.2 (2.9)
$\omega_{34}$	$a$	1061.8 (5.2)	941.8 (0.6)
$\omega_{35}$	$a$	971.4 (1.3)	873.0 (1.4)
$\omega_{36}$	$a$	954.7 (73.9)	854.0 (18.7)
$\omega_{37}$	$a$	913.1 (6.2)	847.3 (20.6)
$\omega_{38}$	$a$	888.9 (1.3)	838.3 (4.5)
$\omega_{39}$	$a$	874.1 (17.2)	786.4 (20.4)
$\omega_{40}$	$a$	821.6 (111.8)	749.2 (84.5)
$\omega_{41}$	$a$	775.2 (1.8)	720.7 (2.1)
$\omega_{42}$	$a$	703.3 (4.1)	648.6 (3.6)

Table C.14: Cont.

Cont.	Sym	SCF/DZP	CCSD/DZP
$\omega_{43}$	<i>a</i>	669.6 (4.2)	619.5 (5.6)
$\omega_{44}$	<i>a</i>	617.5 (2.6)	561.0 (1.7)
$\omega_{45}$	<i>a</i>	557.0 (2.3)	510.3 (1.1)
$\omega_{46}$	<i>a</i>	499.6 (2.4)	463.4 (1.8)
$\omega_{47}$	<i>a</i>	413.4 (11.8)	383.1 (2.1)
$\omega_{48}$	<i>a</i>	398.6 (2.2)	379.6 (9.6)
$\omega_{49}$	<i>a</i>	339.7 (3.1)	312.9 (2.7)
$\omega_{50}$	<i>a</i>	288.8 (1.3)	275.2 (0.6)
$\omega_{51}$	<i>a</i>	274.0 (2.0)	246.4 (1.5)
$\omega_{52}$	<i>a</i>	200.2 (1.9)	181.0 (1.8)
$\omega_{53}$	<i>a</i>	150.3 (0.3)	138.4 (0.1)
$\omega_{54}$	<i>a</i>	134.4 (1.3)	125.9 (1.5)

Table C.15: Harmonic frequencies for conformation **4** in  $\text{cm}^{-1}$ . Infrared intensities in parenthesis in  $\text{km mol}^{-1}$ .

	Sym	SCF/DZP	MP2/DZP	CCSD/DZP
$\omega_1$	<i>a'</i>	3546.8 (0.7)	3331.2 (0.5)	3374.3 (0.6)
$\omega_2$	<i>a'</i>	3363.6 (13.4)	3229.4 (10.1)	3228.8 (15.6)
$\omega_3$	<i>a'</i>	3350.6 (76.9)	3214.5 (36.3)	3211.5 (32.7)
$\omega_4$	<i>a'</i>	3339.5 (25.0)	3204.5 (24.0)	3200.0 (40.8)
$\omega_5$	<i>a'</i>	3319.0 (0.4)	3187.8 (3.6)	3181.2 (3.2)
$\omega_6$	<i>a'</i>	3286.1 (0.0)	3153.6 (0.1)	3146.1 (0.0)
$\omega_7$	<i>a'</i>	1730.1 (2.9)	1640.5 (2.0)	1633.7 (1.4)
$\omega_8$	<i>a'</i>	1710.7 (0.2)	1585.2 (0.0)	1610.5 (0.4)
$\omega_9$	<i>a'</i>	1662.8 (1.3)	1525.9 (0.0)	1548.8 (0.0)
$\omega_{10}$	<i>a'</i>	1570.3 (5.8)	1453.1 (6.9)	1467.4 (3.8)
$\omega_{11}$	<i>a'</i>	1509.9 (0.6)	1401.6 (0.0)	1413.6 (0.1)
$\omega_{12}$	<i>a'</i>	1379.3 (7.4)	1286.0 (7.5)	1294.4 (5.6)
$\omega_{13}$	<i>a'</i>	1279.6 (0.1)	1191.1 (0.1)	1199.5 (0.1)
$\omega_{14}$	<i>a'</i>	1129.9 (3.4)	1047.0 (0.2)	1052.5 (0.0)
$\omega_{15}$	<i>a'</i>	1113.8 (7.1)	981.5 (27.4)	994.4 (24.9)
$\omega_{16}$	<i>a'</i>	1106.3 (10.4)	908.7 (0.8)	944.9 (1.2)
$\omega_{17}$	<i>a'</i>	1080.7 (9.1)	905.7 (1.6)	937.7 (1.4)

Table C.15: Cont.

Cont.	Sym	SCF/DZP	MP2/DZP	CCSD/DZP
$\omega_{18}$	$a'$	1012.8 (2.1)	895.5 (0.7)	896.2 (2.4)
$\omega_{19}$	$a'$	953.2 (12.3)	853.1 (5.4)	868.0 (1.6)
$\omega_{20}$	$a'$	932.1 (11.1)	816.6 (10.3)	837.2 (12.9)
$\omega_{21}$	$a'$	751.6 (38.0)	692.5 (8.9)	698.8 (14.3)
$\omega_{22}$	$a'$	721.0 (64.7)	662.9 (12.3)	670.8 (25.3)
$\omega_{23}$	$a'$	703.3 (10.7)	647.5 (76.5)	656.7 (53.8)
$\omega_{24}$	$a'$	687.3 (0.0)	600.5 (2.9)	609.2 (0.2)
$\omega_{25}$	$a'$	470.3 (5.4)	434.3 (3.2)	438.0 (3.6)
$\omega_{26}$	$a'$	446.3 (0.5)	400.1 (0.4)	404.6 (0.5)
$\omega_{27}$	$a'$	304.8 (0.5)	282.9 (0.4)	284.9 (0.4)
$\omega_{28}$	$a'$	171.7 (3.4)	150.4 (3.5)	157.0 (3.0)
$\omega_{29}$	$a'$	131.0 (0.1)	110.0 (0.0)	112.1 (0.0)
$\omega_{30}$	$a''$	805.7i (9.0)	3229.0 (29.0)	3227.9 (31.4)
$\omega_{31}$	$a''$	3361.7 (47.4)	3213.2 (31.7)	3210.0 (45.7)
$\omega_{32}$	$a''$	3346.1 (64.0)	3198.1 (7.8)	3192.7 (11.4)
$\omega_{33}$	$a''$	3330.2 (6.4)	3172.1 (0.8)	3165.3 (0.7)
$\omega_{34}$	$a''$	3303.8 (0.2)	2069.3 (8.1)	1715.4 (3.3)
$\omega_{35}$	$a''$	1820.6 (12.7)	1691.3 (0.2)	1604.7 (0.5)
$\omega_{36}$	$a''$	1719.0 (0.0)	1578.7 (4.1)	1559.3 (0.0)
$\omega_{37}$	$a''$	1676.1 (0.2)	1533.5 (0.3)	1519.8 (0.2)
$\omega_{38}$	$a''$	1630.8 (0.0)	1500.7 (0.5)	1493.2 (0.1)
$\omega_{39}$	$a''$	1608.7 (0.6)	1469.7 (0.3)	1408.3 (0.1)
$\omega_{40}$	$a''$	1516.0 (1.7)	1372.8 (0.1)	1317.2 (1.0)
$\omega_{41}$	$a''$	1409.1 (0.9)	1306.6 (1.7)	1286.3 (2.0)
$\omega_{42}$	$a''$	1371.1 (2.3)	1271.7 (2.7)	1163.7 (1.0)
$\omega_{43}$	$a''$	1233.5 (0.5)	1143.6 (2.5)	965.2 (0.0)
$\omega_{44}$	$a''$	1111.8 (0.1)	905.8 (0.0)	932.5 (0.0)
$\omega_{45}$	$a''$	1076.4 (0.2)	898.6 (1.5)	905.8 (1.2)
$\omega_{46}$	$a''$	976.4 (0.0)	880.7 (0.7)	869.3 (0.7)
$\omega_{47}$	$a''$	951.5 (2.1)	851.3 (1.3)	852.7 (0.1)
$\omega_{48}$	$a''$	917.3 (0.8)	842.8 (0.1)	736.8 (0.1)
$\omega_{49}$	$a''$	815.9 (0.0)	715.8 (0.0)	659.0 (1.4)
$\omega_{50}$	$a''$	654.3 (0.2)	579.3 (0.0)	577.8 (0.0)
$\omega_{51}$	$a''$	615.3 (0.0)	555.5 (0.0)	492.1 (1.1)

Table C.15: Cont.

Cont.	Sym	SCF/DZP	MP2/DZP	CCSD/DZP
$\omega_{52}$	$a''$	403.2 (0.5)	338.8 (0.1)	303.0 (0.0)
$\omega_{53}$	$a''$	309.4 (0.0)	278.4 (0.0)	213.9 (0.3)
$\omega_{54}$	$a''$	139.5 (0.1)	120.4 (0.0)	111.5 (0.2)

Table C.16: Harmonic frequencies for conformation **5** in  $\text{cm}^{-1}$ . Infrared intensities in parenthesis in  $\text{km mol}^{-1}$ .

	Sym	SCF/DZP	MP2/DZP	CCSD/DZP
$\omega_1$	$a$	3376.7 (3.4)	3249.7 (0.0)	3232.6 (3.2)
$\omega_2$	$a$	3344.5 (25.5)	3204.6 (0.0)	3212.5 (9.0)
$\omega_3$	$a$	3340.7 (68.6)	3204.1 (58.9)	3211.4 (68.2)
$\omega_4$	$a$	3319.3 (10.4)	3184.7 (10.7)	3188.3 (5.4)
$\omega_5$	$a$	3297.2 (1.4)	3184.2 (0.0)	3168.7 (1.5)
$\omega_6$	$a$	1856.2 (0.1)	2371.8 (113.7)	1725.7 (0.0)
$\omega_7$	$a$	1792.2 (6.4)	1587.9 (3.7)	1671.7 (4.0)
$\omega_8$	$a$	1779.5 (6.1)	1578.7 (0.0)	1654.8 (1.0)
$\omega_9$	$a$	1554.2 (1.2)	1478.3 (0.0)	1452.1 (0.7)
$\omega_{10}$	$a$	1434.9 (1.2)	1344.3 (4.7)	1333.0 (0.9)
$\omega_{11}$	$a$	1399.5 (0.1)	1292.8 (0.0)	1305.1 (0.2)
$\omega_{12}$	$a$	1332.4 (0.7)	1280.1 (5.2)	1241.6 (0.3)
$\omega_{13}$	$a$	1298.8 (0.0)	1203.8 (3.3)	1207.2 (0.2)
$\omega_{14}$	$a$	1177.9 (2.4)	1181.5 (0.0)	1121.1 (1.6)
$\omega_{15}$	$a$	1135.8 (0.5)	1090.7 (0.0)	1012.0 (1.0)
$\omega_{16}$	$a$	1109.7 (0.3)	949.6 (0.0)	990.1 (0.8)
$\omega_{17}$	$a$	1092.5 (0.0)	940.1 (0.0)	953.2 (1.8)
$\omega_{18}$	$a$	1013.3 (5.7)	938.9 (4.1)	944.4 (0.3)
$\omega_{19}$	$a$	962.9 (21.3)	932.9 (0.0)	910.5 (1.1)
$\omega_{20}$	$a$	933.9 (28.7)	846.1 (0.0)	836.5 (19.5)
$\omega_{21}$	$a$	848.6 (23.3)	803.0 (28.8)	760.4 (23.5)
$\omega_{22}$	$a$	637.2 (6.1)	599.1 (0.3)	580.5 (2.6)
$\omega_{23}$	$a$	616.7 (0.0)	574.2 (0.0)	573.2 (0.5)
$\omega_{24}$	$a$	581.0 (2.5)	547.8 (0.0)	534.9 (1.9)
$\omega_{25}$	$a$	406.1 (0.1)	500.6 (3.6)	374.8 (0.3)
$\omega_{26}$	$a$	336.0 (0.4)	374.2 (0.0)	309.7 (0.1)



Table C.16: Cont.

Cont.	Sym	SCF/DZP	MP2/DZP	CCSD/DZP
$\omega_{27}$	<i>a</i>	282.7 (2.1)	253.4 (0.0)	265.6 (1.3)
$\omega_{28}$	<i>a</i>	157.2 (0.1)	207.7 (0.1)	146.0 (0.1)
$\omega_{29}$	<i>b</i>	3376.3 (6.5)	3246.8 (5.7)	3232.6 (8.5)
$\omega_{30}$	<i>b</i>	3340.6 (34.4)	3194.2 (64.1)	3207.7 (30.2)
$\omega_{31}$	<i>b</i>	3317.3 (12.9)	3194.0 (0.0)	3188.8 (9.3)
$\omega_{32}$	<i>b</i>	3307.9 (4.8)	3177.3 (2.4)	3179.1 (2.9)
$\omega_{33}$	<i>b</i>	3296.3 (25.6)	3176.3 (0.0)	3167.9 (21.5)
$\omega_{34}$	<i>b</i>	1863.5 (10.3)	1645.3 (0.0)	1731.3 (3.9)
$\omega_{35}$	<i>b</i>	1783.7 (6.7)	1541.3 (3.6)	1654.6 (2.9)
$\omega_{36}$	<i>b</i>	1530.8 (3.3)	1465.0 (0.0)	1427.9 (2.1)
$\omega_{37}$	<i>b</i>	1517.8 (1.9)	1424.5 (15.5)	1412.6 (1.0)
$\omega_{38}$	<i>b</i>	1431.2 (4.3)	1311.8 (0.0)	1328.8 (3.9)
$\omega_{39}$	<i>b</i>	1387.8 (2.7)	1268.4 (20.3)	1292.4 (2.7)
$\omega_{40}$	<i>b</i>	1321.9 (1.6)	1253.9 (0.0)	1233.6 (1.9)
$\omega_{41}$	<i>b</i>	1176.6 (0.3)	1129.9 (0.0)	1113.5 (0.7)
$\omega_{42}$	<i>b</i>	1141.1 (60.8)	1112.6 (13.0)	1055.6 (5.1)
$\omega_{43}$	<i>b</i>	1097.2 (2.3)	1050.1 (80.6)	1003.0 (69.0)
$\omega_{44}$	<i>b</i>	1089.9 (27.5)	921.9 (13.1)	958.0 (2.3)
$\omega_{45}$	<i>b</i>	972.9 (16.1)	883.5 (0.0)	871.5 (9.6)
$\omega_{46}$	<i>b</i>	899.2 (13.5)	822.9 (0.0)	833.2 (8.5)
$\omega_{47}$	<i>b</i>	835.5 (3.7)	798.7 (118.2)	774.6 (3.1)
$\omega_{48}$	<i>b</i>	825.3 (103.5)	761.4 (13.5)	746.6 (84.1)
$\omega_{49}$	<i>b</i>	683.0 (8.6)	706.1 (0.0)	621.4 (8.3)
$\omega_{50}$	<i>b</i>	457.7 (1.7)	387.7 (4.7)	422.6 (0.7)
$\omega_{51}$	<i>b</i>	399.7 (13.6)	372.0 (0.0)	365.5 (10.2)
$\omega_{52}$	<i>b</i>	269.7 (2.8)	341.8 (11.6)	247.4 (2.3)
$\omega_{53}$	<i>b</i>	217.0 (0.7)	218.0 (0.0)	202.7 (0.6)
$\omega_{54}$	<i>b</i>	201.5 (0.2)	180.4 (1.1)	182.5 (0.2)

Table C.17: Harmonic frequencies for conformation **6** in  $\text{cm}^{-1}$ . Infrared intensities in parenthesis in  $\text{km mol}^{-1}$ .

	Sym	SCF/DZP	MP2/DZP	CCSD/DZP
$\omega_1$	<i>a</i>	3341.8 (5.5)	3221.8 (2.0)	3213.3 (3.5)

Table C.17: Cont.

Cont.	Sym	SCF/DZP	MP2/DZP	CCSD/DZP
$\omega_2$	<i>a</i>	3327.1 (9.1)	3209.0 (13.8)	3197.9 (19.3)
$\omega_3$	<i>a</i>	3323.6 (21.0)	3201.1 (0.0)	3194.4 (2.3)
$\omega_4$	<i>a</i>	3309.7 (0.0)	3193.4 (0.0)	3183.4 (0.0)
$\omega_5$	<i>a</i>	3295.7 (0.1)	3182.2 (0.3)	3169.4 (0.0)
$\omega_6$	<i>a</i>	1877.0 (0.7)	1687.6 (2.9)	1744.7 (0.8)
$\omega_7$	<i>a</i>	1865.4 (27.0)	1663.8 (6.5)	1729.2 (11.7)
$\omega_8$	<i>a</i>	1820.8 (0.4)	1633.3 (0.1)	1687.0 (0.5)
$\omega_9$	<i>a</i>	1569.2 (0.3)	1450.7 (0.2)	1464.0 (0.2)
$\omega_{10}$	<i>a</i>	1528.5 (0.8)	1402.6 (0.5)	1419.4 (1.1)
$\omega_{11}$	<i>a</i>	1428.3 (2.8)	1305.7 (0.8)	1326.6 (1.9)
$\omega_{12}$	<i>a</i>	1366.4 (0.5)	1247.5 (0.1)	1264.9 (0.3)
$\omega_{13}$	<i>a</i>	1312.5 (0.2)	1200.6 (0.2)	1215.3 (0.2)
$\omega_{14}$	<i>a</i>	1126.9 (0.0)	1064.9 (1.4)	1059.2 (0.9)
$\omega_{15}$	<i>a</i>	1117.8 (0.4)	1013.1 (0.1)	1016.4 (1.7)
$\omega_{16}$	<i>a</i>	1104.8 (17.7)	970.6 (22.2)	985.9 (24.6)
$\omega_{17}$	<i>a</i>	1076.7 (18.0)	939.6 (1.2)	956.1 (13.6)
$\omega_{18}$	<i>a</i>	1034.9 (20.3)	933.1 (32.0)	947.8 (8.2)
$\omega_{19}$	<i>a</i>	986.5 (6.9)	896.8 (20.1)	918.0 (8.8)
$\omega_{20}$	<i>a</i>	877.6 (0.1)	842.1 (2.0)	831.8 (1.0)
$\omega_{21}$	<i>a</i>	836.7 (1.7)	772.1 (0.1)	773.9 (1.1)
$\omega_{22}$	<i>a</i>	764.0 (19.1)	705.7 (10.6)	707.9 (10.4)
$\omega_{23}$	<i>a</i>	695.9 (35.7)	642.0 (51.1)	640.9 (38.1)
$\omega_{24}$	<i>a</i>	528.8 (4.9)	477.6 (11.0)	483.1 (7.3)
$\omega_{25}$	<i>a</i>	479.4 (19.9)	428.2 (10.8)	436.1 (13.2)
$\omega_{26}$	<i>a</i>	303.1 (0.3)	281.6 (1.0)	277.4 (0.3)
$\omega_{27}$	<i>a</i>	233.9 (1.2)	213.5 (0.8)	214.5 (0.9)
$\omega_{28}$	<i>a</i>	148.9 (0.0)	148.0 (0.1)	144.0 (0.0)
$\omega_{29}$	<i>b</i>	3340.5 (71.6)	3221.5 (51.6)	3212.4 (60.8)
$\omega_{30}$	<i>b</i>	3328.5 (47.0)	3208.0 (45.0)	3198.5 (51.3)
$\omega_{31}$	<i>b</i>	3321.3 (44.0)	3204.1 (12.0)	3193.9 (25.8)
$\omega_{32}$	<i>b</i>	3309.3 (9.7)	3193.9 (2.7)	3183.3 (5.9)
$\omega_{33}$	<i>b</i>	3295.8 (3.3)	3182.4 (2.3)	3169.4 (3.0)
$\omega_{34}$	<i>b</i>	1827.1 (5.1)	1643.8 (0.3)	1697.7 (1.3)
$\omega_{35}$	<i>b</i>	1805.5 (2.6)	1622.5 (0.9)	1670.0 (1.0)

Table C.17: Cont.

Cont.	Sym	SCF/DZP	MP2/DZP	CCSD/DZP
$\omega_{36}$	<i>b</i>	1546.1 (3.8)	1428.7 (2.5)	1441.6 (2.5)
$\omega_{37}$	<i>b</i>	1491.4 (4.5)	1359.0 (0.5)	1381.2 (2.4)
$\omega_{38}$	<i>b</i>	1404.6 (0.5)	1295.9 (0.5)	1309.5 (0.3)
$\omega_{39}$	<i>b</i>	1346.8 (2.9)	1210.2 (1.3)	1237.5 (1.7)
$\omega_{40}$	<i>b</i>	1308.2 (0.1)	1196.3 (0.0)	1212.0 (0.0)
$\omega_{41}$	<i>b</i>	1136.9 (0.1)	1084.1 (0.7)	1077.7 (0.4)
$\omega_{42}$	<i>b</i>	1108.6 (0.0)	969.4 (2.7)	976.3 (1.4)
$\omega_{43}$	<i>b</i>	1104.7 (1.2)	945.8 (1.3)	958.9 (0.0)
$\omega_{44}$	<i>b</i>	992.8 (3.7)	930.4 (0.5)	933.9 (1.0)
$\omega_{45}$	<i>b</i>	969.0 (15.5)	874.8 (4.4)	884.6 (5.8)
$\omega_{46}$	<i>b</i>	909.2 (12.9)	820.7 (25.2)	832.9 (18.1)
$\omega_{47}$	<i>b</i>	836.1 (56.4)	752.9 (34.5)	761.5 (39.0)
$\omega_{48}$	<i>b</i>	793.8 (32.2)	706.0 (18.0)	715.1 (22.4)
$\omega_{49}$	<i>b</i>	598.4 (4.5)	548.2 (1.7)	548.4 (3.7)
$\omega_{50}$	<i>b</i>	536.5 (8.8)	484.1 (5.7)	487.4 (5.6)
$\omega_{51}$	<i>b</i>	381.0 (0.4)	346.7 (0.4)	347.4 (0.4)
$\omega_{52}$	<i>b</i>	300.8 (0.8)	304.4 (0.6)	290.1 (0.5)
$\omega_{53}$	<i>b</i>	209.2 (0.1)	204.8 (0.1)	200.0 (0.1)
$\omega_{54}$	<i>b</i>	176.9 (0.1)	157.4 (0.2)	160.8 (0.1)

## C.5 NMR Shifts

Table C.18: NMR shifts for conformation **2b** in ppm.

	SCF/ DZP	MP2/ DZP	CCSD/ DZP	CCSD(T)/ DZP	CCSD(T)/ tzip
$C_1(2)$	131.0	119.0	114.1	116.7	124.4
$C_3(2)$	135.1	123.3	117.9	120.7	128.7
$C_5(2)$	136.0	122.7	117.6	120.0	127.0
$C_7(2)$	138.2	126.5	120.3	123.2	130.8
$C_9(2)$	138.6	124.0	119.1	121.6	129.3
$H_1(2)$	5.7	5.6	5.3	5.6	5.2
$H_3(2)$	5.9	5.9	5.5	5.8	5.4
$H_5(2)$	5.8	5.5	5.2	5.5	5.2
$H_7(2)$	6.8	6.6	6.1	6.4	6.1

Table C.18: Cont.

	SCF/ DZP	MP2/ DZP	CCSD/ DZP	CCSD(T)/ DZP	CCSD(T)/ tzip
$H_9(2)$	6.5	6.2	5.8	6.1	5.8

Table C.19: NMR shifts for conformation **4** in ppm.

	SCF/ DZP	MP2/ DZP	CCSD/ DZP	CCSD(T)/ DZP	CCSD(T)/ tzip
$C_1(1)$	143.2	129.2	126.5	127.9	133.7
$C_3(2)$	135.9	128.1	122.0	123.5	127.9
$C_5(2)$	136.9	120.9	119.7	121.1	128.4
$C_7(2)$	128.9	119.1	114.1	115.8	123.5
$C_9(2)$	131.8	115.2	114.8	116.4	124.9
$C_{10}(1)$	130.1	119.2	114.7	116.3	124.3
$H_1(1)$	-5.5	-4.9	-4.9	-4.0	-4.5
$H_3(2)$	9.1	9.0	8.4	8.5	8.3
$H_5(2)$	8.6	8.3	7.9	8.1	7.8
$H_7(2)$	8.4	8.5	7.8	8.0	7.8
$H_9(2)$	8.7	8.6	8.1	8.3	8.0
$H_{10}(1)$	8.5	8.6	8.0	8.2	8.0

Table C.20: NMR shifts for conformation **5** in ppm.

	SCF/ DZP	MP2/ DZP	CCSD/ DZP	CCSD(T)/ DZP	CCSD(T)/ tzip
$C_1(2)$	129.7	118.3	117.3	116.3	124.3
$C_3(2)$	136.6	122.6	122.2	120.6	126.9
$C_5(2)$	154.0	139.8	136.5	135.4	143.5
$C_7(2)$	133.8	123.3	120.4	119.5	126.7
$C_9(2)$	138.6	126.0	124.4	123.3	131.1
$H_1(2)$	6.4	6.4	6.1	6.2	5.8
$H_3(2)$	6.9	6.5	6.4	6.4	6.2
$H_5(2)$	6.3	5.9	6.0	5.9	5.5
$H_7(2)$	6.3	6.2	6.0	6.0	5.7

Table C.20: Cont.

	SCF/ DZP	MP2/ DZP	CCSD/ DZP	CCSD(T)/ DZP	CCSD(T)/ tzip
$H_9(2)$	6.7	6.5	6.3	6.3	6.0

Table C.21: NMR shifts for conformation **6** in ppm.

	SCF/ DZP	MP2/ DZP	CCSD/ DZP	CCSD(T)/ DZP	CCSD(T)/ tzip	CCSD(T)/ qz2p
$C_1(2)$	138.9	125.0	123.6	122.3	128.9	133.9
$C_3(2)$	138.3	125.3	123.7	122.6	130.2	135.1
$C_5(2)$	136.6	124.1	122.7	121.7	129.5	134.0
$C_7(2)$	133.5	121.4	120.0	118.9	126.3	130.9
$C_9(2)$	137.9	124.6	123.1	122.0	129.2	134.1
$H_1(2)$	6.3	6.1	5.9	5.9	5.6	5.9
$H_3(2)$	6.5	6.2	6.1	6.1	5.8	6.1
$H_5(2)$	6.5	6.3	6.1	6.2	5.8	6.1
$H_7(2)$	6.2	6.1	5.9	6.0	5.6	5.9
$H_9(2)$	6.2	6.0	5.9	5.9	5.6	5.9

Table C.22:  $^{13}\text{C}$  NMR shifts using CCSD(T)/qz2p for conformation **6** with vibrational correction (v.c.) and temperature correction (t.c.) determined using SCF/tzip in ppm.

	CCSD(T)/ qz2p	CCSD(T)/qz2p + v.c.	CCSD(T)/qz2p + t.c.
$C_1(2)$	133.9	133.5	133.4
$C_3(2)$	135.1	134.6	134.5
$C_5(2)$	134.0	133.7	133.6
$C_7(2)$	130.9	130.5	130.4
$C_9(2)$	134.1	133.9	133.8

## Bibliography

- [1] *AFIPS Conference Proceedings*, volume 30. Thompson Books, Washington, DC, 1967.
- [2] A. M. Ahern, R. L. Garrell, and K. D. Jordan. Theoretical investigation of the normal-mode vibrational frequencies and intensities of ethylene. *J. Phys. Chem.*, 92(22):6228–6232, 1988.
- [3] M. Akiyama. Determination of effective-charge distribution on some deuterobenzenes from their out-of-plane gas-band intensities. *J. Mol. Spectrosc.*, 84:49–56, 1980.
- [4] M. Akiyama, Y. Shimizu, H. Itaya, and M. Kakihana. Charge distribution on benzene determined from infrared band intensities by a new equation. *J. Phys. Chem.*, 93(6):2280–2284, 1989.
- [5] J. Almlöf. *Notes on Hartree-Fock Theory and Related Topics*, pages 1–90. Volume 64 of Roos [192], 1994.
- [6] J. Almlöf and P. R. Taylor. General contraction of gaussian basis sets. I. Atomic natural orbitals for first- and second-row atoms. *J. Chem. Phys.*, 86(7):4070–4077, 1987.
- [7] J. Almlöf and P. R. Taylor. General contraction of gaussian basis sets. II. Atomic natural orbitals and the calculation of atomic and molecular properties. *J. Chem. Phys.*, 92(1):551–560, 1990.

- [8] G. M. Amdahl. *Validity of the single processor approach to achieving large scale computing capabilities*, pages 483–485. Volume 30 of AFIPS Conference Proceedings [1], 1967.
- [9] E. R. Andrews and R. G. Eades. A nuclear magnetic resonance investigation of three solid benzenes. *Pro. R. Soc. London, Ser. A*, 218(1135):537–552, 1953.
- [10] W. R. Angus, C. K. Ingold, and A. H. Leckie. Structure of benzene. Part III. Raman spectra of liquid benzene and liquid hexadeuterobenzene. *J. Chem. Soc.*, pages 925–931, 1936.
- [11] A. A. Auer, J. Gauss, and J. F. Stanton. Quantitative prediction of gas-phase  $^{13}\text{C}$  nuclear magnetic shielding constants. *J. Chem. Phys.*, 118(23):10407–10417, 2003.
- [12] G. E. Bacon, N. A. Curry, and S. A. Wilson. A crystallographic study of solid benzene by neutron diffraction. *Pro. R. Soc. London, Ser. A*, 279(1376):98–110, 1964.
- [13] C. R. Bailey, J. B. Hale, C. K. Ingold, and J. W. Thompson. Structure of benzene. Part IV. Infra-red absorption spectra of benzene and hexadeuterobenzene both as vapour and as liquid. *J. Chem. Soc.*, pages 931–941, 1936.
- [14] J. Barnes and W. H. Fulweiler. The absorption spectrum of liquid benzene. *Physical Rev.*, 32:618–623, 1928.
- [15] R. J. Bartlett. Many-body perturbation-theory and coupled cluster theory for electron correlation in molecules. *Ann. Rev. Phys. Chem.*, 32:359–401, 1981.

- [16] R. J. Bartlett and J. F. Stanton. *Applications of Post-Hartree-Fock Methods: A Tutorial*, pages 65–169. Volume 5 of Lipkowitz and Boyd [124], 1994.
- [17] R. J. Bartlett, J. D. Watts, S. A. Kucharski, and J. Noga. Noniterative fifth-order triple and quadruple excitation-energy corrections in correlated methods. *Chem. Phys. Lett.*, 165(6):513–522, 1990.
- [18] O. Bastiansen. Recent advances in electron-diffraction gas work in Norway. *Acta Cryst.*, 10:861, 1957.
- [19] O. Bastiansen, L. Fernholt, H. M. Seip, H. Kambara, and K. Kuchitsu. Structure of cyclohexane determined by two independent gas electron-diffraction investigations. *J. Mol. Struct.*, 18:163–168, 1973.
- [20] C. W. Bauschlicher, Jr., S.R. Langhoff, and A. Kormornicki. The calculation of the dipole-moments of NiH, TiO and FeO. *Theor. Chim. Acta*, 77(4):263–279, 1990.
- [21] J. L. Bentz, R. M. Olson, M. S. Gordon, M. W. Schmidt, and Ricky A. Kendall. Coupled cluster algorithms for networks of shared memory parallel processors. *Comput. Phys. Comm.*, 176:589–600, 2007.
- [22] S. W. Benson, F. R. Cruickshank, D. M. Golden, G. R. Haugen, H. E. O’Neal, R. Shaw, and R. Walsh. Additivity rules for the estimation of thermochemical properties. *Chem. Rev.*, 69:279, 1969.
- [23] A. Bérces and T. Ziegler. The harmonic force field of benzene. A local density functional study. *J. Chem. Phys.*, 98:4793, 1993.



- [24] J. M. Berman and L. Goodman. The  $a_{2g}$  mode in ground state benzene. *J. Chem. Phys.*, 87(3):1479–1487, 1987.
- [25] B. Bernu, D. M. Ceperley, and Jr. W. A. Lester. The calculation of excited states with quantum Monte Carlo. II. vibrational excited states. *J. Chem. Phys.*, 93(1):552–562, 1990.
- [26] J. E. Bertie and C. D. Keefe. Comparison of infrared absorption intensities of benzene in the liquid and gas phases. *J. Chem. Phys.*, 101(6):4610–4616, 1994.
- [27] J. E. Bertie and C. D. Keefe. Infrared intensities of liquids XXIV: Optical constants of liquid benzene-h<sub>6</sub> at 25° C extended to 11.5 cm<sup>-1</sup> and molar polarizabilities and integrated intensities of benzene-h<sub>6</sub> between 6200 and 11.5 cm<sup>-1</sup>. *J. Mol. Struct.*, 695-696:39–57, 2004.
- [28] A. D. Boese and J. M. L. Martin. Vibrational spectra of the azabenzenes revisited: Anharmonic force fields. *J. Phys. Chem. A.*, 108(14):3085–3096, 2004.
- [29] M. Born and R. Oppenheimer. Zur Quantentheorie der Molekeln. *Ann. d. Phys.*, 84:457–484, 1927.
- [30] J. M. Bowman. The self-consistent-field approach to polyatomic vibrations. *Acc. Chem. Res.*, 19:202–208, 1986.
- [31] J. M. Bowman, K. Christoffel, and F. Tobin. Applications of SCF-SI theory to vibrational motion of polyatomic molecules. *J. Phys. Chem.*, 83(8):905–912, 1979.

- [32] R. G. Bray and M. J. Berry. Intramolecular rate processes in highly vibrationally excited benzene. *J. Chem. Phys.*, 71(12):4909–4922, 1979.
- [33] J. Breidung, W. Thiel, J. Gauss, and J. F. Stanton. Anharmonic force fields from analytic CCSD(T) second derivatives: HOF and F<sub>2</sub>O. *J. Chem. Phys.*, 110(8):3687–3696, 1999.
- [34] I. J. Brenner, J. Senekowitsch, and R. E. Wyatt. Coupled cluster calculation of the in-plane harmonic force field of benzene. *Chem. Phys. Lett.*, 215(1–3):63–71, 1993.
- [35] S. Brodersen and A. Langseth. The infrared spectra of benzene, sym-benzene-d<sub>3</sub> and benzene-d<sub>6</sub>. *Mat. Fys. Skr. Dan. Vid. Selsk.*, 1(1):1–45, 1956.
- [36] E. J. Bylaska, W. A. de Jong, N. Govind, K. Kowalski, T. P. Straatsma, M. Valiev, D. Wang, E. Apra, T. L. Windus, J. Hammond, P. Nichols, S. Hirata, M. T. Hackler, Y. Zhao, P.-D. Fan, R. J. Harrison, M. Dupuis, D. M. A. Smith, J. Nieplocha, V. Tipparaju, M. Krishnan, Q. Wu, T. Van Voorhis, A. A. Auer, M. Nooijen, E. Brown, G. Cisneros, G. I. Fann, H. Fruchtl, J. Garza, K. Hirao, R. Kendall, J. A. Nichols, K. Tsemekhman, K. Wolinski, J. Anchell, D. Bernholdt, P. Borowski, T. Clark, D. Clerc, H. Dachsel, M. Deegan, K. Dyall, D. Elwood, E. Glendening, M. Gutowski, A. Hess, J. Jaffe, B. Johnson, J. Ju, R. Kobayashi, R. Kutteh, Z. Lin, R. Littlefield, X. Long, B. Meng, T. Nakajima, S. Niu, L. Pollack, M. Rosing, G. Sandrone, M. Stave, H. Taylor, G. Thomas, J. van Lenthe, A. Wong, and Z. Zhang. NWChem, a computational chemistry package for parallel computers, Version 5.1. Pacific Northwest National Laboratory, Richland, Washington 99352-0999, USA, 2007.

- [37] A. Cabana, J. Bachand, and J. Giguère. The  $\nu_4$  vibration-rotation bands of  $\text{C}_6\text{H}_6$  and  $\text{C}_6\text{D}_6$ : The analysis of the bands and the determination of the bond lengths. *Can. J. Phys.*, 52(20):1949–1955, 1974.
- [38] S. Califano. *Vibrational States*. John Wiley & Sons, Ltd., London, 1976.
- [39] E. Cané, A. Miani, and A. Trombetti. The  $\nu_6$ ,  $\nu_7$ ,  $\nu_8$  and  $\nu_{19}$  gas phase fundamental frequencies of  $^{12}\text{C}_6\text{H}_6$ . *Chem. Phys. Lett.*, 272:83–85, 1997.
- [40] E. Cané, A. Miani, and A. Trombetti. Some anharmonic constants of  $\text{C}_6\text{H}_6$ . *J. Mol. Spectros.*, 183:204–206, 1997.
- [41] E. Cané, A. Miani, and A. Trombetti. The harmonic vibrational frequencies and the geometry of the  $^{12}\text{C}_6\text{H}_6$ . *Chem. Phys. Lett.*, 340:356–361, 2001.
- [42] S. Carter, J. M. Bowman, and N. Handy. Extensions and tests of ‘multimode’: A code to obtain accurate vibration/rotation energies of many-mode molecules. *Theoretical Chem. Accnts.*, 100:191–198, 1998.
- [43] S. Carter, S. J. Culik, and J. M. Bowman. Vibrational self-consistent field method for many-mode systems: A new approach and application to the vibrations of CO adsorbed on Cu(100). *J. Chem. Phys.*, 107:10485, 1997.
- [44] C. Castro, W. L. Karney, C. M. McShane, and R. P. Pemberton. [10]Annulene: Bond shifting and conformational mechanisms for automerization. *J. Org. Chem.*, 71(8):3001, 2005.

- [45] D. M. Ceperley and L. Mitas. *Quantum Monte Carlo Methods in Chemistry*, pages 1–38. Volume 93 of Prigogine and Rice [173], 1996.
- [46] G. M. Chaban, J. O. Jung, and R. B. Gerber. Ab initio calculation of anharmonic vibrational states of polyatomic systems: Electronic structure combined with vibrational self-consistent field. *J. Chem. Phys.*, 111(5):1823–1829, 1999.
- [47] O. Christiansen. Møller-Plesset perturbation theory for vibrational wave functions. *J. Chem. Phys.*, 119(12):5773–5781, 2003.
- [48] O. Christiansen. Vibrational coupled cluster theory. *J. Chem. Phys.*, 120(5):2149–2159, 2004.
- [49] O. Christiansen and J. M. Luis. Beyond vibrational self-consistent-field methods: Benchmark calculations for the fundamental vibrations of ethylene. *Inter. J. Quant. Chem.*, 104:667–680, 2005.
- [50] J. Čížek. On the correlation problem in atomic and molecular systems. calculation of wavefunction components in Ursell-type expansion using quantum-field theoretical methods. *J. Chem. Phys.*, 45(11):4256–4266, 1966.
- [51] J. Čížek. *On the Use of the Cluster Expansion and the Technique of Diagrams in Calculations of Correlation Effects in Atoms and Molecules*, pages 35–89. Volume 14 of Prigogine and Rice [172], 1969.
- [52] J. Čížek and J. Paldus. Correlation problems in atomic and molecular systems III. Rederivation of the coupled-pair many-electron theory using the traditional quantum chemical method. *Int. J. Quantum Chem.*, 5(4):359–379, 1971.

- [53] J. Clouthier and D. A. Ramsay. The spectroscopy of formaldehyde and thioformaldehyde. *A. Rev. Chem.*, 34:31–58, 1983.
- [54] E. G. Cox. The crystalline structure of benzene. *Pro. R. Soc. London, Ser. A*, 135:491, 1932.
- [55] E. G. Cox, D. W. J. Cruickshank, and J. A. S. Smith. The crystal structure of benzene at  $-3^{\circ}$  C. *Pro. R. Soc. London, Ser. A*, 247(1248):1–21, 1958.
- [56] T. D. Crawford and H. F. Schaefer III. *An Introduction to Coupled Cluster Theory for Computational Chemists*, pages 33–136. Volume 14 of Lipkowitz and Boyd [126], 2000.
- [57] M. Dang-Nhu, G. Blanquet, J. Walrand, and F. Raulin. Spectral intensities in the  $\nu_4$ -band of benzene at  $15\text{ }\mu\text{m}$ . *J. Mol. Spectrosc.*, 134:237–239, 1989.
- [58] B. T. Darling and D. M. Dennison. The water vapor molecule. *Phys. Rev.*, 57(2):128–139, 1940.
- [59] P. A. M. Dirac. Note on exchange phenomena in the Thomas atom. *Proc. Camb. Phil. Soc.*, 26:376–385, 1930.
- [60] A. Domenicano and I. Hargittai, editors. *Accurate Molecular Structures*. Oxford University Press, Oxford, England, 1992.
- [61] T. H. Dunning. Gaussian basis functions for use in molecular calculations. I. Contraction of (9s5p) atomic basis sets for the first-row atoms. *J. Chem. Phys.*, 53(7):2823–2833, 1970.

- [62] T. H. Dunning. Gaussian basis functions for use in molecular calculations. III. Contraction of (10s6p) atomic basis sets for the first-row atoms. *J. Chem. Phys.*, 55(2):716–723, 1971.
- [63] T. H. Dunning. Gaussian basis sets for use in correlated molecular calculations. I. The atoms boron through neon and hydrogen. *J. Chem. Phys.*, 90(2):1007–1023, 1989.
- [64] J. W. Ellis. Molecular absorption spectra of liquids below  $3\mu$ . *Trans. Faraday Soc.*, 25:888–898, 1929.
- [65] S. Eppinger, A. Rabold, T. N. Misra, S. K. Nandy, and H. W. Schrötter. Second-order Raman-spectra of benzene and hexadeuterobenzene in the gaseous-phase. *J. Mol. Struct.*, 266:389–403, 1992.
- [66] U. Erlekam, M. Frankowski, G. Meijer, and G. von Helden. An experimental value for the  $b_{1u}$  C-H stretch mode in benzene. *J. Chem. Phys.*, 124(17):171101–171104, 2006.
- [67] W. C. Ermler and C. W. Kern. Properties of the benzene molecule near the Hartree-Fock limit. *J. Chem. Phys.*, 58(8):3458–3465, 1973.
- [68] P. Esherick, A. Owyong, and J. Plíva. Ionization-detected Raman studies of the  $1600\text{ cm}^{-1}$  Fermi dyad of benzene. *J. Chem. Phys.*, 83(7):3311–3317, 1985.
- [69] L. Farnell, J. Kao, L. Radom, and H. F. Schaefer III. Structures and stabilities of isomeric [10]annulenes. *J. Am. Chem. Soc.*, 103(9):2147–2156, 1981.

- [70] E. Fermi. Über den Ramaneffekt des Kohlendioxyds. *Z. Phys.*, 71(3-4):250–259, 1931.
- [71] G. D. Fletcher, M. W. Schmidt, B. M. Bode, and M. S. Gordon. The distributed data interface in GAMESS. *Comput. Phys. Comm.*, 128:190–200, 2000.
- [72] M. Flynn. Very high-speed computing systems. *Proceedings of the IEEE*, 54(12):1901–1909, 1966.
- [73] V. Fock. Näherungsmethode zur Lösungdes quantenmechanischen Mehrkörperproblems. *Zeits. f. Physik.*, 61:126–148, 1930.
- [74] A. R. Ford, T. Janowski, and P. Pulay. Array files for computational chemistry: MP2 energies. *J. Comput. Chem.*, 28(7):1215–1220, 2007.
- [75] J. Gauss. Effects of electron correlation in the calculation of nuclear-magnetic-resonance chemical-shifts. *J. Chem. Phys.*, 99(5):3629–3643, 1993.
- [76] J. Gauss and D. Cremer. *Analtical Energy Gradients in Møller-Plesset Pertubation and Quadratic Configuration Interaction Methods: Theory and Application*, pages 205–299. Volume 14 of Lipkowitz and Boyd [125], 2000.
- [77] J. Gauss and J. Stanton. Analytic CCSD(T) second derivatives. *Chem. Phys. Lett.*, 276(1–2):70–77, 1997.
- [78] J. Gauss and J. F. Stanton. Coupled-cluster calculations of nuclear magnetic resonance chemical shifts. *J. Chem. Phys.*, 103(9):3561–3577, 1995.

- [79] J. Gauss and J. F. Stanton. The equilibrium structure of benzene. *J. Phys. Chem. A.*, 104(13):2865–2868, 2000.
- [80] J. Gauss and J. F. Stanton. *Electron-Correlated Approaches for the Calculation of NMR Chemical Shifts*, pages 355–422. Volume 123 of Prigogine and Rice [174], 2002.
- [81] J. Gauss, J. F. Stanton, and R. J. Bartlett. Coupled-cluster open-shell analytic gradients: Implementation of the direct product decomposition approach in energy gradient calculations. *J. Chem. Phys.*, 95(4):2623–2638, 1991.
- [82] J. Gerratt and I. M. Mills. Force constants and dipole-moment derivatives of molecules from perturbed hartree-fock calculations. i. *J. Chem. Phys.*, 49(4):1719–1729, 1968.
- [83] L. Goodman, J. M. Berman, and A. G. Ozkaback. The benzene ground state potential surface. III. Analysis of  $b_{2u}$  vibrational mode anharmonicity through two-photon intensity. *J. Chem. Phys.*, 90(5):2544–2554, 1989.
- [84] L. Goodman, A. G. Ozkabak, and S. N. Thakur. A benchmark vibrational potential surface: Ground-state benzene. *J. Phys. Chem.*, 95(23):9044–9058, 1991.
- [85] M. S. Gordon and M. W. Schmidt. Recent advances in qm and qm/mm methods. *Lecture Notes in Computer Science*, 2660:75–83, 2003.
- [86] G. G. Hall. The molecular orbital theory of chemical valency. VIII. A method of calculating ionization potentials. *Proc. Roy. Soc. Lond. A*, 205(1083):541–552, 1951.



- [87] B. L. Hammond, Jr. W. A. Lester, and P. J. Reynolds. *Monte Carlo Methods in Ab Initio Quantum Chemistry*. World Scientific, Singapore, 1994.
- [88] N. C. Handy, R. D. Amos, J. F. Gaw, J. E. Rice, and E. D. Simadiras. The elimination of singularities in derivative calculations. *Chem. Phys. Lett.*, 120(2):151–158, 1985.
- [89] N. C. Handy and H. F. Schaefer III. On the evaluation of analytic energy derivatives for correlated wavefunctions. *J. Chem. Phys.*, 81(2):5031, 1984.
- [90] N. C. Handy, P. E. Maslen, R. D. Amos, J. S. Andrews, C. W. Murray, and G. J. Laming. The harmonic frequencies of benzene. *Chem. Phys. Lett.*, 197(4–5):506–515, 1992.
- [91] N. C. Handy, C. W. Murray, and R. D. Amos. Study of CH<sub>4</sub>, C<sub>2</sub>H<sub>2</sub>, C<sub>2</sub>H<sub>4</sub> and C<sub>6</sub>H<sub>6</sub> using Kohn-Sham theory. *J. Phys. Chem.*, 97(17):4392–4396, 1993.
- [92] M. E. Harding, M. Lenhart, A. A. Auer, and J. Gauss. Quantitative prediction of gas-phase <sup>19</sup>F nuclear magnetic shielding constants. *J. Chem. Phys.*, 128:244111, 2008.
- [93] M. E. Harding, T. Metzroth, J. Gauss, and A. A. Auer. Parallel calculation of CCSD and CCSD(T) analytic first and second derivatives. *J. Chem. Theory Comput.*, 4(1):64–74, 2008.
- [94] R. J. Harrison, G. B. Fitzgerald, W. D. Laidig, and R. J. Bartlett. Analytic MBPT(2) second derivatives. *Chem. Phys. Lett.*, 124(3):291–294, 1986.

- [95] D. R. Hartree. The wave mechanics of an atom with a non-Coulomb central field. Part II. Some results and discussion. *Proc. Camb. Phil. Soc.*, 24:111–132, 1928.
- [96] G. Herzberg. *Infrared and Raman Spectra*. Van Nostrand Reinhold, New York, 1945.
- [97] H. Hollenstein, S. Piccirillo, M. Quack, and M. Snels. High-resolution infrared spectrum and analysis of the  $\nu_{11}$ ,  $A_{2u}(B_2)$  fundamental band of  $^{12}C_6H_6$  and  $^{13}C^{12}C_6H_6$ . *Molecular Physics*, 71(4):759–768, 1990.
- [98] A. B. Hollinger and H. L. Welsh. High resolution rotation- vibration Raman spectra of benzene. I. The totally symmetric bands of  $C_6H_6$ . *Can. J. Phys.*, 56:974–982, 1978.
- [99] A. B. Hollinger and H. L. Welsh. High resolution rotation- vibration Raman spectra of benzene. II. The doubly degenerate bands of  $C_6H_6$ . *Can. J. Phys.*, 56:1513–1525, 1978.
- [100] A. B. Hollinger, H. L. Welsh, and K. S. Jammu. High resolution rotation- vibration Raman spectra of benzene. III. Spectrum of  $C_6D_6$ . *Can. J. Phys.*, 57:767–774, 1979.
- [101] S. Huzinaga. Gaussian-type functions for polyatomic systems. I. *J. Chem. Phys.*, 42(4):1293–1303, 1965.
- [102] T. Janowski, A. R. Ford, and P. Pulay. Parallel calculation of coupled cluster singles and doubles wave functions using array files. *J. Chem. Theory Comput.*, 3(4):1368–1377, 2007.

- [103] F. Jensen. *Introduction to Computational Chemistry*. John Wiley & Sons, Inc., Chichester, England, 1999.
- [104] H. B. Jensen and S. Brodersen. The totally symmetric rotation- vibrational Raman bands of benzene. *J. Raman Spectrosc.*, 8:103–110, 1979.
- [105] J. O. Jung and R. B. Gerber. Vibrational wave functions and spectroscopy of  $(\text{H}_2\text{O})_n$ ,  $n = 2, 3, 4, 5$ : Vibrational self-consistent field with correlation corrections. *J. Chem. Phys.*, 105(23):10332–10348, 1996.
- [106] I. L. Karle. An electron diffraction investigation of cyclotettraene and benzene. *J. Chem. Phys.*, 20(1):65, 1952.
- [107] J. Kauppinen, P. Jensen, and S. Brodersen. Determination of the  $B_0$  constant of  $\text{C}_6\text{H}_6$ . *J. Molec. Spectrosc.*, 83:161–174, 1980.
- [108] C. D. Keefe. The dipole moment derivatives of gaseous benzene: A comparison of experimental and ab initio values. *Chem. Phys.*, 327:180–186, 2006.
- [109] R. A. Kendall, E. Aprá, D. E. Bernholdt, E. J. Bylaska, M. Dupuis, G. I. Fann, R. J. Harrison, J. Ju, J. A. Nichols, J. Nieplocha, T.P. Straatsma, T. L. Windus, and A. T. Wong. High performance computational chemistry: An overview of NWChem a distributed parallel application. *Comput. Phys. Comm.*, 128:260–283, 2000.
- [110] R. D. Kennedy, D. Lloyd, and H. McNab. Annulenes, 1980-2000. *J. Chem. Soc., Perkin Trans.*, 1:1601–1621, 2002.

- [111] M. Khlifi, F. Raulin, and M. Dang-Nhu. Benzene  $\nu_4$  integrated band intensity versus temperature. *J. Mol. Spectrosc.*, 154:235–239, 1992.
- [112] K. Kimura and M. Kubo. Application of least-squares method to gaseous benzene in electron diffraction investigation. *J. Chem. Phys.*, 32(6):1776–1780, 1960.
- [113] R. King, T. D. Crawford, J. F. Stanton, and H. F. Schaefer III. Conformations of [10]annulene: More bad news for density functional theory and perturbation theory. *J. Am. Chem. Soc.*, 121(46):10788–10793, 1999.
- [114] H. Koch, H. J. A. A. Jensen, T. Helgaker, P. Jørgensen, G. E. Scuseria, and H. F. Schaefer III. Coupled cluster energy derivatives. Analytic hessian for the closed-shell coupled cluster singles and doubles wave function: Theory and applications. *J. Chem. Phys.*, 92(8):4924–4940, 1990.
- [115] K. Kuchitsu. *The Potential Energy Surface and Meaning of Internuclear Distance*, pages 14–46. In Domenicano and Hargittai [60], 1992.
- [116] S. R. Langhoff, editor. *Understanding Chemical Reactivity, Volume 13: Quantum Mechanical Electronic Structure Calculations with Chemical Accuracy*. Kulwer Academic Publishers, Dordrecht, Holland, 1995.
- [117] A. Langseth and B. P. Stoicheff. High resolution Raman spectroscopy of gases VI. Rotational spectrum of benzene- $d_3$ . *Can. J. Phys.*, 34:350–353, 1956.
- [118] T. J. Lee, W. D. Allen, and H. F. Schaefer III. The analytic evaluation of energy first derivatives for two-configuration self-consistent-field con-

- figuration interaction (TCSCF-CI) wave functions. Application to ozone and ethylene. *J. Chem. Phys.*, 87(12):7062–7075, 1987.
- [119] T. J. Lee and G. E. Scuseria. *Achieving Chemical Accuracy with coupled-cluster Theory*, pages 47–108. In Langhoff [116], 1995.
- [120] K. K. Lehmann. Beyond the  $x - K$  relations calculation of 1-1 and 2-2 resonance constants with application to HCN and DCN. *Molec. Phys.*, 1989(6):1129–1137, 1989.
- [121] J. Leška and D. J. Loos. Theoretical study of the [10]annulene geometry and stability. *J. Mol. Struct.*, 21(2):245–252, 1974.
- [122] C. Y. Lin, A. T. B. Gilbert, and P. M. W. Gill. Calculating molecular vibrational spectra beyond the harmonic approximation. *Theor. Chem. Account.*, 120:23–35, 2008.
- [123] J. Lindenmayer, U. Magg, and H. Jones. Diode laser spectroscopy of the  $\nu_4$  band of benzene. *J. Molec. Spectrosc.*, 128:172–175, 1988.
- [124] K. B. Lipkowitz and D. B. Boyd, editors. *Reviews in Computational Chemistry*, volume 5. VCH Publishers, Inc., New York, 1994.
- [125] K. B. Lipkowitz and D. B. Boyd, editors. *Reviews in Computational Chemistry*, volume 14. John Wiley & Sons, Inc., Chichester, England, 2000.
- [126] K. B. Lipkowitz and D. B. Boyd, editors. *Reviews in Computational Chemistry*, volume 14. John Wiley & Sons, Inc., Chichester, England, 2000.

- [127] G. Di Lonardo, L. Fusina, G. Masciarelli, and F. Tullini. Integrated band strengths of benzene vapour in the 600-1900  $\text{cm}^{-1}$  region. *Spectrochim. Acta A*, 55:1535–1544, 1999.
- [128] D. J. Loos and J. Leška. Theoretical study of [10] and [12]annulenes. *J. Collect. Czech. Chem. Commun.*, 45(1):187–200, 1980.
- [129] V. Lotrich, N. Flocke, M. Ponton, A. D. Yau, A. Perera, E. Deumens, and R. J. Bartlett. Parallel implementation of electronic structure energy, gradient, and hessian calculations. *J. Chem. Phys.*, 128:194104, 2008.
- [130] P. O. Löwdin, editor. *Int. J. Quantum Chem. Symp.*, volume 13. John Wiley & Sons, Inc., Chichester, England, 1979.
- [131] J. M. L. Martin, J. El-Yazal, and J. P. François. Basis set convergence and performance of density functional theory including exact exchange contributions for geometries and harmonic frequencies. *Mol. Phys.*, 86(6):1437–1450, 1995.
- [132] J. M. L. Martin, T. J. Lee, and P. R. Taylor. An accurate ab initio quartic force field for formaldehyde and its isotopomers. *J. Molec. Spectrosc.*, 160:105–116, 1993.
- [133] J. M. L. Martin, T. J. Lee, and P. R. Taylor. A purely ab initio spectroscopic quality quartic force field for acetylene. *J. Chem. Phys.*, 108(2):676–691, 1998.
- [134] J. M. L. Martin, T. J. Lee, P. R. Taylor, and J. P. François. The anharmonic force field of ethylene,  $\text{C}_2\text{H}_4$ , by means of accurate ab initio calculations. *J. Chem. Phys.*, 103(7):2589–2602, 1995.

- [135] J. M. L. Martin, P. R. Taylor, and T. J. Lee. The harmonic frequencies of benzene. a case for atomic natural orbital basis sets. *Chem. Phys. Lett.*, 275:414–422, 1997.
- [136] S. Masamune and N. Darby. [10]Annulenes and other (CH)<sub>10</sub> hydrocarbons. *Acc. Chem. Res.*, 5:272–281, 1971.
- [137] S. Masamune, K. Hojo, G. Bigam, and D. L. Rabenstein. The geometry of [10]annulenes. *J. Am. Chem. Soc.*, 93(19):4966–4968, 1971.
- [138] S. Masamune and R. T. Seidner. [10]Annulenes. *J. Chem. Soc., Chem. Commun.*, pages 542–544, 1969.
- [139] S. Masamune, R. T. Seidner, H. Zenda, M. Wiesel, N. Nakatsuka, and G. Bigam. Low-temperature photolysis of bicyclo[6.2.0]deca-2,4,6,9-tertaene and trans- and cis-9,10-dihydronaphthalenes. *J. Am. Chem. Soc.*, 90(19):5286–5288, 1968.
- [140] P. E. Maslen, N. C. Handy, R. D. Amos, and D. Jayatilaka. Higher analytic derivatives. IV. Anharmonic effects in the benzene spectrum. *J. Chem. Phys.*, 97(6):4233–4254, 1992.
- [141] D. A. Matthews, J. Vázquez, and J. F. Stanton. Calculated stretching overtone levels and Darling-Dennison resonance in water: a triumph of simple theoretical approaches. *Molec. Phys.*, 105(19):2659–2666, 2007.
- [142] A. B. McCoy and III E. L. Sibert. *Canonical Van Vleck Perturbation Theory and Its Application to Studies of Highly Vibrationally Excited States of Polyatomic Molecules*, pages 151–184. In Wyatt and Zhang [231], 1996.

- [143] A. Miani, E. Cané, P. Palmieri, A. Trombetti, and N. C. Handy. Experimental and theoretical anharmonicity for benzene using density functional theory. *J. Chem. Phys.*, 112(1):248–259, 2000.
- [144] I. M. Mills. *Vibration- Rotation Structure in Asymmetric- and Symmetric-Top Molecules*, pages 115–140. In Rao and Mathews [184], 1972.
- [145] C. Møller and M. S. Plesset. Note on an approximation treatment for many-electron systems. *Phys. Rev.*, 46(7):618–622, 1934.
- [146] J. Nieplocha, R. J. Harrison, and R. J. Littlefield. Global arrays: A nonuniform memory access programming model for high-performance computers. *J. Supercomput.*, 10(2):169–189, 1996.
- [147] J. Nieplocha, B. Palmer, V. Tipparaju, M. Krishnan, H. Trease, and Edo Apr’a. Advances, applications and performance of the global arrays shared memory programming toolkit. *Int. J. of High Performance Computing Applications*, 20(2):203–231, 2006.
- [148] L. S. Norris, M. A. Ratner, A. E. Roitberg, and R. B. Gerber. Møller-Plesset perturbation theory applied to vibrational problems. *J. Chem. Phys.*, 105(24):11261–11267, 1996.
- [149] N. Ohta and M. Ito. Pre-resonance Raman effect and vibronic coupling of benzene and benzene-d<sub>6</sub>. *Chem. Phys.*, 24(2):175–181, 1977.
- [150] M. Oldani and A. Bauder. Pure rotational spectrum of benzene-d<sub>1</sub>. *Chem. Phys. Lett.*, 108(1):7–10, 1984.



- [151] R. M. Olson, J. L. Bentz, R. A. Kendall, M. W. Schmidt, and M. S. Gordon. A novel approach to parallel coupled cluster calculations: Combining distributed and shared memory techniques for modern cluster based systems. *J. Chem. Theory Comput.*, 3(4):1312–1328, 2007.
- [152] G. Orlova and J. D. Goddard. Practical failures from the inclusion of exact exchange: how much exact exchange is appropriate? *Mol. Phys.*, 100(4):483, 2002.
- [153] P. S. Pacheco. *Parallel Programming with MPI*. Morgan Kaufmann Publishers, Inc., San Francisco, 1997.
- [154] R. H. Page, Y. R. Shen, and Y. T. Lee. Local modes of benzene and benzene dimer, studied by infrared-ultraviolet double resonance in a supersonic beam. *J. Chem. Phys.*, 88(8):4621–4636, 1988.
- [155] D. Papoušek and M. R. Aliev. *Molecular Vibrational-Rotational Spectra*. Elsevier, Amsterdam, 1982.
- [156] L. Pauling. Interatomic distances in covalent molecules and resonance between two or more lewis electronic structures. *Proc. Natl. Acad. Sci.*, 18(4):293–297, 1932.
- [157] L. Pauling, L. O. Brockway, and J. Y. Beach. The dependence of interatomic distance on single bond-double bond resonance. *J. Am. Chem. Soc.*, 57:2705–2709, 1935.
- [158] L. Pauling and G. W. Wheland. The nature of the chemical bond. V. The quantum-mechanical calculation of the resonance energy of benzene and naphthalene and the hydrocarbon free radical. *J. Chem. Phys.*, 1:362–374, 1933.

- [159] F. Pawłowski, P. Jørgensen, J. Olsen, F. Hebelund, T. Helgaker, J. Gauss, K. L. Bak, and J. F. Stanton. Molecular equilibrium structures from experimental rotational constants and calculated vibration rotation interaction constants. *J. Chem. Phys.*, 116(15):6482–6496, 2002.
- [160] J. Plíva, P. Esherick, and A. Owyong. Analysis of the simulated Raman spectrum of the  $\nu_{16}/\nu_2+\nu_{18}$  Fermi dyad of benzene. *J. Molec. Spectrosc.*, 125:393–412, 1987.
- [161] J. Plíva and J. W. C. Johns. The  $\nu_{13}$  fundamental band of benzene. *Can. J. Phys.*, 61:269–277, 1983.
- [162] J. Plíva and J. W. C. Johns. The perpendicular band  $\nu_{14}$  of benzene near 10  $\mu\text{m}$ . *J. Mol. Spectrosc.*, 107:318–323, 1984.
- [163] J. Plíva, J. W. C. Johns, and L. Goodman. Infrared bands of isotopic benzenes:  $\nu_{13}$  of  $^{12}\text{C}_6\text{D}_6$  and  $\nu_{12}$  of  $^{13}\text{C}_6\text{H}_6$ . *J. Mol. Spectrosc.*, 140:214–225, 1990.
- [164] J. Plíva, J. W. C. Johns, and L. Goodman. Infrared bands of isotopic benzenes:  $\nu_{13}$  and  $\nu_{14}$  of  $^{13}\text{C}_6\text{D}_6$ . *J. Mol. Spectrosc.*, 148:427–435, 1991.
- [165] J. Plíva, J. W. C. Johns, and Z. Lu. High-resolution study of the difference band  $\nu_{17} - \nu_{20}$  of benzene. *J. Mol. Spectrosc.*, 161:269–274, 1993.
- [166] J. Plíva, J. W. C. Johns, and Z. Lu. The difference band  $\nu_{11} - \nu_4$  and  $\nu_{10} - \nu_{18}$  of benzene at high resolution. *Mol. Phys.*, 87(4):859–863, 1996.
- [167] J. Plíva and A. S. Pine. The spectrum of benzene in the 3- $\mu\text{m}$  region: The  $\nu_{12}$  fundamental band. *J. Mol. Spectrosc.*, 93:209–236, 1982.

- [168] J. Plíva and A. S. Pine. Analysis of the 3- $\mu$ m bands of benzene. *J. Mol. Spectrosc.*, 126:82–98, 1987.
- [169] J. A. Pople, R. Krishman, H. B. Schlegel, and J. S. Binkley. *Derivative Studies in Hartree-Fock and Møller-Plesset Theories*, pages 225–241. Volume 13 of Löwdin [130], 1979.
- [170] Parallel quantum solutions: PQS version 3.2., 2005. See <http://www.pqs-chem.com>.
- [171] D. R. Price and J. F. Stanton. Computational study of [10]annulene NMR spectra. *Org. Lett.*, 4(17):2809–2811, 2002.
- [172] I. Prigogine and S. A Rice, editors. *Advances in Chemical Physics*, volume 14. John Wiley & Sons, Inc., Chichester, England, 1969.
- [173] I. Prigogine and S. A Rice, editors. *Advances in Chemical Physics*, volume 93. John Wiley & Sons, Inc., Chichester, England, 1996.
- [174] I. Prigogine and S. A. Rice, editors. *Advances in Chemical Physics*, volume 123. John Wiley & Sons, Inc., Chichester, England, 2002.
- [175] V. Prudente and P. H. Acioli. Quantum Monte Carlo study of rovibrational states of molecular systems. *Chem. Phys. Lett.*, 302:239–254, 1999.
- [176] V. Prudente, L. S. Costa, and P. H. Acioli. Correlation function quantum Monte Carlo studies of rovibrational excited states in molecules. *J. Phys. B: At. Mol. Opt. Phys.*, 33:R285–R313, 2000.
- [177] P. Pulay. Ab initio calculation of force constants and equilibrium geometries. *Mol. Phys.*, 17(2):197, 1969.

- [178] P. Pulay. Ab initio calculation of force constants and equilibrium geometries in polyatomic molecules ii. force constants of water. *Molec. Phys.*, 18(4):473–480, 1970.
- [179] P. Pulay. Improved SCF convergence acceleration. *J. Comp. Chem.*, 3(4):556–560, 1982.
- [180] P. Pulay, G. Fogarasi, and J. E. Boggs. Force field, dipole moment derivatives and vibronic constants of benzene from a combination of experimental and ab initio quantum chemical information. *J. Chem. Phys.*, 74(7):3999–4014, 1981.
- [181] P. Pulay, G. Fogarasi, F. Pang, and J. E. Boggs. Systematic ab initio gradient calculation of molecular geometries, force constants and dipole moment derivatives. *J. Am. Chem. Soc.*, 101(10):2550–2560, 1979.
- [182] K. G. Raghavachari, G. W. Trucks, J. A. Pople, and M. Head-Gordon. A fifth-order perturbation comparison of electron correlation theories. *Chem. Phys. Lett.*, 157(6):479–483, 1989.
- [183] Raman and Krishnan. *Indian J. Physics*, 2:399, 1928.
- [184] K. N. Rao and C. W. Mathews, editors. *Molecular Spectroscopy: Modern Research*. Academic Press, New York, 1972.
- [185] S. Rashev and D. C. Moule. Empirical determination of the harmonic force constants in benzene. 3. The harmonic frequencies. *J. Phys. Chem. A*, 108(7):1259–1267, 2004.

- [186] M. A. Ratner and R. B. Gerber. Excited vibrational states of polyatomic molecules: The semiclassical self-consistent field approach. *J. Phys. Chem.*, 90(1):20–30, 1986.
- [187] F. Raulin, B. Accaoui, A. Razaghi, M. Dang-Nhu, A. Coustenis, and D. Gautier. Infrared-spectra of gaseous organincs - Application to the atmosphere of Titan. 2. Infrared intensities and frequencies of C-4 alkanenitriles and benzene. *Spectrochim. Acta A*, 46(5):671–683, 1990.
- [188] K. V. Reddy, D. F. Heller, and M. J. Berry. Highly vibrationally excited benzene: Overtone spectroscopy and intramolecular dynamics of C<sub>6</sub>H<sub>6</sub>, C<sub>6</sub>D<sub>6</sub>, and partially deuterated or substituted benzenes. *J. Chem. Phys.*, 76(6):2814–2837, 1982.
- [189] L. T. Redmon and G. D. Purvis amd R. J. Bartlett. Accurate binding-eneries of diborane, borane carbonyl, and borazane determined by many-body perturbation-theory. *J. Am. Chem. Soc.*, 101(11):2856–2862, 1979.
- [190] C. P. Rinsland, V. M. Devi, T. A. Blake, R. L. Sams, S. Sharpe, and L. Chiou. Quantitative measurement of integrated band intensities of benzene vapor in the mid-infrared at 278, 298, and 323 K. *J. Quant. Spectrosc. Ra.*, 109(15):2511–2522, 2008.
- [191] H. Romanowski, J. M. Bowman, and L. B. Harding. Vibrational energy levels of formaldehyde. *J. Chem. Phys*, 82(9):4155–4165, 1985.
- [192] B. O. Roos, editor. *Lecture Notes in Quantum Chemistry II: European Summer School in Quantum Chemistry*, volume 64 of *Lecture Notes in Chemistry*. Springer-Verlag, Berlin, 1994.

- [193] C. C. J. Roothaan. New developments in molecular orbital theory. *Rev. Mod. Phys.*, 23(2):69–89, 1951.
- [194] W. J. Russell and W. Lapraik. On absorption-bands in the visible spectrum produced by certain colourless liquids. *J. Chem. Soc. Trans.*, 19:168–173, 1881.
- [195] E. A. Salter and R. J. Bartlett. Analytic energy derivatives in many-body methods. II. Second derivatives. *J. Chem. Phys.*, 90(3):1767–1773, 1989.
- [196] E. A. Salter, G. W. Trucks, and R. J. Bartlett. Analytic energy derivatives in many-body methods. I. First derivatives. *J. Chem. Phys.*, 90(3):1752–1766, 1989.
- [197] A. Schäfer, H. Horn, and R. Ahlrichs. Fully optimized contracted gaussian basis sets for atoms Li to Kr. *J. Chem. Phys.*, 97(4):2571–2577, 1992.
- [198] A. C. Scheiner, G. E. Scuseria, J. E. Rice, T. J. Lee, and H. F. Schaefer III. Analytic evaluation of energy gradients for the single and double excitation coupled cluster (CCSD) wave function: Theory and application. *J. Chem. Phys.*, 87(9):5361–5373, 1987.
- [199] M. W. Schmidt, K. K. Baldridge, J. A. Boatz, S. T. Elbert, M. S. Gordon, J. H. Jensen, S. Koseki, N. Matsunaga, K. A. Nguyen, S. J. Su, T. L. Windus, M. Dupuis, and J. A. Montgomery. General atomic and molecular electronic structure system. *J. Comput. Chem.*, 14:1347–1363, 1993.

- [200] W. Schneider and W. Thiel. Anharmonic force fields from analytic second derivatives: Method and application to methyl bromide. *Chem. Phys. Lett.*, 154(4):367–373, 1989.
- [201] V. Schomaker and L. Pauling. The electron diffraction investigation of the structure of benzene, pyridine, pyrazine, butadiene-1,3, cyclopentadiene, furan, pyrrole and thiophene. *J. Am. Chem. Soc.*, 61:1769–1780, 1939.
- [202] E. Schrödinger. Quantisierung als Eigenwertproblem. *Ann. d. Phys.*, 384(4):361–376, 1926.
- [203] E. Schrödinger. Quantisierung als Eigenwertproblem. *Ann. d. Phys.*, 384(6):489–527, 1926.
- [204] E. Schrödinger. Quantisierung als Eigenwertproblem. *Ann. d. Phys.*, 385(13):437–490, 1926.
- [205] E. Schrödinger. Quantisierung als Eigenwertproblem. *Ann. d. Phys.*, 386(18):109–139, 1926.
- [206] M. Schütz and R. Lindh. An integral direct, distributed-data, parallel mp2 algorithm. *Theor. Chem. Acta*, 95(1–2):13–34, 1997.
- [207] G. E. Scuseria. Analytic evaluation of energy gradients for the singles and doubles coupled cluster method including perturbative triple excitations: Theory and applications to FOOF and Cr<sub>2</sub>. *J. Chem. Phys.*, 94(1):442–447, 1991.

- [208] E. D. Simandiras, J. E. Rice, T. J. Lee, R. D. Amos, and N. C. Handy. On the necessity of  $f$  basis functions for bending frequencies. *J. Chem. Phys.*, 88(5):3187–3195, 1988.
- [209] J. C. Slater. The theory of complex spectra. *Phys. Rev.*, 34(10):1293–1322, 1929.
- [210] J. C. Slater. *Quantum Theory of Molecules and Solids, Volume 1: Electronic Structure of Molecules*. McGraw-Hill Book Co., Inc., New York, 1963.
- [211] J. F. Stanton, J. Gauss, J. D. Watts, and R. J. Bartlett. A direct product decomposition approach for symmetry exploitation in many-body methods. I. Energy calculations. *J. Chem. Phys.*, 94(6):4334–4345, 1991.
- [212] J. F. Stanton, J. Gauss, J. D. Watts, W. J. Lauderdale, and R. J. Bartlett. The ACESII program system. *Int. J. Quantum Chem. Symp.*, 26:879–894, 1992.
- [213] J. F. Stanton, J. Gauss, J. D. Watts, P. G. Szalay, and R. J. Bartlett. With contributions from A. A. Auer, D. B. Bernholdt, O. Christiansen, M. E. Harding, M. Heckert, O. Heun, C. Huber, D. Jonsson, J. Jusélius, W. J. Lauderdale, T. Metzroth, C. Michauk, D. R. Price, K. Ruud, F. Schiffmann, A. Tajti, M. E. Varner, J. Vázquez and the integral packages: MOLECULE (J. Almlöf and P. R. Taylor), PROPS (P. R. Taylor), and ABACUS (T. Helgaker, H. J. A. A. Jensen, P. Jørgensen, and J. Olsen). See, also Ref. [212]. Current version see <http://www.cfour.de>.



- [214] B. P. Stoicheff. High resolution Raman spectroscopy of gases II. Rotational spectra of  $C_6H_6$  and  $C_6D_6$ , and internuclear distances in the benzene molecule. *Can. J. Phys.*, 32:339–346, 1954.
- [215] H. Sulzbach and H. F. Schaefer III. Exploring the boundary between aromatic and olefinic character: Bad news for second-order perturbation theory and density functional schemes. *J. Am. Chem. Soc.*, 118(14):3519–3520, 1996.
- [216] H. Sulzbach, P. R. Schleyer, H. Jiao, Y. Xie, and H. F. Schaefer III. A [10]annulene isomer may be aromatic, after all! *J. Am. Chem. Soc.*, 117(4):1369–1373, 1995.
- [217] P. Jørgensen T. Helgaker and J. Olsen. *Molecular Electronic-Structure Theory*. John Wiley & Sons, Ltd., Chichester, England, 2000.
- [218] K. Tamagawa, T. Iijima, and M. Kimura. Molecular structure of benzene. *J. Mol. Struct.*, 30:243–253, 1976.
- [219] J. Tennyson, J. R. Henderson, and N. G. Fulton. DVR3D: for the fully pointwise calculation of ro-vibrational spectra of triatomic molecules. *Comp. Phys. Comm.*, 86:175–198, 1995.
- [220] E. E. van Tamelen and T. L. Burkoth. Cyclodecapentaene. *J. Am. Chem. Soc.*, 89(1):151–152, 1967.
- [221] J. Vázquez and J. F. Stanton. Treatment of Fermi resonance effects on transition moments in vibrational perturbation theory. *Molec. Phys.*, 105(1):101–109, 2007.

- [222] J. K. G. Watson. Simplification of the molecular vibration-rotation hamiltonian. *Mol. Phys.*, 15(5):479–490, 1968.
- [223] J. D. Watts. Parallel algorithms for coupled-cluster methods. *Parallel Computing*, 26:857–867, 2000.
- [224] J. D. Watts, J. Gauss, and R. J. Bartlett. Open-shell analytical energy gradients for triple excitation many-body, coupled-cluster methods; MBPT(4), CCSD+T(CCSD), CCSD(T), and QCISD(T). *Chem. Phys. Lett.*, 200(1–2):1–7, 1992.
- [225] H.-J. Werner, P. J. Knowles, R. Lindh, F. R. Manby, M. Schütz, P. Celani, T. Korona, A. Mitrushenkov, G. Rauhut, T. B. Adler, R. D. Amos, A. Bernhardsson, A. Berning, D. L. Cooper, M. J. O. Deegan, A. J. Dobbyn, F. Eckert, E. Goll, C. Hampel, G. Hetzer, T. Hrenar, G. Knizia, C. Köppl, Y. Liu, A. W. Lloyd, R. A. Mata, A. J. May, S. J. McNicholas, W. Meyer, M. E. Mura, A. Nicklass, P. Palmieri, K. Pflüger, R. Pitzer, M. Reiher, U. Schumann, H. Stoll, A. J. Stone, R. Tarroni, T. Thorsteinsson, M. Wang, and A. Wolf. MOLPRO, version 2006.1, a package of ab initio programs, 2006. See <http://www.molpro.net>.
- [226] A. Willetts and N. C. Handy. The anharmonic constants for a symmetric top. *Chem. Phys. Lett.*, 235:286–290, 1995.
- [227] E. B. Wilson. The normal modes and frequencies of vibration of the regular plane hexagon model of the benzene molecule. *Physical Review*, 45:706–714, 1934.
- [228] E. B. Wilson, J. C. Decius, and P. C. Cross. *Molecular Vibrations: The Theory of Infrared and Raman Vibrational Spectra*. McGraw-Hill Book

Co., Inc., New York, 1955.

- [229] K. Wolinski, J. F. Hinton, and P. Pulay. Efficient implementation of the gauge-independent atomic orbital method for NMR chemical shift calculations. *J. Am. Chem. Soc.*, 112(23):8251–8260, 1990.
- [230] L. Wunsch, F. Metz, H. J. Neusser, and E. W. Schlag. Two-photon spectroscopy in the gas phase: Assignments of molecular transitions in benzene. *J. Chem. Phys.*, 66(2):386–400, 1977.
- [231] R. E. Wyatt and J. Z. H. Zhang, editors. *Dynamics of Molecules and Chemical Reactions*. Marcel Dekker, Inc., New York, 1996.
- [232] Y. Xie, H. F. Schaefer III, G. Liang, and J. P. Bowen. [10]annulene: The wealth of energetically low-lying structural isomers of the same  $(\text{CH})_{10}$  connectivity. *J. Am. Chem. Soc.*, 116(4):1442–1449, 1994.
- [233] L. D. Ziegler and B. Hudson. Resonance Raman scattering of benzene and benzene- $d_6$  with 212.8 nm excitation. *J. Chem. Phys.*, 74(2):982–992, 1981.

# Index

- Analytic Derivatives
  - Application
    - Geometry, 92, 139
    - Geometry Optimization, 22, 95, 97, 140
    - Harmonic Frequencies, 95, 109, 139, 140, 153, 207
    - NMR, 139, 140, 160
    - Spectroscopy, 43, 63, 92, 95, 117, 125
  - Coupled Cluster Theory
    - CCSD, 32, 39, 45, 92, 95, 97, 109, 117, 139, 140
    - CCSD(T), 37, 39, 45, 92, 95, 97, 109, 117, 125, 139, 140
  - Density Functional Theory, 92, 139
  - HF, 23
  - MP2, 27, 39, 45, 92, 95, 97, 109, 117, 139, 140
  - SCF, 92, 95, 97, 109, 117, 139, 140
- Annulene
  - Computational Studies
    - Energy, 139, 140, 150, 197
    - Geometry, 139, 140
    - Harmonic Frequencies, 139, 140, 153, 207
    - NMR, 139, 140
  - Conformations, 139
    - 1a**, 141, 198
    - 1b**, 141, 198
    - 2a**, 142, 198, 207
    - 2b**, 144, 199, 209
    - 3a**, 145, 200, 210
    - 3b**, 146, 201, 212
    - 4**, 147, 203, 214
    - 5**, 148, 204, 216
    - 6**, 149, 205, 217
  - Experiment, 138
- Benzene
  - Computational Studies
    - Fundamental Frequencies, 92
    - Harmonic Force Field, 93
    - Harmonic Frequencies, 92
    - Structure, 92
  - Geometry
    - Equilibrium, 182, 184
    - Experiment, 182
  - Harmonic Force Field, 93, 95
  - Harmonic Frequencies, 109, 185
    - Empirical Estimates, 93, 95, 114
  - Spectra, 84
    - Infrared, 86, 90
    - Other, 91
    - Raman, 88
    - Two Photon, 89
  - Structure, 82
  - VPT2
    - Literature, 183
- Energy
  - Annulene, 139, 150, 197
  - Coupled-Cluster Theory, 12

- CCSD, 14
- CCSD(T), 17
- HF, 2
- MP2, 9

#### Geometry

- Distance and Position Averages
  - Benzene, 105, 185
- Effective, 100
  - Benzene, 95, 107
- Equilibrium, 22
  - Annulene, 140
  - Benzene, 95, 97, 100, 182, 184
- Experiment
  - Benzene, 182

#### Parallel, 43

- ACESII, 44
- Analytic Second Derivatives, 45,
  - 95, 109, 117, 125, 140
- Load Balance, 59
- Performance, 48, 168
  - Basis Set, 56
  - Combine, 58
  - Method, 55
  - Symmetry, 60
  - System Size, 57

#### VPT2, 63

- Application
  - Benzene, 117, 183
- Resonance
  - Darling-Dennison, 74
  - Fermi, 72, 121

## Vita

David Reed Price was born in Provo, Utah on the twenty-first day of August 1976, the son of Alexander A. Price and the former Marla Hill. He spent his formative years in San Antonio, Texas before enrolling as a student at William Marsh Rice University. He completed a Bachelor of Arts degree in Chemical Physics in May of 2000, then pursued graduate studies in chemistry at the University of Texas at Austin where he joined the research group of John F. Stanton.

An avid sports fan, he has enjoyed tutoring student-athletes in subjects ranging from organic chemistry to calculus. An amateur poet, he has written over sixty short poems. An opinionated observer, he has also written several essays expressing his views on political and social issues.

Permanent address: 7303 Granite Creek  
San Antonio, Texas 78238

This dissertation was typeset with L<sup>A</sup>T<sub>E</sub>X<sup>†</sup> by the author.

---

<sup>†</sup>L<sup>A</sup>T<sub>E</sub>X is a document preparation system developed by Leslie Lamport as a special version of Donald Knuth's T<sub>E</sub>X Program.